eman ta zabal zazu
Universidad del País Vasco
Euskal Herriko Unibertsitatea

Controlling the fate of stem cells through two- and three-dimensional scaffolds based on bioresorbable polymers and graphene derivatives: a study towards nerve tissue regeneration

Yurena Polo Arroyabe

Industrial PhD Thesis

2022

Thesis (co)supervisors: Dr. Aitor Larrañaga Espartero and Prof. Jose-Ramon Sarasua Oiz

Doctorate Program: Engineering of Materials and Sustainable Processes

Group in Science and Engineering of Polymeric Biomaterials (Zibio Group)

Department of Mining-Metallurgy Engineering and Materials Science

Faculty of Engineering in Bilbao

University of the Basque Country (UPV/EHU)

And Polimerbio

Acknowledgments

I would like to thank the Department of Mining-Metallurgy Engineering and Materials Science for the opportunity to carry out my doctoral thesis with them. I would especially like to acknowledge my thesis supervisors Aitor Larrañaga Espartero and Jose Ramon Sarasua Oíz for the great opportunity of completing this thesis. Thank you very much for all your patience and teachings. Thank you Joserra for all your good advice and thank you Aitor for your great patience, for all the opportunities for personal growth and for teaching me every day to be a better scientist.

I would also like to thank all the people from the Zibio group of the University of the Basque Country (UPV/EHU), who have helped and taught me during these 4 years, especially Ainhoa Lejardi, Ester Zuza, Jone Muñoz, Xabier Larrañaga and Emilio Meaurio. Without them, these 4 years would not have been the same. Special thanks to Carlos Bello for all his help in measuring the mechanical properties of the films in chapter 4 and to Sergio Gonzalez de Langarica for the characterization of the hydrogels in chapter 5. And of course, to Oroitz Sanchez, Iulia Caraseva and Carlos Bello for not only being colleagues, but also a great discovery on a personal level. I would also like to thank Edurne Marín, Gianni Ciofani, Christos Tapeinos and Daniel E. Martínez-Tong and José Luis Toca Herrera for their help in chapter 5 and Jagoba Iturri for the atomic force microscope measurements in chapter 3. Also to Alex and Ricardo from Sgiker for all the help in this thesis.

I would also like to thank the entire Department of Cell Biology of the University of the Basque Country (UPV/EHU) for having welcomed me as one of its members during these years and for having taught me not only everything related to neural and dental stem cell culture, but also how to work in a team and promote multidisciplinary work. You have been an essential pillar for the completion of this thesis, especially Gaskon Ibarretxe, Fernando Unda and Igor Irastorza. You have become great teachers to imitate and, without you, this thesis would not have been the same. I would like to make a special mention to José Ramón Pineda, who, without having any academic ties, has treated me as just another student and has taught me not only to be a better scientist and to improve myself every day, but also to always consider the personal component of our work. On the other hand, Jon Luzuriaga, Beatriz Pardo and Irene Manero also deserve a mention for all their hard work, for always being there and because I am sure they will become great scientists to look up to. Also deserve a mention all the people who have made the day-to-day work more enjoyable; thank you Jokin, Helena, Sandra, Xandra, Noelia, Alba, Irene, Maitane, Miguel, Patricia, Laura, Lucia, Ander, Jone, Maria, Cris, Maddalen, Nerea, Andrea, Iker and Joana.

I must thank Polimerbio for the opportunity to do this thesis, especially Jorge Fernandez who has been an example during these years, thank you for being there, for supporting me and for giving me the opportunity to do this doctoral thesis in the company. Thanks also to the rest of the team for their support in this project: Pablo, Laura, Antonio, Beñat, David, Juan Carlos, Maria.

I would also like to thank all the people who have made me get to where I am. Without the support of the people from Amarna like Machteld, Irene, Sybrand or Walter and the people from Mymetics I would never have made the decision to move back to Spain. Thank you for being an example as scientists and also at personal level. I would especially like to thank Aleksandra Korzystka for putting the idea of doing a PhD in my head and for always supporting me despite the distance. And of course, to all those mice who have given their lives for this project.

Finally, I would like to thank my family for all the support they have given me to pursue this career. Thank you for your unconditional support and for the effort it has taken. Thank you, grandma Toñi, for watching all those documentaries with me, for teaching me to love animals and biology and for always pushing me to be a better person. Thanks, grandpa, for teaching me that life must be enjoyed, and that dreams must be pursued; without that advice I would probably not be here today. Thanks also to my grandmother Pilar, for always reminding me how proud she is with a smile. Thanks to my parents for giving me the opportunity to study. Thank you, mother, for always pushing me to do what really made me happy, even if at the time it was scary and meant pushing me away. Thank you, father, for teaching me to always think in the long term and weigh up the alternatives, there is a little piece of you in this thesis. Thank you Aitor for putting up with all this and for always being proud of me and thank you Boss for all your unconditional love.

Thanks to my friends for putting up with me all these years, for always supporting me and for being there no matter what. Thank you Eukene for all those years of the degree, for continuing to put up with me after so many years and for not letting distance ourselves. Thanks to your unconditional support, this thesis carries a little piece of you. Thanks also to the people of Castro for putting up with me during this stage, the little moments with you have always been and will always be the best part of the summer. Thanks to Leti, Sarai and Leire for all those moments together, for all that advice and all those hours that have filled me with endorphins, for the trips, the concerts, the dinners, the walks... in short, for sharing life with me. Thank you Yera not only for being my friend and showing me that every day for more than 15 years, but also for how proud you make me feel. Thanks also to the teachers Marta González, Henar and Marta Sanz, you were the ones who brought us together. Thank you for all those English lessons that have made it possible for me to be here today and for all those beers afterwards. Thank you, Marta González for still being part of my life, for having seen me grow up and for all the advice you have given me over the years, you have always been and will be an example.

Agradecimientos

Deseo agradecer al Departamento de Ingeniería Minero-Metalúrgica y Ciencia de los Materiales por la oportunidad de poder realizar la tesis doctoral con ellos. En especial a mis directores de Tesis Aitor Larrañaga Espartero y Jose Ramon Sarasua Oíz la gran oportunidad que ha supuesto realizar esta tesis. Muchas gracias por toda la paciencia y las enseñanzas. Gracias Joserra por todos tus buenos consejos y gracias Aitor por la gran paciencia que has tenido, por todas las oportunidades de crecimiento personal y por enseñarme cada día a ser una mejor científica.

También me gustaría agradecer a todas las personas del grupo Zibio de la Universidad del País Vasco (UPV/EHU) que me han ayudado y enseñado durante estos 4 años, especialmente a Ainhoa Lejardi, Ester Zuza, Jone Muñoz, Xabier Larrañaga y Emilio Meaurio. Sin ellos, estos 4 años no hubieran sido los mismo. Agradecer a Carlos Bello en especial toda la ayuda en la medición de las propiedades mecánicas de los filmes del capítulo 4 y a Sergio Gonzalez de Langarica la caracterización de los hidrogeles del capítulo 5. Y como no, a Oroitz Sanchez, Iulia Caraseva y Carlos Bello el haber sido no solo compañeros de trabajo, sino también un gran descubrimiento a nivel personal. Por otro lado, me gustaría agradecer a Edurne Marín, Gianni Ciofani, Christos Tapeinos y Daniel E. Martínez-Tong por su ayuda en el capítulo 5 y a Jagoba Iturri y José Luis Toca Herrera por las medidas en el microscopio de fuerzas atómicas del capítulo 3. También a Alex y Ricardo de Sgiker por toda su ayuda en esta tesis.

Así mismo he de agradecer a todo el departamento de Biología Celular de la Universidad del País Vasco (UPV/EHU) por haberme acogido como una más durante estos años y haberme no solo enseñado todo lo relativo al cultivo de células madre neurales y dentales, sino también a trabajar en equipo y promover un trabajo multidisciplinar. Habéis sido un pilar esencial para la realización de esta tesis, especialmente Gaskon Ibarretxe, Fernando Unda e Igor Irastorza. Os habéis convertido en grandes maestros a los que imitar y sin vosotros esta tesis no hubiera sido lo mismo. Quisiera hacer una mención especial para José Ramón Pineda, quien, sin tener ningún vínculo académico, me ha tratado como una estudiante más y me ha enseñado no solo a ser mejor científica y superarme cada día, sino también a tener siempre en cuenta el componente personal de nuestro trabajo. Por otro lado, también se merecen una mención Jon Luzuriaga, Beatriz Pardo e Irene Manero por todo el esfuerzo dedicado, por estar siempre ahí y porque estoy segura se convertirán en unos grandes científicos a los que admirar. Así mismo, se merecen otra mención todas las personas que han hecho más ameno el día a día con una sonrisa; gracias Jokin, Helena, Sandra, Xandra, Noelia, Alba, Irene, Maitane, Miguel, Patricia, Laura, Lucia, Ander, Jone, Maria, Cris, Maddalen, Nerea, Andrea, Iker, Joana.

Debo agradecer a Polimerbio la oportunidad de realizar esta tesis, especialmente a Jorge Fernandez quien ha sido un ejemplo durante estos años, gracias por estar ahí, por apoyarme y por haberme dado la oportunidad de realizar esta tesis doctoral en la empresa. Gracias también al resto del equipo por el apoyo en este proyecto, Pablo, Laura, Antonio, Beñat, David, Juan Carlos, Maria.

También me gustaría agradecer a todas las personas que me han hecho llegar a donde estoy. Sin el apoyo de la gente de Amarna como Machteld, Irene, Sybrand o Walter y de la gente de Mymetics jamás hubiera tomado la decisión de volverme a España. Gracias por ser un ejemplo como científicos y también como personas. Quisiera agradecer en especial a Aleksandra Korzystka por meterme en la cabeza la idea de hacer un doctorado y por siempre apoyarme a pesar de la distancia que nos separa. Y como no, a los ratones que han dado su vida para que yo hoy presente esta tesis.

Por último, me gustaría agradecer a mi familia todo el apoyo dado para que persiga esta carrera. Gracias por el apoyo incondicional, por el esfuerzo que eso ha supuesto. Gracias a mis aitites estoy hoy donde estoy. Gracias Amama Toñi por ver conmigo todos esos documentales, por enseñarme a amar los animales y la Biología y por empujarme siempre a ser mejor persona. Gracias aitite por inculcarme que la vida hay que disfrutarla y gozarla, y los sueños, perseguirlos; sin esos consejos seguramente hoy no estaría aquí. Gracias también a mi abuela Pilar, por siempre recordarme lo orgullosa que está con una sonrisa. Gracias a mis padres por darme la oportunidad de estudiar y formarme. Gracias Ama por empujarme siempre a hacer lo que realmente me hacía feliz, aunque en ese momento me diera miedo y supusiera alejarme. Gracias aita por enseñarme a pensar siempre a largo plazo y sopesar las alternativas, en esta tesis hay un pedacito vuestro. Gracias Aitor por aguantar todo lo que esto ha supuesto y por siempre estar orgulloso de mí. Y gracias Boss por tu amor incondicional.

Gracias a mis amigas por aguantarme todos estos años, por apoyarme siempre y por estar ahí pasara lo que pasara. Gracias Eukene por todos esos años de carrera, por seguir aguantándome después de tantos años y por no dejar que la distancia nos distancie. Esta tesis lleva un pedacito tuyo, por todo ese apoyo incondicional. Gracias también a la Kuadrilla de Castro por aguantarme durante esta etapa, los ratitos con vosotros siempre han sido y serán lo mejor del verano. Gracias a las de siempre, Leti, Sarai y Leire por todos esos momentos juntas, por todos esos consejos y todas esas horas que me han llenado de endorfinas, por los viajes, los conciertos, las cenas, los paseos… en fin por compartir la vida conmigo. Gracias Yera no solo por ser mi amiga y demostrármelo cada día desde hace más de 15 años, sino por lo orgullosa que me haces sentir de serlo. Gracias también a las profesoras Marta González, Henar y Marta Sanz, vosotras fuisteis quienes nos unisteis. Gracias por todas esas clases de inglés que han hecho que hoy esté aquí y por todas esas cervezas de después. Gracias Marta González por seguir formando parte de mi vida, por haberme visto crecer y por todos los consejos dados durante estos años, siempre has sido y serás un ejemplo.

Eskerrak

Eskerrak eman nahi dizkiot Meatzaritzako Ingeniaritza eta Materialen Zientzia departamentuari, haiekin doktorego-tesia egiteko aukera izategatik. Tesiko zuzendari izan ditudan Aitor Larrañaga Espartero eta Jose Ramon Sarasua Oizi bereziki, tesi hau egiteak ekarri duen aukera paregabeagatik. Eskerrik asko pazientzia eta irakaskuntza guztiengatik. Eskerrik asko Joserra zure aholku on guztiengatik eta eskerrik asko Aitor izan duzun pazientziagatik, hazkunde pertsonalerako aukera guztiengatik eta egunero zientzialari hobea izaten erakusteagatik.

Era berean, eskerrak eman nahi dizkiet 4 urte hauetan lagundu eta irakatsi didaten Euskal Herriko Unibertsitateko (EHU) Zibio taldeko pertsona guztiei, bereziki Ainhoa Lejardi, Ester Zuza, Jone Muñoz, Xabier Larrañaga eta Emilio Meauriori, haiek gabe, 4 urte hauek ez baitziren berdinak izango. Bereziki, eskerrak eman nahi dizkiet Carlos Bellosi, 4. kapituluko filmen propietate mekanikoen neurketan laguntzeagatik, eta Sergio Gonzalez de Langaricari, 5. kapituluaren karakterizazioagatik. Eta nola ez, Oroitz Sanchez, Iulia Caraseva eta Carlos Belloreri, lankideak izateaz gain, aurkikuntza handia izan direlako maila pertsonalean. Bestalde, eskerrak eman nahi dizkiet Edurne Marín, Gianni Ciofani, Christos Tapeinos eta Daniel Martínez-Tongi, 5. kapituluan emandako laguntzagatik, eta Jagoba Iturri eta José Luis Toca Herrerari, 3. kapituluko indarreko mikroskopio atomikoan hartutako neurriengatik. Baita ere Sgikerreko Alex eta Ricardori, beraien laguntzagatik tesi honetan.

Era berean, eskerrak eman behar dizkiot Euskal Herriko Unibertsitateko (UPV/EHU) Zelulen Biologiako departamentu osoari, urte hauetan beste bat bezala hartu nautelako. Zelula ama neuralen eta hortzetako zelulen hazkuntzari buruzko guztia erakusteaz gain, taldean lan egiten eta diziplina anitzeko lana sustatzen irakatsi didatelako. Tesi hau egiteko funtsezko zutabea izan zarete, bereziki Gaskon Ibarretxe, Fernando Unda, Igor Irastorza. Maisu handi bihurtu zarete eta zuek gabe tesi hau ez zen gauza bera izango. Aipamen berezia egin nahi nioke José Ramón Pinedari; izan ere, inolako lotura akademikorik gabe, beste ikasle bat bezala tratatu nau, eta zientzialari hobea izaten eta egunetik egunera nire burua gainditzen irakatsi dit, beti gure lanaren osagai pertsonala kontuan hartuz. Bestalde, Jon Luzuriagak, Beatriz Pardok eta Irene Manerok ere aipamen bat merezi dute, egindako ahalegin guztiengatik, beti hor egoteagatik eta ziur nagoelako miresteko moduko zientzialari handi bihurtuko direla. Era berean, beste aipamen bat merezi dute irribarre batekin egunerokotasuna atseginago egin duten pertsona guztiek; eskerrik asko Jokin, Helena, Sandra, Xandra, Noelia, Alba, Irene, Maitane, Miguel, Patricia, Laura, Lucia, Ander, Jone, Maria, Cris, Maddalen, Nerea, Andrea, Iker, Joana.

Eskerrak eman behar dizkiot Polimerbiori tesi hau egiteko aukeragatik, bereziki Jorge Fernandezi, urte hauetan eredu izan baita, eskerrik asko hor egoteagatik, laguntzeagatik eta doktorego-tesi hau enpresan egiteko aukera eman didazulako. Taldeko gainerako kideei ere eskerrik asko proiektu honetan laguntzeagatik: Pablo, Laura, Antonio, Beñat, David, Juan Carlos, Maria.

Era berean, eskerrak eman nahi dizkiet nagoen tokira helarazi nauten pertsona guztiei. Amarnako Machteld, Irene, Sybrand edo Walter bezalakoen eta Mymeticseko jendearen babesik gabe, ez nuen inoiz Espainiara itzultzeko erabakia hartuko. Eskerrik asko zientzialari eta pertsona gisa eredu izateagatik. Eskerrak eman nahi nizkioke bereziki Aleksandra Korzystkari doktoretza egiteko ideia buruan sartzeagatik eta beti bermatzeagatik, nahiz eta urrun egon. Eta nola ez sagu horiei guztiei, beren bizia eman baitute nik gaur tesi hau aurkez dezadan.

Azkenik, nire familiari eskerrak eman nahi dizkiot, baldintzarik gabeko laguntzagatik eta horrek ekarri duen ahaleginagatik. Eskerrik asko nire aititeei, eskerrik asko Amama Toñi nirekin dokumental horiek guztiak ikusteagatik, animaliak eta Biologia maitatzen erakusteagatik eta beti pertsona hobea izatera bultzatzeagatik. Eskerrik asko, aitite, bizitza gozatu egin behar dela irakatsi didazulako, eta ametsak, berriz, jazarri; aholku horiek gabe, segur aski, gaur ez nintzateke hemen egongo. Eskerrik asko baita ere nire amona Pilarri, beti gogorarazten didazulako zein harro zauden irribarre batekin. Eskerrik asko nire gurasoei ikasteko eta prestatzeko aukera emateagatik. Eskerrik asko Ama, benetan zoriontsu egiten ninduena egitera bultzatzeagatik beti, nahiz eta une horretan urruntzea ekartzen zuen. Eskerrik asko aita, beti epe luzera pentsatzen erakusteagatik, tesi honetan zuen zati txiki bat dago. Eskerrik asko Aitor honek suposatu duen guztia jasateagatik eta beti nitaz harro egoteagatik. Eta eskerrik asko Boss zure zure baldintzarik gabeko maitasunagatik.

Eskerrik asko nire lagunei urte hauetan jasan izanagatik eta beti laguntzeagatik. Eskerrik asko Eukene karrera urte horiengatik, hainbeste urteren ondoren niri eusten jarraitzeagatik eta distantziak urruntzen ez uzteagatik. Tesi honek zure zatitxo bat darama, baldintzarik gabeko babes guztiagatik. Eskerrik asko Castroko Kuadrillari etapa honetan ni jasateagatik, zuekiko tartetxoak beti izan dira eta izango dira udako onenak. Eskerrik asko betikoei, Leti, Sarai eta Leire une horiengatik guztiengatik, aholku horiengatik guztiengatik eta endorfinaz bete nauten ordu horiengatik, bidaiengatik, kontzertuengatik, afariengatik, paseoengatik, azkenik bizitza nirekin partekatzeagatik. Eskerrik asko Yera, ez bakarrik nire laguna izateagatik eta egunero erakutsi didazulako duela 15 urte baino gehiagotik, baizik eta harro sentiarazten nauzulako. Marta González, Henar eta Marta Sanz irakasleei ere eskerrik gu batzeagatik. Eskerrik asko ingeles klase horiengatik eta geroko garagardo guztiengatik. Eskerrik asko Marta González nire bizitzaren parte izaten jarraitzeagatik, hazten ikusi nauzulako eta urte hauetan emandako aholku guztiengatik, beti eredu izan eta izango zara.

Abstract

Neurological disorders are the major cause of long-term impairment and the second largest cause of death worldwide. Among them, central nervous system (CNS) disorders are the major socio-economical concerns due to their impact on the quality of life of patients and their relatives. Hence, there is an urgent need for new treatments that allow the functional recovery of the damaged tissue or, at least, improve the quality of life and minimize the risks associated with CNS injuries.

In this regard, among the experimental treatments, bioresorbable polyester materials are showing great results in preclinical and clinical trials due to their biocompatibility, tunable degradability, versatility and physicochemical and mechanical properties. Nevertheless, their hydrophobic nature sometimes delays cell attachment and subsequent regeneration of the injured tissue. To overcome this problem, most researchers coat the surface of their materials with extracellular matrix (ECM)-like compounds. However, one of the most abundant ECM compounds in neural tissue (i.e., laminin) has a low prognosis in reaching the clinic, due to the cytotoxicity of some of its byproducts. Thus, alternative strategies are needed to enhance biocompatibility and cell adhesion of polymeric materials while avoiding the use of potentially toxic compounds that could clearly hinder the translation of the devices to the clinical practice.

In this PhD thesis, we present the development of bioresorbable elastomeric scaffolds based on L-lactide and ε-caprolactone (PLCL) with an ordered nanotopography and surface-functionalized with graphene oxide (GO) to boost the attachment, aligned growth, migration and differentiation of murine and human stem cells, avoiding the use of ECM-like compounds coatings. We first explored the biocompatibility, attachment and guided migration of murine neural stem cells (NSCs) *in vitro*, to study the possibility of creating migration paths that will potentially favor a guided restoration of the damaged neural tissue *in vivo*. Besides, we also investigated the independent effect of the nanotopography and the presence of GO on the differentiation capabilities towards both neuronal and glial-like lineages. Our strategy then, focuses on achieving a balanced neuronal and glial support for a long-term survival of the cultures and an enhanced neural regeneration (Chapter 3).

For a future use in clinic, NSCs-based approaches have the limitation of achieving autologous cell sources. Additionally, the possibility of creating a tumor due to their pluripotent features also represent an important risk for their bench-to-bedside translation. Hence, we also explored more reliable cell sources for a future therapeutic use in clinic. In this regard, mesenchymal stem cells (MSCs) are achieving great results in preclinical and clinical trials on the restoration of injured CNS. MSCs possess intrinsic immunomodulatory features which enhance their restoration capabilities by minimizing inflammatory responses. Here, we propose a new MSC source for the restoration of future CNS injuries: the human dental pulp stem cells (hDPSCs). They can be easily and

autologously obtained. Thanks to their neural crest origin, they own the differentiation potential towards the neural tissue. With the aim of achieving a combinatorial approach of bioresorbable polymeric nanostructured scaffolds grafted with human stem cells for the restoration of injured CNS, we studied the biocompatibility, motility and neurodifferentiation pattern of the hDPSCs over our nanostructured scaffolds towards neuronal, astroglial and myelinating-like cells (Chapter 4).

In spite of being necessary for proof of concept and addressing questions so important as biocompatibility or cell motion, *in vitro* tests lack the actual integration and restoration of the injured neural tissue. Thus, we also tested the restoration capabilities of our nanostructured scaffolds in injured rodent CNS. For that, we first impaired the rostral migratory stream (RMS) that connects the subventricular zone with the olfactory bulb and studied the guided reconnection capabilities of our nanostructured scaffolds either functionalized or not with GO. Again, with the aim of addressing the enhanced restoration capabilities of the personalized advanced medical products combining polymeric materials and human stem cells, we also compared the regeneration of the RMS when grafting hDPSCs alone or in combination with our nanostructured scaffolds (Chapter 4).

Finally, with the aim of producing scaffolds that better resemble the neural niche *in vitro*, we fabricated graphene derivatives-based three-dimensional (3D) scaffolds (Chapter 5). Graphene derivatives-based materials are widely used for neural tissue engineering due to their mechanical and conductive properties, but still further investigation is needed to elucidate their effect on cell behavior, especially in cell survival and differentiation. By just varying the content of the reducing agent (i.e., ascorbic acid (AsA)), we fabricated graphene derivatives-based materials with different geometrical, mechanical and conductive properties to study their effect on NSCs proliferation and differentiation towards neuronal, glial and myelinating precursor cells. We also incorporated cerium oxide (CeO_2) nanoparticles to provide enhanced antioxidant and neuroprotective features to our 3D scaffolds and studied their effect on the establishment of balanced neuronal and glial co-cultures.

Overall, here we explored the fabrication of polymeric and graphene-based materials for the modulation of stem cell behavior and their commitment towards neural tissue both *in vitro* and *in vivo*. Moreover, we also investigated the effect of the geometry, mechanical, electrical conductivity and antioxidant properties on stem cell proliferation and differentiation. This thesis gives new insights into the design of polymeric materials based on graphene derivatives for future personalized advanced medical products in combination with human stem cells in the restoration of CNS injuries.

Resumen

Los trastornos neurológicos son la principal causa de discapacidad a largo plazo y la segunda causa de muerte en todo el mundo. Entre ellos, las alteraciones del sistema nervioso central (SNC) causan el mayor impacto socioeconómico por su efecto en la calidad de vida de los pacientes y sus familiares. Por ello, es urgente encontrar nuevos tratamientos que permitan la recuperación funcional del tejido dañado o, al menos, mejorar la calidad de vida y minimizar los riesgos asociados a las lesiones del SNC.

En este sentido, en ensayos preclínicos y clínicos, los materiales basados en poliésteres biorreabsorbibles están mostrando grandes resultados gracias a su biocompatibilidad, ajustable degradabilidad, versatilidad y propiedades fisicoquímicas y mecánicas. Sin embargo, su naturaleza hidrofóbica a veces retrasa la fijación de las células y la posterior regeneración del tejido lesionado. Como alternativa, la mayoría de los investigadores recubren la superficie de sus materiales con compuestos similares a la matriz extracelular (MEC). Pero algunos de estos compuestos presentes en el SNC, como la laminina, tienen un bajo pronóstico de llegar a mercado, debido a la citotoxicidad de sus subproductos. Estos inconvenientes, se traducen en la necesidad de nuevas estrategias para mejorar la biocompatibilidad y la adhesión celular de los materiales poliméricos evitando el uso de compuestos potencialmente tóxicos, que podrían dificultar claramente la traslación de estos dispositivos a la práctica clínica.

En esta tesis doctoral, presentamos el desarrollo de matrices de anclaje biorreabsorbibles basadas en un copolímeros elastomérico de la L-lactida y ε-caprolactona (PLCL), con una nanotopografía alineada y una funcionalización superficial con óxido de grafeno (GO) para potenciar la adhesión, el crecimiento alineado, la migración y la diferenciación de células madre murinas y humanas, evitando el uso de recubrimientos con compuestos de la MEC. En primer lugar, se exploró la biocompatibilidad, la adhesión y la migración guiada de las células madre neurales (NSC) murinas *in vitro*, para estudiar la posibilidad de crear vías de migración que puedan favorecer la restauración guiada del tejido neural dañado *in vivo*. Además, también se investigó el efecto independiente de la nanotopografía y la presencia de GO en las capacidades de diferenciación hacia linajes neuronales y gliales. Nuestra estrategia se centró en conseguir un soporte neuronal y glial equilibrado para una supervivencia a largo plazo de los cultivos y una regeneración neuronal mejorada (capítulo 3).

Para un futuro uso en la clínica, los enfoques basados en células madre, como las NSCs tienen la limitación de poder conseguir fuentes celulares autólogas. Además, la posibilidad de crear un tumor debido a sus características pluripotentes también representa un riesgo importante para su traslación. Por lo tanto, en esta tesis, se han explorado fuentes celulares más fiables para un futuro uso terapéutico en la clínica. En este sentido, las células madre mesenquimales (MSC) están logrando grandes resultados en ensayos preclínicos y clínicos sobre la restauración del SNC lesionado. Las MSCs poseen

características inmunomoduladoras intrínsecas que mejoran su capacidad de restauración al minimizar las respuestas inflamatorias. Aquí, proponemos una nueva fuente de MSCs para la restauración de futuras lesiones del SNC: las células madre de la pulpa dental humana (hDPSCs). Pueden obtenerse fácilmente y de forma autóloga y gracias a su origen en la cresta neural, poseen el potencial de diferenciación hacia tejido neural. Con el objetivo de lograr un enfoque combinatorio que aúne matrices de anclaje poliméricas biorreabsorbibles y nanoestructuradas con células madre humanas para la restauración del SNC lesionado, se estudió la biocompatibilidad, la motilidad y el patrón de neurodiferenciación de las hDPSCs sobre las matrices de anclajes nanoestructuradas hacia células neuronales, astrogliales y mielinizantes (capítulo 4).

A pesar de ser necesarios para pruebas de concepto y abordar cuestiones tan importantes como la biocompatibilidad o el movimiento celular, los ensayos *in vitro* carecen de la integración y restauración real del tejido neural lesionado. Por ello, también se probó la capacidad de restauración de las matrices de anclaje nanoestructuradas en el SNC lesionado en roedores. Primero se dañó la vía rostral migratoria (VRM) que conecta la zona subventricular con el bulbo olfatorio y se estudiaron las capacidades de reconexión guiada de las matrices de anclaje nanoestructuradas y funcionalizadas o no con GO. De nuevo, con el objetivo de abordar las capacidades regenerativas de posibles productos de terapia avanzada personalizada, basados en materiales poliméricos y células madre humanas, también se comparó la regeneración de la VRM tras la inserción de hDPSCs solas o en combinación con nuestras matrices de anclaje nanoestructuradas (Capítulo 4).

Por último, con el objetivo de producir matrices de anclaje que se asemejen mejor al nicho neural *in vitro*, se fabricaron matrices de anclaje tridimensionales (3D) basadas en derivados del grafeno (Capítulo 5). Los materiales basados en derivados del grafeno se utilizan ampliamente para la ingeniería de tejidos neuronales, debido a sus propiedades mecánicas y conductoras, pero aún es necesario investigar más para dilucidar su efecto en el comportamiento celular, especialmente en la supervivencia y diferenciación de las células. Con sólo variar el contenido del agente reductor (es decir, el ácido ascórbico (AsA)), se fabricaron matrices basadas en derivados del grafeno con diferentes propiedades geométricas, mecánicas y conductoras para, así, estudiar su efecto sobre la proliferación y diferenciación de las NSCs hacia células precursoras neuronales, gliales y mielinizantes. También se incorporaron nanopartículas de óxido de cerio (CeO_2) para dotar a las matrices de anclaje en 3D de características antioxidantes y neuroprotectoras y se estudió su efecto en el establecimiento de cocultivos equilibrados de células neuronales y gliales.

En general, se han explorado la fabricación de materiales poliméricos y basados en grafeno para la modulación del comportamiento de las células madre y su compromiso con el tejido neural tanto *in vitro* como *in vivo*. Además, se ha investigado el efecto de la geometría, las propiedades mecánicas, la conductividad eléctrica y las capacidades antioxidantes sobre la proliferación y diferenciación de las células madre. Esta tesis aporta

nuevos conocimientos sobre el diseño de materiales poliméricos y basados en derivados del grafeno para la creación de futuros productos personalizados de terapia avanzada en combinación con células madre humanas en la restauración de lesiones del SNC.

Laburpena

Asaldura neurologikoak epe luzeko desgaitasunaren kausa nagusia eta heriotzaren bigarren kausa dira mundu osoan. Horien artean, nerbio-sistema zentralaren (NSZ) alterazioek inpaktu sozioekonomiko handiena eragiten dute, pazienteen eta haien senideen bizi-kalitatean duten eraginagatik. Beraz, premiazkoa da tratamendu berriak aurkitzea, kaltetutako ehuna funtzionalki berreskuratzeko edo, gutxienez, bizi-kalitatea hobetzeko eta NSZen lesioekin lotutako arriskuak minimizatzeko.

Ildo horretan, saiakuntza aurreklinikoetan eta klinikoetan, poliester bioxurgagarrietan oinarritutako materialek emaitza handiak izan dituzte, biobateragarritasunari, degradagarritasunari, aldagarritasunari eta propietate fisiko-kimiko eta mekanikoei esker. Hala ere, bere izaera hidrofobikoak atzeratu dezake zelulen finkapena eta, berez, ehun lesionatuaren birsorkuntza. Alternatiba gisa, ikertzaile gehienek beren materialen azalera zelulaz kanpoko matrizearen (ZKM) antzeko konposatuekin estaltzen dute. Baina ZKMan dauden konposatu horietako batzuek, hala nola, lamininak, merkatura iristeko pronostiko txikia dute, sortu dezaketen azpiprodukTuen zitotoxikotasuna dela eta. Eragozpen horien ondorioz, material polimerikoen biobateragarritasuna eta atxikipen zelularra hobetzeko estrategia berriak behar dira, toxikoak izan daitezkeen konposatuak erabiltzea saihestuz, eta praktika klinikorako bidea erraztuz.

Doktorego-tesi honetan, polimero elastomerikoetan oinarritutako L-laktida eta ε-caprolaktonazko ainguraketa matrize bioxurgagarrien garapena aurkezten dugu. Lerrokatutako nanotopografia eta gainazaleko funtzionalizazioak grafeno oxidoarekin (GO), sagu eta gizaki zelulen atxikipena, lerrokatutako hazkundea, migrazioa eta bereizketa sustatuko dute, ZKMen antzerako konposatuen erabilera saihestuz. Lehenik eta behin, *in vitro* sagu zelula ama neuralen (NSC) biobateragarritasuna, atxikipena eta migrazio gidatua aztertu ziren, *in vivo* kaltetutako ehun neuralaren berreskurapen gidatua erraztu dezaketen migrazio-bideak sortzeko aukera aztertzeko. Gainera, nanotopografiaren eta GOren eragin independentea aztertu ziren, NSCen leinu neuronal eta glialetarantz bereizteko gaitasunetan. Gure estrategiaren ardatza euskarri neuronal eta glial orekatu bat lortzea izan zen, epe luzeko biziraupenerako kultiboetan eta hobetutako berreskurapen neural baterako (3. kapitulua).

Etorkizunean klinikan erabiltzeko, zelula ametan oinarritutako ikuspegiek, hala nola NSCek, mugatuta dute iturri zelular autologoak lortzea. Gainera, tumore bat sortzeko aukera dute, haren ezaugarri pluripotenteak direla eta. Beraz, tesi honetan, zelula-iturri fidagarriagoak aztertu dira etorkizunean klinikan erabilera terapeutikoa izateko. Zentzu horretan, zelula ama mesenkimalak (MSC) emaitza handiak lortzen ari dira lesionatutako NSZren berreskurapen saiakuntza aurrekliniko eta klinikoetan. MSCek berezko ezaugarri inmunomodulatzaileak dituzte, eta horrek birsortze gaitasuna hobetzen du, hanturazko erantzunak minimizatuz. Hemen, MSCen iturri berri bat proposatzen dugu NSZren etorkizuneko lesioak birsortzeko: giza hortz-mamiaren zelula amak (hDPSCs). Erraz eta

modu autologoan lor daitezke, eta gailur neuralean duten jatorriari esker, ehun neuralerantz bereizteko ahalmena dute. Lesionatutako NSZ berrezartzeko, ainguratze matrize polimeriko bioxurgagarriak eta nanoegituratuak, giza zelula amekin batuko dituen ikuspegi pertsonalizatu konbinatorio bat lortzeko helburuarekin, hDPSCen biobateragarritasuna, mugikortasuna eta neurodesberdintze-eredua aztertu ziren leinu neuronal, astroglial eta mielinizatzaileekiko, nanoegituratutako ainguraketa matrizeen gainean (4. kapitulua).

Kontzeptu-probetarako eta biobateragarritasuna edo mugimendu zelularra bezalako gai garrantzitsuei erantzuteko beharrezkoak izan arren, *in vitro* saiakuntzek ez dute lesionatutako ehun neuralaren benetako integrazio eta birsortze errealik. Horregatik, lesionatutako sagu NSZan nanoegituratutako ainguraketa-matrizeen birsortze gaitasuna ere probatu zen. Lehenik, eremu azpibentrikularra usain-erraboarekin lotzen duen aurpegiko migrazio-korrontea (AMK) kaltetu zen, eta funtzionalizatutako edo ez ainguraketa-matrize nanoegituratuen birkonexio gidaturako gaitasunak aztertu ziren. Berriro ere, material polimerikoetan eta giza zelula ametan oinarritutako terapia aurreratu pertsonalizatuen birsorkuntza-ahalmenei heltzeko helburuarekin, hDPSCak bakarrik edo gure ainguratze-matrize nanoegituratuekin batera txertatu ziren eta AKMren birsorkuntza ahalmena aztertu zen (4. kapitulua).

Azkenik, *in vitro* nitxo neurala hobeto antzeratzen duten ainguraketa-matrizeak ekoizteko, grafenoaren deribatuetan oinarritutako hiru dimentsioko (3D) ainguraketa-matrizeak sortu ziren (5. kapitulua). Grafenoaren deribatuetan oinarritutako materialak anitz erabiltzen dira ehun neuronalen ingeniaritzarako, haien propietate mekanikoak eta eroaleak direla eta, baina oraindik portaera zelularrean duten eragina, batez ere zelulen biziraupenean eta bereizketan, argitu behar dira. Agente erreduktorearen edukia aldatze hutsarekin (hau da, azido askorbikoa (AsA)), grafenoaren deribatuetan oinarritutako matrizeak fabrikatu ziren propietate geometriko, mekaniko eta eroale desberdinekin, horrela NSCak zelula aitzindari neuronal, glial eta mielinizatzaileekiko hazkuntza eta bereizketan duten eragina aztertzeko. Era berean, zerio oxidoaren (CeO_2) nanopartikulak gehitu ziren, 3D ainguraketa matrizeei ezaugarri antioxidatzaile eta neurobabesleak emateko, eta horien eragina aztertu zen zelula neuronal eta glialen kultibo orekatuak ezartzeko.

Publications related to this thesis

- Y. Polo, J. Luzuriaga, J. Iturri, I. Irastorza, J.L. Toca-Herrera, G. Ibarretxe, F. Unda, J.-R. Sarasua, J.R. Pineda, A. Larrañaga, *Nanostructured scaffolds based on bioresorbable polymers and graphene oxide induce the aligned migration and accelerate the neuronal differentiation of neural stem cells*, Nanomedicine Nanotechnol. Biol. Med. 31 (2021) 102314. https://doi.org/10.1016/j.nano.2020.102314.
- Y. Polo, J. Luzuriaga, S. Gonzalez de Langarica, B. Pardo-Rodríguez, D.E. Martínez-Tong, C. Tapeinos, E. Marin, J. Muñoz-Ugartemendia, G. Ciofani, G. Ibarretxe, F. Unda, J.-R. Sarasua, J.R. Pineda, A. Larrañaga, *Self-assembled three-dimensional hydrogels based on graphene derivatives and cerium oxide nanoparticles: scaffolds for co-culture of oligodendrocytes and neurons derived from neural stem cells*. (Under review in Nanoscale).

Other publications

- J. Luzuriaga, Y. Polo, O. Pastor-Alonso, B. Pardo-Rodríguez, A. Larrañaga, F. Unda, J.-R. Sarasua, J.R. Pineda, G. Ibarretxe, *Advances and Perspectives in Dental Pulp Stem Cell Based Neuroregeneration Therapies*, Int. J. Mol. Sci. 22 (2021) 3546. https://doi.org/10.3390/ijms22073546.
- J.R. Pineda, Y. Polo, B. Pardo-Rodríguez, J. Luzuriaga, V. Uribe-Etxebarria, P. García-Gallastegui, J.-R. Sarasua, A. Larrañaga, G. Ibarretxe, *In vitro preparation of human Dental Pulp Stem Cell grafts with biodegradable polymer scaffolds for nerve tissue engineering*, Methods Cell Biol. 170 (2022) 147–167. https://doi.org/10.1016/bs.mcb.2022.02.012.

Participation in congresses

- Y. Polo, J. Luzuriaga, J. Iturri, I. Irastorza, J.M. Encinas, J.R. Pineda, G. Ibarretxe, F. Unda, A. Larrañaga, J.-R. Sarasua, *Nanostructured scaffolds based on bioresorbable polymers and graphene oxide to promote neurodifferentiation of dental pulp-derived stem cells*. TERMIS European Chapter Meeting 2019. Oral Presentation. Rodhes, Greece, May 2019.
- J.R. Pineda, Y. Polo, J. Luzuriaga, J. Iturri, I. Irastorza, J.L. Toca-Herrera, G. Ibarretxe, F. Unda, J.-R. Sarasua, A. Larrañaga, *Nanopatterned scaffolds based on bioresorbable polymers and graphene derivatives induce aligned migration and accelerates the neuronal differentiation of neural stem cells*. FENS 2020. Poster. Glasgow, United Kingdom, July 2020.
- Y. Polo, J. Luzuriaga, J. Iturri, I. Irastorza, J.L. Toca-Herrera, G. Ibarretxe, F. Unda, J.-R. Sarasua, J.R. Pineda, A. Larrañaga, *Nanostructured scaffolds based on bioresorbable polymers and graphene oxide to promote neurodifferentiation of stem cells*. WBC 2020 virtual_11TH WORLD BIOMATERIALS CONGRESS. Oral Presentation. Glasgow, United Kingdom, December 2020.
- J.R. Pineda, Y. Polo, J. Luzuriaga, J. Iturri, I. Irastorza, J.L. Toca-Herrera, G. Ibarretxe, F. Unda, J.-R. Sarasua, A. Larrañaga, *Nanopatterned scaffolds based on bioresorbable polymers and graphene oxide induce the aligned migration and*

accelerates the neuronal differentiation of neural stem cells. Cell Bio virtual 2020. Poster. Rockville, United States. December 2020.

- Y. Polo, J. Luzuriaga, S. Gonzalez de Langarica, B. Pardo-Rodríguez, E. Marin, D.E. Martínez-Tong, G. Ibarretxe, F. Unda, J.-R. Sarasua, J.R. Pineda, A. Larrañaga. Self-assembled hybrid hydrogels based on graphene derivatives and cerium oxide nanoparticles as three-dimensional substrates for neural stem cells. ESB 2021 31st Conference. Oral Presentation. Porto, Portugal, September 2021.
- Y. Polo, J. Luzuriaga, S. Gonzalez de Langarica, B. Pardo Rodriguez, E. Marin, D.E. Martínez-Tong; G. Ibarretxe; F. Unda; J.-R. Sarasua, A. Larrañaga, J.R. Pineda, *Self-assembled hybrid hydrogels based on graphene derivates and cerium oxide nanoparticles as three-dimensional substrates for neural stem cells*. SENC 2021 19th meeting. Poster. Lleida, Spain; November 2021.
- J. Luzuriaga, J. Salvador, A. Martin, B. Pardo-Rodriguez, I. Manero-Roig, I. Irastorza, Y.Polo, F. Unda, I. Badiola, G. Ibarretxe, J.R. Pineda, A. Valdivia, *Human dental pulp stem cells express the angiotensin-renin system and its stimulation increases cell proliferation, while retaining their neurodifferentiation potential*. Neurogune 2022. Poster. Pamplona, Spain, July 2022.
- I. Manero-Roig, Y. Polo, B. Pardo-Rodriguez, I. Romayor, J. Luzuriaga, L. Rubio-Emazabel, C. Eguizábal, G. Ibarretxe, F. Unda, J.-R. Sarasua, A. Larrañaga, J.R. Pineda, *Use of bioresorbable nanopatterned polymer scaffolds as a strategy to guide the migration of neural and dental stem and progenitor cells*. Neurogune 2022. Poster. Pamplona, Spain, July 2022.
- B. Pardo-Rodriguez, I. Manero-Roig, J. Luzuriaga, Y. Polo, F. Unda, G. Ibarretxe, J.R. Pineda, *Optimization of neurodifferentiation protocols of human dental pulp stem cells in serum free media*. Neurogune 2022. Poster. Pamplona, Spain, July 2022.
- Y. Polo, J. Luzuriaga, S. Gonzalez de Langarica, B. Pardo-Rodríguez, E. Marin, D.E. Martínez-Tong, I. Manero-Roig, , G. Ibarretxe, F. Unda, J.-R. Sarasua, J.R. Pineda, A. Larrañaga, *Graphene derivatives and cerium oxide nanoparticles based hydrogels as three-dimensional substrates for neural stem cell differentiation towards astroglial, neuronal and oligodendroglial lineages*. Neurogune 2022. Poster. Pamplona, Spain, July 2022.
- B. Pardo-Rodriguez, I. Manero-Roig, J. Luzuriaga, Y. Polo, I. Romayor, F. Unda, G. Ibarretxe, J.R. Pineda, *Influence of serum presence on the neurodifferentiation process of human dental pulp stem cells*. Sehit 2022. Poster. Granada, Spain, September 2022.
- I. Manero-Roig, Y. Polo, B. Pardo-Rodriguez, I. Romayor, J. Luzuriaga, L. Rubio-Emazabel, C. Eguizábal, G. Ibarretxe, F. Unda, J.-R. Sarasua, A. Larrañaga, J.R. Pineda, *Study of the capacity of alignment and migration of neural and dental stem and progenitor cells cultured on nanopatterned polydopamine bioresorbable polymer scaffolds for cell therapy*. Sehit 2022. Poster. Granada, Spain, September 2022.
- I. Romayor, I. Manero-Roig, Y. Polo, J. Luzuriaga, R. Basanta, O. Pastor-Alonso, J.M. Encinas, C. Eguizabal, F. Unda, G. Ibarretxe, J.R. Pineda, *HB-EGF participates in ERBB signaling pathway including chemotaxis migration and invasive properties of neural stem cells*. Sehit 2022. Oral presentation. Granada, Spain, September 2022.

Table of content

Chapter 1

Hypothesis and Aims

Hypothesis and Aims

Hypothesis

The use of bioresorbable polymers and graphene derivative-based scaffolds can promote the alignment, guided migration, integration and differentiation of stem cells without the need of extracellular matrix-like compounds. Besides, their interplay in cell behavior and differentiation may support the establishment of a neurogenic lineage that combines stem cell sustenance together with immature and mature neuronal, astroglial and myelinating cell support capable of restoring the functionality of the central nervous system, both *in vitro* and *in vivo*.

Aims

The main aim of this thesis is the formulation of scaffolds based on bioresorbable polymers and graphene derivatives that, without the use of extracellular matrix-like compounds, promote the adhesion, guided migration and differentiation of stem cells into neural tissue. To achieve this main aim, three secondary objectives were established:

1. To develop nanostructured scaffolds based on the combination of graphene derivatives and bioresorbable polymers for guided mouse neural stem cell (NSCs) attachment and neurodifferentiation *in vitro*.
2. To develop nanostructured scaffolds based on the combination of graphene derivatives and bioresorbable polymers for guided human dental pulp stem cell (hDPSCs) attachment and neurodifferentiation both *in vitro* and *in vivo*.
3. To fabricate self-assembled three-dimensional scaffolds based on graphene derivatives and cerium oxide (CeO_2) nanoparticles for neural stem cell (NSCs) attachment and neurodifferentiation.

Each of these secondary objectives has been divided in three matching experimental chapters with the corresponding sub-objectives:

1. **Nanostructured scaffolds based on bioresorbable polymers and graphene oxide induce the aligned migration and accelerate the neuronal differentiation of neural stem cells.**
   - 1.1. Fabrication and characterization of nanostructured polymeric scaffolds functionalized with graphene oxide.
     - 1.1.1. Fabrication of a biodegradable nanostructured film based on a L-lactide and ε-caprolactone (PLCL) copolymer.
     - 1.1.2. Functionalization of the surface with graphene oxide.
     - 1.1.3. Morphological and physicochemical analysis.

1.2. Evaluation of the *in vitro* compatibility and neurodifferentiation pattern of the NSCs seeded on the nanostructured polymeric scaffolds.
   1.2.1. Analysis of the attachment, alignment and elongation of NSCs.
   1.2.2. Study of the migration pattern over the nanostructured polymeric scaffolds.
   1.2.3. Analysis of the astroglial-like and neuronal-like lineage commitment.

2. Nanostructured scaffolds based on bioresorbable polymers and graphene oxide facilitate the adhesion, alignment, neural commitment and migration of human dental pulp stem cells and allow the intracerebral implantation to promote the restoration of the injured rostral migratory stream on a rodent brain model.

2.1. Fabrication and characterization of nanostructured polymeric scaffolds functionalized with graphene oxide.
   2.1.1. Synthesis of a biodegradable copolymer based on L-lactide and ε-caprolactone (PLCL).
   2.1.2. Fabrication of a biodegradable nanostructured film based on the synthesized copolymer.
   2.1.3. Functionalization of the surface with graphene oxide.
   2.1.4. Analysis of the impact of the functionalization in mechanical properties and hydrolytic degradation profile.

2.2. Evaluation of the *in vitro* compatibility and neurodifferentiation pattern of hDPSCs seeded on the nanostructured polymeric scaffolds.
   2.2.1. Analysis of the migration pattern over the nanostructured polymeric scaffolds.
   2.2.2. Assessment of the stemness profile of the hDPSCs.
   2.2.3. Analysis of the astroglial-like, neuronal-like and myelinating-like lineage commitment.

2.3. Evaluation of the functionality of the nanostructured polymeric scaffolds in a partially bulbectomized murine animal model, by implantation in the cerebral cortex.
   2.3.1. Analysis of the biocompatibility of the scaffolds.
   2.3.2. Study of the capabilities of the scaffold to modulate survival and migration of cells.

3. Self-assembled three-dimensional hydrogels based on graphene derivatives and cerium oxide nanoparticles: scaffolds for co-culture of oligodendrocytes and neurons derived from neural stem cells.

3.1. Fabrication and characterization of three-dimensional scaffolds based on graphene derivatives and CeO_2 nanoparticles.

3.1.1. Evaluation of the effect of reducing agent (i.e., ascorbic acid) on the self-assembly of three-dimensional graphene derivatives-based hydrogels and the resulting morphological, mechanical and electrical properties.

3.1.2. Evaluation of the effect of CeO_2 nanoparticles on the self-assembly of three-dimensional graphene derivatives-based hydrogels and the resulting morphological, mechanical, electrical and antioxidant properties.

3.2. Evaluation of the *in vitro* compatibility and neurodifferentiation pattern of NSCs on the self-assembled three-dimensional graphene derivatives-based hydrogels.

3.2.1. Analysis of the biocompatibility of the self-assembled three-dimensional graphene derivatives-based hydrogels.

3.2.2. Assessment the stemness profile of NSCs.

3.2.3. Analysis of the astroglial-like, oligodendrogial-like and neuronal-like lineage commitment.

Chapter 2

General introduction: Studying the potential of bioresorbable polymeric materials to enhance stem cell integration and tissue recovery in central nervous system traumatic clinical approaches

General introduction: Studying the potential of bioresorbable polymeric materials to enhance stem cell integration and tissue recovery in central nervous system traumatic clinical approaches

Abstract

Regeneration of the nervous system is of great interest due to the current socio-economical impact associated to neurological diseases. Although both stem cells and polymeric materials are showing promising results *in vitro* and *in vivo*, most of them fail on achieving clinically relevant outcomes. First, stem cells lack an effective survival and integration on the injured tissue and some of them even can acquire tumorigenic properties in long-term neurological clinical trials. Second, polymeric materials by their own fail on achieving complete functional restoration of the injured neural tissue. Hence, lately, the combinatorial approaches based on stem cells grafted into bioresorbable scaffolds have gained increasing interest. This combinatorial approach could offer a better restoration of the tissue than the scaffolds implanted alone, and they can also enhance the survival and integration of the stem cells while avoiding tumorigenic features *in vivo*. In this general introduction, we summarize the latest results on combinatorial stem cell and scaffold implantation together with the future perspectives.

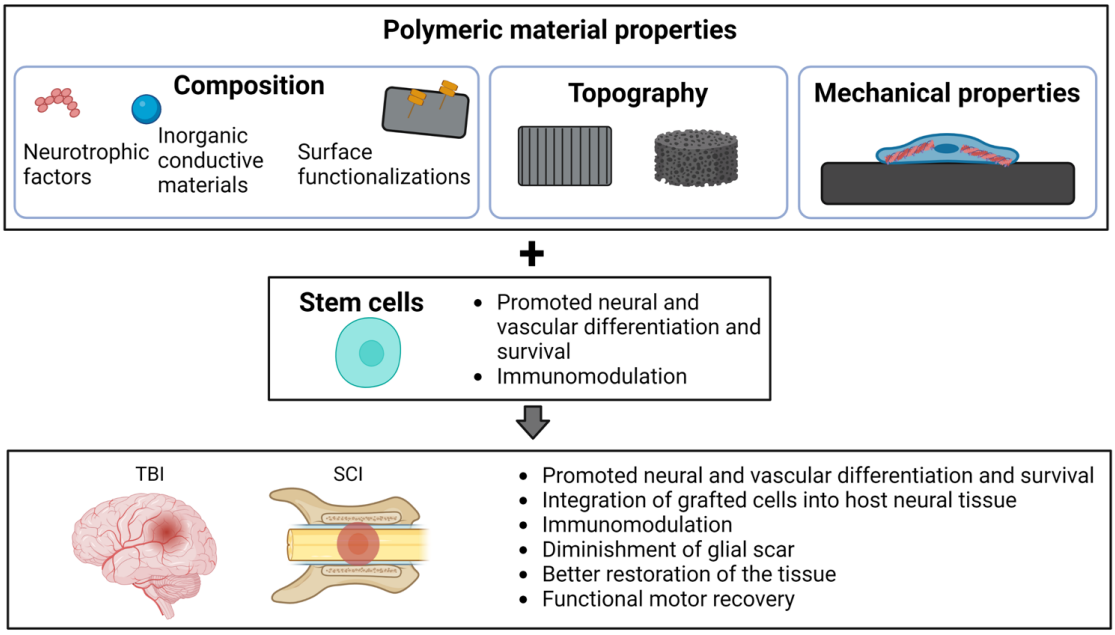

2.1. Introduction

2.1.1. Central nervous system

The nervous system consists of central nervous system (CNS) and the peripheral nervous system (PNS). The PNS is comprised of cranial and spinal nerves, as well as the ganglia that are connected to them, whereas the CNS is comprised of the brain and spinal cord [1]. Two types of cells are present in the CNS: neurons and astroglial cells. While neurons are the primary excitable cell type responsible for transmitting and receiving signals via action potentials and neurotransmitters, astroglial cells are supportive cells that are divided into microglia, astrocytes, ependymal cells, oligodendrocytes and Schwann cells [2].

Astrocytes perform diverse functions, including anchoring capillaries with neuronal somas and dendrites, establishing contact with ependymal cells, controlling the extracellular environment of the CNS, assisting in the development of the blood barrier, and repairing injured tissue by controlling neurogenesis [2]. On the other hand, oligodendrocytes are the main myelinating cells of the CNS. The myelin sheets they create protect the neuronal axons and enable potential actions. But, under appropriate circumstances, oligodendrocyte precursor cells can also become Schwann cells and remyelinate injured axons. Moreover, lately, Schwann cells have been described to migrate over capillaries to guide axonal regrowth in injured CNS [3]. Microglia cells comprise the immune system of the CNS and are involved in immune response, homeostasis maintenance and neural repair [4]. Finally, ependymal cells originated from the radial glial (precursor also of oligodendrocytes, astrocytes and some neurons), are ciliated epithelial cells. They are essential for maintaining the balance of the cerebrospinal fluid (CSF), the removal of waste from the brain, homeostasis and metabolic activities [5].

Surrounding the neural cells there is the extracellular matrix (ECM) and the mostly unknown interstitial system (ISS), a dynamic and intricate area that connects the circulatory system and neural networks, which is essential for the movement of substances and the transmission of signals between neurons [6]. This system takes up 15% to 20% of the entire neural tissue in the brain. It serves as anchoring scaffold and helps on nutrient supply, coordinated reaction to perturbations in the brain's inner and outer surroundings, neural cell communication and information processing and integration [6,7].

2.1.2. Physiopathology after traumatic injury on the central nervous system

As a result of a traumatic injury, all the neural microenvironment (including neural cells, ECM, fluids, vasculature and ISS) is affected and, because of the specialization of the CNS, it is essentially incapable of self-healing. Additionally, the inherent capacity for regeneration is self-limited to the nature of the lesion, being traumatic injuries one of the most difficult to regenerate due to the physiopathology of the injury itself [8]. Traumatic injuries in the CNS occur after a direct mechanical impact and are divided into spinal cord injury (SCI) and traumatic brain injury (TBI). Both SCI and TBI physiopathology are characterized for having a first primary injury caused by the trauma itself in the first hours, followed by a second injury caused by the inflammatory and neurotoxic environment created by the loss of neural cells, activation of the immune system and overproduction of reactive oxygen and nitrogen species (RONS) [9] (Figure 2.1.).

2.1.2.1. Primary injury

Immediately after an impact, the compression forces result in a mechanical disturbance of cellular membranes and cytoskeleton. The compression of the cellular membrane causes a rapid and uncontrolled inflow of sodium (Na^+), efflux of potassium (K^+) and elevations in intra-axonal calcium (Ca^{2+}). Lipid peroxidases, proteases, and phospholipases are activated by Ca^{2+}, which raises the content of lipids and free radicals within cells. As a result of the vast intra-axonal Ca^{2+} entry, some proteolytic mechanisms like calpain protease are activated, causing the degradation of cytoskeletal proteins and irreversible axonal damage [10]. Besides, N-methyl-D-aspartate (NMDA) receptor is also activated promoting the depolarization of the neurons through glutamate imbalance. Hence, there is a prolonged activation of the pumps to compensate the ionic misbalance, which results in fast glucose absorption and the exhaustion of energy reserves [11]. Furthermore, the homeostatic imbalance produces the release of endonucleases, translocases, and caspases to the microenvironment, which causes conformational alterations on biological membranes and deoxyribonucleic acid (DNA). Together, these processes cause the degradation of neural and vascular membranes, which ultimately result in activation of necrotic or programmed (apoptosis) cell death [12].

On the other hand, Ca^{2+} enters the mitochondria, altering oxidative metabolism and creating lactate, which causes acidosis and edema, exacerbating the energetical imbalance [13]. Moreover, as a cause of the Ca^{2+} entry, there is an increased caspase function and the release of RONS, enhancing the acidic and oxidative environment and subsequent neuronal and myelinating cell death [14]. The lipid peroxidation process is also exacerbated by elevated RONS, resulting in a membrane modification and consequent alteration of the signaling pathways [15].

The mechanical impact also causes the destabilization of microtubules, causing a further axonal lost and retraction. Hence, there is a physical axonal lost which causes accumulation of molecules on the sides of the lesion [16]. The vasculature is also affected after the traumatic impact: small blood arteries and capillaries explode releasing the blood into the neural microenvironment. Moreover, there is a disruption of the barriers (either blood-spinal cord barrier (BSCB) or the blood-brain barrier (BBB)) enabling the entry of immune system cells such as neutrophils or macrophages and the consequent secretion of inflammatory molecules such as the cytokines tumor necrosis factor-α [TNF-α] or interleukin-1β [IL-1β] [17]. In addition, this scenario activates microglia, increasing the recruitment of pro-inflammatory cells. The recruitment of immune cells enables phagocytes to remove debris generated during tissue rupture, but they also generate cytotoxic molecules such as oxygen and nitrogen free radicals, causing a further protein and lipid oxidation and DNA damage, leading to increased neural cell death [4]. Finally, astrocytes around the injured site are mechanically activated due to conformational changes in the extracellular focal adhesion kinases (FAK) and the Ca^{2+} entry that activates ERK pathway, which further involves structural modifications in the junctions with blood vessels, and neurons, aggravating the already altered trophic support [18].

2.1.2.2. Secondary injury

The secondary injury is developed over the course of the next few hours to days due to metabolic alterations (e.g., excitotoxicity, mitochondrial dysfunction, lipid peroxidation, etc.), inflammation, edema (i.e., accumulation of fluids), and the release of numerous prooxidative, proapoptotic and proinflammatory intermediates and lasts until the wound is closed and the glial scar reaches maturity [19]. Starting from the center of the injury, there is an inflammatory signaling cascade promoting cell death, including the nearby axons of neurons that survived the initial blow. These inflammatory signals are driven by damage associated molecular patterns (DAMPs) that includes cell debris, adenine triphosphate (ATP), the high mobility group box 1 proteins (HMGB1), S100 calcium-binding protein β (S100β), histones, or IL-1β release, increasing apoptosis and necrosis around [1]. DAMPs act as warning signals, activating the immune response to start the clearance of the debris and other molecules. At the same time, the released DAMPs directly impact the immune reactivity and hence the severity of the secondary injury [20].

In response to DAMPs, nearby microglia are polarized and secrete proinflammatory molecules, which further increase the recruitment of distal microglia towards the injured site [20]. Microglia eliminate cell debris and other molecules from the microenvironment and, together with astrocytes, seal the injured site, promote angiogenesis, tissue healing and regulate harmful immunological responses [4,21,22]. Microglia also became activated due to the proinflammatory molecules undergoing a

morphological change from M2 morphology to the M1 [23]. This morphological change contributes to the release of cytokines and RONS, which have a neurotoxic effect in nearby astrocytes, oligodendrocytes and neurons [24]. Finally, the activation of microglia provokes the phagocytosis of neuronal dendrites and axons, together with the creation of the glial scar [25].

Activated M1 microglia also emit cytokines that affect the activity of astrocytes. In normal conditions, astrocytes modulate the excitotoxic glutamate levels and enhance secretion of neurotrophic factors, preventing neuronal death and enabling axonal growth [26]. But, when activated, microglia release chondroitin sulfate proteoglycan-based inhibitory extracellular matrix, that is accumulated around the injured site. This glial scar is a physical and chemical barrier that prevents the establishment of functional connections and axonal regeneration [27]. Together with the glial scar, the sudden cell death over the injury provokes a lost in the tissue volume. This is filled by fluids, macrophages and thin bands of connective tissue creating cystic microcavitations or cavities [28] and representing another physical barrier for cell migration and axonal and vascular reconnection. Finally, the oligodendrocyte precursor cells that migrate towards the injured site, together with pericytes and fibroblast, are integrated in the glial scar, surrounding the cavities and secreting dense ECM proteins from connective tissue (mainly collagen) that further enhance the physical and chemical barrier for network reconnection [29].

Another main characteristic of the pathophysiology of the secondary injury is the damaged vasculature including hemorrhage, edema, alterations in blood flow, and disruption of the blood barrier. The mechanical disruption of the vasculature provokes an hemorrhage, which creates a structural compression, increasing the pressure and causing vasospasm (i.e., arterial shrinkage produced by a prolonged blood vessel constriction) [30]. Moreover, the bleeding causes the accumulation of ferritin and hemosiderin, which are two neurotoxic proteins that further increase neural cell death and the activation of the immune response [31]. The edema, an excessive increase of water in the extracellular space, can be caused by the ionic imbalance, which increases vascular permeability, but also by the disturbance of the vasculature, which affects the blood barrier [32].

Regarding disruption of the blood barrier, both BBB and BSCB are selective active barriers formed by astrocytes, pericytes and endothelial cells. However, they are disrupted after an injury, allowing the entry of potentially neurotoxic molecules and inflammatory cells to the CNS [33]. It might be taken in consideration that their selective transport for various molecules is different, which may alter the restoration capabilities of the chosen therapy [33]. Anyways, in both cases, endothelial cell damage reduces the production of occludins and claudins, two of the proteins involved in tight junctions, producing a loosening of them [34]. Pericytes start segregating cytokines, nitric oxide,

and metalloproteinases (MMP) and astrocytes start swelling, thus resulting in an increased permeability towards the CNS [34].

Overall, vascular and neuronal death caused by the excitatory and neurotoxic molecules, inflammation, ischemia, and calcium dysregulation ends up on the damaged neural circuits and the remodeling and reorganization of both neural and vascular networks. However, the substantial cell loss and the development of cavities produce a significant barrier that prevents cell migration and axon regrowth. In addition, biochemicals secreted by astrocytes, pericytes, and ependymal cells form a fibrous scar, which results in the collapse of the axonal growth cone and the ultimate failure of regeneration. Due to the intracellular and extracellular CNS components that prevent regeneration, currently there are only palliative alternatives for traumatic CNS disorders [35]. Hence, regeneration of the CNS is a major social, clinical and scientific challenge. In this regard, scientists are working on new therapies for traumatic neural injuries, including TBI and SCI. Among them, stem cell-based therapies and polymeric materials are achieving promising results *in vivo* and in clinical trials, which are described in the following sections.

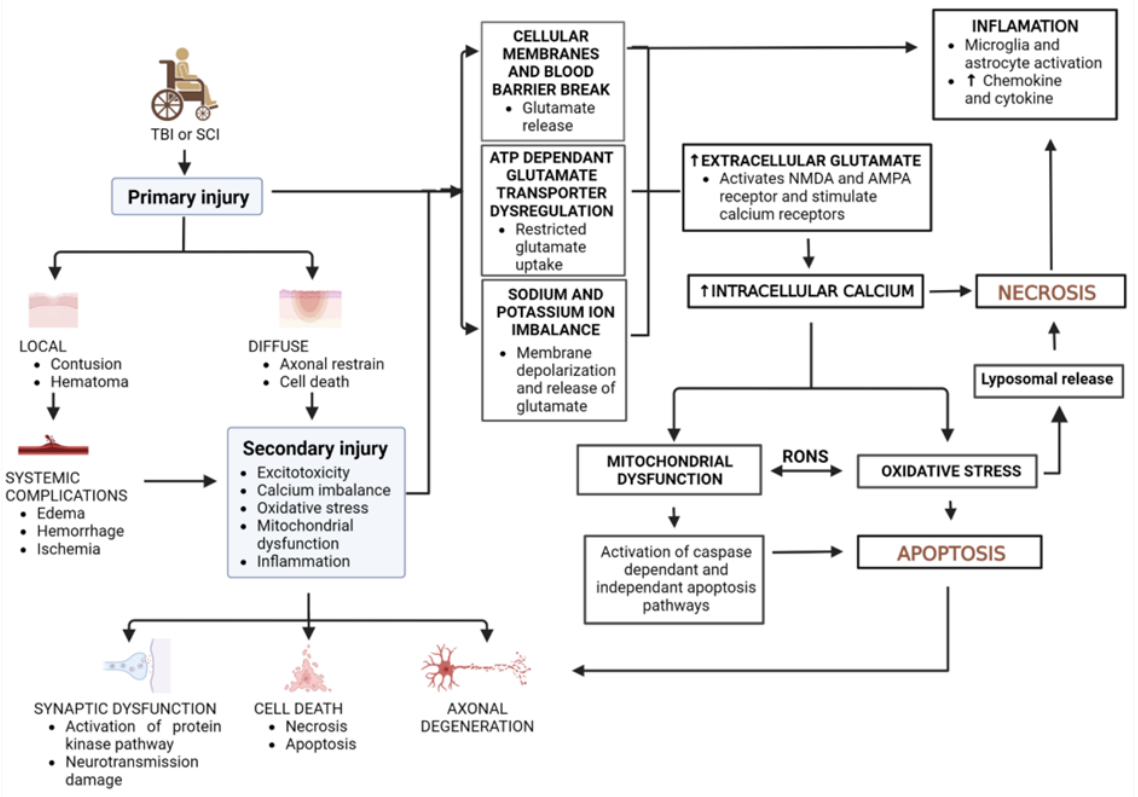

Figure 2.1.: Pathophysiology after traumatic injury in the central nervous system.
After traumatic injury, the architecture of the CNS is dramatically modified as a result of both primary and secondary injuries that activate several mechanisms at the cellular and molecular levels.

2.2. Current stem cell-based approaches in preclinical and clinical trials

Stem cell therapies are achieving promising results *in vitro*, *in vivo* and also in clinical trials. Their immunomodulatory properties, together with their trophic factor secretion and the ability to differentiate towards neuronal and astroglial lineages, make them ideal for modulating the inflammatory response and the generation of a new neural network. Nevertheless, as it will be explained in this section, they still fail in the functional regeneration of the injured CNS due to their poor integration and possible tumorigenic properties associated to their pluripotent features (Figure 2.2.).

2.2.1. Embryonic stem cells (ESCs)

In humans, early-stage embryos that have been rejected from *in vitro* fertilization are used to create embryonic stem cells (ESCs) [36]. ESCs have an infinite capacity for self-renewal and are in principle capable of producing every type of stem and progenitor cell [37]. However, they are also unpredictable after transplantation and can result to be tumorigenic [38]. Hence, although widely used in the past, the new trend is to promote a neural pre-differentiation of ESCs into neural stem cells (NSCs) before transplantation [39].

2.2.2. Neural stem and neural pluripotent stem cells (NSCs)

Neural stem cells can be extracted from the subventricular zone (SVZ), hippocampus subgranular zone (SGZ), and ventricular zone of the spinal cord from human fetal miscarriages [40–42]. Neural stem cells are divided into neural stem cells (NSCs) and neural pluripotent cells (NPCs). Although NPCs are more committed than NSCs, overall, both can differentiate and replace lost cells in the nervous tissue [43] thanks to their ability to influence immunological processes [44,45] and release growth factors that increase host cell survival after injury, promoting also tissue recovery [46]. Nevertheless, their regional origin might interfere with their ability to restore the neural tissue. For example, spinal cord derived NPCs appear to have a boosted differentiation compared to forebrain-derived NPCs after traumatic injury [47].

Regarding CNS regeneration, after transplantation, NPCs have the capacity to develop into neurons and glia and thereby restore missing tissue. Indeed, both grafted human and pig NPCs demonstrated to differentiate towards neurons, interact with host brain circuits, and support functional recovery after SCI in a rodent model [48–51]. Grafted rodent and human NPCs influence a series of biochemical and cellular processes in the acute and subacute stages of SCI, resulting in a better survival of the surrounding damaged host neurons, and an enhanced functional recovery [52–54]. Moreover, the release of neurotrophic factors from NPCs promotes neuroprotection [52,55,56] and modifies the microenvironment, lowering inflammation and promoting neuronal survival after SCI [57,58]. Besides, the creation of gap junctions between host and

grafted cells may enhance the homeostatic support of the host damaged cells while committing grafted cells towards neuronal or astroglial lineages [59]. In clinical experiments, NPCs from a cell line (NSI-566) transplanted into human chronic SCI patients demonstrated the safety of these cells. However, only two of the six studied patients experienced functional improvement [60].

Similarly, NPCs exhibit therapeutic effects in TBI through neuroprotection and induction of anti-inflammatory features. NPCs grafted into an adult mouse TBI model exhibited an enhanced neuroprotection and decreased microglia activation [61]. Mouse NPCs grafted into a rat model TBI resulted in an increased B-cell lymphoma-extra large (Bcl-xL) expression, and in a decreased neuronal death in the cerebral cortex and enhanced motor restoration [62]. Regarding anti-inflammatory features, NPCs have been shown to precisely modulate microglia phenotype, specifically raising the M2 (anti-inflammatory) to M1 (pro-inflammatory) phenotypes (M2/M1 ratio) after TBI, thus modulating inflammation, restoration and degradation of the tissue [4,21,63]. Even in more chronic scenarios, human NPCs implanted one month after TBI improved cognitive abilities, decreased neuroinflammation, and promoted host neuronal survival.

Overall, NSCs and NPCs exhibit great regeneration capacities both *in vitro* and *in vivo* and even in human clinical trials. However, their difficulties in autologous extraction together with the possible creation of tumors due to remaining pluripotent features and ethical concerns is delaying their clinical application [64,65]. Indeed, the required continuous extraction of NSCs or NPCs from abortions for a standardized treatment together with the necessary immunosuppression of the patients make essential the consideration of other stem cell sources [66].

2.2.3. Oligodendrocyte precursor neural cells (oPNCs)

Oligodendrocyte precursor neural cells (oPNCs) are extracted from human fetal CNS and they provide the advantage of achieving greater populations of oligodendroglial cells than NSCs or NPCs [67]. Indeed, oPNCs grafted in a rodent SCI model demonstrated a boosted oligodendrocyte differentiation and migration, together with an enhanced motor functional recovery thanks to axonal remyelination and tissue preservation on the injured site [67,68]. In chronic scenarios, where regeneration is impaired due to the microenvironment [69], the combination of chondroitinase ABC proteoglycan treatment together with human oPNCs enhanced functional recovery in a rat model of chronic SCI [70]. Nevertheless, these cells still have the disadvantage of challenging autologous extraction and ethical concerns due to their fetal origin [67].

2.2.4. Induced pluripotent stem cells (iPSCs)

Nowadays, widely known reprogramming agents (Oct3/4, Sox2, Klf4, and c-Myc) allow to convert somatic cells into induced pluripotent stem cells (iPSCs). Hence, iPSCs can be autologously obtained, offering a reduced risk of immunological rejection [71,72]. Grafted iPSCs generate both neurons and oligodendrocytes when grafted *in vivo*, while iPSC-derived neurons demonstrated to fully integrate into the neural network including the establishment of functional synaptic axons with healthy neurons on opposite sides of a SCI injury [73,74]. Accordingly, human iPSC-derived NPCs enhanced axonal remyelination and functional motor recovery on rodent and primate chronic SCI models, either combined or not with pharmacological suppression of gamma-secretases [73–78]. Regarding brain injury, iPSCs have demonstrated motor and cognitive functional recovery after TBI at long term, but not after one day transplantation [79–81].

Although *in vivo* studies have demonstrated functional recovery after iPSCs transplantation, in human clinical trials iPSCs grafted in the brain created a tumor at long-term, showing that their pluripotent capacity may be a handicap for human therapy [82]. Furthermore, the amount of time needed for cell reprogramming and growth is another drawback of iPSCs for acute-subacute therapy. Hence, autologous therapy is only possible at chronic phases. Nowadays, the establishment of international cell banks of clinical-grade iPSCs from a variety of donors with most of the human leukocyte antigen (HLA) matched, are lowering the need for immunosuppressive therapies in future clinical trials [83], but there is still a need for other stem cell sources.

2.2.5. Mesenchymal stem cells (MSCs)

Mesenchymal stem cells (MSCs) are obtained from numerous organs and tissues such as bone marrow, umbilical cord, amniotic fluid, and adipose tissue, allowing the autologous grafts and minimizing ethical concerns. Compared with other stem cells, MSCs have the advantage of being immunomodulatory, which minimizes the risk of immunorejection even in allogenic transplants [84]. Besides, they secrete trophic factors such as glial cell-derived neurotrophic factor (GDNF), vascular endothelial growth factor (VEGF), brain-derived neurotrophic factor (BDNF) and nerve growth factor (NGF), which may decrease the secondary injury of the CNS [85,86]. Nevertheless, the origin of the MSCs impacts their neural regeneration capabilities. Although MSCs originating from umbilical cord have the most immunomodulatory effects, those deriving from adipose tissue revealed similar neuronal commitment and functional SCI regeneration capabilities, making these two sources the best for CNS restoration [87].

In vivo, grafted MSCs reduce inflammation and modulate the immune response by augmenting the conversion of M1 into M2 macrophages in rodent SCI model [88]. Even in chronic rodent SCI, intravenously grafted MSCs demonstrated a functional recovery [89]. Similarly, clinical trials for SCI demonstrated beneficial motor and sensory functions

in phase I and II [90–93], but fail in phase III, where only 2 of the 16 patients experienced a neurological recovery [94]. Regarding brain injury, intravenous administration of human MSCs demonstrated an increased neural cell generation together with neuroprotective and enhanced cognition thanks to the release of Wnt3a in a rodent TBI model [95]. In clinical trials, human allogenic MSCs (SB623, containing the human *Notch-1* intracellular domain) stereotactically administered in the brain showed a motor recovery and no rejection, but no other functional restoration [96]. Overall, although promising, more research is needed to assess safety concerns and restoration capabilities of the MSCs. Among them, human dental pulp stem cells (hDPSCs) are achieving promising results. Thus, they are explained in a separate section.

2.2.6. Dental pulp stem cells (DPSCs)

Dental pulp stem cells (DPSCs) are easily extracted from third molars of healthy donors, and hence can be achieved autologously in a minimal invasive manner. Among MSCs, DPSCs are one of the most promising thanks to their immunomodulatory effect, trophic factor release and the ability to generate both pericytes and Schwann cells [97]. In this regard, DPSCs have demonstrated promising results when grafted into healthy rodent brain by stereotaxis, integrating inside the brain vasculature and providing an enhanced neovascularization [98]. In injured CNS, grafted human DPSCs inhibited host neural cell death, regenerated axonal regrowth and developed into myelinating cells, which was directly associated with a functional motor recovery in rodent SCI model [99]. Despite more research is needed, the fact that DPSCs are no tumorigenic and can be obtained autologously [97], make them a promising cell source for future neural regeneration.

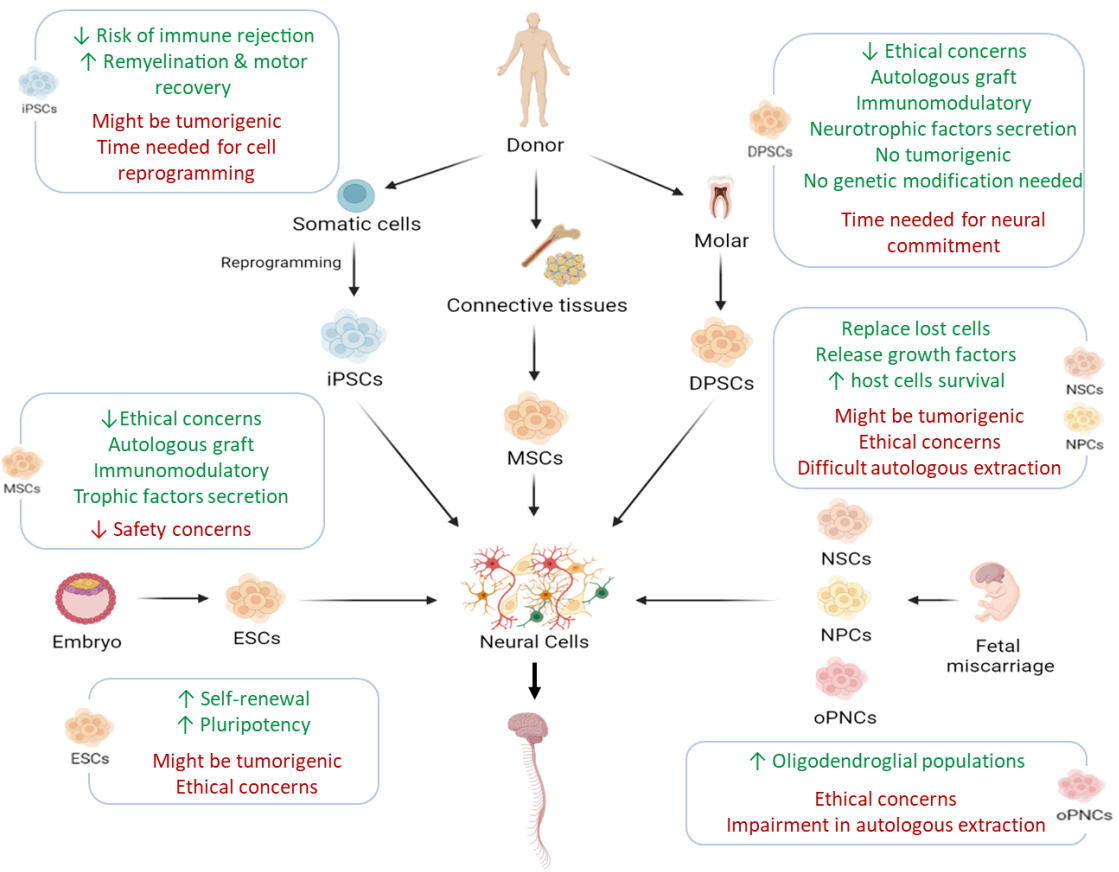

Figure 2.2.: **Schematic representation of the stem cells used for traumatic CNS regeneration highlighting their advantages and disadvantages.**

Stem cells can be obtained autologously or not and, depending on their origin, they have a different prognostic regarding cell differentiation and replacement, integration and even immunomodulation.

2.3. Bioresorbable polymeric materials as modulators of stem cell differentiation and integration

Although promising results are being reported for stem cells in neural tissue restoration, most preclinical and clinical trials highlight the suboptimal functional restoration due to the poor integration of stem cells into the host neural circuitry [100]. A possible approach to increase cell engraftment relies on the use of polymeric materials acting as anchoring scaffolds for stem cells [101]. Moreover, neurological disorders cause variations on the ECM and its constituents, its biochemical properties and transport of nutrients that can alter the neural microenvironment composition [102,103]. Polymeric materials can mimic the ECM and modulate the stem cell integration and commitment, enhancing accordingly the recovery of the injured neural tissue (Figure 2.3).

2.3.1. Composition matters: guiding cell fate through material composition

After an injury in the CNS, the immune system and the glial cells, like macrophages, lymphocytes and astrocytes, are accumulated around the injured site promoting inflammation and the formation of the glial scar. In this regard, the composition of the materials for neural regeneration needs to be finely adjusted to minimize the exacerbated immune reaction while enabling the cell attachment through the interaction of the cells with the surface of the scaffolds [104].

In general, polymeric materials offer the opportunity to serve as a cell anchoring scaffold for host cells but can also serve as a platform to deliver stem cells and promote their integration and regeneration capabilities in the injured CNS [105]. Polymeric materials can be divided into natural and synthetic polymers, which can be further modified via several strategies to improve their regeneration capacity and interaction with cells.

2.3.1.1. Natural polymeric materials

Natural polymers have the benefit of being highly similar or even identical to biomacromolecular components found in the ECM (e.g., collagen, hyaluronic acid, elastin, chitosan, gelatin, polysaccharides or generic mixtures of ECM compounds). Consequently, they are easily recognized by cells and can minimize the detection by the immune system and consequent rejection [106]. Moreover, many of these polymers are bioresorbable and biocompatible, and can promote cell attachment and expansion. Natural origin biomaterials can be found in a wide variety of formats, including *in situ* gellable solutions, scaffolds, fibers, or tubular conduits. Lately, three-dimensional (3D) porous biomaterials have attracted great interest due to their enhanced cell-biomaterial interactions, ECM deposition and adequate transfer of oxygen and nutrients. Natural polymers are, however, associated to batch-to-batch variations, making the design of the final devices complex due to unpredictable mechanical and physico-chemical properties, as well as degradation rates [107].

- **Collagen:** Collagen is the most abundant natural polymer in the ECM and ISS (30% of the mass) of vertebrates and is composed of about 28 proteins [108]. Its highly conserved structure offers no immunogenic reactions together with cell binding motifs that promote attachment, growth, migration, and even cell commitment [109].

  Regarding the use of collagen in SCI models, the combination of collagen with NSCs promoted survival of the grafted cells, but failed on the functional motor restoration in a rodent SCI model [110]. Anyway, when structured collagen supports were combined with human MSCs, the neuronal and functional motor regeneration in canine SCI model was promoted [111], suggesting that either the aligned fiber orientation or MSCs were responsible of these outcomes. In clinical studies, collagen based NeuroRegen scaffold together with MSCs showed no adverse effects in any patient but the motor recovery was limited in both acute and chronic SCI [112,113]. Overall, collagen scaffolds are achieving impressive results, offering a good alternative for neural regeneration. Nevertheless, compared with other tissues, the CNS presents a lower proportion of collagen in its ECM, where collagen rich deposits have been even associated with glial scar and dura matter [114–117], making other natural polymeric options more attractive to restore traumatic CNS injuries.

- **Gelatin:** Gelatin is produced when collagen is partially hydrolyzed, and hence it has similar bioresorbable and biocompatible features. In CNS injury, gelatin-based scaffolds can fill the cavity and reduce death and inflammation [118]. The combination of gelatin with neural committed iPSCs demonstrated immunomodulatory effects together with decreased collagen deposition and cavities in a rodent SCI model [119].

- **Chitosan:** Deacetylation of chitin produces chitosan, a copolymer of N-glucosamine and N-acetylglucosamine that is abundantly present in the cell walls of arthropods, bacteria, and fungi [120]. Chitosan scaffolds restrained both immune response and glial scar formation, while favoring the restoration of the neural and vascular systems including *de novo* growth of myelinated axons promoting motor function on rodent SCI [121].

  In combination with stem cells, chitosan hydrogels grafted with either human MSCs or DPSCs showed motor recovery thanks to the secretion of brain-derived neurotrophic factor (BDNF), glial cell line-derived neurotrophic factor (GDNF), neurotrophin-3 (NT-3) and beta nerve growth factor (bNGF). Altogether, this combination diminished active-caspase 3 and prevented axonal loss in rodent SCI models [122,123]. In conclusion, these studies highly encourage the inclusion of stem cells together with polymeric natural scaffolds for nerve regeneration [124]. But, in clinical trials, chitosan grafted with MSCs failed to regenerate human chronic SCI and reported negative effects including hematoma formation [125], highlighting the

necessity to improve the biocompatibility and mechanical properties of this material before reaching the clinic. Moreover, when inserting chitosan scaffolds on rodent brain, no improvement on neural network was observed, discouraging its use in TBI [126].

- **Hyaluronic acid:** Hyaluronic acid is composed by N-acetyl-glucosamide and D-glucuronic acid in a disaccharide form and is especially prominent in the ECM and ISS of the CNS, making it suitable for neural regeneration. Remarkably, by preventing lymphocyte accumulation, chemotaxis, and growth, hyaluronic acid hinders the creation of glial scar and decreases secondary injury, enhancing hence, neuroprotection [127,128].

  Hyaluronic acid hydrogels have been reported to enhance neural differentiation of human NPCs towards both neural and astroglial lineages. These differences on cell commitment *in vitro* can be finely adjusted by controlling the mechanical properties via different crosslinking degrees [129]. Accordingly, human MSCs incubated over cylinder-shaped polyvinyl alcohol (PVA)/hyaluronic acid hydrogel with a wide-range of stiffness values (between 20 kPa to 200 kPa), exhibited improved neural differentiation in the softest hydrogels (i.e., 20 kPa) [130]. In a similar example, collagen-hyaluronic acid hydrogels designed with specific mechanical properties showed increasing nerve regeneration in rodent SCI model [131]. Hyaluronic acid mixed with heparin and collagen and grafted with NSCs also showed immunomodulation on TBI rodent models [132], further encouraging its potential use in CNS restoration. Despite these promising results, hyaluronic acid is known to have low water solubility, poor mechanical properties and lack of moieties for cell attachment, making necessary the research on alternative materials or modification strategies with bioactive molecules [131].

- **Alginate:** Alginate is a polysaccharide extracted, among others, from seaweed, and shows good biocompatibility and bioresorbable properties. Alginate hydrogels have shown to promote both neuronal and astroglial differentiation of NSCs depending on the mechanical properties [133–135], highlighting the role of mechanical properties on cell commitment. In combination with stem cells, alginate hydrogels grafted with NSCs lowered the immune response, the cavities and the caspase-3 enzyme in a rodent SCI model [136]. However, no improvement was observed when alginate hydrogels were placed inside rodent or primate brain, discouraging their use for TBI [126].

- **Agarose:** Agarose is another biocompatible polysaccharide extracted from seaweed. Together with Matrigel, agarose scaffolds demonstrated an enhanced axonal growth and functional motor recovery in a rodent SCI model [110]. In combination with MSCs, agarose, carbomer and arginine-glycine-aspartic acid hydrogels were able to attenuate the proinflammatory response mediated by macrophages and promote

regeneration in a rodent SCI model [137], which again highlights the combinatorial use of natural polymers and stem cells for restoration of traumatic CNS injuries. However, no studies have been found reporting the use of agarose in TBI.

- **Fibrin:** Fibrin is extracted from animal blood or tissue plasma, which confers it enhanced biocompatibility. Regarding CNS restoration, fibrin-based scaffolds alone were able to increase neural and vascular regrowth and inhibit the deposition of reactive astrocytes at the injury site in rodent SCI models [138,139]. In combination with NPCs, fibrin matrix promoted functional recovery of rats and nonhuman primates suffering SCI. Remarkably, through novel synapses, the neurons produced from human and monkey NPCs were physically and functionally integrated with the host neuronal circuitry at the injured site [140,141]. In another study, fibrin hydrogels grafted with MSCs promoted neural reconnection and lowered cavities giving as a result a boosted motor functionality on a rodent SCI [142]. No studies have been found on the use of fibrin in TBI, but the good results of fibrin combined with stem cells, encourages its use for this pathology.

- **Decellularized scaffolds:** Lately, a new trend is arising with the possibility of removing cells from the actual tissue and leaving the whole ECM and ISS structure formed by carbohydrates, lipids and proteins [143]. In this way, not only the chemical clues are preserved but also the structural and other mechanical properties of the tissue that promotes attachment, growth, migration and differentiation of the grafted or host stem cells [144]. Although no examples are yet available using decellularized scaffolds alone, decellularized spinal cord scaffolds grafted with MSCs diminished glial scar and macrophage- and lymphocyte-mediated immune response and promoted axonal regrowth and motor functionality in rodent SCI models [145,146]. In TBI, decellularized scaffolds either grafted with ESCs or NSCs, diminished neural lost and improved cognitive and motor functions in rodent SCI models [147,148]. Hence, decellularized scaffolds in combination with stem cells are showing great results *in vivo*, although the complications on achieving autologous samples may delay their clinical use.

2.3.1.2. Synthetic polymeric materials

Some synthetic polymers offer minimal immune reaction, high biocompatibility, low or non-toxicity, tailored degradability, porosity, and physicochemical and mechanical features. Moreover, they can be tailored to better resemble the neural microenvironment at the atomic, molecular and macromolecular level, resulting in enhanced functionalities, specific geometries, and topological structures that can be controlled in ranges from 1 nm to various μm [113, 114]. Hence, relevant properties of synthetic polymeric materials understood as degradability, molecular affinity, or porosity can be tuned to allow the regulation of extracellular signals displayed to stem

cells, allowing the modification of the differentiation pattern. Studies of biomaterial-stem cell interactions have reported that synthetic materials itself are able to modulate stem cell differentiation even when there is no biomolecule delivery [151]. Nowadays, synthetic absorbable scaffolds are mostly based in poly(caprolactone) (PCL), poly(lactide) (PLA), poly(lactide-co-glycolide) (PLGA) and poly(ethylene glycol) (PEG).

- **Poly(ε-caprolactone) (PCL):** Poly(ε-caprolactone) (PCL) is an aliphatic polyester that shows slow degradation rate [152], which enables a long-term stability of the implanted scaffold. Thanks to the thermoplastic properties of PCL, different architectures can be designed with the aim of enhancing cell attachment and migrated direction of cells. In animal studies, porous or patterned PCL promoted cell attachment and aligned axonal proliferation inside and outside the tubular device in rodent SCI models [153–155]. In combination with stem cells, PCL grafted with ESCs diminished the cavity and regenerated the injured site [156]. When compared to other bioresorbable polymers, PCL showed an increased immunomodulation and host cell integration in a rodent TBI model [157], further supporting the use of PCL on traumatic CNS injuries.

- **Poly(lactide) (PLA):** Poly(lactide) (PLA) is a bioresorbable material synthesized by processing sustainable plant-source starch. PLA has been widely employed in biomedical engineering due to its great biocompatibility and degradability. PLA can be progressively metabolized to lactic acid and digested in 6 to 12 months. In CNS regeneration, aligned PLA scaffolds promoted aligned axonal growth and diminished cavity in rodent SCI models [158,159]. Besides, PLA-based 3D porous scaffolds also promoted axonal regeneration and functional motor recovery in rodent SCI models [160,161]. Although no studies with stem cells or TBI have been found, overall, the reported studies highlight the versatility of PLA to fabricate scaffolds with different features, like morphologies or degradation rates for CNS regeneration.

- **Poly(lactide-co-glycolide) (PLGA):** Poly(lactide-co-glycolide) (PLGA) is produced after the copolymerization of glycolide and lactide. It is bioresorbable, biocompatible, food and drug administration (FDA)-approved and offers tunable architectural capabilities [162,163]. Porous scaffolds of PLGA alone, either arranged in a tubular form or not, showed aligned myelinated axonal regrowth, immunomodulation, tissue regeneration and cavity diminishment in both rodent and pig SCI models [164]. Besides, when the porous scaffolds where also tubularly arranged, an aligned axonal regrowth was also observed in rodent SCI models [165,166]. In clinical trials, PLGA combined with poly-L-lysine scaffold is showing promising results regarding safety, although no functional recovery data has been published yet [167]. Together with stem cells, PLGA porous scaffolds grafted with human NSCs or MSCs showed migration and integration in rodent, canine and primate SCI models [168–170], suggesting again that the incorporation of stem cells together with synthetic scaffolds

may promote regeneration of the CNS. In TBI, PLGA showed increased host neuronal infiltration and survival in the injured rodent brain [171], but in comparison with PCL, it also showed increased glial formation and infiltration of immune cells, delaying hence the host tissue remodeling [157].

- **Poly(ethylene glycol) (PEG)**: Poly(ethylene glycol) (PEG) offers superior water-holding capacity, water-solubility and biocompatibility [172]. Due to these characteristics, several studies have demonstrated that PEG scaffolds alone diminished glial scar formation and promoted myelinated axonal proliferation and functional recovery in rodent and pig SCI models [173–177]. Moreover, when injected intravenously, PEG hydrogels, alone or combined with PLA, protected axons around the injured site in rodent TBI models [178,179]. Although more investigation is needed, these results encourage the use of PEG together with other natural or synthetic polymers for the neuroprotection of the affected area after a traumatic injury on the CNS.

2.3.1.3. Modification of polymeric scaffolds with neurotrophic factors and other bioactive molecules

Neurotrophic factors and other bioactive molecules increase attachment, proliferation, differentiation and even provide immunomodulatory features to the polymeric materials, also boosting the integration of the grafted stem cells. Natural and synthetic polymeric scaffolds have been widely used in combination with neurotrophic factors to enhance CNS regeneration. Among the available neurotrophic factors, brain derived neurotrophic factor (BDNF), basic fibroblast growth factor (bFGF), nerve growth factor (NGF) and neurotrophin 3 (NT3) are the most commonly reported examples.

- **Brain derived neurotrophic factor (BDNF)**: Brain derived neurotrophic factor (BDNF) is involved in neuronal flexibility, neurotransmitter regulation, and neuronal survival and proliferation [180]. BDNF has been recently combined with natural polymers to enhance restoration. Hyaluronic acid hydrogel combined with BDNF and MSCs diminished both inflammation and glial scar formation to enhance functional regeneration in a rodent SCI model [181]. In another study, linear agarose scaffolds combined with BDNF and grafted with MSCs showed a more aligned growth of the axons in a rodent SCI model [182], suggesting a possible enhanced outcome when combining MSCs with BDNF, independently of the natural polymer chosen.

- **Basic fibroblast growth factor (bFGF):** Basic fibroblast growth factor (bFGF) is known to be involved in cell growth, migration, differentiation and survival, promoting tissue repair [183]. Regarding its combination with natural polymers and stem cells, the combination of gelatin with bFGF showed to be immunomodulatory, lowered host cell death and had neuroprotective features in a rodent SCI model [184]. In the case of synthetic polymers, poloxamer/heparin hydrogels grafted with human DPSCs and

combined with bFGF showed functional locomotor recovery in rodent SCI model, thanks to the upregulation of the antiapoptotic protooncogene B-cell lymphoma 2 (Bcl-2) and downregulation of Bcl-2 associated X apoptosis regulator (Bax), as well as other apoptotic indicators like cleaved caspase-3 [185]. In an associated work, poloxamer/heparin hydrogels grafted with human DPSCs and combined with bFGF effectively decreased pro-inflammatory cytokine production in rodent SCI [186]. Overall, these works highlight the inclusion of bFGF for the restoration of the injured CNS.

- **Nerve growth factor (NGF):** Nerve growth factor (NGF) controls neuronal growth, survival, maintenance, and development. In combination with alginate and fibrin scaffolds, NGF demonstrated enhanced axonal growth, neuronal regeneration and functional motor features in a rodent SCI [187].

- **Neurotrophin 3 (NT3):** Neurotrophin 3 (NT3) growth factor stimulates the development and maturation of new synapses as well as the maintenance and maturation of existing neurons in CNS [188]. The incorporation of NT3 has shown beneficial results in combination with natural polymers. The combination of collagen together with NT3 considerably augmented the neurons and fiber-like structures and decreased glial scar and collagen accumulation in the injury. Consequently, the functional recovery of rodent and non-primate SCI models was achieved [189–191]. Also chitosan scaffolds in combination with NT3 and MSCs showed immunomodulation properties and enhanced motor function in a rodent SCI model [192]. Similarly, gelatin scaffolds modified with TrkC NT3 receptor and NT3 itself derived from NSCs or Schwann cells showed increased axonal and synaptic regeneration in a rodent SCI model [193]. Overall, these results encourage the combinatorial use of neurotrophins with natural polymers for the CNS restoration.

Apart from neurotrophic factors, other molecules are also being investigated. Among them, molecules that enhance angiogenesis like vascular endothelial growth factors or more simple molecules like peptides are among the most used.

- **Vascular endothelial growth factor (VEGF):** Due to the importance of vasculature regeneration for guidance and restructuration of lost axons in CNS injuries, vascular endothelial growth factors (VEGF) are also being investigated. Although most of the data has been done *in vitro*, *in vivo* PLGA microinjection has shown promising results in combination with NSCs and VEGF in a rodent stroke model. VEGF helped to attract endothelial cells from the host tissue, starting the process of neovascularization in the lesion cavity, which enhanced integration and differentiation of grafted cells [194].

- **Peptides:** The combination of natural polymers with diverse peptides has demonstrated enhanced neural regeneration. Chitosan hydrogels in combination with NSCs and SB216763 (an inhibitor of glycogen synthase kinase 3) and decellularized glioma ECM showed an enhanced neural differentiation towards neuronal, glial and oligodendrocyte lineages together with an increased motor function in rodent SCI model [195]. In another study, TKKTLRT collagenase-derived peptide was combined with aligned collagen fibers obtaining nerve growth electrophysiological functional recovery in canine SCI. Finally, when functionalizing collagen porous scaffolds with ephrin type-A receptor 4 (EphA4) and Plexin-B1 associated ligand-binding motifs, enhanced neurite growth and functional recovery of a rodent SCI model was reported [196].

  In vivo, hyaluronic acid combined with PPFLMLLKGSTR peptide and MSCs diminished glial scar and inflammatory response of the tissue, enhancing functional regeneration on rodent SCI model [197]. In another study, oligodendrocyte progenitor prediferentiated iPSCs grafted in a hyaluronan and methylcellulose hydrogel functionalized with RGD peptide and platelet-derived growth factor (PDGF-A), exhibited an enhanced survival and integration on the injured rat SCI in comparison with the cells grafted alone. Moreover, the formation of a teratoma was decreased when grafted together with the hydrogel in favor of an astroglial commitment [198], suggesting again the benefits of combining bioactive molecules and stem cells with scaffolds for functional neural regeneration.

2.3.1.4. Modification of polymeric scaffolds with nanoentities: nanocomposites

Inorganic materials in the form of nanoentitites can confer enhanced biocompatibility and electrical conductivity to the polymeric scaffolds, thus promoting the dissemination of the action potentials across the injured CNS [199]. In this regard, inorganic nanoentities and carbon-based materials like graphene and carbon-nanotubes have been widely explored.

- **Inorganic nanoentities:** Inorganic nanoentities based on ceramic and metallic substances have the advantage of promoting electrical conductivity and RONS scavenging. In this sense, both gold and cerium oxide nanoparticles in combination with synthetic polymers showed immunomodulation, neuronal growth and survival, remyelination and functional motor recovery in SCI [200,201] and antioxidant features on TBI rodent models [202].

  In combination with stem cells, electrospun gold nanocomposite-based tubular nerve conduits promoted the adhesion and growth of Schwann cells, while *in vivo* tests revealed neither harmful nor immunogenic effects with increased myelinization and motor recovery on a rodent SCI model [203]. Similarly, manganese oxide nanoparticles combined with NSCs demonstrated an enhanced differentiation of the

grafted cells in a rodent SCI model [204]. Overall, these data support the combinatorial use of bioresorbable polymeric scaffolds together with inorganic nanoentities for the treatment of traumatic CNS injuries.

Carbon-based materials are an emerging trend in CNS restoration due to their biophysical, mechanical and enhanced electrical conductivity. Among them, most of the studies in traumatic CNS like TBI and SCI have been done with carbon nanotubes and graphene derivatives.

- **Graphene derivatives:** Graphene is a stiff, thermally and electrically conductive two-dimensional carbon nanostructure [205]. Thanks to its physical, chemical, mechanical and electrical properties, it has been widely used *in vitro* for neural differentiation, either in its pure graphene form, or for a better biocompatibility as graphene oxide (GO) [206]. Some studies even reported neural cell action potential stimulation thanks to the activation of P2Y receptor when incorporating graphene derivatives [207]. Nevertheless, its compatibility is still controversial: although several studies have demonstrated its biocompatibility and capacity to promote neuronal and oligodendroglial differentiation when combined with natural and synthetic polymers [133,208], other studies have reported detrimental outcomes [209].

  Lately, graphene-based materials are being used as electrode arrays for neural stimulation, showing promising biocompatibility results after implantation in rodent brains [210]. Moreover, when PCL was combined with graphene, neuronal and vascular growth was promoted together with the regulation of glial and Schwann cells. As a result, the functional motor restoration in a rodent SCI model was achieved [211]. These results highly support the use of graphene-based materials for enhancing the biocompatibility, neuronal differentiation and electrical conductivity of the materials, boosting the regenerative capacities *in vivo*. However, it should be highlighted that in both TBI and SCI treatments, graphene was used in combination with polymeric scaffolds at low dosage; higher dosages have been described to produce an exacerbated inflammation, granuloma and even pulmonary edema [209].

- **Carbon nanotubes:** Regarding carbon nanotubes, they are nanometer size cylinders formed by wrapped graphene layers and can also be modified to increase biocompatibility. Even in the absence of exogenous differentiation factors, carbon nanotubes stimulated neuronal differentiation when implanted in rodent brain, although they were unable to avoid the formation of the glial scar [212,213]. Nevertheless, by coupling them with neurotrophin, their biocompatibility and bioactivity was improved, thus increasing neuronal outgrowth, lowering also the inflammatory response [214]. Combining the carbon nanotubes with PEG resulted in an improved axonal regeneration and functional motor recovery without glial scar formation in rodent SCI models [215,216], supporting the idea of combining bioresorbable synthetic polymers with carbon nanotubes for CNS injury restoration.

2.3.1.5. Modification of polymeric scaffolds via surface functionalization

Most of the synthetic polymeric materials discussed above have the handicap of being hydrophobic. To overcome this limitation, researches are following surface functionalization strategies to enhance biocompatibility and promote cell attachment [217]. As in a natural neural network cells mainly attach to ECM proteins, ECM-like compounds are the preferred choice for surface functionalization [218]. Indeed, in most of the studies, scaffolds are coated with ECM-like components like laminin, fibronectin, hyaluronic acid or collagen before *in vivo* studies [219]. Some of these compounds have the RGD (arginine–glycine–aspartic acid) integrin binding peptide sequence in their formulation that enhance cell attachment and differentiation [220]. The surface functionalization with this ECM-like compounds have been shown to increase biocompatibility and restoration of the tissue in SCI rodent models [221]. However, these ECM-like proteins can also be harmful for their use *in vivo* if they are not correctly handled. For example, laminin in its $\alpha_2\beta_2\gamma_1$ (Lm211) form, inhibit signaling pathways required to initiate myelination [222] and can even boost cancerous phenotype [223]. With the aim of avoiding ECM-like compounds and promote cell attachment, polymeric materials are being alternatively functionalized with conductive substances like polydopamine (PDA) or graphene oxide (GO) [224,225]. As explained before, GO in combination with polymeric materials has been reported to facilitate neural regeneration and functional recovery in SCI rodent models [211]. Regarding PDA, the product derived from the self-polymerization of dopamine that is formed by catechol and amino groups, it can easily form covalent and non-covalent bindings with almost any material, facilitating surface functionalization [224,226,227]. Moreover, PDA might have an immunomodulatory capacity thanks to the entrapment of proteins. PLGA scaffolds coated with PDA have been shown to regulate the immune response by diminishing the available cytokines thanks to the PDA coating, improving the restoration of the nerve tissue in a rodent SCI model [228].

Overall, these results support the functionalization of the hydrophobic polymeric materials either with proteins, natural polymers, or inorganic materials like GO for an enhanced biocompatibility, cell attachment and functional restoration of the injured CNS *in vivo*.

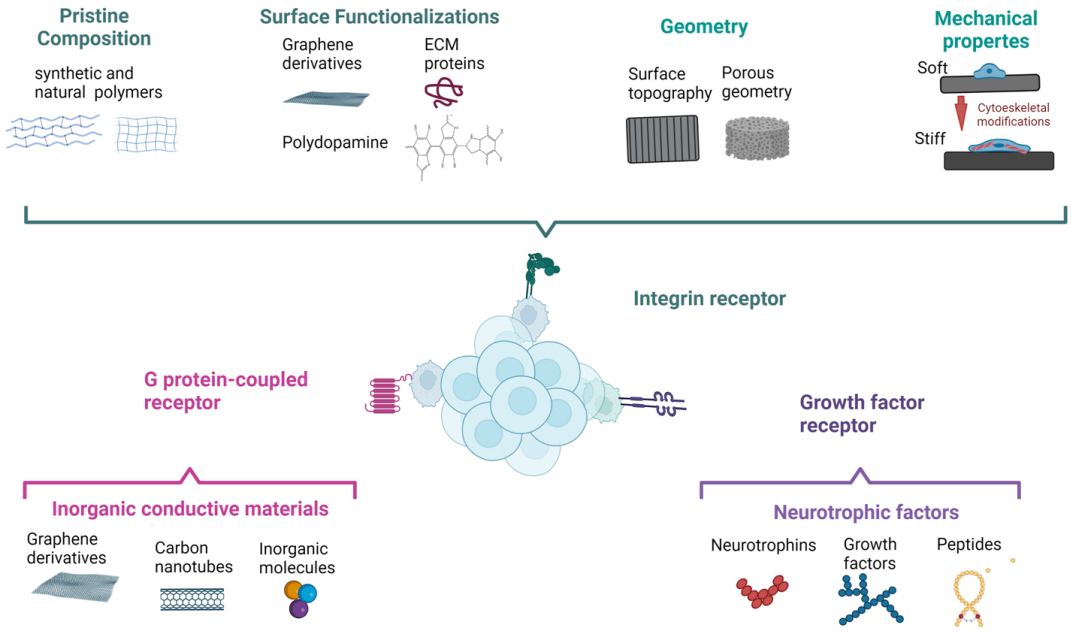

Figure 2.3.: **Components of the material properties that affect grafted or host cell survival and integration**.
Material properties and environment signals induce the activation of cell membrane receptors provoking a molecular cascade that affects host and grafted cell survival and integration.

2.3.2. Guiding cell fate through geometrical cues

Neural cells tend to proliferate and differentiate better in tubular-like structures, maybe due to the structure similarities with the neural tube (the embryonic precursor to the central nervous system), the spinal cord, or even the brain tracks [229]. But as the neural tissue develops, matures, and ages, the geometry varies, including the ISS architecture. These changes are correlated with neuronal migration, differentiation, synapse creation, myelination, regressive processes, and the organization and reorganization of the tissue [230,231]. Moreover, neurological disorders cause geometrical variations on the conformation of the neural tissue, including changes in volume fraction and morphology of the connective tissue [232]. Hence, architectural heterogeneity and changes of the neural microenvironment must be considered when designing scaffolds for neural regeneration. Indeed, polymeric materials can be modulated to mimic the topographical cues of the cellular microenvioronment and guide cell activities like proliferation, differentiation or directional movement and growth by just varying the surface topography in two or three dimensions (Figure 2.4.).

2.3.2.1. Two-dimensional materials topography

Cells react to topographical features of biomaterials through the binding of integrin receptors and the generation of focal adhesions [233,234], but neural tissue cells like NSCs are more sensitive to topographical guidance than other types of stem cells due to their ability to move over greater distances after a lesion [235]. These cells can even modify their form and continue to remodel their cytoskeleton while they are constrained. For example, a two dimensional grooved or porous nano- or micro-pattern can be sensed by the cell, inducing a change on its cytoplasmic membrane surface roughness that can be sensed by the cells nearby [236], modifying hence a whole group of cells. In this regard, nanofibers have been reported to boost self-renewal and maintenance of the stem phenotype in rodent embryos through stimulation of Rac and phosphoinositide-3-kinase signaling pathways [237]. Moreover, stem phenotype retention was further enhanced by increasing nanofiber diameter (from 12 to 600 nm) and promoting the alignment by triggering ERK1/2 and JNK pathways [238–240]. Finally, aligned nanopatterns have been reported to better retain cell stemness than hexagonal patterns [241]. Indeed, hexagonal patterns like graphene boost neurodifferentiation specially towards neuronal commitment [242]. Anisotropic (different properties in different directions) gradient substrates with a wavelength of 26 μm and a height of 2.9 μm also promoted neuronal differentiation [243]. Nevertheless, even in anisotropic substrates, hierarchical parallel features significantly enhanced neural differentiation of human MSCs. In this regard, the diminished nuclear Yes-associated protein amount (YAP)/TAZ and lower cell contractions indicated that the neurogenesis was driven by the cell tension and YAP/TAZ pathway due to topographical cues [243], suggesting that the aligned nanotopography is beneficial for both maintenance of the stem phenotype and neurodifferentation. Indeed, when compared to nanofibrous scaffolds that are arbitrarily aligned, those with an organized arrangement enhance NSC or ESC differentiation into several neural lineages [244–246]. For instance, in the presence of neural induction factors, nanofibrous scaffolds with 230 nm-thick fibers promote neuronal differentiation [247]. Indeed, by simply modifying the diameter of the nanofibers, with no external neural inductor, it is possible to precisely control the differentiation process, enhancing oligodendroglial differentiation by just increasing few nanometers the diameter size till 280 nm [248]. Surprisingly, increasing again the diameter size from 283 to 1452 nm resulted in the promotion of attachment and neuronal commitment and suppression of astroglial differentiation [248,249]. Nevertheless, at the nanometer size, 350 to 480 nm-thick nanofibers induce greater neurogenesis, as a result of Wnt signaling activation [246,249]. On the other hand, when reaching the scale of μm, substrates between 1 and 30 μm inhibited the creation of new neural cells in a size-dependent manner, further supporting the ability of nanotopographical cues on promoting neural cell proliferation and differentiation. These bigger patterns (from 10 to 20 μm) demonstrated to support the infiltration of

astroglial and vascular cells and the aligned growth of axons *in vivo* [246,250,251]. Hence, the combination of nanotopographical cues embedded in larger µm scale topographies might be beneficial for future CNS regeneration strategies. This strategy may promote neuronal differentiation of the stem cells rather than astroglial commitment, which may be interesting for the generation of a balanced neuronal and astroglial populations for regeneration. Indeed, nanopatterns themselves may provide helpful structural cues for the regeneration of brain tissue [252,253] by providing nanofiber alignment that boosts blood vessel healing [254,255] and directed neural growth [256], which ultimately enhances neural regeneration.

2.3.2.2. Three-dimensional porous scaffolds

Studies have demonstrated that three-dimensional (3D) architectures better resemble the natural environment of the cells, making them to behave more like *in vivo* models [257]. It has been reported that 3D continuous porous structures are beneficial for cell invasion and proliferation inside the scaffold and for the maintenance of the stem phenotype [258]. Indeed, pore size can be modulated to promote attachment, infiltration and differentiation of grafted and host cells. Scaffolds with pores of 20 or 100 µm diameter rather than 10 or 30 µm showed the best MSCs attachment, growth, infiltration and differentiation towards both neuronal and astroglial lineages *in vitro* [259,260], while those between 90 and 230 µm enhanced host cell integration and vasculogenesis in a rodent TBI model [261].

In addition to pore size, pore conformation has also an impact on neural regeneration. The actual alignment on the pore connection (40-80 µm) enhanced both neural and vascular cell growth when implanted on rodent brain [262], showing that alignment is also important when designing 3D scaffolds. But the level of porosity and pore dimension also affects the degradation rate [263]. The CNS is composed by water, which enables the hydrolytic degradation of the scaffolds, but also by immunological cells and enzymes, which facilitates the enzymatic degradation [264], which might be taken in consideration when designing scaffolds for *in vivo* neural regeneration [263]. On the other hand, neural tissue is an heterogeneous three-dimensional tissue with unique microenvironment, composed by veins (1-3 mm), dendrites (500 µm), neuronal cell bodies (10–50 µm) and capillaries (4–8 µm) [265]. Hence, the ISS in between cells (continually linked tubes and sheets around each neural cell) has multiple compartments and a range of pore diameters to fit all these architectures filled with an aqueous interstitial fluid [6]. Hence, 3D materials may resemble this complex architecture but also the microfluidics and water content. Regarding water quantity, 3D scaffolds can be categorized in solid systems (sponges or nanofibers) and polymer gels or hydrogels.

While solid systems have a poor content of water, polymer gels or hydrogels are defined as soft and/or solid-like systems made of one or more polymers and are more suitable for neural regeneration [266]. In general, hydrogels are polymer/solvent systems, in which there subsists a 3D network made of macromolecules and their aggregates enabling to retain a larger volume of solvents and water. Hence, they also promote the flow of nutrients, oxygen, and bioactive substances that are necessary for cell survival and proliferation *in vivo*. These polymeric gel systems can also comprise elastic cross-linked networks and fluid filling into the interstitial gaps of the natural network and, hence, they suffer from larger deformations [267]. Hydrogels can regulate cell behavior and provide tools for neural cell expansion and differentiation prior to their transplantation. For example, 3D printed hydrogels were able to support NSCs encapsulation, growth and guided cell migration inside microchannels [268], and even boost oligodendroglial differentiation thanks to the resembled architectural and mechanical properties of the neonatal neural tissue using collagen, hyaluronic acid, and laminin [266]. In another study, NSCs grafted on porous collagen-based hydrogels were able to efficiently deliver NSCs to the injured site and protect them in a SCI rodent model [269].

Finally, in the last decade, the combination of polymeric bioinks based on polymeric materials with stem cells are gaining interest. This new technique offers the possibility of better resembling the neural microenvironment and using the stem cells as scaffold itself. In this regard, 3D porous alginate, carboxymethyl-chitosan, and agarose obtained by cross-linking after NSCs incorporation have demonstrated promising results in neural cell differentiation *in vitro* [270].

2.3.3. The role of mechanical properties to modulate stem cell fate

The dynamic process of early development is characterized by the quick conversion of a fertilized cell into a three-dimensional (3D) embryo. A variety of mechanical signals present in the cellular microenvironment coordinate directed growth, commitment, and mobility in a highly controlled and sequential manner. Between the physical cues, cells produce contractions that stimulate the ECM, to which they are attached, as they pull on their niche, such as when they migrate [271,272]. Hence, cells continuously recognize the topographical and mechanical characteristics of the microenvironment around them and adjust their functional phenotypes accordingly to preserve homeostasis. Indeed, cell-cell and cell-ECM interactions establish physical connections between the exterior and the interior of individual cells that control a variety of cellular processes, including attachment, migration, growth, and cell differentiation [273]. For example, a transmembrane protein called integrin is actively involved in outside-in and inside-out signaling that is mediated by cytoskeleton contraction and polymerization, which is known to regulate cellular mechanotransduction pathways [274]. Therefore, integrin-

ECM interaction is a main target for influencing cell activity through the material characteristics. Indeed, cytoskeletal filaments that closely bind the nuclear membrane to the integrin-based focal adhesion can transfer extrinsic mechanical stimuli or cytoskeletal tension to the nuclear membrane, resulting in conformational displacement of the nucleus and highlighting the importance of nuclear mechanosensation as a mechanism to control physical inputs [275]. In addition to altering the geometry of the nucleus, applied forces also control the configuration of several proteins found in the nuclear membrane that are linked to different biochemical signals [276]. Signal pathways for nuclear mechanosensation have been reported to regulate even cellular adaptation mechanisms, including stem cell differentiation, through transcriptional regulatory mechanisms, such as histone modification and transcription factor activity, which are controlled by force-mediated nuclear deformation [277]. Indeed, mechanical stimuli play a significant role in controlling the regeneration of natural tissues. Cells recognize these signals and convert them into biochemical data, which can then be translated back into mechanical signals [278].

It has been widely demonstrated the importance of the stimulus in cellular differentiation. Indeed, mechanical stimuli must be delivered in an optimal spatial and temporal manner to stimulate development [279]. Lately, it has been reported that in cell development, it is more important a balanced stimuli of mechanical forces over time, than the exact time when the mechanical stimuli happens [279,280]. Indeed, stem cells need balanced forces across their cell-cell junctions to proliferate, while they tend to die when they are isolated [281]. For example, the elimination of physical cues stops embryogenesis, highlighting the significance of physical forces for cell development [282,283].

To explore how cell fate is influenced by the mechanical properties of the extracellular matrix, several research studies have developed polymer-based scaffolds and hydrogels with a wide range of mechanical properties and have subsequently analyzed their impact on cell adhesion, migration and differentiation [284] (Figure 2.4.).

2.3.3.1. Stiffness

The mechanical cues of the substrates are also important for cell development. Substrates with very low elastic moduli (0.00001 kPa) suppress cell proliferation, self-renewal, and maturation of NSCs [285]. Soft scaffolds (Young's modulus of 0.5 kPa) better maintain MSCs stem phenotype than stiffer ones (Young's modulus of 30 kPa), suggesting that the intrinsic mechanical properties of the substrates are able to modulate stem phenotype and differentiation [286].

To minimize microtraumas associated with an elastic mismatch, any biomaterial chosen for neural regeneration should ideally mimic the Young's modulus of the targeted neural tissue [287]. As an heterogeneous organ, human brain exhibits a Young's modulus of

0.1-2.5 kPa [288,289] depending on the region, while the spinal cord has a modulus in the range of 250-300 kPa [290]. Several studies highlight the benefits on approaching neural tissue stiffness when designing scaffolds for neural regeneration [285]. The differences on neural commitment depend on the Young´s modulus of the biomaterial, promoting the stiffer substrates (1–34 kPa) the astroglial differentiation, while the softer ones (0.1–1 kPa) enhance the neuronal commitment *in vitro* [285,291–294]. Regarding oligodendrocyte differentiation, it seems to be favored in stiffer substrates (< 7 kPa), but this is still controversial [295]. Nevertheless, when designing scaffolds for neural regeneration, it must be generally considered that stiffer substrates can also provoke the activation of the focal adhesions and the redistribution of the actin cytoskeleton into stress fibers [296], which may also be harmful for *in vivo* and clinical approaches.

Similarly, regarding three-dimensional substrates, stiffer structures (2.6 kPa) impede neurogenesis while softer ones (1.5 kPa) promote neuronal differentiation and maturation. Importantly, when human NPCs were cultured in hydrogels with higher elastic modulus (7.2 kPa), apoptosis occurred [129] due to the high cross-linking density of the hydrogels that limited cell activities [134]. Aside from that, in another study, hydrogels of 1.5 kPa enhanced neurite outgrowth while softer alginate hydrogels (0.18 kPa) were better for neuronal differentiation [135]. Moreover, rigid substrates (460 kPa) rather than softer ones (50 kPa), promoted the activation of synaptic connection and transmission of cultured hippocampus neural network. Indeed, stiffer materials regulated voltage-gated calcium channel currents, calcium oscillations, synaptic connection, spontaneous excitatory postsynaptic activity, excitatory transmitter release, and excitatory postsynaptic currents of the achieved neurons, highlighting the importance of the mechanical properties of the material on achieving a functional neural culture *in vitro* [297]. *In vivo,* when polyacrylamide (PAA) gels of 0.1 kPa (soft) or 30 kPa (stiff) were implanted into Sprague-Dawley rat brains, the stiff hydrogel triggered an increased inflammatory response of the astrocytes and microglia. These results further indicated that due to the mechanosensitivity of the glia, mechanical mismatch was associated with polymeric medical devices failure due to foreign body reaction and the creation of the glial scar, resulting on the encapsulation of the implant and the impairment of the restoration [298].

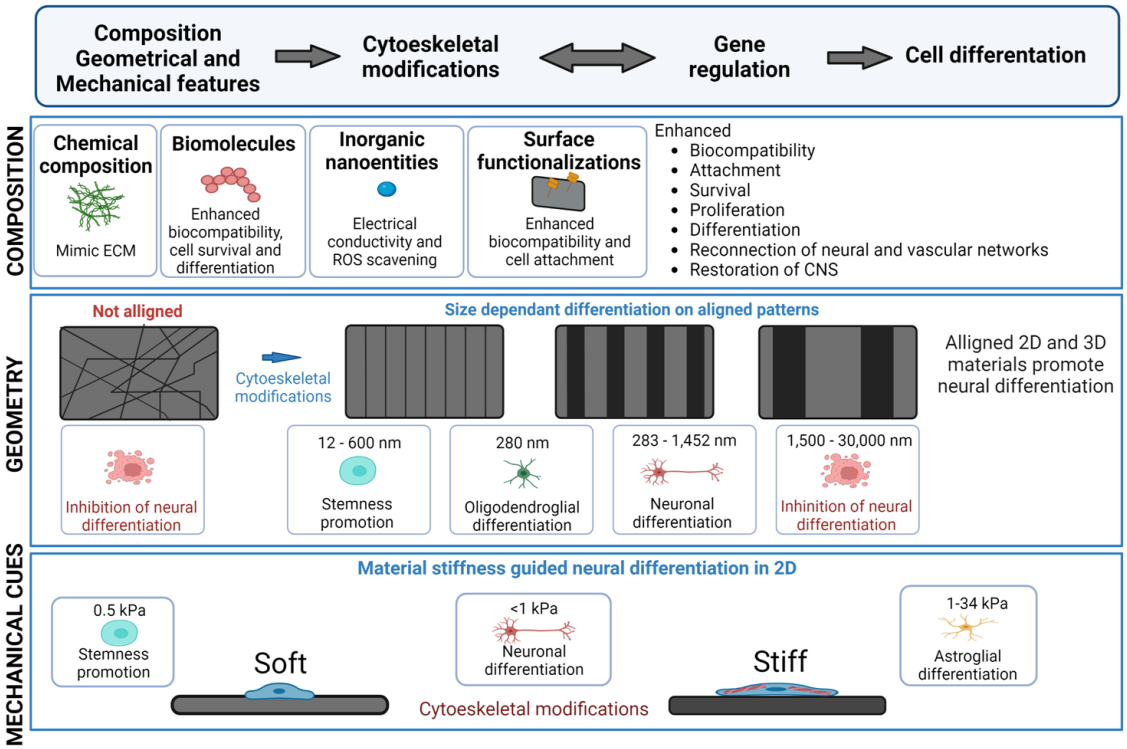

Figure 2.4.: Effect of the composition, geometry and mechanical properties on cell differentiation.

Material pristine composition can be modulated with biomolecules, inorganic nanoentities or via surface functionalization to enhance biocompatibility, attachment and differentiation of host and stem cells after a traumatic CNS injury. In aligned scaffolds, those with nm scale better promote glial and neuronal differentiation, while aligned clues in µm scale inhibit neural differentiation. Regarding mechanical properties, softer scaffolds promote neuronal differentiation while stiffer ones enhance astroglial differentiation.

2.3.3.2. Other mechanical stimuli

Mechanical forces also modulate crucial cellular processes including YAP-mediated cell motility induction [299]. For instance, in organogenesis, oscillating waves able to expand and compact huge areas of cells regulate YAP/TAZ signaling, delimitating tissue edges and accomplishing controlled organ growth [300]. Thus, while in 2D materials the mechanical cues are based on the mechanotransduction of the stiffness driven by cell-matrix interactions, the main mechanical factors controlling cell proliferation in 3D scaffolds include viscoelasticity [301]. In this regard, even with the same degradability, morphology and elastic modulus, neurogenesis was modulated due to the viscoelasticity of hyaluronic acid and collagen hydrogels. Indeed, the accelerated stress relaxation of the hydrogel increased neurogenesis and elongation of axons of NSCs both *in vitro* and *in vivo* in a SCI rodent model by YAP/TAZ signaling [302].

Finally, there must be also considered that nanotopography can also be sensed as mechanical stimuli and hence activate integrin mediated gene regulation [236]. In this

sense, mechanical properties also tune cell migration in a process called mechanotaxis [303]. Mechanotaxis is divided into four categories: cohesotaxis (migration directed by gradients of intracellular tension), plithotaxis (directional collective migration caused by tensile forces), solitary migration caused by ECM deformation, and durotaxis (stiffness-mediated migration) and has been described to be involved in neural development. For example, scaffolds of up to 5 kPa promoted neural cell movement [304–306]. Overall, although more investigation is needed, viscoelasticity of the materials may modulate the cell fate enhancing stem cell division on the injured site and influencing the regeneration. On the other hand, mechanical cues not only guide cell differentiation, but apparently, they can also stimulate migration paths, which may enhance guided axonal regrowth for SCI.

2.4. Conclusions

Every single characteristic of the material can play a key role in cell fate. Hence, composition, degradability, topography or mechanical and conductivity features need to be finely modulated to mimic neural ECM and consequently promote CNS regeneration. Nevertheless, CNS is a complex tissue composed by neural and vascular cells, ECM and also ISS. New materials should also focus on the compositional, mechanical and microfluidic properties of the ISS in order to achieve a better restoration of the CNS. Indeed, 3D scaffolds with similar water content to that exhibited by the CNS achieved better restoration capabilities thanks to a better nutrient, oxygen and other bioactive molecules supply. Accordingly, the microfluidics of the scaffolds should be taken in consideration when designing scaffolds for CNS regeneration in future studies.

In addition, although most of the attention is placed on the characteristics of the materials that modulate cell differentiation towards neuronal commitment, for a functional CNS restoration, other cell-types like astrocytes, myelinating cells, ependymal cells or even vascular cells are required. Future studies should focus on the achievement of a balanced heterocellular culture containing at least stem, astroglial, myelinating and neuronal cells *in vitro*. These cells should be also accompanied by endothelial cells to achieve better results in animal experiments. In this regard, materials in combination with bioactive molecules may enhance the achievement of the different populations and even provide the materials with new characteristics, like stem cell migration, or immune system regulation that have been shown to be effective in the restoration of lost tissue in animal models of SCI and TBI.

Finally, animal experiments highly encourage the functionalization of the surface of the materials to enhance biocompatibility and electrical conductivity while minimizing the use of ECM-like compounds. In addition, the use of combinatorial treatments that include bioresorbable polymeric scaffolds in combination with stem cells is also advisable. Stem cells alone, although promising, are exhibiting a lack of integration and survival inside the injured CNS. Their combination with bioresorbable scaffolds can enhance the integration while serving as anchoring scaffold for host cells. Moreover, these constructs can be further functionalized with bioactive molecules that, as explained before, might hinder apoptosis and necrosis, promote cell migration, and even modulate the immune response. In addition, the combination of bioresorbable polymeric scaffold grafted with stem cells should allow in the future the simultaneous incorporation of a heterogenic population of stem, progenitor and predifferentiated cells for a better restoration of the CNS.

References

[1] S.P. Gadani, J.T. Walsh, J.R. Lukens, J. Kipnis, Dealing with Danger in the CNS: The Response of the Immune System to Injury, Neuron. 87 (2015) 47–62. https://doi.org/10.1016/j.neuron.2015.05.019.

[2] S. Jäkel, L. Dimou, Glial Cells and Their Function in the Adult Brain: A Journey through the History of Their Ablation, Front. Cell. Neurosci. 11 (2017) 24. https://doi.org/10.3389/fncel.2017.00024.

[3] C.Z. Chen, B. Neumann, S. Förster, R.J.M. Franklin, Schwann cell remyelination of the central nervous system: why does it happen and what are the benefits?, Open Biol. 11 (n.d.) 200352. https://doi.org/10.1098/rsob.200352.

[4] N.A. Devanney, A.N. Stewart, J.C. Gensel, Microglia and macrophage metabolism in CNS injury and disease: The role of immunometabolism in neurodegeneration and neurotrauma, Exp. Neurol. 329 (2020) 113310. https://doi.org/10.1016/j.expneurol.2020.113310.

[5] A. MacDonald, B. Lu, M. Caron, N. Caporicci-Dinucci, D. Hatrock, K. Petrecca, G. Bourque, J.A. Stratton, Single Cell Transcriptomics of Ependymal Cells Across Age, Region and Species Reveals Cilia-Related and Metal Ion Regulatory Roles as Major Conserved Ependymal Cell Functions, Front. Cell. Neurosci. 15 (2021). https://www.frontiersin.org/articles/10.3389/fncel.2021.703951 (accessed September 2, 2022).

[6] Y. Lei, H. Han, F. Yuan, A. Javeed, Y. Zhao, The brain interstitial system: Anatomy, modeling, in vivo measurement, and applications, Prog. Neurobiol. 157 (2017) 230–246. https://doi.org/10.1016/j.pneurobio.2015.12.007.

[7] C. He, F. Chen, B. Li, Z. Hu, Neurophysiology of HCN channels: from cellular functions to multiple regulations, Prog. Neurobiol. 112 (2014) 1–23. https://doi.org/10.1016/j.pneurobio.2013.10.001.

[8] G. Gutiérrez-Gutiérrez, M. Sereno, A. Miralles, E. Casado-Sáenz, E. Gutiérrez-Rivas, Chemotherapy-induced peripheral neuropathy: clinical features, diagnosis, prevention and treatment strategies, Clin. Transl. Oncol. 12 (2010) 81–91. https://doi.org/10.1007/S12094-010-0474-z.

[9] S. Sulhan, K.A. Lyon, L.A. Shapiro, J.H. Huang, Neuroinflammation and blood–brain barrier disruption following traumatic brain injury: Pathophysiology and potential therapeutic targets, J. Neurosci. Res. 98 (2020) 19–28. https://doi.org/10.1002/jnr.24331.

[10] V.E. Johnson, W. Stewart, D.H. Smith, Axonal pathology in traumatic brain injury, Exp. Neurol. 246 (2013) 35–43. https://doi.org/10.1016/j.expneurol.2012.01.013.

[11] M.L. Pearn, I.R. Niesman, J. Egawa, A. Sawada, A. Almenar-Queralt, S.B. Shah, J.L. Duckworth, B.P. Head, Pathophysiology Associated with Traumatic Brain Injury: Current Treatments and Potential Novel Therapeutics, Cell. Mol. Neurobiol. 37 (2017) 571–585. https://doi.org/10.1007/s10571-016-0400-1.

[12] J. Hazeldine, R.J. Dinsdale, D.N. Naumann, A. Acharjee, J.R.B. Bishop, J.M. Lord, P. Harrison, Traumatic injury is associated with reduced deoxyribonuclease activity and dysregulation of the actin scavenging system, Burns Trauma. 9 (2021) tkab001. https://doi.org/10.1093/burnst/tkab001.

[13] B.H. Verweij, J.P. Muizelaar, F.C. Vinas, P.L. Peterson, Y. Xiong, C.P. Lee, Impaired cerebral mitochondrial function after traumatic brain injury in humans, J. Neurosurg. 93 (2000) 815–820. https://doi.org/10.3171/jns.2000.93.5.0815.

[14] G. Cheng, R. Kong, L. Zhang, J. Zhang, Mitochondria in traumatic brain injury and mitochondrial-targeted multipotential therapeutic strategies, Br. J. Pharmacol. 167 (2012) 699–719. https://doi.org/10.1111/j.1476-5381.2012.02025.x.

[15] M.A. Anwar, T.S. Al Shehabi, A.H. Eid, Inflammogenesis of Secondary Spinal Cord Injury, Front. Cell. Neurosci. 10 (2016) 98. https://doi.org/10.3389/fncel.2016.00098.

[16] M.D. Tang-Schomer, A.R. Patel, P.W. Baas, D.H. Smith, Mechanical breaking of microtubules in axons during dynamic stretch injury underlies delayed elasticity, microtubule disassembly, and axon degeneration, FASEB J. 24 (2010) 1401–1410. https://doi.org/10.1096/fj.09-142844.

[17] E.A. Winkler, D. Minter, J.K. Yue, G.T. Manley, Cerebral Edema in Traumatic Brain Injury: Pathophysiology and Prospective Therapeutic Targets, Neurosurg. Clin. N. Am. 27 (2016) 473–488. https://doi.org/10.1016/j.nec.2016.05.008.

[18] G. Yu, Y. Zhang, B. Ning, Reactive Astrocytes in Central Nervous System Injury: Subgroup and Potential Therapy, Front. Cell. Neurosci. 15 (2021) 792764. https://doi.org/10.3389/fncel.2021.792764.

[19] V.C. Nikolian, S.E. Dekker, T. Bambakidis, G.A. Higgins, I.S. Dennahy, P.E. Georgoff, A.M. Williams, A.V. Andjelkovic, H.B. Alam, Improvement of Blood-Brain Barrier Integrity in Traumatic Brain Injury and Hemorrhagic Shock Following Treatment With Valproic Acid and Fresh Frozen Plasma, Crit. Care Med. 46 (2018) e59. https://doi.org/10.1097/CCM.0000000000002800.

[20] M.E. Bianchi, DAMPs, PAMPs and alarmins: all we need to know about danger, J. Leukoc. Biol. 81 (2007) 1–5. https://doi.org/10.1189/jlb.0306164.

[21] H. Xu, Z. Wang, J. Li, H. Wu, Y. Peng, L. Fan, J. Chen, C. Gu, F. Yan, L. Wang, G. Chen, The Polarization States of Microglia in TBI: A New Paradigm for Pharmacological Intervention, Neural Plast. 2017 (2017) 5405104. https://doi.org/10.1155/2017/5405104.

[22] J. Gao, R.J. Grill, T.J. Dunn, S. Bedi, J.A. Labastida, R.A. Hetz, H. Xue, J.R. Thonhoff, D.S. DeWitt, D.S. Prough, C.S. Cox, P. Wu, Human Neural Stem Cell Transplantation-Mediated Alteration of Microglial/Macrophage Phenotypes after Traumatic Brain Injury, Cell Transplant. 25 (2016) 1863–1877. https://doi.org/10.3727/096368916X691150.

[23] M.T. Fitch, C. Doller, C.K. Combs, G.E. Landreth, J. Silver, Cellular and Molecular Mechanisms of Glial Scarring and Progressive Cavitation: In Vivo and In VitroAnalysis of Inflammation-Induced Secondary Injury after CNS Trauma, J. Neurosci. 19 (1999) 8182–8198. https://doi.org/10.1523/JNEUROSCI.19-19-08182.1999.

[24] S.L. Shuman, J.C. Bresnahan, M.S. Beattie, Apoptosis of microglia and oligodendrocytes after spinal cord contusion in rats, J. Neurosci. Res. 50 (1997) 798–808. https://doi.org/10.1002/(SICI)1097-4547(19971201)50:5<798::AID-JNR16>3.0.CO;2-Y.

[25] A.D. Greenhalgh, S. David, Differences in the Phagocytic Response of Microglia and Peripheral Macrophages after Spinal Cord Injury and Its Effects on Cell Death, J. Neurosci. 34 (2014) 6316–6322. https://doi.org/10.1523/JNEUROSCI.4912-13.2014.

[26] A. Kumar, D.J. Loane, Neuroinflammation after traumatic brain injury: opportunities for therapeutic intervention, Brain. Behav. Immun. 26 (2012) 1191–1201. https://doi.org/10.1016/j.bbi.2012.06.008.

[27] A.P. Tran, P.M. Warren, J. Silver, New insights into glial scar formation after spinal cord injury, Cell Tissue Res. 387 (2022) 319–336. https://doi.org/10.1007/s00441-021-03477-w.

[28] C.S. Ahuja, S. Nori, L. Tetreault, J. Wilson, B. Kwon, J. Harrop, D. Choi, M.G. Fehlings, Traumatic Spinal Cord Injury-Repair and Regeneration, Neurosurgery. 80 (2017) S9–S22. https://doi.org/10.1093/neuros/nyw080.

[29] J.M. Cregg, M.A. DePaul, A.R. Filous, B.T. Lang, A. Tran, J. Silver, Functional regeneration beyond the glial scar, Exp. Neurol. 253 (2014) 197–207. https://doi.org/10.1016/j.expneurol.2013.12.024.

[30] K. Faust, P. Horn, U.C. Schneider, P. Vajkoczy, Blood pressure changes after aneurysmal subarachnoid hemorrhage and their relationship to cerebral vasospasm and clinical outcome, Clin. Neurol. Neurosurg. 125 (2014) 36–40. https://doi.org/10.1016/j.clineuro.2014.06.023.

[31] J.A. Gaasch, P.R. Lockman, W.J. Geldenhuys, D.D. Allen, C.J. Van der Schyf, Brain iron toxicity: differential responses of astrocytes, neurons, and endothelial cells, Neurochem. Res. 32 (2007) 1196–1208. https://doi.org/10.1007/s11064-007-9290-4.

[32] A. Salehi, J.H. Zhang, A. Obenaus, Response of the cerebral vasculature following traumatic brain injury, J. Cereb. Blood Flow Metab. 37 (2017) 2320–2339. https://doi.org/10.1177/0271678X17701460.
[33] V. Bartanusz, D. Jezova, B. Alajajian, M. Digicaylioglu, The blood–spinal cord barrier: Morphology and Clinical Implications, Ann. Neurol. 70 (2011) 194–206. https://doi.org/10.1002/ana.22421.
[34] A.K. Shetty, V. Mishra, M. Kodali, B. Hattiangady, Blood brain barrier dysfunction and delayed neurological deficits in mild traumatic brain injury induced by blast shock waves, Front. Cell. Neurosci. 8 (2014) 232. https://doi.org/10.3389/fncel.2014.00232.
[35] C.E. Schmidt, J.B. Leach, Neural tissue engineering: strategies for repair and regeneration, Annu. Rev. Biomed. Eng. 5 (2003) 293–347. https://doi.org/10.1146/annurev.bioeng.5.011303.120731.
[36] ESHRE Takforce on Ethics and Law, IV. Stem cells, Hum. Reprod. Oxf. Engl. 17 (2002) 1409–1410. https://doi.org/10.1093/humrep/17.5.1409.
[37] K. Blair, J. Wray, A. Smith, The Liberation of Embryonic Stem Cells, PLOS Genet. 7 (2011) e1002019. https://doi.org/10.1371/journal.pgen.1002019.
[38] B. Blum, N. Benvenisty, The tumorigenicity of human embryonic stem cells, Adv. Cancer Res. 100 (2008) 133–158. https://doi.org/10.1016/S0065-230X(08)00005-5.
[39] X. Li, E. Sundström, Stem Cell Therapies for Central Nervous System Trauma: The 4 Ws—What, When, Where, and Why, Stem Cells Transl. Med. 11 (2022) 14–25. https://doi.org/10.1093/stcltm/szab006.
[40] X. Li, E.M. Floriddia, K. Toskas, K.J.L. Fernandes, N. Guérout, F. Barnabé-Heider, Regenerative Potential of Ependymal Cells for Spinal Cord Injuries Over Time, EBioMedicine. 13 (2016) 55–65. https://doi.org/10.1016/j.ebiom.2016.10.035.
[41] X. Li, E.M. Floriddia, K. Toskas, C. Chalfouh, A. Honore, A. Aumont, N. Vallières, S. Lacroix, K.J.L. Fernandes, N. Guérout, F. Barnabé-Heider, FoxJ1 regulates spinal cord development and is required for the maintenance of spinal cord stem cell potential, Exp. Cell Res. 368 (2018) 84–100. https://doi.org/10.1016/j.yexcr.2018.04.017.
[42] W. Xu, N. Lakshman, C.M. Morshead, Building a central nervous system: The neural stem cell lineage revealed, Neurogenesis. 4 (2017) e1300037. https://doi.org/10.1080/23262133.2017.1300037.
[43] N. Uchida, D.W. Buck, D. He, M.J. Reitsma, M. Masek, T.V. Phan, A.S. Tsukamoto, F.H. Gage, I.L. Weissman, Direct isolation of human central nervous system stem cells, Proc. Natl. Acad. Sci. 97 (2000) 14720–14725. https://doi.org/10.1073/pnas.97.26.14720.
[44] S. Pluchino, L. Zanotti, B. Rossi, E. Brambilla, L. Ottoboni, G. Salani, M. Martinello, A. Cattalini, A. Bergami, R. Furlan, G. Comi, G. Constantin, G. Martino, Neurosphere-derived multipotent precursors promote neuroprotection by an immunomodulatory mechanism, Nature. 436 (2005) 266–271. https://doi.org/10.1038/nature03889.
[45] V. Börger, M. Bremer, R. Ferrer-Tur, L. Gockeln, O. Stambouli, A. Becic, B. Giebel, Mesenchymal Stem/Stromal Cell-Derived Extracellular Vesicles and Their Potential as Novel Immunomodulatory Therapeutic Agents, Int. J. Mol. Sci. 18 (2017) 1450. https://doi.org/10.3390/ijms18071450.
[46] J. Gao, D.S. Prough, D.J. McAdoo, J.J. Grady, M.O. Parsley, L. Ma, Y.I. Tarensenko, P. Wu, Transplantation of primed human fetal neural stem cells improves cognitive function in rats after traumatic brain injury, Exp. Neurol. 201 (2006) 281–292. https://doi.org/10.1016/j.expneurol.2006.04.039.
[47] M.T. Dell'Anno, X. Wang, M. Onorati, M. Li, F. Talpo, Y. Sekine, S. Ma, F. Liu, W.B.J. Cafferty, N. Sestan, S.M. Strittmatter, Human neuroepithelial stem cell regional specificity enables spinal cord repair through a relay circuit, Nat. Commun. 9 (2018) 3419. https://doi.org/10.1038/s41467-018-05844-8.
[48] J.-R. Yang, C.-H. Liao, C.-Y. Pang, L.L.-H. Huang, Y.-L. Chen, Y.-L. Shiue, L.-R. Chen, Transplantation of porcine embryonic stem cells and their derived neuronal progenitors in

a spinal cord injury rat model, Cytotherapy. 15 (2013) 201–208. https://doi.org/10.1016/j.jcyt.2012.09.001.

[49] H. Kumamaru, K. Kadoya, A.F. Adler, Y. Takashima, L. Graham, G. Coppola, M.H. Tuszynski, Generation and post-injury integration of human spinal cord neural stem cells, Nat. Methods. 15 (2018) 723–731. https://doi.org/10.1038/s41592-018-0074-3.

[50] K. Kadoya, P. Lu, K. Nguyen, C. Lee-Kubli, H. Kumamaru, L. Yao, J. Knackert, G. Poplawski, J.N. Dulin, H. Strobl, Y. Takashima, J. Biane, J. Conner, S.-C. Zhang, M.H. Tuszynski, Spinal cord reconstitution with homologous neural grafts enables robust corticospinal regeneration, Nat. Med. 22 (2016) 479–487. https://doi.org/10.1038/nm.4066.

[51] P. Lu, Y. Wang, L. Graham, K. McHale, M. Gao, D. Wu, J. Brock, A. Blesch, E.S. Rosenzweig, L.A. Havton, B. Zheng, J.M. Conner, M. Marsala, M.H. Tuszynski, Long-distance growth and connectivity of neural stem cells after severe spinal cord injury, Cell. 150 (2012) 1264–1273. https://doi.org/10.1016/j.cell.2012.08.020.

[52] G.W.J. Hawryluk, A. Mothe, J. Wang, S. Wang, C. Tator, M.G. Fehlings, An In Vivo Characterization of Trophic Factor Production Following Neural Precursor Cell or Bone Marrow Stromal Cell Transplantation for Spinal Cord Injury, Stem Cells Dev. 21 (2012) 2222–2238. https://doi.org/10.1089/scd.2011.0596.

[53] M. Emgård, J. Piao, H. Aineskog, J. Liu, C. Calzarossa, J. Odeberg, L. Holmberg, E.-B. Samuelsson, B. Bezubik, P.H. Vincent, S.P. Falci, Å. Seiger, E. Åkesson, E. Sundström, Neuroprotective effects of human spinal cord-derived neural precursor cells after transplantation to the injured spinal cord, Exp. Neurol. 253 (2014) 138–145. https://doi.org/10.1016/j.expneurol.2013.12.022.

[54] J. Gao, R.J. Grill, T.J. Dunn, S. Bedi, J.A. Labastida, R.A. Hetz, H. Xue, J.R. Thonhoff, D.S. DeWitt, D.S. Prough, C.S. Cox, P. Wu, Human Neural Stem Cell Transplantation-Mediated Alteration of Microglial/Macrophage Phenotypes after Traumatic Brain Injury, Cell Transplant. 25 (2016) 1863–1877. https://doi.org/10.3727/096368916X691150.

[55] C.P. Hofstetter, N.A.V. Holmström, J.A. Lilja, P. Schweinhardt, J. Hao, C. Spenger, Z. Wiesenfeld-Hallin, S.N. Kurpad, J. Frisén, L. Olson, Allodynia limits the usefulness of intraspinal neural stem cell grafts; directed differentiation improves outcome, Nat. Neurosci. 8 (2005) 346–353. https://doi.org/10.1038/nn1405.

[56] H. Kumamaru, H. Saiwai, K. Kubota, K. Kobayakawa, K. Yokota, Y. Ohkawa, K. Shiba, Y. Iwamoto, S. Okada, Therapeutic activities of engrafted neural stem/precursor cells are not dormant in the chronically injured spinal cord, Stem Cells Dayt. Ohio. 31 (2013) 1535–1547. https://doi.org/10.1002/stem.1404.

[57] Y.-C. Hsu, D.-C. Lee, I.-M. Chiu, Neural Stem Cells, Neural Progenitors, and Neurotrophic Factors, Cell Transplant. 16 (2007) 133–150. https://doi.org/10.3727/000000007783464678.

[58] P. Lu, L.L. Jones, E.Y. Snyder, M.H. Tuszynski, Neural stem cells constitutively secrete neurotrophic factors and promote extensive host axonal growth after spinal cord injury, Exp. Neurol. 181 (2003) 115–129. https://doi.org/10.1016/S0014-4886(03)00037-2.

[59] J. Jäderstad, L.M. Jäderstad, J. Li, S. Chintawar, C. Salto, M. Pandolfo, V. Ourednik, Y.D. Teng, R.L. Sidman, E. Arenas, E.Y. Snyder, E. Herlenius, Communication via gap junctions underlies early functional and beneficial interactions between grafted neural stem cells and the host, Proc. Natl. Acad. Sci. 107 (2010) 5184–5189. https://doi.org/10.1073/pnas.0915134107.

[60] E. Curtis, J.R. Martin, B. Gabel, N. Sidhu, T.K. Rzesiewicz, R. Mandeville, S.V. Gorp, M. Leerink, T. Tadokoro, S. Marsala, C. Jamieson, M. Marsala, J.D. Ciacci, A First-in-Human, Phase I Study of Neural Stem Cell Transplantation for Chronic Spinal Cord Injury, Cell Stem Cell. 22 (2018) 941-950.e6. https://doi.org/10.1016/j.stem.2018.05.014.

[61] M. Nasser, N. Ballout, S. Mantash, F. Bejjani, F. Najdi, N. Ramadan, J. Soueid, K. Zibara, F. Kobeissy, Transplantation of Embryonic Neural Stem Cells and Differentiated Cells in a Controlled Cortical Impact (CCI) Model of Adult Mouse Somatosensory Cortex, Front.

Neurol. 9 (2018). https://www.frontiersin.org/articles/10.3389/fneur.2018.00895 (accessed August 30, 2022).

[62] A.-L. Pang, L.-L. Xiong, Q.-J. Xia, F. Liu, Y.-C. Wang, F. Liu, P. Zhang, B.-L. Meng, S. Tan, T.-H. Wang, Neural Stem Cell Transplantation Is Associated with Inhibition of Apoptosis, Bcl-xL Upregulation, and Recovery of Neurological Function in a Rat Model of Traumatic Brain Injury, Cell Transplant. 26 (2017) 1262–1275. https://doi.org/10.1177/0963689717715168.

[63] J. Gao, R.J. Grill, T.J. Dunn, S. Bedi, J.A. Labastida, R.A. Hetz, H. Xue, J.R. Thonhoff, D.S. DeWitt, D.S. Prough, C.S. Cox, P. Wu, Human Neural Stem Cell Transplantation-Mediated Alteration of Microglial/Macrophage Phenotypes after Traumatic Brain Injury, Cell Transplant. 25 (2016) 1863–1877. https://doi.org/10.3727/096368916X691150.

[64] F. Barnabé-Heider, C. Göritz, H. Sabelström, H. Takebayashi, F.W. Pfrieger, K. Meletis, J. Frisén, Origin of New Glial Cells in Intact and Injured Adult Spinal Cord, Cell Stem Cell. 7 (2010) 470–482. https://doi.org/10.1016/j.stem.2010.07.014.

[65] M. Sundberg, P.-H. Andersson, E. Åkesson, J. Odeberg, L. Holmberg, J. Inzunza, S. Falci, J. Öhman, R. Suuronen, H. Skottman, K. Lehtimäki, O. Hovatta, S. Narkilahti, E. Sundström, Markers of Pluripotency and Differentiation in Human Neural Precursor Cells Derived from Embryonic Stem Cells and CNS Tissue, Cell Transplant. 20 (2011) 177–192. https://doi.org/10.3727/096368910X527266.

[66] E. Akesson, J.-H. Piao, E.-B. Samuelsson, L. Holmberg, A. Kjaeldgaard, S. Falci, E. Sundström, A. Seiger, Long-term culture and neuronal survival after intraspinal transplantation of human spinal cord-derived neurospheres, Physiol. Behav. 92 (2007) 60–66. https://doi.org/10.1016/j.physbeh.2007.05.056.

[67] H. Zhou, S. Lu, K. Li, Y. Yang, C. Hu, Z. Wang, Q. Wang, Y. He, X. Wang, D. Ye, Q. Guan, J. Zang, C. Liu, S. Qu, Z. Luan, Study on the Safety of Human Oligodendrocyte Precursor Cell Transplantation in Young Animals and Its Efficacy on Myelination, Stem Cells Dev. 30 (2021) 587–600. https://doi.org/10.1089/scd.2021.0012.

[68] N. Nagoshi, M. Khazaei, J. Ahlfors, C.S. Ahuja, S. Nori, J. Wang, S. Shibata, M.G. Fehlings, Human Spinal Oligodendrogenic Neural Progenitor Cells Promote Functional Recovery After Spinal Cord Injury by Axonal Remyelination and Tissue Sparing, Stem Cells Transl. Med. 7 (2018) 806–818. https://doi.org/10.1002/sctm.17-0269.

[69] A.P. Tran, P.M. Warren, J. Silver, The Biology of Regeneration Failure and Success After Spinal Cord Injury, Physiol. Rev. 98 (2018) 881–917. https://doi.org/10.1152/physrev.00017.2017.

[70] S. Nori, M. Khazaei, C.S. Ahuja, K. Yokota, J.-E. Ahlfors, Y. Liu, J. Wang, S. Shibata, J. Chio, M.H. Hettiaratchi, T. Führmann, M.S. Shoichet, M.G. Fehlings, Human Oligodendrogenic Neural Progenitor Cells Delivered with Chondroitinase ABC Facilitate Functional Repair of Chronic Spinal Cord Injury, Stem Cell Rep. 11 (2018) 1433–1448. https://doi.org/10.1016/j.stemcr.2018.10.017.

[71] K. Takahashi, S. Yamanaka, Induction of pluripotent stem cells from mouse embryonic and adult fibroblast cultures by defined factors, Cell. 126 (2006) 663–676. https://doi.org/10.1016/j.cell.2006.07.024.

[72] K. Takahashi, K. Tanabe, M. Ohnuki, M. Narita, T. Ichisaka, K. Tomoda, S. Yamanaka, Induction of pluripotent stem cells from adult human fibroblasts by defined factors, Cell. 131 (2007) 861–872. https://doi.org/10.1016/j.cell.2007.11.019.

[73] S. Kawabata, M. Takano, Y. Numasawa-Kuroiwa, G. Itakura, Y. Kobayashi, Y. Nishiyama, K. Sugai, S. Nishimura, H. Iwai, M. Isoda, S. Shibata, J. Kohyama, A. Iwanami, Y. Toyama, M. Matsumoto, M. Nakamura, H. Okano, Grafted Human iPS Cell-Derived Oligodendrocyte Precursor Cells Contribute to Robust Remyelination of Demyelinated Axons after Spinal Cord Injury, Stem Cell Rep. 6 (2016) 1–8. https://doi.org/10.1016/j.stemcr.2015.11.013.

[74] P. Lu, G. Woodruff, Y. Wang, L. Graham, M. Hunt, D. Wu, E. Boehle, R. Ahmad, G. Poplawski, J. Brock, L.S.B. Goldstein, M.H. Tuszynski, Long-distance axonal growth from human induced

pluripotent stem cells after spinal cord injury, Neuron. 83 (2014) 789–796. https://doi.org/10.1016/j.neuron.2014.07.014.

[75] Y. Kobayashi, Y. Okada, G. Itakura, H. Iwai, S. Nishimura, A. Yasuda, S. Nori, K. Hikishima, T. Konomi, K. Fujiyoshi, O. Tsuji, Y. Toyama, S. Yamanaka, M. Nakamura, H. Okano, Pre-evaluated safe human iPSC-derived neural stem cells promote functional recovery after spinal cord injury in common marmoset without tumorigenicity, PloS One. 7 (2012) e52787. https://doi.org/10.1371/journal.pone.0052787.

[76] S. Nori, Y. Okada, A. Yasuda, O. Tsuji, Y. Takahashi, Y. Kobayashi, K. Fujiyoshi, M. Koike, Y. Uchiyama, E. Ikeda, Y. Toyama, S. Yamanaka, M. Nakamura, H. Okano, Grafted human-induced pluripotent stem-cell–derived neurospheres promote motor functional recovery after spinal cord injury in mice, Proc. Natl. Acad. Sci. 108 (2011) 16825–16830. https://doi.org/10.1073/pnas.1108077108.

[77] R.P. Salewski, R.A. Mitchell, L. Li, C. Shen, M. Milekovskaia, A. Nagy, M.G. Fehlings, Transplantation of Induced Pluripotent Stem Cell-Derived Neural Stem Cells Mediate Functional Recovery Following Thoracic Spinal Cord Injury Through Remyelination of Axons, Stem Cells Transl. Med. 4 (2015) 743–754. https://doi.org/10.5966/sctm.2014-0236.

[78] T. Okubo, N. Nagoshi, J. Kohyama, O. Tsuji, M. Shinozaki, S. Shibata, Y. Kase, M. Matsumoto, M. Nakamura, H. Okano, Treatment with a Gamma-Secretase Inhibitor Promotes Functional Recovery in Human iPSC- Derived Transplants for Chronic Spinal Cord Injury, Stem Cell Rep. 11 (2018) 1416–1432. https://doi.org/10.1016/j.stemcr.2018.10.022.

[79] J. Dunkerson, K.E. Moritz, J. Young, T. Pionk, K. Fink, J. Rossignol, G. Dunbar, J.S. Smith, Combining enriched environment and induced pluripotent stem cell therapy results in improved cognitive and motor function following traumatic brain injury, Restor. Neurol. Neurosci. 32 (2014) 675–687. https://doi.org/10.3233/RNN-140408.

[80] H. Tang, H. Sha, H. Sun, X. Wu, L. Xie, P. Wang, C. Xu, C. Larsen, H.L. Zhang, Y. Gong, Y. Mao, X. Chen, L. Zhou, X. Feng, J. Zhu, Tracking induced pluripotent stem cells-derived neural stem cells in the central nervous system of rats and monkeys, Cell. Reprogramming. 15 (2013) 435–442. https://doi.org/10.1089/cell.2012.0081.

[81] M.D. Nieves, O. Furmanski, M.L. Doughty, Host sex and transplanted human induced pluripotent stem cell phenotype interact to influence sensorimotor recovery in a mouse model of cortical contusion injury, Brain Res. 1748 (2020) 147120. https://doi.org/10.1016/j.brainres.2020.147120.

[82] N. Amariglio, A. Hirshberg, B.W. Scheithauer, Y. Cohen, R. Loewenthal, L. Trakhtenbrot, N. Paz, M. Koren-Michowitz, D. Waldman, L. Leider-Trejo, A. Toren, S. Constantini, G. Rechavi, Donor-Derived Brain Tumor Following Neural Stem Cell Transplantation in an Ataxia Telangiectasia Patient, PLOS Med. 6 (2009) e1000029. https://doi.org/10.1371/journal.pmed.1000029.

[83] C.-Y. Huang, C.-L. Liu, C.-Y. Ting, Y.-T. Chiu, Y.-C. Cheng, M.W. Nicholson, P.C.H. Hsieh, Human iPSC banking: barriers and opportunities, J. Biomed. Sci. 26 (2019) 87. https://doi.org/10.1186/s12929-019-0578-x.

[84] V.R. Dasari, K.K. Veeravalli, D.H. Dinh, Mesenchymal stem cells in the treatment of spinal cord injuries: A review, World J. Stem Cells. 6 (2014) 120–133. https://doi.org/10.4252/wjsc.v6.i2.120.

[85] Y. Ohta, M. Takenaga, Y. Tokura, A. Hamaguchi, T. Matsumoto, K. Kano, H. Mugishima, H. Okano, R. Igarashi, Mature adipocyte-derived cells, dedifferentiated fat cells (DFAT), promoted functional recovery from spinal cord injury-induced motor dysfunction in rats, Cell Transplant. 17 (2008) 877–886. https://doi.org/10.3727/096368908786576516.

[86] V. Neirinckx, B. Rogister, R. Franzen, S. Wislet-Gendebien, Bone marrow stromal stem cells transplantation in mice with acute spinal cord injury, Methods Mol. Biol. Clifton NJ. 1213 (2014) 257–264. https://doi.org/10.1007/978-1-4939-1453-1_21.

[87] A.-M. Liu, B.-L. Chen, L.-T. Yu, T. Liu, L.-L. Shi, P.-P. Yu, Y.-B. Qu, K.-F. So, L.-B. Zhou, Human adipose tissue- and umbilical cord-derived stem cells: which is a better alternative to treat

spinal cord injury?, Neural Regen. Res. 15 (2020) 2306–2317. https://doi.org/10.4103/1673-5374.284997.

[88] H. Nakajima, K. Uchida, A.R. Guerrero, S. Watanabe, D. Sugita, N. Takeura, A. Yoshida, G. Long, K.T. Wright, W.E.B. Johnson, H. Baba, Transplantation of mesenchymal stem cells promotes an alternative pathway of macrophage activation and functional recovery after spinal cord injury, J. Neurotrauma. 29 (2012) 1614–1625. https://doi.org/10.1089/neu.2011.2109.

[89] T. Morita, M. Sasaki, Y. Kataoka-Sasaki, M. Nakazaki, H. Nagahama, S. Oka, T. Oshigiri, T. Takebayashi, T. Yamashita, J.D. Kocsis, O. Honmou, Intravenous infusion of mesenchymal stem cells promotes functional recovery in a model of chronic spinal cord injury, Neuroscience. 335 (2016) 221–231. https://doi.org/10.1016/j.neuroscience.2016.08.037.

[90] P.-C. Jiang, W.-P. Xiong, G. Wang, C. Ma, W.-Q. Yao, S.F. Kendell, B.M. Mehling, X.-H. Yuan, D.-C. Wu, A clinical trial report of autologous bone marrow-derived mesenchymal stem cell transplantation in patients with spinal cord injury, Exp. Ther. Med. 6 (2013) 140–146. https://doi.org/10.3892/etm.2013.1083.

[91] D. Jarocha, O. Milczarek, A. Wedrychowicz, S. Kwiatkowski, M. Majka, Continuous improvement after multiple mesenchymal stem cell transplantations in a patient with complete spinal cord injury, Cell Transplant. 24 (2015) 661–672. https://doi.org/10.3727/096368915X687796.

[92] W.A. El-Kheir, H. Gabr, M.R. Awad, O. Ghannam, Y. Barakat, H.A.M.A. Farghali, Z.M. El Maadawi, I. Ewes, H.E. Sabaawy, Autologous bone marrow-derived cell therapy combined with physical therapy induces functional improvement in chronic spinal cord injury patients, Cell Transplant. 23 (2014) 729–745. https://doi.org/10.3727/096368913X664540.

[93] G. Dai, X. Liu, Z. Zhang, Z. Yang, Y. Dai, R. Xu, Transplantation of autologous bone marrow mesenchymal stem cells in the treatment of complete and chronic cervical spinal cord injury, Brain Res. 1533 (2013) 73–79. https://doi.org/10.1016/j.brainres.2013.08.016.

[94] S.K. Oh, K.H. Choi, J.Y. Yoo, D.Y. Kim, S.J. Kim, S.R. Jeon, A Phase III Clinical Trial Showing Limited Efficacy of Autologous Mesenchymal Stem Cell Therapy for Spinal Cord Injury, Neurosurgery. 78 (2016) 436–447; discussion 447. https://doi.org/10.1227/NEU.0000000000001056.

[95] Y. Zhao, S.L. Gibb, J. Zhao, A.N. Moore, M.J. Hylin, T. Menge, H. Xue, G. Baimukanova, D. Potter, E.M. Johnson, J.B. Holcomb, C.S. Cox Jr, P.K. Dash, S. Pati, Wnt3a, a Protein Secreted by Mesenchymal Stem Cells Is Neuroprotective and Promotes Neurocognitive Recovery Following Traumatic Brain Injury, Stem Cells. 34 (2016) 1263–1272. https://doi.org/10.1002/stem.2310.

[96] M. Kawabori, A.H. Weintraub, H. Imai, I. Zinkevych, P. McAllister, G.K. Steinberg, B.M. Frishberg, T. Yasuhara, J.W. Chen, S.C. Cramer, A.S. Achrol, N.E. Schwartz, J. Suenaga, D.C. Lu, I. Semeniv, H. Nakamura, D. Kondziolka, D. Chida, T. Kaneko, Y. Karasawa, S. Paadre, B. Nejadnik, D. Bates, A.H. Stonehouse, R.M. Richardson, D.O. Okonkwo, Cell Therapy for Chronic TBI: Interim Analysis of the Randomized Controlled STEMTRA Trial, Neurology. 96 (2021) e1202–e1214. https://doi.org/10.1212/WNL.0000000000011450.

[97] J. Luzuriaga, Y. Polo, O. Pastor-Alonso, B. Pardo-Rodríguez, A. Larrañaga, F. Unda, J.-R. Sarasua, J.R. Pineda, G. Ibarretxe, Advances and Perspectives in Dental Pulp Stem Cell Based Neuroregeneration Therapies, Int. J. Mol. Sci. 22 (2021) 3546. https://doi.org/10.3390/ijms22073546.

[98] J. Luzuriaga, O. Pastor-Alonso, J.M. Encinas, F. Unda, G. Ibarretxe, J.R. Pineda, Human Dental Pulp Stem Cells Grown in Neurogenic Media Differentiate Into Endothelial Cells and Promote Neovasculogenesis in the Mouse Brain, Front. Physiol. 10 (2019) 347. https://doi.org/10.3389/fphys.2019.00347.

[99] K. Sakai, A. Yamamoto, K. Matsubara, S. Nakamura, M. Naruse, M. Yamagata, K. Sakamoto, R. Tauchi, N. Wakao, S. Imagama, H. Hibi, K. Kadomatsu, N. Ishiguro, M. Ueda, Human dental pulp-derived stem cells promote locomotor recovery after complete transection of the rat

spinal cord by multiple neuro-regenerative mechanisms, J. Clin. Invest. 122 (2012) 80–90. https://doi.org/10.1172/JCI59251.

[100] D. Henriques, R. Moreira, J. Schwamborn, L. Pereira de Almeida, L.S. Mendonça, Successes and Hurdles in Stem Cells Application and Production for Brain Transplantation, Front. Neurosci. 13 (2019). https://www.frontiersin.org/articles/10.3389/fnins.2019.01194 (accessed August 22, 2022).

[101] S.M. Willerth, S.E. Sakiyama-Elbert, Combining Stem Cells and Biomaterial Scaffolds for Constructing Tissues and Cell Delivery, StemJournal. 1 (2019) 1–25. https://doi.org/10.3233/STJ-180001.

[102] M.Y. Chen, A. Hoffer, P.F. Morrison, J.F. Hamilton, J. Hughes, K.S. Schlageter, J. Lee, B.R. Kelly, E.H. Oldfield, Surface properties, more than size, limiting convective distribution of virus-sized particles and viruses in the central nervous system, J. Neurosurg. 103 (2005) 311–319. https://doi.org/10.3171/jns.2005.103.2.0311.

[103] Y. Bekku, L. Vargová, Y. Goto, I. Vorísek, L. Dmytrenko, M. Narasaki, A. Ohtsuka, R. Fässler, Y. Ninomiya, E. Syková, T. Oohashi, Bral1: its role in diffusion barrier formation and conduction velocity in the CNS, J. Neurosci. Off. J. Soc. Neurosci. 30 (2010) 3113–3123. https://doi.org/10.1523/JNEUROSCI.5598-09.2010.

[104] G. Dumsile Mahumane, P. Kumar, L.C. du Toit, Y. Essop Choonara, V. Pillay, 3D scaffolds for brain tissue regeneration: architectural challenges, Biomater. Sci. 6 (2018) 2812–2837. https://doi.org/10.1039/C8BM00422F.

[105] S. Liu, Y.-Y. Xie, B. Wang, Role and prospects of regenerative biomaterials in the repair of spinal cord injury, Neural Regen. Res. 14 (2019) 1352–1363. https://doi.org/10.4103/1673-5374.253512.

[106] C.M.A.P. Schuh, A.G.E. Day, H. Redl, J. Phillips, An Optimized Collagen-Fibrin Blend Engineered Neural Tissue Promotes Peripheral Nerve Repair, Tissue Eng. Part A. 24 (2018) 1332–1340. https://doi.org/10.1089/ten.TEA.2017.0457.

[107] S. Pina, V.P. Ribeiro, C.F. Marques, F.R. Maia, T.H. Silva, R.L. Reis, J.M. Oliveira, Scaffolding Strategies for Tissue Engineering and Regenerative Medicine Applications, Materials. 12 (2019) 1824. https://doi.org/10.3390/ma12111824.

[108] V.R. Sherman, W. Yang, M.A. Meyers, The materials science of collagen, J. Mech. Behav. Biomed. Mater. 52 (2015) 22–50. https://doi.org/10.1016/j.jmbbm.2015.05.023.

[109] A.R. Murphy, A. Laslett, C.M. O'Brien, N.R. Cameron, Scaffolds for 3D in vitro culture of neural lineage cells, Acta Biomater. 54 (2017) 1–20. https://doi.org/10.1016/j.actbio.2017.02.046.

[110] S. Han, J.Y. Lee, E.Y. Heo, I.K. Kwon, T.Y. Yune, I. Youn, Implantation of a Matrigel-loaded agarose scaffold promotes functional regeneration of axons after spinal cord injury in rat, Biochem. Biophys. Res. Commun. 496 (2018) 785–791. https://doi.org/10.1016/j.bbrc.2018.01.157.

[111] S. Han, Z. Xiao, X. Li, H. Zhao, B. Wang, Z. Qiu, Z. Li, X. Mei, B. Xu, C. Fan, B. Chen, J. Han, Y. Gu, H. Yang, Q. Shi, J. Dai, Human placenta-derived mesenchymal stem cells loaded on linear ordered collagen scaffold improves functional recovery after completely transected spinal cord injury in canine, Sci. China Life Sci. 61 (2018) 2–13. https://doi.org/10.1007/s11427-016-9002-6.

[112] Y. Zhao, F. Tang, Z. Xiao, G. Han, N. Wang, N. Yin, B. Chen, X. Jiang, C. Yun, W. Han, C. Zhao, S. Cheng, S. Zhang, J. Dai, Clinical Study of NeuroRegen Scaffold Combined with Human Mesenchymal Stem Cells for the Repair of Chronic Complete Spinal Cord Injury, Cell Transplant. 26 (2017) 891–900. https://doi.org/10.3727/096368917X695038.

[113] Z. Xiao, F. Tang, Y. Zhao, G. Han, N. Yin, X. Li, B. Chen, S. Han, X. Jiang, C. Yun, C. Zhao, S. Cheng, S. Zhang, J. Dai, Significant Improvement of Acute Complete Spinal Cord Injury Patients Diagnosed by a Combined Criteria Implanted with NeuroRegen Scaffolds and Mesenchymal Stem Cells, Cell Transplant. 27 (2018) 907–915. https://doi.org/10.1177/0963689718766279.

[114] N. Klapka, H.W. Müller, Collagen matrix in spinal cord injury, J. Neurotrauma. 23 (2006) 422–435. https://doi.org/10.1089/neu.2006.23.422.

[115] A. Seppänen, T. Suuronen, S.C. Hofmann, K. Majamaa, I. Alafuzoff, Distribution of collagen XVII in the human brain, Brain Res. 1158 (2007) 50–56. https://doi.org/10.1016/j.brainres.2007.04.073.

[116] L.M. Rappl, Physiological changes in tissues denervated by spinal cord injury tissues and possible effects on wound healing, Int. Wound J. 5 (2008) 435–444. https://doi.org/10.1111/j.1742-481X.2007.00360.x.

[117] M.A. Reina, A. López, M. Dittmann, J.A. De Andrés, Ultrastructure of Spinal Dura Mater, in: M.A. Reina, J.A. De Andrés, A. Hadzic, A. Prats-Galino, X. Sala-Blanch, A.A.J. van Zundert (Eds.), Atlas Funct. Anat. Reg. Anesth. Pain Med. Hum. Struct. Ultrastruct. 3D Reconstr. Images, Springer International Publishing, Cham, 2015: pp. 411–434. https://doi.org/10.1007/978-3-319-09522-6_20.

[118] X. Wang, Q. Ao, X. Tian, J. Fan, H. Tong, W. Hou, S. Bai, Gelatin-Based Hydrogels for Organ 3D Bioprinting, Polymers. 9 (2017) 401. https://doi.org/10.3390/polym9090401.

[119] L. Fan, C. Liu, X. Chen, Y. Zou, Z. Zhou, C. Lin, G. Tan, L. Zhou, C. Ning, Q. Wang, Directing Induced Pluripotent Stem Cell Derived Neural Stem Cell Fate with a Three-Dimensional Biomimetic Hydrogel for Spinal Cord Injury Repair, ACS Appl. Mater. Interfaces. 10 (2018) 17742–17755. https://doi.org/10.1021/acsami.8b05293.

[120] T. Ikeda, K. Ikeda, K. Yamamoto, H. Ishizaki, Y. Yoshizawa, K. Yanagiguchi, S. Yamada, Y. Hayashi, Fabrication and Characteristics of Chitosan Sponge as a Tissue Engineering Scaffold, BioMed Res. Int. 2014 (2014) 786892. https://doi.org/10.1155/2014/786892.

[121] J. Chedly, S. Soares, A. Montembault, Y. von Boxberg, M. Veron-Ravaille, C. Mouffle, M.-N. Benassy, J. Taxi, L. David, F. Nothias, Physical chitosan microhydrogels as scaffolds for spinal cord injury restoration and axon regeneration, Biomaterials. 138 (2017) 91–107. https://doi.org/10.1016/j.biomaterials.2017.05.024.

[122] Z. Hua-bin, L. Lin, C. Lu, Tissue-engineered spinal cord construction by chitosan alginate scaffold and adipose-derived mesenchymal stem cells in the treatment of acute spinal cord injury, Chin. J. Tissue Eng. Res. 21 (2017) 4199. https://doi.org/10.3969/j.issn.2095-4344.2017.26.017.

[123] J. Zhang, X. Lu, G. Feng, Z. Gu, Y. Sun, G. Bao, G. Xu, Y. Lu, J. Chen, L. Xu, X. Feng, Z. Cui, Chitosan scaffolds induce human dental pulp stem cells to neural differentiation: potential roles for spinal cord injury therapy, Cell Tissue Res. 366 (2016) 129–142. https://doi.org/10.1007/s00441-016-2402-1.

[124] S.-H. Hsu, W.-C. Kuo, Y.-T. Chen, C.-T. Yen, Y.-F. Chen, K.-S. Chen, W.-C. Huang, H. Cheng, New nerve regeneration strategy combining laminin-coated chitosan conduits and stem cell therapy, Acta Biomater. 9 (2013) 6606–6615. https://doi.org/10.1016/j.actbio.2013.01.025.

[125] S.M. Amr, A. Gouda, W.T. Koptan, A.A. Galal, D.S. Abdel-Fattah, L.A. Rashed, H.M. Atta, M.T. Abdel-Aziz, Bridging defects in chronic spinal cord injury using peripheral nerve grafts combined with a chitosan-laminin scaffold and enhancing regeneration through them by co-transplantation with bone-marrow-derived mesenchymal stem cells: Case series of 14 patients, J. Spinal Cord Med. 37 (2014) 54–71. https://doi.org/10.1179/2045772312Y.0000000069.

[126] V.A. Kornev, E.A. Grebenik, A.B. Solovieva, R.I. Dmitriev, P.S. Timashev, Hydrogel-assisted neuroregeneration approaches towards brain injury therapy: A state-of-the-art review, Comput. Struct. Biotechnol. J. 16 (2018) 488–502. https://doi.org/10.1016/j.csbj.2018.10.011.

[127] S.V. Kushchayev, M.B. Giers, D. Hom Eng, N.L. Martirosyan, J.M. Eschbacher, M.M. Mortazavi, N. Theodore, A. Panitch, M.C. Preul, Hyaluronic acid scaffold has a neuroprotective effect in hemisection spinal cord injury, J. Neurosurg. Spine. 25 (2016) 114–124. https://doi.org/10.3171/2015.9.SPINE15628.

[128] P. Sensharma, G. Madhumathi, R.D. Jayant, A.K. Jaiswal, Biomaterials and cells for neural tissue engineering: Current choices, Mater. Sci. Eng. C Mater. Biol. Appl. 77 (2017) 1302–1315. https://doi.org/10.1016/j.msec.2017.03.264.

[129] S.K. Seidlits, Z.Z. Khaing, R.R. Petersen, J.D. Nickels, J.E. Vanscoy, J.B. Shear, C.E. Schmidt, The effects of hyaluronic acid hydrogels with tunable mechanical properties on neural progenitor cell differentiation, Biomaterials. 31 (2010) 3930–3940. https://doi.org/10.1016/j.biomaterials.2010.01.125.

[130] S.H. Oh, D.B. An, T.H. Kim, J.H. Lee, Wide-range stiffness gradient PVA/HA hydrogel to investigate stem cell differentiation behavior, Acta Biomater. 35 (2016) 23–31. https://doi.org/10.1016/j.actbio.2016.02.016.

[131] X. Wang, J. He, Y. Wang, F.-Z. Cui, Hyaluronic acid-based scaffold for central neural tissue engineering, Interface Focus. 2 (2012) 278–291. https://doi.org/10.1098/rsfs.2012.0016.

[132] J. Zhong, A. Chan, L. Morad, H.I. Kornblum, G. Fan, S.T. Carmichael, Hydrogel Matrix to Support Stem Cell Survival After Brain Transplantation in Stroke, Neurorehabil. Neural Repair. 24 (2010) 636–644. https://doi.org/10.1177/1545968310361958.

[133] N. Mansouri, S.F. Al-Sarawi, J. Mazumdar, D. Losic, Advancing fabrication and properties of three-dimensional graphene–alginate scaffolds for application in neural tissue engineering, RSC Adv. 9 (2019) 36838–36848. https://doi.org/10.1039/C9RA07481C.

[134] A. Banerjee, M. Arha, S. Choudhary, R.S. Ashton, S.R. Bhatia, D.V. Schaffer, R.S. Kane, The influence of hydrogel modulus on the proliferation and differentiation of encapsulated neural stem cells, Biomaterials. 30 (2009) 4695–4699. https://doi.org/10.1016/j.biomaterials.2009.05.050.

[135] M. Matyash, F. Despang, C. Ikonomidou, M. Gelinsky, Swelling and mechanical properties of alginate hydrogels with respect to promotion of neural growth, Tissue Eng. Part C Methods. 20 (2014) 401–411. https://doi.org/10.1089/ten.TEC.2013.0252.

[136] S.M. Hosseini, A. Sharafkhah, O. Koohi-Hosseinabadi, M. Semsar-Kazerooni, Transplantation of Neural Stem Cells Cultured in Alginate Scaffold for Spinal Cord Injury in Rats, Asian Spine J. 10 (2016) 611–618. https://doi.org/10.4184/asj.2016.10.4.611.

[137] I. Caron, F. Rossi, S. Papa, R. Aloe, M. Sculco, E. Mauri, A. Sacchetti, E. Erba, N. Panini, V. Parazzi, M. Barilani, G. Forloni, G. Perale, L. Lazzari, P. Veglianese, A new three dimensional biomimetic hydrogel to deliver factors secreted by human mesenchymal stem cells in spinal cord injury, Biomaterials. 75 (2016) 135–147. https://doi.org/10.1016/j.biomaterials.2015.10.024.

[138] P.J. Johnson, S.R. Parker, S.E. Sakiyama-Elbert, Fibrin-based tissue engineering scaffolds enhance neural fiber sprouting and delays the accumulation of reactive astrocytes at the lesion in a subacute model of spinal cord injury, J. Biomed. Mater. Res. A. 92 (2010) 152–163. https://doi.org/10.1002/jbm.a.32343.

[139] S. Yao, S. Yu, Z. Cao, Y. Yang, X. Yu, H.-Q. Mao, L.-N. Wang, X. Sun, L. Zhao, X. Wang, Hierarchically aligned fibrin nanofiber hydrogel accelerated axonal regrowth and locomotor function recovery in rat spinal cord injury, Int. J. Nanomedicine. 13 (2018) 2883–2895. https://doi.org/10.2147/IJN.S159356.

[140] E.S. Rosenzweig, J.H. Brock, P. Lu, H. Kumamaru, E.A. Salegio, K. Kadoya, J.L. Weber, J.J. Liang, R. Moseanko, S. Hawbecker, J.R. Huie, L.A. Havton, Y.S. Nout-Lomas, A.R. Ferguson, M.S. Beattie, J.C. Bresnahan, M.H. Tuszynski, Restorative Effects of Human Neural Stem Cell Grafts to the Primate Spinal Cord, Nat. Med. 24 (2018) 484–490. https://doi.org/10.1038/nm.4502.

[141] H. Iwai, H. Shimada, S. Nishimura, Y. Kobayashi, G. Itakura, K. Hori, K. Hikishima, H. Ebise, N. Negishi, S. Shibata, S. Habu, Y. Toyama, M. Nakamura, H. Okano, Allogeneic Neural Stem/Progenitor Cells Derived From Embryonic Stem Cells Promote Functional Recovery After Transplantation Into Injured Spinal Cord of Nonhuman Primates, Stem Cells Transl. Med. 4 (2015) 708–719. https://doi.org/10.5966/sctm.2014-0215.

[142] Y.O. Mukhamedshina, E.R. Akhmetzyanova, A.A. Kostennikov, E.Y. Zakirova, L.R. Galieva, E.E. Garanina, A.A. Rogozin, A.P. Kiassov, A.A. Rizvanov, Adipose-Derived Mesenchymal Stem Cell Application Combined With Fibrin Matrix Promotes Structural and Functional Recovery Following Spinal Cord Injury in Rats, Front. Pharmacol. 9 (2018) 343. https://doi.org/10.3389/fphar.2018.00343.

[143] M.J. Buckenmeyer, T.J. Meder, T.A. Prest, B.N. Brown, Decellularization techniques and their applications for the repair and regeneration of the nervous system, Methods San Diego Calif. 171 (2020) 41–61. https://doi.org/10.1016/j.ymeth.2019.07.023.

[144] P.M. Crapo, C.J. Medberry, J.E. Reing, S. Tottey, Y. van der Merwe, K.E. Jones, S.F. Badylak, Biologic scaffolds composed of central nervous system extracellular matrix, Biomaterials. 33 (2012) 3539–3547. https://doi.org/10.1016/j.biomaterials.2012.01.044.

[145] Y.-H. Wang, J. Chen, J. Zhou, F. Nong, J.-H. Lv, J. Liu, Reduced inflammatory cell recruitment and tissue damage in spinal cord injury by acellular spinal cord scaffold seeded with mesenchymal stem cells, Exp. Ther. Med. 13 (2017) 203–207. https://doi.org/10.3892/etm.2016.3941.

[146] H. Yin, T. Jiang, X. Deng, M. Yu, H. Xing, X. Ren, A cellular spinal cord scaffold seeded with rat adipose-derived stem cells facilitates functional recovery via enhancing axon regeneration in spinal cord injured rats, Mol. Med. Rep. 17 (2018) 2998–3004. https://doi.org/10.3892/mmr.2017.8238.

[147] L. Zhang, F. Zhang, Z. Weng, B.N. Brown, H. Yan, X.M. Ma, P.S. Vosler, S.F. Badylak, C.E. Dixon, X.T. Cui, J. Chen, Effect of an Inductive Hydrogel Composed of Urinary Bladder Matrix Upon Functional Recovery Following Traumatic Brain Injury, Tissue Eng. Part A. 19 (2013) 1909–1918. https://doi.org/10.1089/ten.tea.2012.0622.

[148] J.Y. Wang, A.K.F. Liou, Z.H. Ren, L. Zhang, B.N. Brown, X.T. Cui, S.F. Badylak, Y.N. Cai, Y.Q. Guan, R.K. Leak, J. Chen, X. Ji, L. Chen, Neurorestorative Effect of Urinary Bladder Matrix-Mediated Neural Stem Cell Transplantation Following Traumatic Brain Injury in Rats, CNS Neurol. Disord. - Drug Targets. 12 (n.d.) 413–425. https://www.eurekaselect.com/article/51418 (accessed September 3, 2022).

[149] H. Shin, S. Jo, A.G. Mikos, Biomimetic materials for tissue engineering., Biomaterials. 24 (2003) 4353–4364. https://doi.org/10.1016/s0142-9612(03)00339-9.

[150] M.P. Lutolf, P.M. Gilbert, H.M. Blau, Designing materials to direct stem-cell fate., Nature. 462 (2009) 433–441. https://doi.org/10.1038/nature08602.

[151] A.M. Bratt-Leal, R.L. Carpenedo, M.D. Ungrin, P.W. Zandstra, T.C. McDevitt, Incorporation of biomaterials in multicellular aggregates modulates pluripotent stem cell differentiation., Biomaterials. 32 (2011) 48–56. https://doi.org/10.1016/j.biomaterials.2010.08.113.

[152] A. Larrañaga, P. Aldazabal, F.J. Martin, J.R. Sarasua, Hydrolytic degradation and bioactivity of lactide and caprolactone based sponge-like scaffolds loaded with bioactive glass particles, Polym. Degrad. Stab. 110 (2014) 121–128. https://doi.org/10.1016/j.polymdegradstab.2014.08.021.

[153] D. Shahriari, J.Y. Koffler, M.H. Tuszynski, W.M. Campana, J.S. Sakamoto, Hierarchically Ordered Porous and High-Volume Polycaprolactone Microchannel Scaffolds Enhanced Axon Growth in Transected Spinal Cords, Tissue Eng. Part A. 23 (2017) 415–425. https://doi.org/10.1089/ten.tea.2016.0378.

[154] P.S. Donoghue, R. Lamond, S.D. Boomkamp, T. Sun, N. Gadegaard, M.O. Riehle, S.C. Barnett, The development of a ε-polycaprolactone scaffold for central nervous system repair, Tissue Eng. Part A. 19 (2013) 497–507. https://doi.org/10.1089/ten.TEA.2012.0382.

[155] N.A. Silva, R.A. Sousa, J.S. Fraga, M. Fontes, H. Leite-Almeida, R. Cerqueira, A. Almeida, N. Sousa, R.L. Reis, A.J. Salgado, Benefits of spine stabilization with biodegradable scaffolds in spinal cord injured rats, Tissue Eng. Part C Methods. 19 (2013) 101–108. https://doi.org/10.1089/ten.TEC.2012.0264.

[156] P. Terraf, S.M. Kouhsari, J. Ai, H. Babaloo, Tissue-Engineered Regeneration of Hemisected Spinal Cord Using Human Endometrial Stem Cells, Poly ε-Caprolactone Scaffolds, and Crocin as a Neuroprotective Agent, Mol. Neurobiol. 54 (2017) 5657–5667. https://doi.org/10.1007/s12035-016-0089-7.

[157] D.Y. Wong, S.J. Hollister, P.H. Krebsbach, C. Nosrat, Poly(epsilon-caprolactone) and poly (L-lactic-co-glycolic acid) degradable polymer sponges attenuate astrocyte response and lesion growth in acute traumatic brain injury, Tissue Eng. 13 (2007) 2515–2523. https://doi.org/10.1089/ten.2006.0440.

[158] A. Hurtado, J.M. Cregg, H.B. Wang, D.F. Wendell, M. Oudega, R.J. Gilbert, J.W. McDonald, Robust CNS regeneration after complete spinal cord transection using aligned poly-l-lactic acid microfibers, Biomaterials. 32 (2011) 6068–6079. https://doi.org/10.1016/j.biomaterials.2011.05.006.

[159] R.J. Colello, W.N. Chow, J.W. Bigbee, C. Lin, D. Dalton, D. Brown, B.S. Jha, B.E. Mathern, K.D. Lee, D.G. Simpson, The incorporation of growth factor and chondroitinase ABC into an electrospun scaffold to promote axon regrowth following spinal cord injury, J. Tissue Eng. Regen. Med. 10 (2016) 656–668. https://doi.org/10.1002/term.1805.

[160] A. Hurtado, L.D.F. Moon, V. Maquet, B. Blits, R. Jérôme, M. Oudega, Poly (d,l-lactic acid) macroporous guidance scaffolds seeded with Schwann cells genetically modified to secrete a bi-functional neurotrophin implanted in the completely transected adult rat thoracic spinal cord, Biomaterials. 27 (2006) 430–442. https://doi.org/10.1016/j.biomaterials.2005.07.014.

[161] J. Cai, K.S. Ziemba, G.M. Smith, Y. Jin, Evaluation of cellular organization and axonal regeneration through linear PLA foam implants in acute and chronic spinal cord injury, J. Biomed. Mater. Res. A. 83 (2007) 512–520. https://doi.org/10.1002/jbm.a.31296.

[162] J. Ding, J. Zhang, J. Li, D. Li, C. Xiao, H. Xiao, H. Yang, X. Zhuang, X. Chen, Electrospun polymer biomaterials, Prog. Polym. Sci. 90 (2019) 1–34. https://doi.org/10.1016/j.progpolymsci.2019.01.002.

[163] C. Martins, F. Sousa, F. Araújo, B. Sarmento, Functionalizing PLGA and PLGA Derivatives for Drug Delivery and Tissue Regeneration Applications, Adv. Healthc. Mater. 7 (2018) 1701035. https://doi.org/10.1002/adhm.201701035.

[164] J.D. Guest, S.W. Moore, A.A. Aimetti, A.B. Kutikov, A.J. Santamaria, C.P. Hofstetter, A.E. Ropper, N. Theodore, T.R. Ulich, R.T. Layer, Internal decompression of the acutely contused spinal cord: Differential effects of irrigation only versus biodegradable scaffold implantation, Biomaterials. 185 (2018) 284–300. https://doi.org/10.1016/j.biomaterials.2018.09.025.

[165] A.J. Krych, G.E. Rooney, B. Chen, T.C. Schermerhorn, S. Ameenuddin, L. Gross, M.J. Moore, B.L. Currier, R.J. Spinner, J.A. Friedman, M.J. Yaszemski, A.J. Windebank, Relationship between scaffold channel diameter and number of regenerating axons in the transected rat spinal cord, Acta Biomater. 5 (2009) 2551–2559. https://doi.org/10.1016/j.actbio.2009.03.021.

[166] L. He, Y. Zhang, C. Zeng, M. Ngiam, S. Liao, D. Quan, Y. Zeng, J. Lu, S. Ramakrishna, Manufacture of PLGA multiple-channel conduits with precise hierarchical pore architectures and in vitro/vivo evaluation for spinal cord injury, Tissue Eng. Part C Methods. 15 (2009) 243–255. https://doi.org/10.1089/ten.tec.2008.0255.

[167] N. Theodore, R. Hlubek, J. Danielson, K. Neff, L. Vaickus, T.R. Ulich, A.E. Ropper, First Human Implantation of a Bioresorbable Polymer Scaffold for Acute Traumatic Spinal Cord Injury: A Clinical Pilot Study for Safety and Feasibility, Neurosurgery. 79 (2016) E305-312. https://doi.org/10.1227/NEU.0000000000001283.

[168] B.G. Kim, Y.M. Kang, J.H. Phi, Y.-H. Kim, D.H. Hwang, J.Y. Choi, S. Ryu, A.-E. Elastal, S.H. Paek, K.-C. Wang, S.-H. Lee, S.U. Kim, B.-W. Yoon, Implantation of polymer scaffolds seeded with neural stem cells in a canine spinal cord injury model, Cytotherapy. 12 (2010) 841–845. https://doi.org/10.3109/14653249.2010.501784.

[169] C.D. Pritchard, J.R. Slotkin, D. Yu, H. Dai, M.S. Lawrence, R.T. Bronson, F.M. Reynolds, Y.D. Teng, E.J. Woodard, R.S. Langer, Establishing a model spinal cord injury in the African green monkey for the preclinical evaluation of biodegradable polymer scaffolds seeded with human neural stem cells, J. Neurosci. Methods. 188 (2010) 258–269. https://doi.org/10.1016/j.jneumeth.2010.02.019.

[170] K.N. Kang, J.Y. Lee, D.Y. Kim, B.N. Lee, H.H. Ahn, B. Lee, G. Khang, S.R. Park, B.H. Min, J.H. Kim, H.B. Lee, M.S. Kim, Regeneration of Completely Transected Spinal Cord Using Scaffold of Poly(D,L-Lactide-co-Glycolide)/Small Intestinal Submucosa Seeded with Rat Bone Marrow Stem Cells, Tissue Eng. Part A. 17 (2011) 2143–2152. https://doi.org/10.1089/ten.tea.2011.0122.

[171] W. Tang, F. Fang, K. Liu, Z. Huang, H. Li, Y. Yin, J. Wang, G. Wang, L. Wei, Y. Ou, Y. Wang, Aligned Biofunctional Electrospun PLGA-LysoGM1 Scaffold for Traumatic Brain Injury Repair, ACS Biomater. Sci. Eng. 6 (2020) 2209–2218. https://doi.org/10.1021/acsbiomaterials.9b01636.

[172] A.A. D'souza, R. Shegokar, Polyethylene glycol (PEG): a versatile polymer for pharmaceutical applications, Expert Opin. Drug Deliv. 13 (2016) 1257–1275. https://doi.org/10.1080/17425247.2016.1182485.

[173] J. Luo, R. Shi, Diffusive oxidative stress following acute spinal cord injury in guinea pigs and its inhibition by polyethylene glycol, Neurosci. Lett. 359 (2004) 167–170. https://doi.org/10.1016/j.neulet.2004.02.027.

[174] J. Luo, R. Shi, Polyethylene glycol inhibits apoptotic cell death following traumatic spinal cord injury, Brain Res. 1155 (2007) 10–16. https://doi.org/10.1016/j.brainres.2007.03.091.

[175] R.B. Borgens, R. Shi, D. Bohnert, Behavioral recovery from spinal cord injury following delayed application of polyethylene glycol, J. Exp. Biol. 205 (2002) 1–12. https://doi.org/10.1242/jeb.205.1.1.

[176] R. Shi, R.B. Borgens, Acute repair of crushed guinea pig spinal cord by polyethylene glycol, J. Neurophysiol. 81 (1999) 2406–2414. https://doi.org/10.1152/jn.1999.81.5.2406.

[177] R.B. Borgens, R. Shi, Immediate recovery from spinal cord injury through molecular repair of nerve membranes with polyethylene glycol, FASEB J. Off. Publ. Fed. Am. Soc. Exp. Biol. 14 (2000) 27–35. https://doi.org/10.1096/fasebj.14.1.27.

[178] X. Ping, K. Jiang, S.-Y. Lee, J.-X. Cheng, X. Jin, PEG-PDLLA micelle treatment improves axonal function of the corpus callosum following traumatic brain injury, J. Neurotrauma. 31 (2014) 1172–1179. https://doi.org/10.1089/neu.2013.3147.

[179] A.O. Koob, B.S. Duerstock, C.F. Babbs, Y. Sun, R.B. Borgens, Intravenous polyethylene glycol inhibits the loss of cerebral cells after brain injury, J. Neurotrauma. 22 (2005) 1092–1111. https://doi.org/10.1089/neu.2005.22.1092.

[180] S. Bathina, U.N. Das, Brain-derived neurotrophic factor and its clinical implications, Arch. Med. Sci. AMS. 11 (2015) 1164–1178. https://doi.org/10.5114/aoms.2015.56342.

[181] L.-M. Li, L.-L. Huang, X.-C. Jiang, J.-C. Chen, H.-W. OuYang, J.-Q. Gao, Transplantation of BDNF Gene Recombinant Mesenchymal Stem Cells and Adhesive Peptide-modified Hydrogel Scaffold for Spinal Cord Repair, Curr. Gene Ther. 18 (2018) 29–39. https://doi.org/10.2174/1566523218666180413150023.

[182] M. Gao, P. Lu, B. Bednark, D. Lynam, J.M. Conner, J. Sakamoto, M. Tuszynski, Templated Agarose Scaffolds for the Support of Motor Axon Regeneration Into Sites of Complete Spinal Cord Transection, Biomaterials. 34 (2013) 1529–1536. https://doi.org/10.1016/j.biomaterials.2012.10.070.

[183] Y.-R. Yun, J.E. Won, E. Jeon, S. Lee, W. Kang, H. Jo, J.-H. Jang, U.S. Shin, H.-W. Kim, Fibroblast Growth Factors: Biology, Function, and Application for Tissue Regeneration, J. Tissue Eng. 2010 (2010) 218142. https://doi.org/10.4061/2010/218142.

[184] L. Lan, F.-R. Tian, D.-L. ZhuGe, Q.-C. ZhuGe, B.-X. Shen, B.-H. Jin, J.-P. Huang, M.-Z. Wu, L.-X. Fan, Y.-Z. Zhao, H.-L. Xu, Implantable porous gelatin microspheres sustained release of

bFGF and improved its neuroprotective effect on rats after spinal cord injury, PLoS ONE. 12 (2017) e0173814. https://doi.org/10.1371/journal.pone.0173814.

[185] L. Luo, A.A. Albashari, X. Wang, L. Jin, Y. Zhang, L. Zheng, J. Xia, H. Xu, Y. Zhao, J. Xiao, Y. He, Q. Ye, Effects of Transplanted Heparin-Poloxamer Hydrogel Combining Dental Pulp Stem Cells and bFGF on Spinal Cord Injury Repair, Stem Cells Int. 2018 (2018) 2398521. https://doi.org/10.1155/2018/2398521.

[186] A. Albashari, Y. He, Y. Zhang, J. Ali, F. Lin, Z. Zheng, K. Zhang, Y. Cao, C. Xu, L. Luo, J. Wang, Q. Ye, Thermosensitive bFGF-Modified Hydrogel with Dental Pulp Stem Cells on Neuroinflammation of Spinal Cord Injury, ACS Omega. 5 (2020) 16064–16075. https://doi.org/10.1021/acsomega.0c01379.

[187] G. Jiao, Y. Pan, C. Wang, Z. Li, Z. Li, R. Guo, A bridging SF/Alg composite scaffold loaded NGF for spinal cord injury repair, Mater. Sci. Eng. C Mater. Biol. Appl. 76 (2017) 81–87. https://doi.org/10.1016/j.msec.2017.02.102.

[188] P.C. Maisonpierre, L. Belluscio, S. Squinto, N.Y. Ip, M.E. Furth, R.M. Lindsay, G.D. Yancopoulos, Neurotrophin-3: a neurotrophic factor related to NGF and BDNF, Science. 247 (1990) 1446–1451. https://doi.org/10.1126/science.247.4949.1446.

[189] S. Han, W. Yin, X. Li, S. Wu, Y. Cao, J. Tan, Y. Zhao, X. Hou, L. Wang, C. Ren, J. Li, X. Hu, Y. Mao, G. Li, B. Li, H. Zhang, J. Han, B. Chen, Z. Xiao, X. Jiang, J. Dai, Pre-Clinical Evaluation of CBD-NT3 Modified Collagen Scaffolds in Completely Spinal Cord Transected Non-Human Primates, J. Neurotrauma. 36 (2019) 2316–2324. https://doi.org/10.1089/neu.2018.6078.

[190] L. Yao, W. Daly, B. Newland, S. Yao, W. Wang, B.K.K. Chen, N. Madigan, A. Windebank, A. Pandit, Improved axonal regeneration of transected spinal cord mediated by multichannel collagen conduits functionalized with neurotrophin-3 gene, Gene Ther. 20 (2013) 1149–1157. https://doi.org/10.1038/gt.2013.42.

[191] B.A. Breen, H. Kraskiewicz, R. Ronan, A. Kshiragar, A. Patar, T. Sargeant, A. Pandit, S.S. McMahon, Therapeutic Effect of Neurotrophin-3 Treatment in an Injectable Collagen Scaffold Following Rat Spinal Cord Hemisection Injury, ACS Biomater. Sci. Eng. 3 (2017) 1287–1295. https://doi.org/10.1021/acsbiomaterials.6b00167.

[192] G. Sun, J. Shao, D. Deng, Z. Zhou, X. Zhou, Y. Lin, Z. Li, A chitosan scaffold infused with neurotrophin-3 and human umbilical cord mesenchymal stem cells suppresses inflammation and promotes functional recovery after spinal cord injury in mice, (n.d.) 8.

[193] B.-Q. Lai, M.-T. Che, B.-L. Du, X. Zeng, Y.-H. Ma, B. Feng, X.-C. Qiu, K. Zhang, S. Liu, H.-Y. Shen, J.-L. Wu, E.-A. Ling, Y.-S. Zeng, Transplantation of tissue engineering neural network and formation of neuronal relay into the transected rat spinal cord, Biomaterials. 109 (2016) 40–54. https://doi.org/10.1016/j.biomaterials.2016.08.005.

[194] E. Bible, O. Qutachi, D.Y.S. Chau, M.R. Alexander, K.M. Shakesheff, M. Modo, Neo-vascularization of the stroke cavity by implantation of human neural stem cells on VEGF-releasing PLGA microparticles, Biomaterials. 33 (2012) 7435–7446. https://doi.org/10.1016/j.biomaterials.2012.06.085.

[195] R. Jian, Y. Yixu, L. Sheyu, S. Jianhong, Y. Yaohua, S. Xing, H. Qingfeng, L. Xiaojian, Z. Lei, Z. Yan, X. Fangling, G. Huasong, G. Yilu, Repair of spinal cord injury by chitosan scaffold with glioma ECM and SB216763 implantation in adult rats, J. Biomed. Mater. Res. A. 103 (2015) 3259–3272. https://doi.org/10.1002/jbm.a.35466.

[196] X. Li, J. Han, Y. Zhao, W. Ding, J. Wei, S. Han, X. Shang, B. Wang, B. Chen, Z. Xiao, J. Dai, Functionalized Collagen Scaffold Neutralizing the Myelin-Inhibitory Molecules Promoted Neurites Outgrowth in Vitro and Facilitated Spinal Cord Regeneration in Vivo, ACS Appl. Mater. Interfaces. 7 (2015) 13960–13971. https://doi.org/10.1021/acsami.5b03879.

[197] L.-M. Li, M. Han, X.-C. Jiang, X.-Z. Yin, F. Chen, T.-Y. Zhang, H. Ren, J.-W. Zhang, T.-J. Hou, Z. Chen, H.-W. Ou-Yang, Y. Tabata, Y.-Q. Shen, J.-Q. Gao, Peptide-Tethered Hydrogel Scaffold Promotes Recovery from Spinal Cord Transection via Synergism with Mesenchymal Stem Cells, ACS Appl. Mater. Interfaces. 9 (2017) 3330–3342. https://doi.org/10.1021/acsami.6b12829.

[198] T. Führmann, R.Y. Tam, B. Ballarin, B. Coles, I. Elliott Donaghue, D. van der Kooy, A. Nagy, C.H. Tator, C.M. Morshead, M.S. Shoichet, Injectable hydrogel promotes early survival of induced pluripotent stem cell-derived oligodendrocytes and attenuates longterm teratoma formation in a spinal cord injury model, Biomaterials. 83 (2016) 23–36. https://doi.org/10.1016/j.biomaterials.2015.12.032.

[199] Y. Cho, R.B. Borgens, Polymer and nano-technology applications for repair and reconstruction of the central nervous system, Exp. Neurol. 233 (2012) 126–144. https://doi.org/10.1016/j.expneurol.2011.09.028.

[200] F. Papastefanaki, I. Jakovcevski, N. Poulia, N. Djogo, F. Schulz, T. Martinovic, D. Ciric, G. Loers, T. Vossmeyer, H. Weller, M. Schachner, R. Matsas, Intraspinal Delivery of Polyethylene Glycol-coated Gold Nanoparticles Promotes Functional Recovery After Spinal Cord Injury, Mol. Ther. 23 (2015) 993–1002. https://doi.org/10.1038/mt.2015.50.

[201] L. Dong, X. Kang, Q. Ma, Z. Xu, H. Sun, D. Hao, X. Chen, Novel Approach for Efficient Recovery for Spinal Cord Injury Repair via Biofabricated Nano-Cerium Oxide Loaded PCL With Resveratrol to Improve in Vitro Biocompatibility and Autorecovery Abilities, Dose-Response. 18 (2020) 1559325820933518. https://doi.org/10.1177/1559325820933518.

[202] Z.S. Bailey, E. Nilson, J.A. Bates, A. Oyalowo, K.S. Hockey, V.S.S.S. Sajja, C. Thorpe, H. Rogers, B. Dunn, A.S. Frey, M.J. Billings, C.A. Sholar, A. Hermundstad, C. Kumar, P.J. VandeVord, B.A. Rzigalinski, Cerium Oxide Nanoparticles Improve Outcome after In Vitro and In Vivo Mild Traumatic Brain Injury, J. Neurotrauma. 37 (2020) 1452–1462. https://doi.org/10.1089/neu.2016.4644.

[203] S. Das, M. Sharma, D. Saharia, K.K. Sarma, M.G. Sarma, B.B. Borthakur, U. Bora, In vivo studies of silk based gold nano-composite conduits for functional peripheral nerve regeneration, Biomaterials. 62 (2015) 66–75. https://doi.org/10.1016/j.biomaterials.2015.04.047.

[204] L. Yang, S.-T.D. Chueng, Y. Li, M. Patel, C. Rathnam, G. Dey, L. Wang, L. Cai, K.-B. Lee, A biodegradable hybrid inorganic nanoscaffold for advanced stem cell therapy, Nat. Commun. 9 (2018) 3147. https://doi.org/10.1038/s41467-018-05599-2.

[205] V. Palmieri, G. Perini, M. De Spirito, M. Papi, Graphene oxide touches blood: in vivo interactions of bio-coronated 2D materials, Nanoscale Horiz. 4 (2019) 273–290. https://doi.org/10.1039/c8nh00318a.

[206] X. Huang, X. Qi, F. Boey, H. Zhang, Graphene-based composites, Chem. Soc. Rev. 41 (2012) 666–686. https://doi.org/10.1039/c1cs15078b.

[207] K.E. Kitko, T. Hong, R.M. Lazarenko, D. Ying, Y.-Q. Xu, Q. Zhang, Membrane cholesterol mediates the cellular effects of monolayer graphene substrates, Nat. Commun. 9 (2018) 796. https://doi.org/10.1038/s41467-018-03185-0.

[208] S. Shah, P.T. Yin, T.M. Uehara, S.-T.D. Chueng, L. Yang, K.-B. Lee, Guiding Stem Cell Differentiation into Oligodendrocytes Using Graphene-Nanofiber Hybrid Scaffolds, Adv. Mater. 26 (2014) 3673–3680. https://doi.org/10.1002/adma.201400523.

[209] C. Liao, Y. Li, S.C. Tjong, Graphene Nanomaterials: Synthesis, Biocompatibility, and Cytotoxicity, Int. J. Mol. Sci. 19 (2018) 3564. https://doi.org/10.3390/ijms19113564.

[210] D.-W. Park, A.A. Schendel, S. Mikael, S.K. Brodnick, T.J. Richner, J.P. Ness, M.R. Hayat, F. Atry, S.T. Frye, R. Pashaie, S. Thongpang, Z. Ma, J.C. Williams, Graphene-based carbon-layered electrode array technology for neural imaging and optogenetic applications, Nat. Commun. 5 (2014) 5258. https://doi.org/10.1038/ncomms6258.

[211] Y. Qian, X. Wang, J. Song, W. Chen, S. Chen, Y. Jin, Y. Ouyang, W.-E. Yuan, C. Fan, Preclinical assessment on neuronal regeneration in the injury-related microenvironment of graphene-based scaffolds, Npj Regen. Med. 6 (2021) 1–8. https://doi.org/10.1038/s41536-021-00142-2.

[212] Y.-S. Chen, G.-H. Hsiue, Directing neural differentiation of mesenchymal stem cells by carboxylated multiwalled carbon nanotubes, Biomaterials. 34 (2013) 4936–4944. https://doi.org/10.1016/j.biomaterials.2013.03.063.

[213] G. Bardi, A. Nunes, L. Gherardini, K. Bates, K.T. Al-Jamal, C. Gaillard, M. Prato, A. Bianco, T. Pizzorusso, K. Kostarelos, Functionalized Carbon Nanotubes in the Brain: Cellular Internalization and Neuroinflammatory Responses, PLOS ONE. 8 (2013) e80964. https://doi.org/10.1371/journal.pone.0080964.

[214] K. Matsumoto, C. Sato, Y. Naka, A. Kitazawa, R.L.D. Whitby, N. Shimizu, Neurite outgrowths of neurons with neurotrophin-coated carbon nanotubes, J. Biosci. Bioeng. 103 (2007) 216–220. https://doi.org/10.1263/jbb.103.216.

[215] S. Usmani, A. Franceschi Biagioni, M. Medelin, D. Scaini, R. Casani, E.R. Aurand, D. Padro, A. Egimendia, P. Ramos Cabrer, M. Scarselli, M. De Crescenzi, M. Prato, L. Ballerini, Functional rewiring across spinal injuries via biomimetic nanofiber scaffolds, Proc. Natl. Acad. Sci. 117 (2020) 25212–25218. https://doi.org/10.1073/pnas.2005708117.

[216] J.A. Roman, T.L. Niedzielko, R.C. Haddon, V. Parpura, C.L. Floyd, Single-Walled Carbon Nanotubes Chemically Functionalized with Polyethylene Glycol Promote Tissue Repair in a Rat Model of Spinal Cord Injury, J. Neurotrauma. 28 (2011) 2349–2362. https://doi.org/10.1089/neu.2010.1409.

[217] J.D. Krutty, S.K. Schmitt, P. Gopalan, W.L. Murphy, Surface Functionalization and Dynamics of Polymeric Cell Culture Substrates, Curr. Opin. Biotechnol. 40 (2016) 164–169. https://doi.org/10.1016/j.copbio.2016.05.006.

[218] D.-H. Kim, S. Cho, D. Wirtz, Tight coupling between nucleus and cell migration through the perinuclear actin cap, J. Cell Sci. 127 (2014) 2528–2541. https://doi.org/10.1242/jcs.144345.

[219] P. Sengupta, B.L.V. Prasad, Surface Modification of Polymers for Tissue Engineering Applications: Arginine Acts as a Sticky Protein Equivalent for Viable Cell Accommodation, ACS Omega. 3 (2018) 4242–4251. https://doi.org/10.1021/acsomega.8b00215.

[220] L. He, S. Tang, M.P. Prabhakaran, S. Liao, L. Tian, Y. Zhang, W. Xue, S. Ramakrishna, Surface modification of PLLA nano-scaffolds with laminin multilayer by LbL assembly for enhancing neurite outgrowth, Macromol. Biosci. 13 (2013) 1601–1609. https://doi.org/10.1002/mabi.201300177.

[221] R. Boni, A. Ali, A. Shavandi, A.N. Clarkson, Current and novel polymeric biomaterials for neural tissue engineering, J. Biomed. Sci. 25 (2018) 90. https://doi.org/10.1186/s12929-018-0491-8.

[222] M. Ghidinelli, Y. Poitelon, Y.K. Shin, D. Ameroso, C. Williamson, C. Ferri, M. Pellegatta, K. Espino, A. Mogha, K. Monk, P. Podini, C. Taveggia, K.-A. Nave, L. Wrabetz, H.T. Park, M.L. Feltri, Laminin 211 inhibits protein kinase A in Schwann cells to modulate neuregulin 1 type III-driven myelination, PLoS Biol. 15 (2017) e2001408. https://doi.org/10.1371/journal.pbio.2001408.

[223] J.D. Lathia, M. Li, P.E. Hall, J. Gallagher, J.S. Hale, Q. Wu, M. Venere, E. Levy, M.S. Rani, P. Huang, E. Bae, J. Selfridge, L. Cheng, H. Guvenc, R.E. McLendon, I. Nakano, A.E. Sloan, H.S. Phillips, A. Lai, C. Gladson, M. Bredel, S. Bao, A.B. Hjelmeland, J.N. Rich, Laminin alpha 2 enables glioblastoma stem cell growth, Ann. Neurol. 72 (2012) 766–778. https://doi.org/10.1002/ana.23674.

[224] K. Yang, J.S. Lee, J. Kim, Y.B. Lee, H. Shin, S.H. Um, J.B. Kim, K.I. Park, H. Lee, S.-W. Cho, Polydopamine-mediated surface modification of scaffold materials for human neural stem cell engineering, Biomaterials. 33 (2012) 6952–6964. https://doi.org/10.1016/j.biomaterials.2012.06.067.

[225] M. Bramini, G. Alberini, E. Colombo, M. Chiacchiaretta, M.L. DiFrancesco, J.F. Maya-Vetencourt, L. Maragliano, F. Benfenati, F. Cesca, Interfacing Graphene-Based Materials With Neural Cells, Front. Syst. Neurosci. 12 (2018) 12. https://doi.org/10.3389/fnsys.2018.00012.

[226] D.J. Miller, D.R. Dreyer, C.W. Bielawski, D.R. Paul, B.D. Freeman, Surface Modification of Water Purification Membranes, Angew. Chem. Int. Ed Engl. 56 (2017) 4662–4711. https://doi.org/10.1002/anie.201601509.

[227] X. Jing, H.-Y. Mi, B.N. Napiwocki, X.-F. Peng, L.-S. Turng, Mussel-inspired electroactive chitosan/graphene oxide composite hydrogel with rapid self-healing and recovery behavior for tissue engineering, Carbon. 125 (2017) 557–570. https://doi.org/10.1016/j.carbon.2017.09.071.

[228] G. Wei, D. Jiang, S. Hu, Z. Yang, Z. Zhang, W. Li, W. Cai, D. Liu, Polydopamine-Decorated Microcomposites Promote Functional Recovery of an Injured Spinal Cord by Inhibiting Neuroinflammation, ACS Appl. Mater. Interfaces. 13 (2021) 47341–47353. https://doi.org/10.1021/acsami.1c11772.

[229] S. Liu, X. Sun, T. Wang, S. Chen, C. Zeng, G. Xie, Q. Zhu, X. Liu, D. Quan, Nano-fibrous and ladder-like multi-channel nerve conduits: Degradation and modification by gelatin, Mater. Sci. Eng. C. 83 (2018) 130–142. https://doi.org/10.1016/j.msec.2017.11.020.

[230] A. Faissner, M. Pyka, M. Geissler, T. Sobik, R. Frischknecht, E.D. Gundelfinger, C. Seidenbecher, Contributions of astrocytes to synapse formation and maturation - Potential functions of the perisynaptic extracellular matrix, Brain Res. Rev. 63 (2010) 26–38. https://doi.org/10.1016/j.brainresrev.2010.01.001.

[231] M. Florio, W.B. Huttner, Neural progenitors, neurogenesis and the evolution of the neocortex, Dev. Camb. Engl. 141 (2014) 2182–2194. https://doi.org/10.1242/dev.090571.

[232] S. Hrabětová, D. Masri, L. Tao, F. Xiao, C. Nicholson, Calcium diffusion enhanced after cleavage of negatively charged components of brain extracellular matrix by chondroitinase ABC, J. Physiol. 587 (2009) 4029–4049. https://doi.org/10.1113/jphysiol.2009.170092.

[233] D. Lehnert, B. Wehrle-Haller, C. David, U. Weiland, C. Ballestrem, B.A. Imhof, M. Bastmeyer, Cell behaviour on micropatterned substrata: limits of extracellular matrix geometry for spreading and adhesion, J. Cell Sci. 117 (2004) 41–52. https://doi.org/10.1242/jcs.00836.

[234] M.J. Dalby, N. Gadegaard, R.O.C. Oreffo, Harnessing nanotopography and integrin-matrix interactions to influence stem cell fate, Nat. Mater. 13 (2014) 558–569. https://doi.org/10.1038/nmat3980.

[235] S. Yip, K.S. Aboody, M. Burns, J. Imitola, J.A. Boockvar, J. Allport, K.I. Park, Y.D. Teng, M. Lachyankar, T. McIntosh, D.M. O'Rourke, S. Khoury, R. Weissleder, P.M. Black, W. Weiss, E.Y. Snyder, Neural stem cell biology may be well suited for improving brain tumor therapies, Cancer J. Sudbury Mass. 9 (2003) 189–204. https://doi.org/10.1097/00130404-200305000-00007.

[236] J.M. Mann, R.H.W. Lam, S. Weng, Y. Sun, J. Fu, A silicone-based stretchable micropost array membrane for monitoring live-cell subcellular cytoskeletal response, Lab. Chip. 12 (2012) 731–740. https://doi.org/10.1039/c2lc20896b.

[237] A. Nur-E-Kamal, I. Ahmed, J. Kamal, M. Schindler, S. Meiners, Three-dimensional nanofibrillar surfaces promote self-renewal in mouse embryonic stem cells, Stem Cells Dayt. Ohio. 24 (2006) 426–433. https://doi.org/10.1634/stemcells.2005-0170.

[238] P.M. Tsimbouri, R.J. McMurray, K.V. Burgess, E.V. Alakpa, P.M. Reynolds, K. Murawski, E. Kingham, R.O.C. Oreffo, N. Gadegaard, M.J. Dalby, Using nanotopography and metabolomics to identify biochemical effectors of multipotency, ACS Nano. 6 (2012) 10239–10249. https://doi.org/10.1021/nn304046m.

[239] L. Liu, Q. Yuan, J. Shi, X. Li, D. Jung, L. Wang, K. Yamauchi, N. Nakatsuji, K. Kamei, Y. Chen, Chemically-defined scaffolds created with electrospun synthetic nanofibers to maintain mouse embryonic stem cell culture under feeder-free conditions, Biotechnol. Lett. 34 (2012) 1951–1957. https://doi.org/10.1007/s10529-012-0973-9.

[240] L. Ji, V.L.S. LaPointe, N.D. Evans, M.M. Stevens, Changes in embryonic stem cell colony morphology and early differentiation markers driven by colloidal crystal topographical cues, Eur. Cell. Mater. 23 (2012) 135–146. https://doi.org/10.22203/ecm.v023a10.

[241] Y.P. Kong, C.H. Tu, P.J. Donovan, A.F. Yee, Expression of Oct4 in human embryonic stem cells is dependent on nanotopographical configuration, Acta Biomater. 9 (2013) 6369–6380. https://doi.org/10.1016/j.actbio.2013.01.036.

[242] N. Rodriguez-Losada, R. Wendelbob, M.C. Ocaña, A.D. Casares, R. Guzman de Villoría, J.A. Aguirre Gomez, M.A. Arraez, P. Gonzalez-Alegre, M.A. Medina, E. Arenas, J.A. Narvaez, Graphene Oxide and Reduced Derivatives, as Powder or Film Scaffolds, Differentially Promote Dopaminergic Neuron Differentiation and Survival, Front. Neurosci. 14 (2020). https://www.frontiersin.org/articles/10.3389/fnins.2020.570409 (accessed September 6, 2022).

[243] L. Yang, K.M. Jurczak, L. Ge, P. van Rijn, High-Throughput Screening and Hierarchical Topography-Mediated Neural Differentiation of Mesenchymal Stem Cells, Adv. Healthc. Mater. 9 (2020) e2000117. https://doi.org/10.1002/adhm.202000117.

[244] E. Kijeńska, M.P. Prabhakaran, W. Swieszkowski, K.J. Kurzydlowski, S. Ramakrishna, Electrospun bio-composite P(LLA-CL)/collagen I/collagen III scaffolds for nerve tissue engineering, J. Biomed. Mater. Res. B Appl. Biomater. 100B (2012) 1093–1102. https://doi.org/10.1002/jbm.b.32676.

[245] S.H. Lim, X.Y. Liu, H. Song, K.J. Yarema, H.-Q. Mao, The effect of nanofiber-guided cell alignment on the preferential differentiation of neural stem cells, Biomaterials. 31 (2010) 9031–9039. https://doi.org/10.1016/j.biomaterials.2010.08.021.

[246] J. Xie, S.M. Willerth, X. Li, M.R. Macewan, A. Rader, S.E. Sakiyama-Elbert, Y. Xia, The differentiation of embryonic stem cells seeded on electrospun nanofibers into neural lineages, Biomaterials. 30 (2009) 354–362. https://doi.org/10.1016/j.biomaterials.2008.09.046.

[247] M.P. Prabhakaran, J.R. Venugopal, S. Ramakrishna, Mesenchymal stem cell differentiation to neuronal cells on electrospun nanofibrous substrates for nerve tissue engineering, Biomaterials. 30 (2009) 4996–5003. https://doi.org/10.1016/j.biomaterials.2009.05.057.

[248] G.T. Christopherson, H. Song, H.-Q. Mao, The influence of fiber diameter of electrospun substrates on neural stem cell differentiation and proliferation, Biomaterials. 30 (2009) 556–564. https://doi.org/10.1016/j.biomaterials.2008.10.004.

[249] S.Y. Chew, W.C. Low, Scaffold-based approach to direct stem cell neural and cardiovascular differentiation: An analysis of physical and biochemical effects, J. Biomed. Mater. Res. A. 97A (2011) 355–374. https://doi.org/10.1002/jbm.a.33064.

[250] S. Baiguera, C. Del Gaudio, L. Fioravanzo, A. Bianco, M. Grigioni, M. Folin, In vitro astrocyte and cerebral endothelial cell response to electrospun poly(epsilon-caprolactone) mats of different architecture, J. Mater. Sci. Mater. Med. 21 (2010) 1353–1362. https://doi.org/10.1007/s10856-009-3944-5.

[251] M. Sun, M. McGowan, P.J. Kingham, G. Terenghi, S. Downes, Novel thin-walled nerve conduit with microgrooved surface patterns for enhanced peripheral nerve repair, J. Mater. Sci. Mater. Med. 21 (2010) 2765–2774. https://doi.org/10.1007/s10856-010-4120-7.

[252] J. Gerardo-Nava, T. Führmann, K. Klinkhammer, N. Seiler, J. Mey, D. Klee, M. Möller, P.D. Dalton, G.A. Brook, Human neural cell interactions with orientated electrospun nanofibers in vitro, Nanomed. 4 (2009) 11–30. https://doi.org/10.2217/17435889.4.1.11.

[253] W. Chen, Y. Shao, X. Li, G. Zhao, J. Fu, Nanotopographical Surfaces for Stem Cell Fate Control: Engineering Mechanobiology from the Bottom, Nano Today. 9 (2014) 759–784. https://doi.org/10.1016/j.nantod.2014.12.002.

[254] M. Zhu, Z. Wang, J. Zhang, L. Wang, X. Yang, J. Chen, G. Fan, S. Ji, C. Xing, K. Wang, Q. Zhao, Y. Zhu, D. Kong, L. Wang, Circumferentially aligned fibers guided functional neoartery regeneration in vivo, Biomaterials. 61 (2015) 85–94. https://doi.org/10.1016/j.biomaterials.2015.05.024.

[255] Aligned-Braided Nanofibrillar Scaffold with Endothelial Cells Enhances Arteriogenesis | ACS Nano, (n.d.). https://pubs.acs.org/doi/10.1021/acsnano.5b00545 (accessed August 29, 2022).

[256] E.J. Berns, S. Sur, L. Pan, J.E. Goldberger, S. Suresh, S. Zhang, J.A. Kessler, S.I. Stupp, Aligned neurite outgrowth and directed cell migration in self-assembled monodomain gels, Biomaterials. 35 (2014) 185–195. https://doi.org/10.1016/j.biomaterials.2013.09.077.

[257] C. Fischbach, R. Chen, T. Matsumoto, T. Schmelzle, J.S. Brugge, P.J. Polverini, D.J. Mooney, Engineering tumors with 3D scaffolds, Nat. Methods. 4 (2007) 855–860. https://doi.org/10.1038/nmeth1085.

[258] R.J. McMurray, N. Gadegaard, P.M. Tsimbouri, K.V. Burgess, L.E. McNamara, R. Tare, K. Murawski, E. Kingham, R.O.C. Oreffo, M.J. Dalby, Nanoscale surfaces for the long-term maintenance of mesenchymal stem cell phenotype and multipotency, Nat. Mater. 10 (2011) 637–644. https://doi.org/10.1038/nmat3058.

[259] M.T. Raimondi, S.M. Eaton, M. Laganà, V. Aprile, M.M. Nava, G. Cerullo, R. Osellame, Three-dimensional structural niches engineered via two-photon laser polymerization promote stem cell homing, Acta Biomater. 9 (2013) 4579–4584. https://doi.org/10.1016/j.actbio.2012.08.022.

[260] M.K. Lee, M.H. Rich, J. Lee, H. Kong, A bio-inspired, microchanneled hydrogel with controlled spacing of cell adhesion ligands regulates 3D spatial organization of cells and tissue, Biomaterials. 58 (2015) 26–34. https://doi.org/10.1016/j.biomaterials.2015.04.014.

[261] W.M. Tian, S.P. Hou, J. Ma, C.L. Zhang, Q.Y. Xu, I.S. Lee, H.D. Li, M. Spector, F.Z. Cui, Hyaluronic acid-poly-D-lysine-based three-dimensional hydrogel for traumatic brain injury, Tissue Eng. 11 (2005) 513–525. https://doi.org/10.1089/ten.2005.11.513.

[262] C. Martínez-Ramos, A. Vallés-Lluch, J.M.G. Verdugo, J.L.G. Ribelles, J.A. Barcia Albacar, A.B. Orts, J.M. Soria López, M.M. Pradas, Channeled scaffolds implanted in adult rat brain, J. Biomed. Mater. Res. A. 100 (2012) 3276–3286. https://doi.org/10.1002/jbm.a.34273.

[263] K. Odelius, A. Höglund, S. Kumar, M. Hakkarainen, A.K. Ghosh, N. Bhatnagar, A.-C. Albertsson, Porosity and Pore Size Regulate the Degradation Product Profile of Polylactide, Biomacromolecules. 12 (2011) 1250–1258. https://doi.org/10.1021/bm1015464.

[264] F.K. Ma, J. Li, M. Kong, Y. Liu, Y. An, X.G. Chen, Preparation and hydrolytic erosion of differently structured PLGA nanoparticles with chitosan modification, Int. J. Biol. Macromol. 54 (2013) 174–179. https://doi.org/10.1016/j.ijbiomac.2012.12.019.

[265] M.A. Hemphill, S. Dauth, C.J. Yu, B.E. Dabiri, K.K. Parker, Traumatic brain injury and the neuronal microenvironment: a potential role for neuropathological mechanotransduction, Neuron. 85 (2015) 1177–1192. https://doi.org/10.1016/j.neuron.2015.02.041.

[266] S.A. Geissler, A.L. Sabin, R.R. Besser, O.M. Gooden, B.D. Shirk, Q.M. Nguyen, Z.Z. Khaing, C.E. Schmidt, Biomimetic hydrogels direct spinal progenitor cell differentiation and promote functional recovery after spinal cord injury., J. Neural Eng. 15 (2018) 25004. https://doi.org/10.1088/1741-2552/aaa55c.

[267] A.K. Nayak, B. Das, 1 - Introduction to polymeric gels, in: K. Pal, I. Banerjee (Eds.), Polym. Gels, Woodhead Publishing, 2018: pp. 3–27. https://doi.org/10.1016/B978-0-08-102179-8.00001-6.

[268] C. Li, M. Kuss, Y. Kong, F. Nie, X. Liu, B. Liu, A. Dunaevsky, P. Fayad, B. Duan, X. Li, 3D Printed Hydrogels with Aligned Microchannels to Guide Neural Stem Cell Migration, ACS Biomater. Sci. Eng. 7 (2021) 690–700. https://doi.org/10.1021/acsbiomaterials.0c01619.

[269] A. Kourgiantaki, D.S. Tzeranis, K. Karali, K. Georgelou, E. Bampoula, S. Psilodimitrakopoulos, I.V. Yannas, E. Stratakis, K. Sidiropoulou, I. Charalampopoulos, A. Gravanis, Neural stem cell delivery via porous collagen scaffolds promotes neuronal differentiation and locomotion recovery in spinal cord injury, Npj Regen. Med. 5 (2020) 1–14. https://doi.org/10.1038/s41536-020-0097-0.

[270] Q. Gu, E. Tomaskovic-Crook, R. Lozano, Y. Chen, R.M. Kapsa, Q. Zhou, G.G. Wallace, J.M. Crook, Functional 3D Neural Mini-Tissues from Printed Gel-Based Bioink and Human Neural Stem Cells, Adv. Healthc. Mater. 5 (2016) 1429–1438. https://doi.org/10.1002/adhm.201600095.

[271] R. Loganathan, B.J. Rongish, C.M. Smith, M.B. Filla, A. Czirok, B. Bénazéraf, C.D. Little, Extracellular matrix motion and early morphogenesis, Dev. Camb. Engl. 143 (2016) 2056–2065. https://doi.org/10.1242/dev.127886.

[272] D.E. Discher, D.J. Mooney, P.W. Zandstra, Growth factors, matrices, and forces combine and control stem cells, Science. 324 (2009) 1673–1677. https://doi.org/10.1126/science.1171643.

[273] D.A. Fletcher, R.D. Mullins, Cell mechanics and the cytoskeleton, Nature. 463 (2010) 485–492. https://doi.org/10.1038/nature08908.

[274] B. Shen, M.K. Delaney, X. Du, Inside-out, outside-in, and inside-outside-in: G protein signaling in integrin-mediated cell adhesion, spreading, and retraction, Curr. Opin. Cell Biol. 24 (2012) 600–606. https://doi.org/10.1016/j.ceb.2012.08.011.

[275] A. Sneider, J. Hah, D. Wirtz, D.-H. Kim, Recapitulation of molecular regulators of nuclear motion during cell migration, Cell Adhes. Migr. 13 (2019) 50–62. https://doi.org/10.1080/19336918.2018.1506654.

[276] D.-H. Kim, B. Li, F. Si, J.M. Phillip, D. Wirtz, S.X. Sun, Volume regulation and shape bifurcation in the cell nucleus, J. Cell Sci. 128 (2015) 3375–3385. https://doi.org/10.1242/jcs.166330.

[277] S. Cho, J. Irianto, D.E. Discher, Mechanosensing by the nucleus: From pathways to scaling relationships, J. Cell Biol. 216 (2017) 305–315. https://doi.org/10.1083/jcb.201610042.

[278] N. Huebsch, D.J. Mooney, Inspiration and application in the evolution of biomaterials, Nature. 462 (2009) 426–432. https://doi.org/10.1038/nature08601.

[279] D.E. Discher, P. Janmey, Y.-L. Wang, Tissue cells feel and respond to the stiffness of their substrate, Science. 310 (2005) 1139–1143. https://doi.org/10.1126/science.1116995.

[280] Of Extracellular Matrix, Scaffolds, and Signaling: Tissue Architecture Regulates Development, Homeostasis, and Cancer - PMC, (n.d.). https://www.ncbi.nlm.nih.gov/pmc/articles/PMC2933192/ (accessed August 29, 2022).

[281] V. Maruthamuthu, B. Sabass, U.S. Schwarz, M.L. Gardel, Cell-ECM traction force modulates endogenous tension at cell-cell contacts, Proc. Natl. Acad. Sci. U. S. A. 108 (2011) 4708–4713. https://doi.org/10.1073/pnas.1011123108.

[282] M. Behrndt, G. Salbreux, P. Campinho, R. Hauschild, F. Oswald, J. Roensch, S.W. Grill, C.-P. Heisenberg, Forces driving epithelial spreading in zebrafish gastrulation, Science. 338 (2012) 257–260. https://doi.org/10.1126/science.1224143.

[283] A.C. Martin, M. Kaschube, E.F. Wieschaus, Pulsed actin-myosin network contractions drive apical constriction, Nature. 457 (2009) 495. https://doi.org/10.1038/nature07522.

[284] T. Naganuma, The relationship between cell adhesion force activation on nano/micro-topographical surfaces and temporal dependence of cell morphology, Nanoscale. 9 (2017) 13171–13186. https://doi.org/10.1039/c7nr04785a.

[285] K. Saha, A.J. Keung, E.F. Irwin, Y. Li, L. Little, D.V. Schaffer, K.E. Healy, Substrate Modulus Directs Neural Stem Cell Behavior, Biophys. J. 95 (2008) 4426–4438. https://doi.org/10.1529/biophysj.108.132217.

[286] A. Skardal, D. Mack, A. Atala, S. Soker, Substrate elasticity controls cell proliferation, surface marker expression and motile phenotype in amniotic fluid-derived stem cells, J. Mech. Behav. Biomed. Mater. 17 (2013) 307–316. https://doi.org/10.1016/j.jmbbm.2012.10.001.

[287] T.H. Kim, D.B. An, S.H. Oh, M.K. Kang, H.H. Song, J.H. Lee, Creating stiffness gradient polyvinyl alcohol hydrogel using a simple gradual freezing-thawing method to investigate stem cell differentiation behaviors, Biomaterials. 40 (2015) 51–60. https://doi.org/10.1016/j.biomaterials.2014.11.017.

[288] S. Budday, R. Nay, R. de Rooij, P. Steinmann, T. Wyrobek, T.C. Ovaert, E. Kuhl, Mechanical properties of gray and white matter brain tissue by indentation, J. Mech. Behav. Biomed. Mater. 46 (2015) 318–330. https://doi.org/10.1016/j.jmbbm.2015.02.024.

[289] E. Nicolas, S. Callé, S. Nicolle, D. Mitton, J.-P. Remenieras, Biomechanical characterization of ex vivo human brain using ultrasound shear wave spectroscopy, Ultrasonics. 84 (2018) 119–125. https://doi.org/10.1016/j.ultras.2017.10.009.

[290] S. Cheng, E.C. Clarke, L.E. Bilston, Rheological properties of the tissues of the central nervous system: a review, Med. Eng. Phys. 30 (2008) 1318–1337. https://doi.org/10.1016/j.medengphy.2008.06.003.

[291] A.J. Engler, F. Rehfeldt, S. Sen, D.E. Discher, Microtissue elasticity: measurements by atomic force microscopy and its influence on cell differentiation, Methods Cell Biol. 83 (2007) 521–545. https://doi.org/10.1016/S0091-679X(07)83022-6.

[292] G. Chu, Z. Yuan, C. Zhu, P. Zhou, H. Wang, W. Zhang, Y. Cai, X. Zhu, H. Yang, B. Li, Substrate stiffness- and topography-dependent differentiation of annulus fibrosus-derived stem cells is regulated by Yes-associated protein, Acta Biomater. 92 (2019) 254–264. https://doi.org/10.1016/j.actbio.2019.05.013.

[293] Q. Ma, L. Yang, Z. Jiang, Q. Song, M. Xiao, D. Zhang, X. Ma, T. Wen, G. Cheng, Three-Dimensional Stiff Graphene Scaffold on Neural Stem Cells Behavior, ACS Appl. Mater. Interfaces. 8 (2016) 34227–34233. https://doi.org/10.1021/acsami.6b12305.

[294] A.J. Engler, S. Sen, H.L. Sweeney, D.E. Discher, Matrix elasticity directs stem cell lineage specification, Cell. 126 (2006) 677–689. https://doi.org/10.1016/j.cell.2006.06.044.

[295] N.D. Leipzig, M.S. Shoichet, The effect of substrate stiffness on adult neural stem cell behavior, Biomaterials. 30 (2009) 6867–6878. https://doi.org/10.1016/j.biomaterials.2009.09.002.

[296] V. Vogel, M. Sheetz, Local force and geometry sensing regulate cell functions, Nat. Rev. Mol. Cell Biol. 7 (2006) 265–275. https://doi.org/10.1038/nrm1890.

[297] Q.-Y. Zhang, Y.-Y. Zhang, J. Xie, C.-X. Li, W.-Y. Chen, B.-L. Liu, X. Wu, S.-N. Li, B. Huo, L.-H. Jiang, H.-C. Zhao, Stiff substrates enhance cultured neuronal network activity, Sci. Rep. 4 (2014) 6215. https://doi.org/10.1038/srep06215.

[298] P. Moshayedi, G. Ng, J.C.F. Kwok, G.S.H. Yeo, C.E. Bryant, J.W. Fawcett, K. Franze, J. Guck, The relationship between glial cell mechanosensitivity and foreign body reactions in the central nervous system, Biomaterials. 35 (2014) 3919–3925. https://doi.org/10.1016/j.biomaterials.2014.01.038.

[299] H.J. Lee, M.F. Diaz, K.M. Price, J.A. Ozuna, S. Zhang, E.M. Sevick-Muraca, J.P. Hagan, P.L. Wenzel, Fluid shear stress activates YAP1 to promote cancer cell motility, Nat. Commun. 8 (2017) 14122. https://doi.org/10.1038/ncomms14122.

[300] A. Hubaud, I. Regev, L. Mahadevan, O. Pourquié, Excitable Dynamics and Yap-Dependent Mechanical Cues Drive the Segmentation Clock, Cell. 171 (2017) 668-682.e11. https://doi.org/10.1016/j.cell.2017.08.043.

[301] O. Chaudhuri, J. Cooper-White, P.A. Janmey, D.J. Mooney, V.B. Shenoy, Effects of extracellular matrix viscoelasticity on cellular behaviour, Nature. 584 (2020) 535–546. https://doi.org/10.1038/s41586-020-2612-2.

[302] S. Chen, A. Liu, C. Wu, Y. Chen, C. Liu, Y. Zhang, K. Wu, D. Wei, J. Sun, L. Zhou, H. Fan, Static–Dynamic Profited Viscoelastic Hydrogels for Motor-Clutch-Regulated Neurogenesis, ACS Appl. Mater. Interfaces. 13 (2021) 24463–24476. https://doi.org/10.1021/acsami.1c03821.

[303] B.J. Dubin-Thaler, G. Giannone, H.-G. Döbereiner, M.P. Sheetz, Nanometer Analysis of Cell Spreading on Matrix-Coated Surfaces Reveals Two Distinct Cell States and STEPs, Biophys. J. 86 (2004) 1794–1806. https://www.ncbi.nlm.nih.gov/pmc/articles/PMC1304013/ (accessed August 29, 2022).

[304] D. Koch, W.J. Rosoff, J. Jiang, H.M. Geller, J.S. Urbach, Strength in the Periphery: Growth Cone Biomechanics and Substrate Rigidity Response in Peripheral and Central Nervous System Neurons, Biophys. J. 102 (2012) 452–460. https://doi.org/10.1016/j.bpj.2011.12.025.

[305] L.A. Flanagan, Y.-E. Ju, B. Marg, M. Osterfield, P.A. Janmey, Neurite branching on deformable substrates, Neuroreport. 13 (2002) 2411–2415. https://doi.org/10.1097/00001756-200212200-00007.

[306] J. Lantoine, T. Grevesse, A. Villers, G. Delhaye, C. Mestdagh, M. Versaevel, D. Mohammed, C. Bruyère, L. Alaimo, S.P. Lacour, L. Ris, S. Gabriele, Matrix stiffness modulates formation and activity of neuronal networks of controlled architectures, Biomaterials. 89 (2016) 14–24. https://doi.org/10.1016/j.biomaterials.2016.02.041.

Chapter 3

Nanostructured scaffolds based on bioresorbable polymers and graphene oxide induce the aligned migration and accelerate the neuronal differentiation of neural stem cells

Nanostructured scaffolds based on bioresorbable polymers and graphene oxide induce the aligned migration and accelerate the neuronal differentiation of neural stem cells

Abstract

Within the field of neural tissue engineering, there is a huge need for the development of materials that promote the adhesion, aligned migration and differentiation of stem cells into neuronal and supportive glial cells. In this first experimental chapter, we have fabricated bioresorbable elastomeric scaffolds combining an ordered nanopatterned topography together with a surface functionalization with graphene oxide (GO) in mild conditions. These scaffolds allowed the attachment of murine neural stem cells (NSCs) without the need of any further coating of its surface with extracellular matrix adhesion proteins. The NSCs were able to give rise to both immature neurons and supporting glial cells over the nanostructured scaffolds *in vitro*, promoting their aligned migration in cell clusters following the nanostructured grooves. This system has the potential to reestablish spatially oriented neural precursor cell connectivity, constituting a promising tool for future cellular therapy including nerve tissue regeneration.

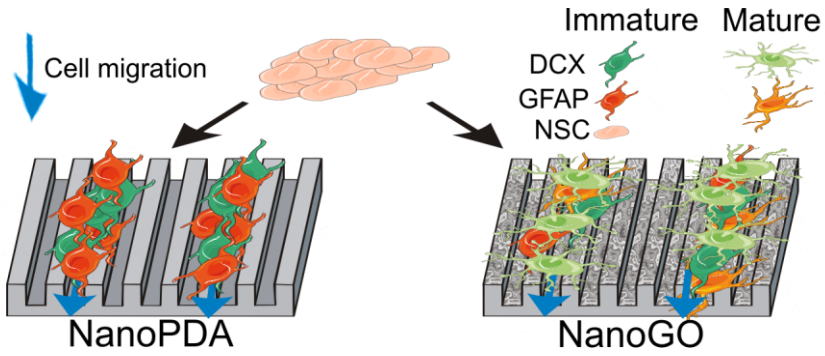

3.1. Introduction

Neurological disorders cause death or disability to more than 94 million people worldwide every year and this number is expected to rise to 103 million by 2030 [1]. Hence, further research is necessary to develop effective strategies for a guided neural regeneration and reestablishment of the lost nerve connectivity.

Within the field of neural tissue regeneration, the discovery and/or optimization of biomaterials that fulfill the complex requirements for this specific biomedical application play a pivotal role. Much progress has been made in determining the ideal features a biomaterial should have for its use as a neural replacement graft, and in understanding the interactions of growing axons within these biomaterials; however, the regeneration levels induced by the biomaterial usually do not match those obtained by nerve tissue autografts and the development of new and effective nerve regeneration therapies is still an urgent clinical need [2,3].

The biomaterials for nerve tissue regeneration should be biocompatible and biodegradable, while providing structural cues that promote oriented axon regeneration and guidance signals from extracellular matrix (ECM)-like components. Additionally, they should also present long-term storage capability and ease of handling/suturing [4–6]. One important aspect to take in consideration is that the ECM is more than just a structural component. Indeed, for stem cells in particular, both the topography and composition of the ECM are pivotal in instructing cell fate choices by selective contact guidance, promotion of cell adhesion and concentration of growth factors and/or signaling ligands to defined niches [7]. However, negative effects produced by an inappropriate choice of ECM can also be identified. For instance, an excess of the typically employed ECM adhesion protein laminin $\alpha_2\beta_2\gamma_1$ (Lm211) can inhibit signaling pathways required to initiate myelination [8]. Furthermore, laminin ECM proteins may represent a lethal risk if at some point resident and/or grafted cells became cancerous. It has been demonstrated that laminin primes the proliferation of brain tumor cells such as ependymoma or glioblastoma cancer stem cells, becoming strongly correlated to negative patient prognosis [9]. For all these reasons, it is urgent to design a biomaterial scaffold with the ability to allow the attachment of neural stem cells and progenitors without the need of a laminin coating.

To overcome these challenges, the use of polymeric substrates that mimic the mechanical (e.g., elasticity, stiffness), geometrical and chemical features of the ECM has been described to satisfactorily promote the differentiation of stem cells towards neural lineages [10]. Among the available polymeric substrates, bioresorbable (co)polyesters based on L-lactide and ε-caprolactone are of particular interest. These systems show inherent biodegradability, biocompatibility and the possibility to tune the mechanical properties and degradation rates depending on the specific application, via the precise

control of the L-lactide-to-ε-caprolactone ratio and synthesis conditions (e.g., catalyst, reaction temperature and time) [11–13]. Nevertheless, nowadays, polymeric devices are not just bioinert support materials for cell growth. To fit within the new discipline of materiobiology [14], they also need to mimic the morphological, topographical and mechanical properties of the desired tissue [15]. To fulfill these requisites, nanopattern construction represents a promising strategy to endow the material surface with specific geometrical and mechanical signals. Nanopatterns can potentially elicit a stem cell response, as surface nanotopography could induce pronounced changes to cell shape, and consequently also in gene expression [16]. In this regard, the importance of nanotopography was shown on the differentiation of adult stem cells towards neuronal lineages, compared to unpatterned and micro-patterned control surfaces [17]. Moreover, the combination of nanotopography with graphene derivatives (e.g., graphene oxide (GO), reduced graphene oxide (rGO)) has been shown to promote neuronal differentiation and axon alignment [18]. In the recent years, GO-based materials have been extensively explored as some of the most promising biomaterials for neural regeneration [19] thanks to their unique properties [20].

However, there is still much to investigate regarding the impact of nanotopography and graphene derivatives on the mobility of the cells along the scaffold device, the *in situ* differentiation of stem cells into glial or neuronal cells and the necessary equilibrium between both pathways, to achieve a functional recovery of the neural tissue. Therefore, we have developed novel two-dimensional nanostructured tissue engineering scaffolds based on bioresorbable polymers and GO as a new alternative to promote the neurodifferentiation of murine neural stem cells (NSCs) and progenitors, which are competent to give rise to both mature neuronal and glial cells. The high efficiency shown by these nanopatterned scaffolds, even under long incubation periods compatible with usual differentiation protocols, turns them into an optimal and easy-to-produce tool.

3.2. Materials and methods

3.2.1. Fabrication of scaffolds

PURASORB PLC 7015 (Corbion, The Netherlands) (PLCL 7015) is a biodegradable copolymer of L-lactide and ε-caprolactone in a 70/30 molar ratio, with a weight average molecular weight (M_w) of 154.6 kDa and dispersity index (DI) of 2.10, as determined by gel permeation chromatography (GPC). For the fabrication of the scaffolds, PLCL films of around 150 µm were first obtained by compression molding in a Collin P 200 E (Germany) hydraulic press at 175 ^{o}C. These films were subsequently nanostructured by a thermo-pressing process at 190 ^{o}C and 20 N with the aid of a commercially available silicon stamp (NIL Technology, Denmark) (period: 700 nm; linewidth: 365 nm; depth: 350 nm) (Figure 3.1.). For the surface-functionalization with GO, the nanostructured PLCL scaffolds were incubated in a 2 mg/ml dopamine-hydrocholoride (cat# H8502, Sigma-Aldrich, Spain) solution in 2-amino-2-(hydroxymethyl)-1,3-propanediol (TRIS) buffer (cat# T1503, Sigma-Aldrich, Spain) at pH = 8.5 for 1 h to form a homogeneous layer of polydopamine (PDA). To eliminate the excess of PDA and reagents, the films were thoroughly washed with distilled water. Afterwards, PDA-coated films were incubated in a 0.25 mg/ml GO solution (cat# 947-768-1, Graphenea, Spain) for 30 min to allow the deposition of GO on the surface of the nanostructured scaffolds. Finally, the scaffolds were extensively washed with distilled water prior to their use and characterization. Circular samples of 6 mm diameter were punched out for subsequent characterization and cell culture studies.

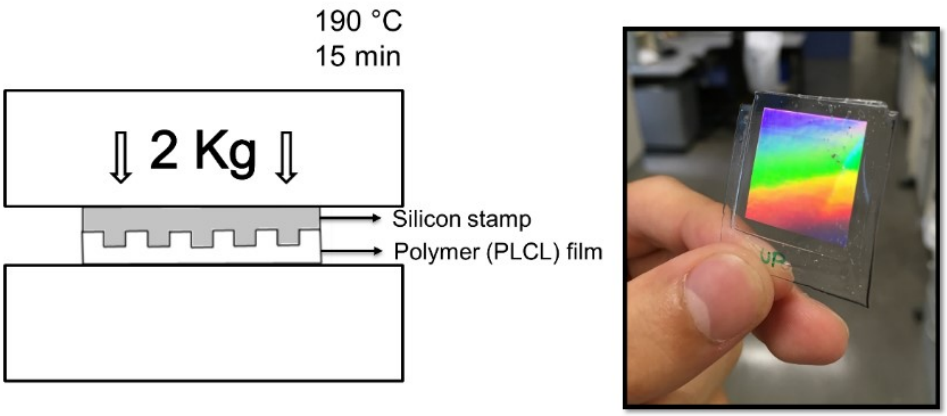

Figure 3.1.: Schematic representation of the fabrication process of nanostructured PLCL. Thanks to the thermoplastic features of the PLCL, scaffolds are fabricated by applying heat and force to replicate the nanotopography of a silicon stamp (left). A photograph of the resulting sample (right).

3.2.2. Morphological and physico-chemical characterization of the scaffolds

3.2.2.1. Scanning electron microscopy (SEM)

The surface morphology of the scaffolds was examined via scanning electron microscopy (SEM) (HITACHI S-4800). Prior to their analysis, samples were coated with a 150 Å layer of gold in a JEL Ion Sputter JFC-1100 at 1200 V and 5 mA.

3.2.2.2. Atomic force microscopy (AFM)

For the measurement of topographical and mechanical properties of PLCL-based flat and nanostructured scaffolds, AFM measurements were performed in both imaging and force spectroscopy modes, respectively, on a Nanowizard 3 (JPK Instruments, Berlin, Germany). Experiments were conducted in liquid environment (1x PBS) at room temperature (25 ^{o}C).

AFM imaging of the prepared samples was performed in contact mode with a setpoint (applied force) of 5 nN at a scan rate of 1 Hz and for 10x10 μm². Topographical analysis involved the use of uncoated silicon nitride cantilevers mounting a quadratic pyramidal tip (22 nm radius, DNP-S10, Bruker, USA) at the end. In turn, for adhesion measurements 10 μm silicon dioxide colloidal probes (CP-PNPS-SiO_2 cantilevers, NanoAndMore GmbH, Germany) were utilized. Thermal noise calibration allowed determining the spring constant of the corresponding cantilevers, being around 0.12 N/m and 0.3 N/m, respectively. The colloidal particle, after short (ca. 30 s) oxygen plasma treatment (GaLaInstrumente GmbH, Bad Schwalbach, Germany) was chemically modified either by 1*H*,1*H*,2*H*,2*H*-perfluorododecyltrichlorosilane hydrophobic (cat# 729965, Sigma-Aldrich, Germany) fluorinated silane (FSi) overnight vapor deposition or by dip coating in 20 μM fibronectin (cat# F1141, Sigma-Aldrich, Germany) in PBS (incubation time = 120 min) prior to employment. Force measurements were carried out at constant approach/retracting rate (1.5 μm/s) with a maximum loading force of 10 nN being applied. To evaluate the adhesion-related factors of the different systems under analysis, the focus was set on the retraction segment from the resulting force-distance curves (Figure 3.2.), which allowed calculating the maximum adhesion force and work of adhesion. Based on the different responses obtained, validity of the coatings applied on the PLCL specimens was confirmed. Control experiments were carried out on laminin-coated borosilicate glass slides.

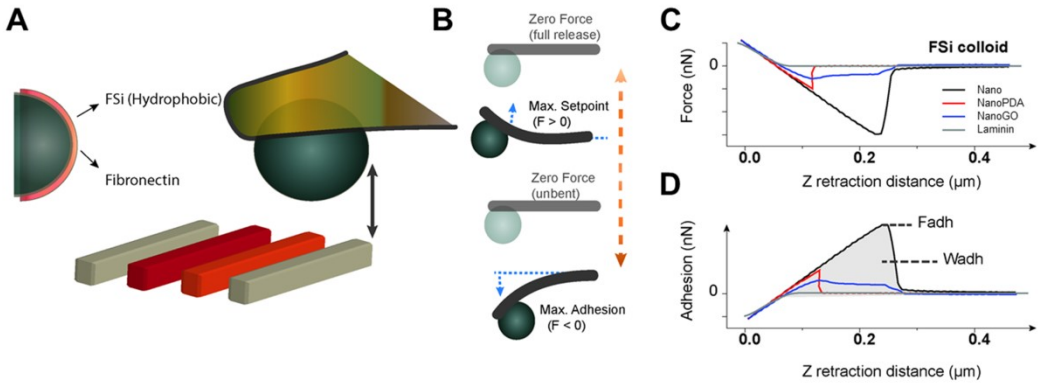

Figure 3.2.: AFM method schematic representation.
(A) General experimental scheme of the force measurements performed on PLCL substrates. The colored blocks reflect the different systems under analysis. **(B)** The motion of the colloidal probe is restricted to Z axis, where the existing forces induce a cantilever bending. The chemical properties of the probing colloid can be tuned depending on the coating (FSi vs FN) applied. **(C)** Representative retraction force plots for fluorinated probes (FSi) in contact with the PLCL substrates and **(D)** their transformation into adhesion vs retraction distance.

3.2.2.3. Raman spectroscopy

Raman spectra of the scaffolds were collected by using a Renishaw In Via Raman spectrometer, joined to a Leica DMLM microscope. The spectra were acquired with the Leica 50x N Plan (0.75 aperture) objective. Besides, for the visualization and focusing, another Leica 5x N Plan (0.12 aperture) and a 20x N Plan EPI (0.40 aperture) objectives were used. The spatial resolution for the 50x objectives is 1-2 μm. For the focusing and searching of the points of interest, the microscope implements a prior scientific motorized stage (XYZ) with a joystick. The measurements were performed with a laser of 785 nm (diode laser, Torsana). In this case, the power at the source is 350 mW, being the maximum power at the sample 150 mW. In all the measurements, the power of the laser was reduced in order to avoid photodecomposition of the samples (burning) by using neutral density filters. For each spectrum 10 s were employed and ten scans were accumulated.

3.2.2.4. X-ray photoelectron spectroscopy (XPS)

To confirm the successful functionalization with PDA and GO, scaffolds were subjected to XPS analysis with a SPECS (Germany) instrument equipped with Phoibos 150 1D-DLD analyzer and monochromatized Al Kα (1486.6 eV) radiation source. Survey scans (1100 to 0 eV binding energy, BE; step energy 1 eV; dwell time 0.1 s; pass energy 40 eV) were acquired with an electron take-off angle of 90º. High-resolution scans (step energy 0.1 eV; dwell time 0.1 s; pass energy 30 eV) were also acquired with an electron take-off angle of 90º. The hydrocarbon peak component in the C 1s spectra was set at 285.0 eV

to correct sample charging. The spectrometer was previously calibrated with the peak of Ag 3d 5/2 (368.28 eV).

3.2.2.5. Contact angle measurements

Surface wettability changes due to the stepwise coating procedure (PDA, GO) were determined on flat samples with a Kruess EasyDrop instrument (Kruess, Hamburg, Germany). The water droplets (8 µl) were deposited perpendicularly on the samples (3x) by means of a glass syringe.

3.2.3. Cell culture

NSCs were obtained, cultured in Neurocult proliferation media and passaged as previously described [7,21]. Cells were seeded at a density of either 10,000 or 5,000 cells per scaffold. For the control assays, NSCs were seeded onto 12 mm coverslips either coated with laminin or non-coated (L2020, Sigma, St. Louis, MO), as previously described [22]. Cell differentiation was induced using Neurocult differentiation supplement (cat# 05752, Stem Cell Technologies, Vancouver, Canada) at 9:1 ratio, 2% B27 supplement (cat# 17504044, Gibco, Waltham, MA USA), in the presence of 100 U/ml penicillin and 150 µg/ml streptomycin antibiotics. Fresh medium was replaced every three days. Cell orientations were calculated by measuring the orientation angle of the leading edge relative to a common reference point using ImageJ software.

3.2.3.1. Immunostaining

Samples were fixed using a phosphate buffer saline (PBS) solution of 4% paraformaldehyde (PFA) (cat# 158127, Sigma Aldrich, Spain) and 3% sucrose (cat# S0389, Sigma Aldrich, Spain). Then, cells were permeabilized with PBS containing 0.3% triton-X100 in 1% Bovine Serum Albumin (BSA) (cat# A7906, Sigma-Aldrich, Spain) and incubated with the respective primary antibodies overnight (o.n.) at 4 ^{o}C. To characterize commitment to neuronal lineages, DCX and NeuN were used as immature and mature neuronal markers, respectively (1:400, sc8066, Santa Cruz, Dallas, USA; 1:200, ab177487, Abcam, Cambridge, UK). To characterize commitment to astroglial lineages, both GFAP and S100β (1:400, MAB360, Merck Chemicals & Life Science S.A.; 1:400, Dako Cytomation, Glostrup, Denmark) were used. After three washes with PBS, scaffolds were incubated with donkey anti-mouse, anti-rabbit or anti-goat Alexa secondary antibodies 488, 594, 647 or 680 (Life Technologies, Carlsbad, USA) and counterstained with DAPI (1:1000, Sigma, St. Louis, USA), dried and mounted using DAKO fluorescence mounting medium (cat# S3023, Dako Cytomation, Glostrup, Denmark).

3.2.3.2. Scanning electron microscopy (SEM)

Samples were fixed using 2% glutaraldehyde (cat# 50-262-19, Fisher Scientific, Pittsburgh, USA) diluted in 0.1 M cacodylate buffer (cat# C0250, Sigma-Aldrich, Spain) at pH = 7.4 for 1 h at room temperature (RT). Then, the fixative solution was rinsed using cacodylate buffer plus isosmolar sucrose (cat# S7903, Sigma-Aldrich, Spain). Samples were post fixed using 1% osmium tetraoxide (OsO_4) (cat# O5500, Sigma-Aldrich, Spain) in cacodylate for 1 h in the dark at 4 ^oC. Then, OsO_4 was removed by three rinses of 10 min with cacodylate buffer. Samples were immediately dehydrated with increasing series of EtOH (30^o, 50^o, 70^o, 90^o, 96^o, 100^o and 2x100^o absolute) during 10 min each. The desiccation at critical point was performed with two washes of 10 min of hexamethyldisilazane (cat# 440191, Sigma-Aldrich, Spain) and then the samples were dried. Immediately after this point, samples were placed on scanning electron microscope stands using conductive cement. Finally, a metallic coating was made using gold sputtered in an Argon atmosphere. Samples were visualized using a scanning electron microscope Hitachi S-3400 N (Hitachi, Tokio, Japan).

3.2.3.3. Videomicroscopy

Neurospheres were disaggregated and 60,000 NSCs were cultured in a petri µ-Dish 35 mm (Ibidi, Gräfelfing, Germany) containing nanostructured scaffolds either functionalized with GO or not. Cells were allowed to attach during 2 h and then recorded for a total of 72 h using a Nikon BioStation IM-Q videomicroscopy (Nikon Instruments Europe BV, Amsterdam, Netherlands). Imaging conditions were maintained at 37 ^oC, 5% CO_2 and 95% relative humidity. Images of four-six fields per condition were taken every 15 min using a 20x objective. Tracking and overlay of individual cell tracks over a reduced period of 8 h were carried out using the MTrackJ plugin in ImageJ software. Dynamic parameters (migration velocity, pausing time, persistence and total traveled distance) were calculated with an Excel macro developed by F. Cordelières (Bordeaux imaging center, UMS 3420 CNRS, Bordeaux, France) [23].

3.2.4. Statistical analysis

Comparisons between multiple groups were made using Kruskal-Wallis followed by Dunn´s post hoc test or Holm-Šídák method. In turn, comparisons between only two groups were made using U-Mann Whitney test, where $p < 0.05$ was considered as statistically significant. Results were presented as mean ± SD or SEM (indicated accordingly). The number of independent experiments is shown in the respective figure legend. For the mechanical properties of the samples via AFM, the statistical difference between groups was tested by t-test and two-way analysis of variance (ANOVA) at a confidence level of 95% ($p < 0.05$).

3.3. Results and discussion

3.3.1. PLCL scaffolds were successfully fabricated, nanostructured and functionalized

Although the use of nanostructured scaffolds as a tool to promote cell alignment and differentiation is well reported in bibliography from a conceptual perspective, most of the studies either employ non-biodegradable substrates or complex procedures for the fabrication of the scaffolds, which enormously limit their potential in the biomedical field [16,24–27]. Herein, we employed a fully bioresorbable, FDA-approved polymeric material based on L-lactide and ε-caprolactone (70/30 molar ratio) [28]. This copolymer undergoes a random-scission of its ester linkages in aqueous solutions and starts losing weight after approximately 80 days in PBS [29]. Considering also that, in the bulk degradation process, the degrading chains are not expelled out to the surrounding environment until the end of the degradation process [30], we do not expect any interference of the degradation by-products with the cell differentiation process studied herein.

Thanks to the thermoplastic nature of the copolymer, the nanotopography of a commercially available silicon stamp was faithfully replicated on the PLCL films, yielding nanostructured PLCL scaffolds with a well-defined grooved pattern (Figure 3.3. A). This process was performed in an ease, quick and easy to scale up way without the need of any organic solvent or complex processes, which highlights the robustness, scalability and versatility of this methodology. The surface of the scaffolds was characterized by ridges of 496.5±29.8 nm and grooves of 203.3±22.8 nm. For a more detailed morphological characterization, atomic force microscopy (AFM) was employed (Figure 3.3. B). As evidenced from these images, some ridges appeared slightly distorted, which can be ascribed to the soft mechanical behavior of this copolymer at room temperature [31].

The fabrication and post-functionalization processes are frequently performed in the presence of organic solvents that may induce a cytotoxic effect if they are not completely eliminated [32]. Following this solvent-free strategy, the post-functionalization of the nanostructured scaffolds was achieved by exploiting the multiple interactions between PDA and virtually any substrate in slightly basic aqueous solutions [33]. First, the nanostructured scaffolds were coated with a thin and homogeneously distributed layer of PDA with no detrimental effect on the nanotopography (Figure 3.3. A and B). The concentration of the initial dopamine hydrochloride solution and the reaction time were carefully controlled to avoid the excessive deposition of PDA agglomerates that could deteriorate the native nanostructured topography of the scaffolds (Figure 3.4. A). This nanostructured topography was also preserved after the final functionalization with GO (Figure 3.3. A and B). Working at higher GO concentrations in this step resulted in the

excessive deposition of GO, which, again, covered some areas of the polymeric film (Figure 3.4. B).

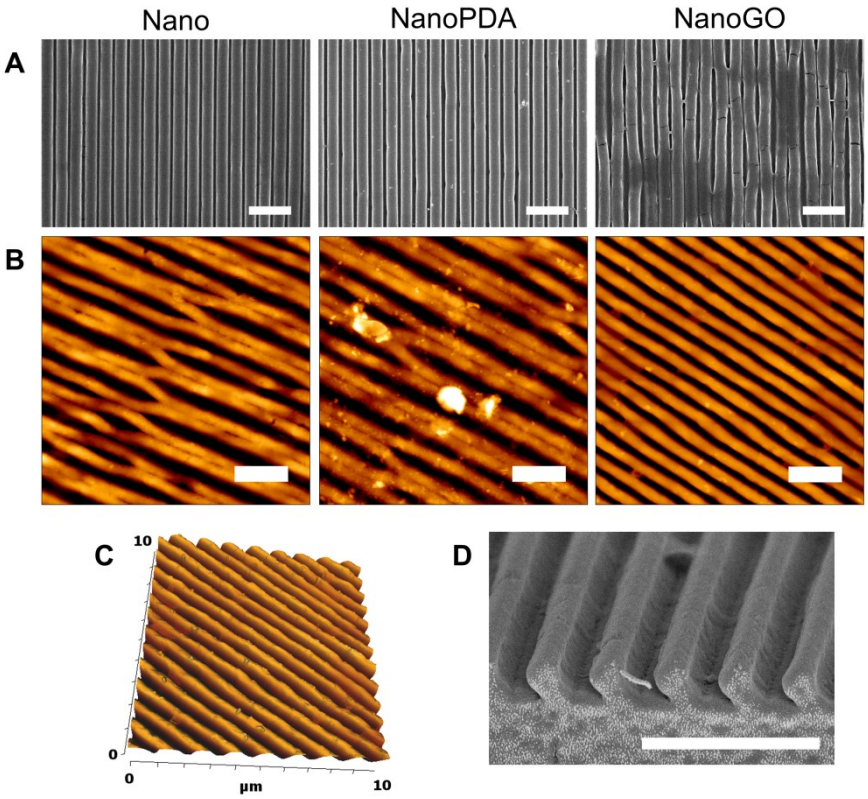

Figure 3.3.: Morphological characterization of the nanostructured scaffolds.
(A) SEM and **(B)** AFM micrographs of nanostructured PLCL (Nano), nanostructured PLCL coated with PDA (NanoPDA) and further functionalized with GO (NanoGO). **(C)** AFM 3-dimensional micrograph and **(D)** SEM cross-section micrograph of a nanostructured PLCL scaffold. Scale bars, 2 µm.

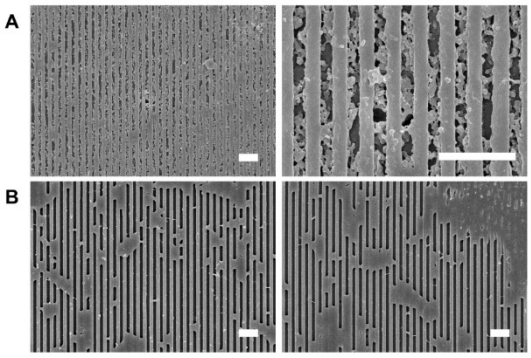

Figure 3.4.: Polydopamine and GO deposition at different concentrations and incubation times.
(A) SEM micrographs of nanostructured PLCL scaffolds coated with PDA at a concentration of 0.5 mg/ml for 2 h. **(B)** SEM micrographs of nanostructured PLCL scaffolds coated with PDA and further functionalized with GO at a concentration of 0.5 (left) or 1 mg/ml (right) of GO. Scale bars 2 µm.

In the case of non-nanostructured PLCL scaffolds (Figure 3.5. A and B), a slight increase in the overall roughness was observed as PDA and GO were deposited, similar to the results observed for the nanostructured scaffolds.

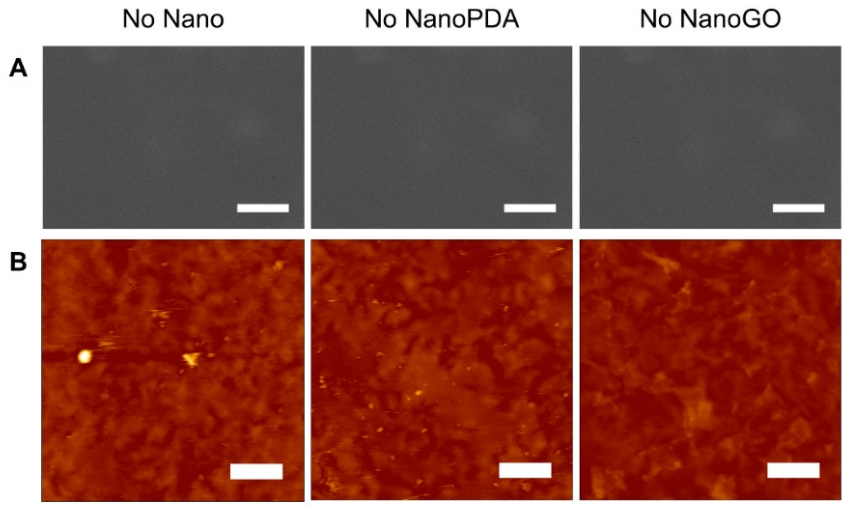

Figure 3.5.: Morphological characterization of the non-nanostructured scaffolds.
(A) SEM and **(B)** AFM micrographs of non-nanostructured PLCL (No Nano), non-nanostructured PLCL coated with PDA (No NanoPDA) and further functionalized with GO (No NanoGO). Scale bars, 5 µm for SEM and 2 µm for AFM.

To confirm the successful functionalization of the scaffolds with PDA and GO, the samples were subjected to XPS, Raman spectroscopy and AFM in force spectroscopy mode analysis. After PDA coating, an increase (from 29 to 41%) of the contribution at 285.0 eV, that corresponds to C-C/C-H bonds, was observed in the C 1s spectrum with respect to the pristine PLCL scaffold (Figure 3.6. A). Additionally, in the N 1s spectra a peak centered at 400.0 eV appeared, which can be ascribed to secondary and primary amine groups, and imine functionalities from PDA. The differences in the XPS spectra after surface functionalization with GO with respect to PDA-coated films was negligible and only a slight decrease (from 3.1 to 1.6%) in the nitrogen signal was detected.

Raman spectroscopy however, truly confirmed the presence of GO on the surface of the PLCL scaffolds (Figure 3.6. B). The intensities of the D and G bands, which are associated respectively to the disordered structure of graphene in sp^2-hybridized carbon and stretching of the C-C bond in graphitic materials [34], increased with the concentration of the employed GO solution for the incubation. Note that the D and G bands were not present in the scaffold incubated with a 0.25 mg/ml GO solution but in the absence of PDA adlayer, which highlights the importance of the PDA coating for the successful functionalization of the surface with GO. This can be associated to several interactions between PDA and GO, including hydrogen bonding between amine and hydroxyl groups of PDA and GO respectively and π-π stacking between catechol groups of PDA and the hexagonal lattice of GO [35]**.** Subsequent experiments were performed with the scaffolds functionalized with a GO concentration of 0.25 mg/ml, which ensured a successful surface functionalization while preserving the native nanotopography of the PLCL scaffolds.

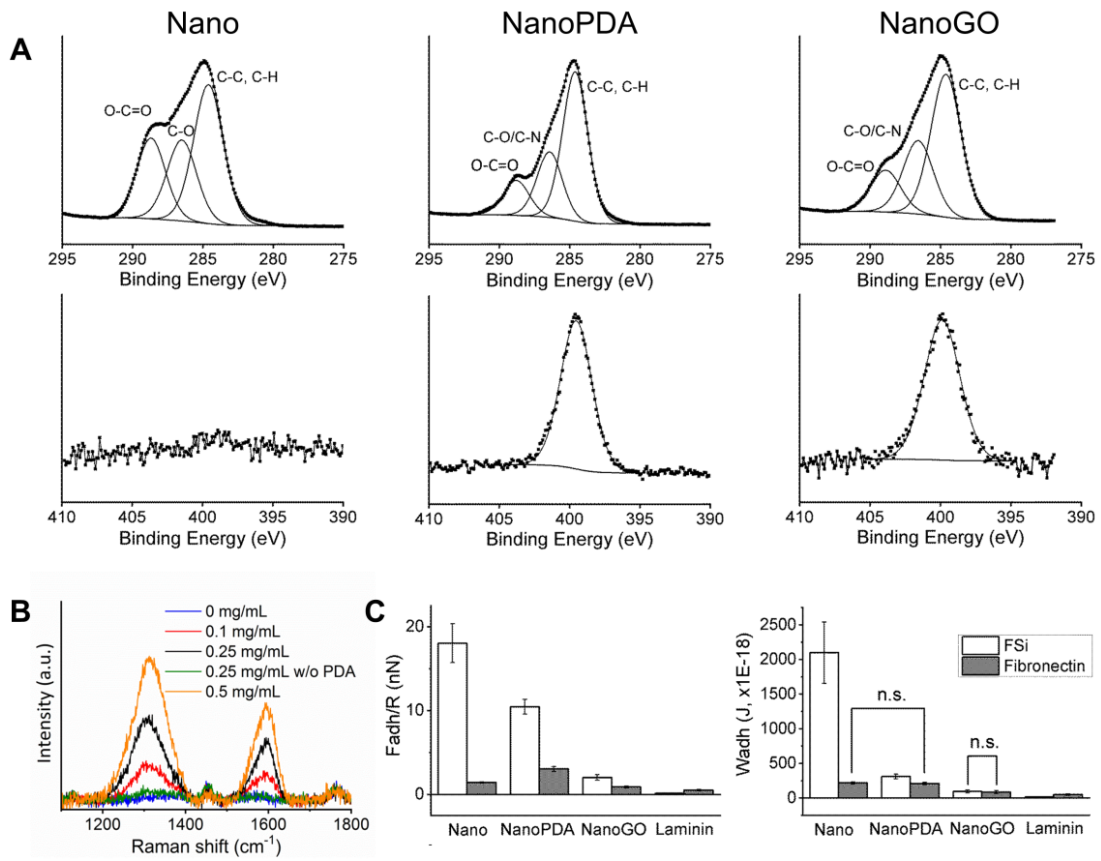

Figure 3.6.: Surface characterization of the scaffolds.

(A) High resolution C 1s (top) and N 1s (bottom) XPS spectra of nanostructured PLCL (Nano), nanostructured PLCL coated with PDA (NanoPDA) and further functionalized with GO (NanoGO). **(B)** Raman spectra of NanoGO scaffolds at different concentrations of GO solution. **(C)** Mean adhesion force (left) and work of adhesion (right) values for FSi (white) and fibronectin-coated (grey) probes. The error bars correspond to the standard error of the mean (SEM). Statistically significant differences ($p < 0.05$) were observed in all the cases, except in those indicated by n.s.

The employment of AFM in force spectroscopy mode enabled the quantitative evaluation of the mechanical properties (adhesion) at the interface between cells and the substrate. Hydrophobic probes led to larger forces than fibronectin-coated ones (used as control), independently of the substrate under analysis (Figure 3.6. C). For the hydrophobic probes, the maximum adhesion value, together with the corresponding adhesion work, decreased with the different coatings applied (Table 3.1.). This could be explained by the higher hydrophobic character of PLCL (water contact angle-WCA ≈ 90-100^{o}), in comparison with thin PDA (WCA ≈ 50^{o}), GO (WCA ≈ 15-30^{o}) and laminin (< 10^{o}) films, which were gradually more hydrophilic. This behavior highlights the fact that level-wise modification of PLCL took place satisfactorily, and that just a few nanometers are enough to change the character of the interface.

For fibronectin-coated colloids, and despite the much lower values calculated, the different content of the substrate also led to a variation in the adhesion-related response. In this case, forces of hydrophobic nature were not the dominant ones anymore. Indeed, adhesion factors for bare PLCL suffered a 10-fold drop in comparison with hydrophobic probe measurements (Figure 3.6. C and Table 3.1.). Here, PDA-coated scaffolds appeared as the predominant ones while those containing GO on top presented lower affinity for fibronectin, although still higher than control laminin films. Therefore, the effective action of the surface modification is again confirmed.

Table 3.1.: Table of FSi and fibronectin-coated probes showing the values of the maximum adhesion value and the adhesion work after applying the different coatings to the nanostructured PLCL scaffolds. Samples of nanostructured PLCL (Nano), nanostructured PLCL coated with PDA (NanoPDA) and further functionalized with GO (NanoGO) were compared to the laminin control (laminin). SEM values correspond to the standard error of the mean.

	Fsi probe				Fibronectin			
	F_{adh}	SEM	W_{adh}	SEM	F_{adh}	SEM	W_{adh}	SEM
	nN		$x10^{-18}$ J		nN		$x10^{-18}$ J	
Nano	18.04	2.32	2098.47	442.06	1.42	0.07	218.53	14.91
NanoPDA	10.46	0.88	312.75	34.78	3.03	0.31	209.52	17.37
NanoGO	2.03	0.32	95.13	19.77	0.88	0.11	86.06	22.96
Laminin	0.15	0.02	13.57	1.69	0.50	0.08	49.01	9.78

3.3.2. Neural stem cells and progenitors attach and align following nanopattern shape without the need of a laminin coating

Laminin has been extensively used for monolayer coating of NSC cultures. To test whether NSCs were able to adhere and survive to surfaces without laminin coating, 5,000 NSCs were seeded into nanostructured and non-nanostructured scaffolds. Alternatively to laminin, GO has been employed owing to its reported physico-chemical features to improve cell adhesion and neuronal differentiation [11,36]. Forty-five minutes after initial seeding, only nanostructured surfaces showed a clear cellular orientation and attachment as evidenced by the guided growth of the cell leading edge (Figure 3.7. A). We noticed that most of the adhered cells shared the same orientation following the surface nanopattern. A quantification representing the variation of angle measurements was performed and determined that 70% of the cells were perfectly aligned with nanostructured scaffolds functionalized with GO (NanoGO), meanwhile nanostructured scaffolds without GO functionalization (NanoPDA) showed a 67% of cells aligned with a variation of 30^{o}. Non-nanostructured scaffolds had shorter leading-edge processes with no preferential orientation (Figure 3.7. B).

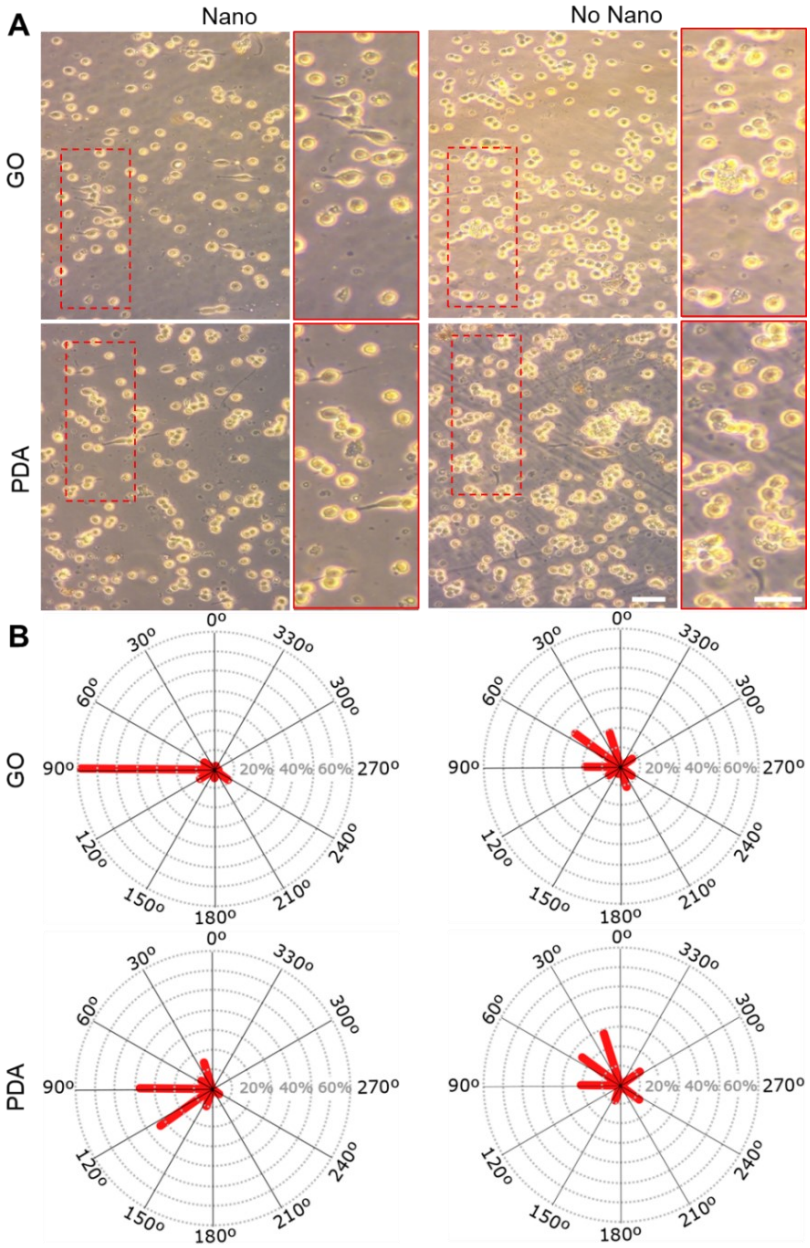

Figure 3.7.: Neural stem cells and progenitors (NSCs) alignment on the nanostructured scaffolds without ECM-like compound coating.

(A) Brightfield microscopy images of NSCs forty-five minutes after seeding, showing the parallel alignment of cell elongations on nanostructured scaffolds. **(B)** Distribution of cell orientation measuring angle degrees around the mean (90^{o}) in NanoGO (78 cells analyzed), NanoPDA (45 cells), No NanoGO (31 cells) and No NanoPDA (26 cells). Scale bars, 25 µm.

Additionally, two hours post-seeding, the length of the leading cellular process was determined. The cells seeded on NanoGO showed the maximal elongation with an average of 32.45±6.74 µm while NanoPDA showed a reduced length of 23.66±5.41 µm (Figure 3.8.). On the contrary, the leading processes of the cells seeded on non-nanostructured scaffolds functionalized with GO (NoNanoGO) were smaller than without the functionalization (NoNanoPDA) (13.74±1.29 and 23.86±9.19 µm respectively; $p < 0.001$ One-way ANOVA).

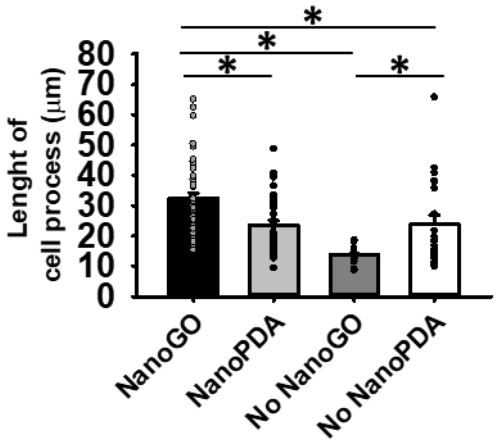

Figure 3.8.: Length of cell processes on different scaffolds.
Quantification of the length of cellular process for each condition. Bars are shown as mean ± SEM. Dots show individual data. *p < 0.05, after Kruskal-Wallis One Way Analysis of Variance on Ranks.

To test whether nanostructured scaffolds were able to guide the orientation and migration of NSCs for longer periods that are compatible with neuronal differentiation protocols, the experiment was repeated by allowing the seeded NSCs to grow for three days *in vitro* (DIV3) in proliferation medium. Afterwards, the culture medium was changed to differentiation medium to allow cellular neurodifferentiation. The culture was kept for another seven days (total DIV10, Figure 3.9. A). The nanostructured materials induced an oriented growth and migration of NSCs along the parallel grooves during the initial three days of culture, independently of the GO functionalization. Non-nanostructured surfaces only showed large spheroid-shaped cellular structures as in (non-coated glass control) standard free-floating neurosphere cultures (Figure 3.9. B). To further confirm the results and corroborate that 1) cells were aligning according to the nanograting axis and 2) the alignment could be maintained after cell differentiation, cells were seeded and allowed to attach in proliferation medium for 24 h. Thereafter, the medium was changed to induce cell differentiation and cells were fixed at DIV7 or DIV14. SEM analysis demonstrated the alignment of cell clusters following the nanostructured grooves both at DIV7 (Figure 3.10. A) and DIV14 (Figure 3.10. B). Thus, NSCs grew aligned with the surface nanopattern in a timescale compatible with neural cell differentiation protocols.

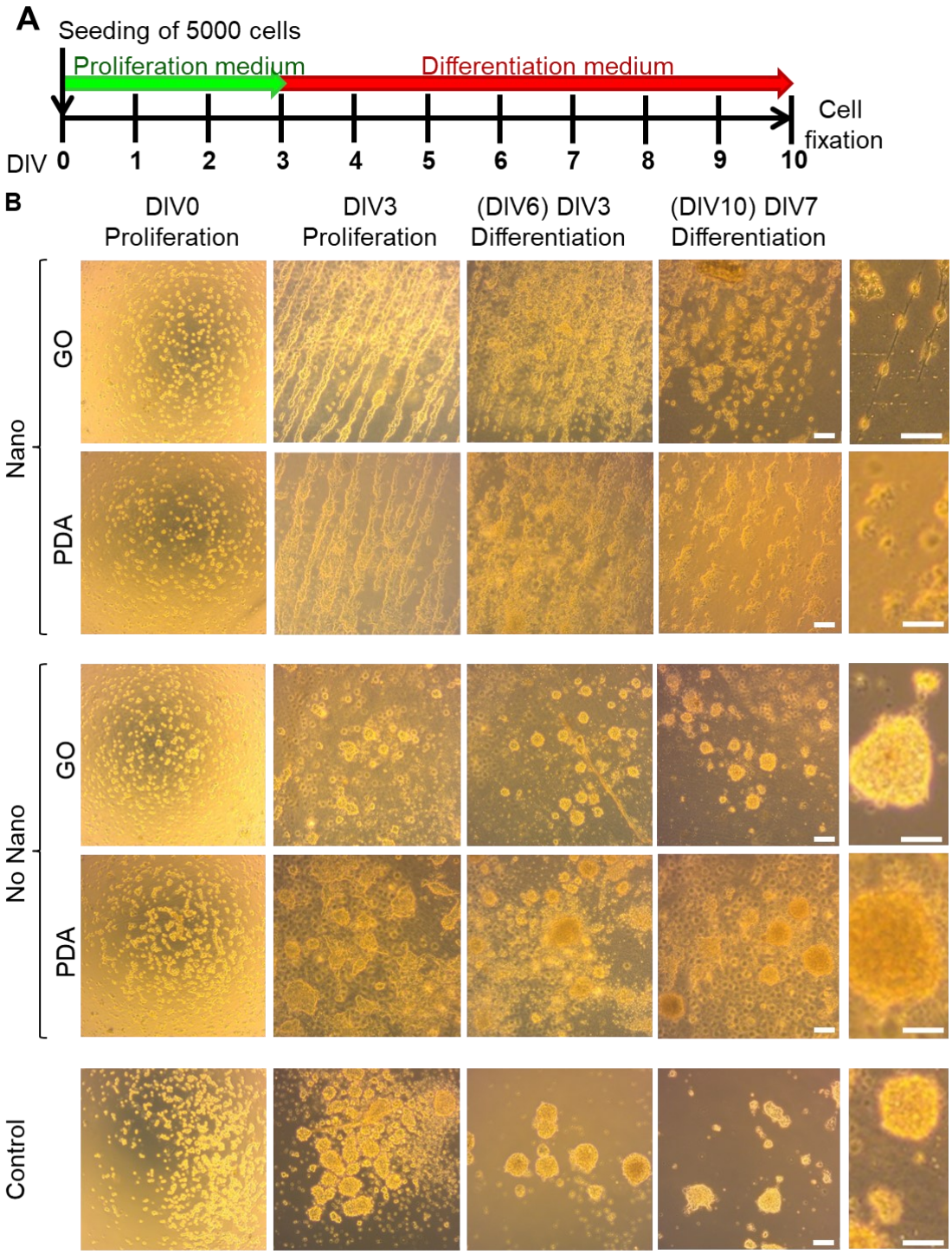

Figure 3.9.: NSCs attachment and alignment without ECM-like coating.
(A) Scheme of experimental design. **(B)** Images showing the evolution of NSC cultures over the different substrates with no ECM protein coating in any of them. Cells align during the initial three days following the nanostructured grooves and do not detach during one-week differentiation. Cultures with non-nanostructured grooves grow forming cell clusters without any preferential cell alignment. Control condition using a coverslip without any ECM protein coating shows that cells do not attach, growing as neurospheres. Scale bars, 100 µm.

Overall, the intrinsic properties of our nanostructured scaffolds offer the advantage of NSC adhesion without the need of an extracellular matrix (ECM)-like compound like laminin coating. Additionally, the nanostructured scaffolds NanoGO and NanoPDA offered the advantage of cell alignment and elongation along the nanostructured grooves. Even though the induction of cell alignment and elongation according to a determined nanograting axis has been reported before [16,37,38], most of the times the structure is covered with ECM-like compounds to allow the attachment of the cells. But ECM-like compounds may represent a lethal risk *in vivo* which hinder their future use in clinic [9]. Here, we present an ECM-like compound free strategy for the alignment of NSCs, providing a tool for both *in vitro* and *in vivo* studies.

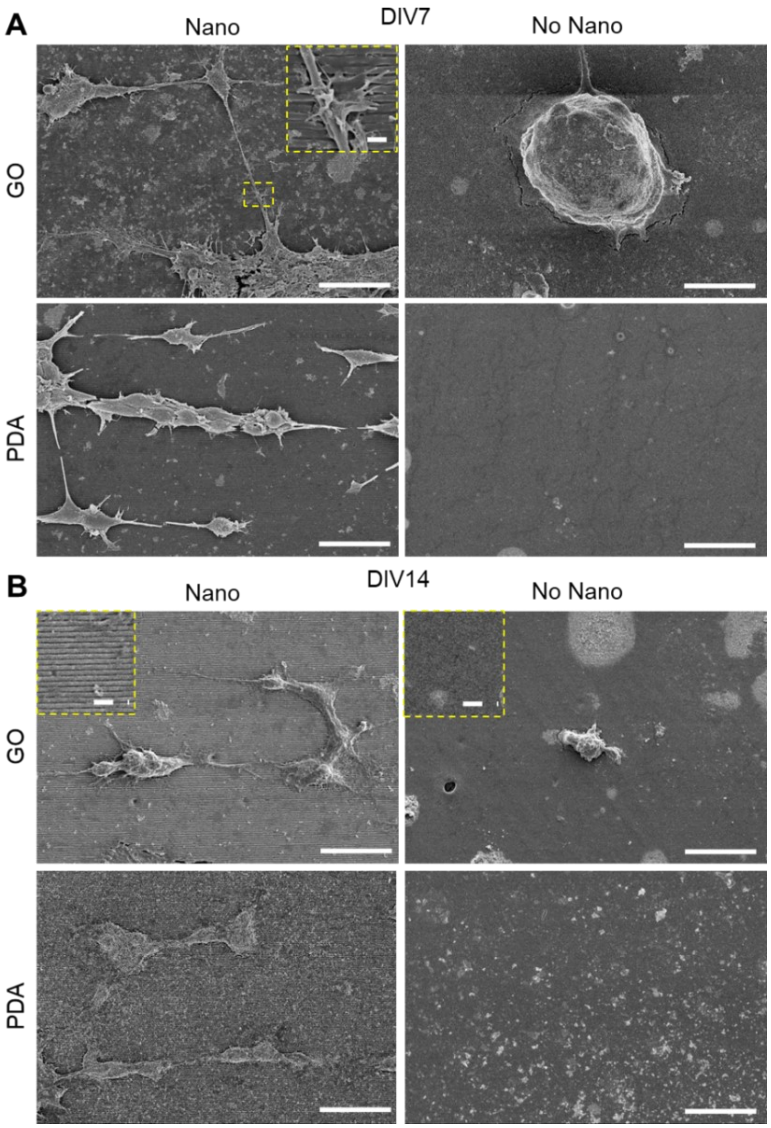

Figure 3.10.: Images of NSCs alignment and elongation according to the nanograting axis.
(A) SEM of NSC culture at DIV7 showing pack of cells aligned in the nanostructured scaffolds and detail of cell-to-cell contacts (inset). Non-nanostructured scaffolds impede cell attachment and spreading. **(B)** Fourteen days post seeding, cells remain attached and the alignment of the nanopatterning (inset) serve as guide for cell projections. On the contrary, the absence of nanopatterning maintained NSCs as rounded spheres impeding cell attachment and dissemination. Scale bar 50 µm and Inset 2 µm.

3.3.3. Surface nanostructured grooves allow the oriented migration of neural stem and progenitor cells

Since cell migration is a critical factor for complete tissue regeneration (e.g., wound healing), the next step was to assess the dynamics of cell growth and adhesion over the different biomaterials. Hence, NSCs were seeded on the scaffolds and videorecorded for 72 h to characterize its migratory properties. Cells cultured over nanostructured scaffolds independently on the functionalization with GO (NanoPDA vs NanoGO) displayed a lower motility with respect to cells cultured over laminin (mean velocity of 12.67±1.54 μm/h (NanoPDA), 15.23±1.17 μm/h (NanoGO) and 26.49±0.68 μm/h (laminin control)), ($p < 0.001$ One-way ANOVA, Figures 3.11. A and B). Remarkably, the difference between GO presence and GO absence conditions was not statistically significant ($p < 0.075$, One-way ANOVA, Figure 3.11. B). Persistence time characterizes the average time between significant changes in the direction of a translocation of a cell [39–41]. This value allows a quantitative analysis of the differences in migration behavior. The results are shown in the percentage of time. The cells cultured on nanostructured NanoPDA and NanoGO scaffolds showed significantly more persistence than the cells cultured on laminin control (35.81±19.19% (NanoPDA) and 17.82±5.51% (NanoGO) with respect to 7.31±1.42% (laminin control)), ($p < 0.001$, One-way ANOVA, Figure 3.11. C). According to these results, nanostructured scaffolds showed an increased pausing time in comparison with those coated with laminin (98.81±0.96% (NanoPDA), 97.37±0.72% (NanoGO) and 91.14±1.31% (laminin control)), ($p < 0.001$, One-way ANOVA, Figure 3.11. D). Also, the total traveled distance for an interval of 8 h was similar on nanostructured scaffolds NanoPDA and NanoGO and much higher in the case of laminin control (40.79±35.89 μm (NanoPDA), 68.59±16.95 μm (NanoGO), and 316.91±45.01 μm (laminin control)), ($p < 0.001$, One-way ANOVA, Figure 3.11. E).

Overall, we found that nanostructured scaffolds allowed the directionality of cell migration along the nanostructured grooves. Thus, our strategy goes a step further allowing the possibility of creating migration paths of NSCs and most surely their differentiated cell progeny that follow a determined orientation according to the desired nanopatterning.

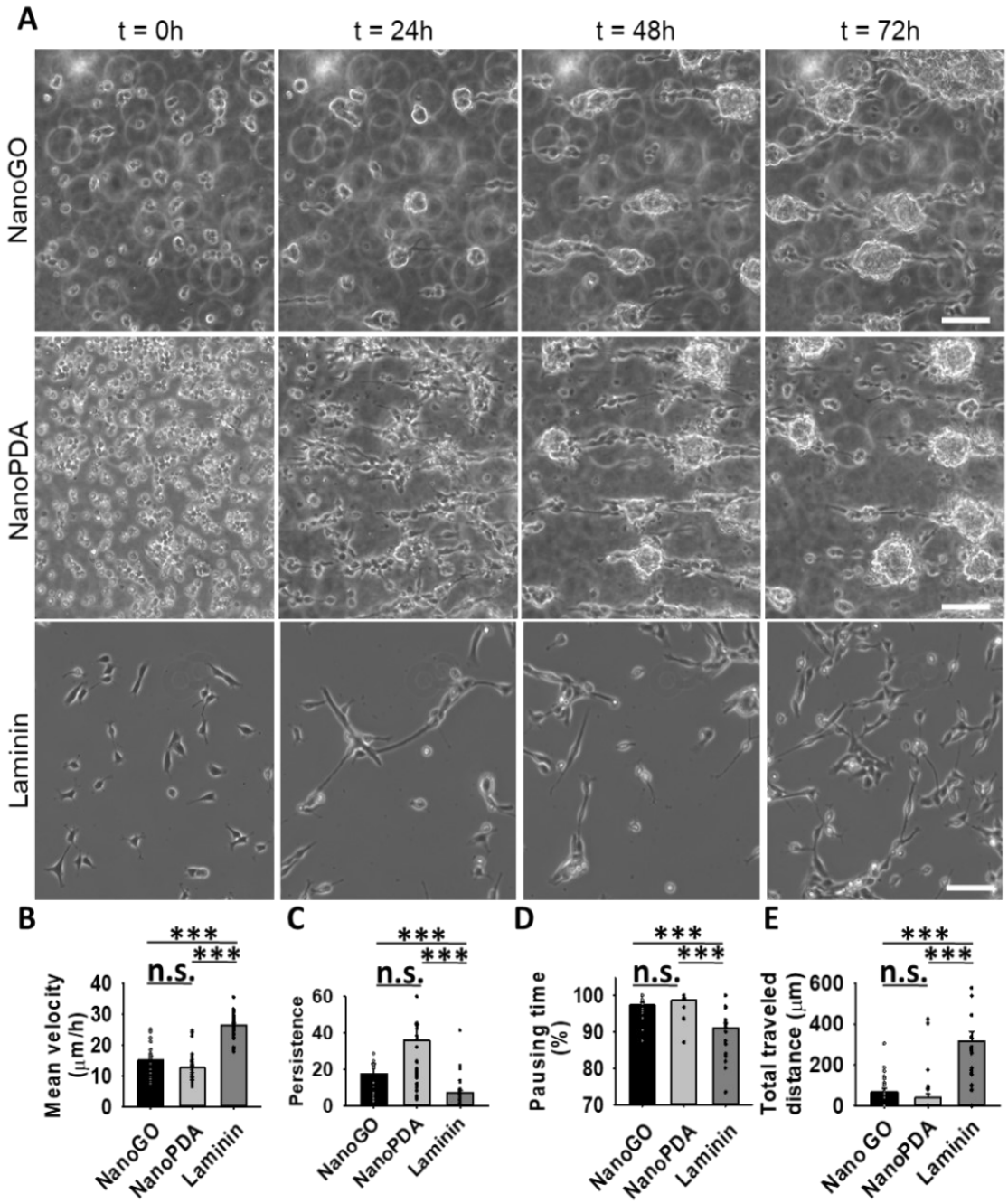

Figure 3.11.: Dynamic movement pattern of NSCs and progenitor cells over the NanoGO and NanoPDA scaffolds.

(A) Videomicroscopy snapshots at 0, 24, 48 and 72 h post seeding in nanostructured scaffolds illustrates the dynamic process of the parallel cell alignment. On the contrary, NSCs seeded on laminin-coated surfaces show a random distribution over time. **(B)** Mean cell velocity, **(C)** Cell persistence, **(D)** Pausing time and **(E)** Total traveled distance of the cells over the NanoPDA and NanoGO scaffolds compared to laminin control. Bars are shown as mean ± SEM. Dots show individual data. ***p < 0.001, Kruskal-Wallis One Way Analysis of Variance on Ranks. Scale bars, 50 μm.

3.3.4. Neural stem and progenitor cells cultured on nanostructured scaffolds are able to generate neuronal and astroglial lineage cells

Another important aspect for neural tissue cell therapy is to preserve the capabilities to generate newborn neurons as well as their supportive glial cells. To check whether nanostructured scaffolds were permissive to the generation of both neuronal and astroglial lineage, NSCs were first kept for 24 h in proliferation medium and then switched to differentiation medium. At DIV7 with differentiation medium, both nanostructured and non-nanostructured scaffolds with or without GO were fixed for immunostaining. Neuroblasts are neuronal precursors with migratory properties that strongly express the protein doublecortin (DCX) [42–44]. On the other hand, astrocytes are other abundant cells in the central nervous system that abundantly express glial acidic fibrillary protein (GFAP) [45]. Double immunofluorescence against DCX and GFAP showed the presence of both these cell types on the nanostructured scaffolds (Figure 3.12.). In the case of non-nanostructured scaffolds, due to the lack of adhesion, only few cells were counted on the immunostaining (data not shown).

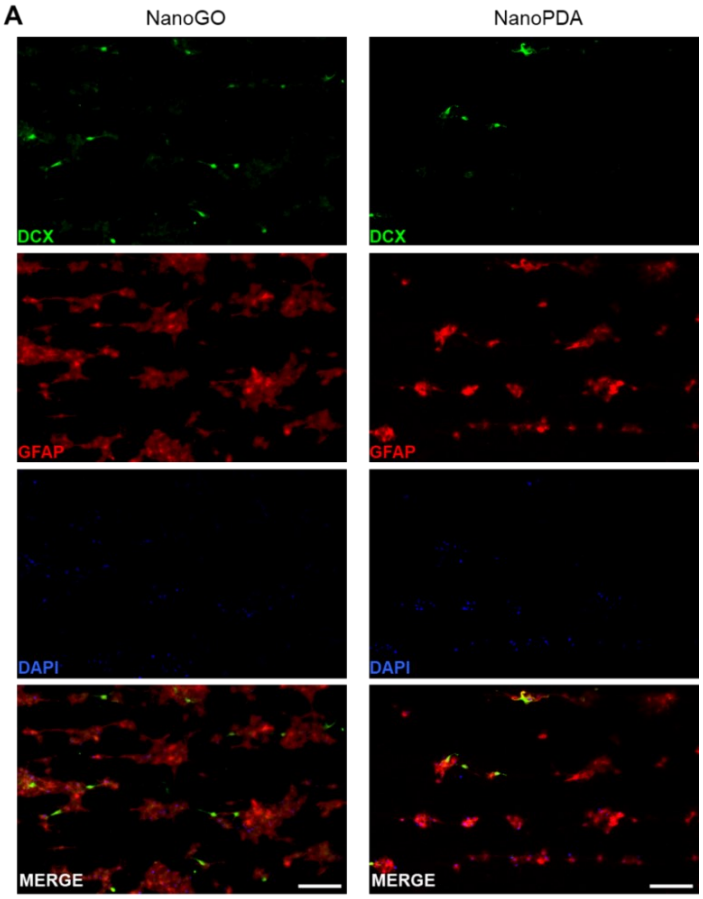

Figure 3.12.: NSCs cultured on nanostructured scaffolds showing a co-culture of neuronal and astroglial precursor cells.
Confocal microscopy images of DCX (neuroblasts) and GFAP (astrocytes) immunostaining on nanostructured surfaces. Aligned clusters containing neuronal and glial lineage cells are observed at DIV7 after switch to differentiation medium. DAPI was used as a counterstain for cell nuclei. Scale bar, 75 µm.

3.3.5. NSC differentiation to neuronal lineage is enhanced by the combination of nanostructured grooves and GO

Once we have demonstrated the differentiation capabilities of the NSCs towards both immature neuronal and astroglial-like cells, we wanted to address the differentiation pattern towards more mature phenotypes. NSCs cultured with differentiation medium on laminin-coated coverslips progressively differentiate towards mature neuronal fates over time, losing DCX and expressing instead NeuN (Figure 3.13.). The level of neuronal maturation was determined by: i) immunostaining for DCX and the absence of the nuclear neuronal marker NeuN (immature neurons), ii) the presence of both markers (maturing neurons) and iii) the absence of DCX and presence of NeuN (fully mature neurons). In control laminin-coating conditions, the DCX positive cell population dropped significantly (from 30.85±2.41% at DIV7 to 15.90±0.02% at DIV10, $p < 0.05$, One-way ANOVA). The percentage of maturing neurons co-expressing DCX+/NeuN+ was stable at DIV7 and 10 (15.66±3.31% and 14.46±2.05% for DIV7 and DIV10, respectively, $p < 0.108$, One-way ANOVA). All these results demonstrated that NSCs were able to neurodifferentiate towards neuronal lineage cells.

Interestingly, when we turned to evaluate mature cell differentiation over scaffolds, we found an enhanced neurodifferentiation of the cells on NanoGO and NanoPDA compared to laminin control. We found that both NanoGO and NanoPDA scaffolds increased the amount of NeuN positive cells at DIV10, compared to laminin control (NanoGO 90.41±0.20, NanoPDA 96.72±3.06% and laminin control 28.62±1.30%, $p < 0.05$, One-way ANOVA), demonstrating that both NanoGO and NanoPDA induced the differentiation towards neuronal lineages at earlier times than those of the ECM adhesion protein laminin. Accordingly, the PDA-coated NanoPDA scaffolds were able to increase DCX (49.10±1.47%) and NeuN (96.72±3.05%) cell populations at DIV10 even without a need of neither laminin nor GO ($p < 0.05$, One-way ANOVA). Again, the induction of neurodifferentiation of stem cells thanks to a synthetic nanostructure has been previously reported [17], which may explain these results.

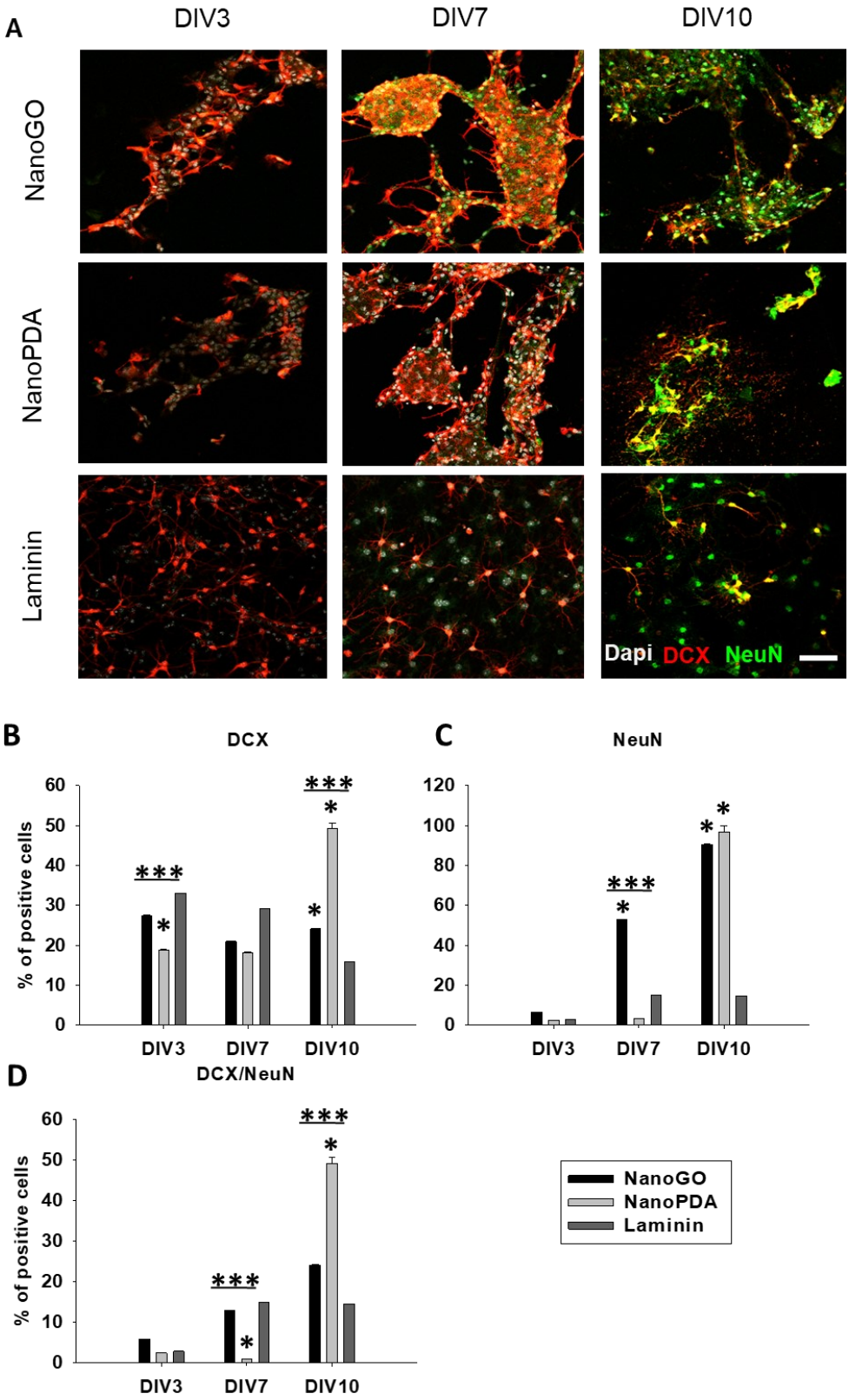

Figure 3.13.: Neuronal differentiation of NSCs over NanoGO and NanoPDA scaffolds.
(A) Double immunofluorescence for the neuronal lineage markers DCX (red) and NeuN (green) at DIV 3, 7 and 10 post-seeding in the different conditions. **(B)** Quantification of the proportion of DCX+, **(C)** NeuN+ and (D) DCX+/NeuN+ double stained positive cells. *p < 0.05 compared to laminin. ***p < 0.001 between the treatments NanoPDA and NanoGO, Holm-Šídák method One Way Analysis of Variance on Ranks. Scale bar, 50 µm.

Remarkably, overall, NanoGO scaffolds seemed to better accelerate the NSC differentiation into neuronal pathway with an increased number of NeuN positive cells with respect to both laminin control and NanoPDA at DIV7 (NanoGO 52.50±0.04%; NanoPDA 3.2±0.01% and laminin control 18.46±3.20%, $p < 0.05$, One-way ANOVA), thus considerably shortening the time needed for complete neuronal differentiation (Figure 3.13.). Nevertheless, the number of neurons co-expressing DCX+/NeuN+ was significantly increased on the NanoPDA scaffolds at DIV10 with respect to NanoGO and laminin control (NanoPDA 49.18±0.03%; NanoGO 24.08±0.02% and laminin control 14.46±2.05%, $p < 0.05$, One-way ANOVA). This phenomenon may be ascribed again to a more rapid neurodifferentiation over NanoGO scaffolds compared to NanoPDA. Indeed, NSCs cultured over NanoGO scaffolds loose DCX but retain NeuN expression. Accordingly, it has been previously reported that the presence of GO enhances cellular neurodifferentiation [46], while the combination of GO with electrical stimulation induces NSC proliferation, neuronal differentiation and neurite elongation [47]. Although GO has been widely chosen instead of pure graphene due to its better capability for laminin assembly, not much data has been reported for the effects of GO-coated scaffolds without the use of ECM-like intermediates [46,47]. We found that laminin-free NanoGO scaffolds reduced the time cells need to express neuronal markers with respect to standard laminin coating and NanoPDA scaffolds. Thus, both nanopatterning and GO surface functionalization can be combined to enhance and accelerate neuronal differentiation.

3.3.6. NSC differentiation to astroglial lineage is accelerated by the presence of both nanostructured grooves and GO

Once we had addressed the neuronal differentiation patterns, we studied the astroglial-like cell differentiation towards both immature (GFAP) and mature (S100β) astroglial-like cells over the nanostructured scaffolds NanoPDA and NanoGO again in comparison with a laminin coated glass cover. NSCs cultured with differentiation medium on laminin-coated coverslips progressively differentiated towards mature astroglial fates over time (Figure 3.14.). The level of glia maturation can be determined as follows: i) immunostaining for GFAP and the absence of S100β (immature glia), ii) the presence of both markers (maturing glia) and iii) the absence of GFAP and presence of S100β (fully mature glia). In control (laminin-coating) conditions, GFAP positive cells increased over time (DIV3 0.64±0.13%; DIV10 28.35±3.13%, $p < 0.005$, One-way ANOVA) (Figure 3.14.). These cells also presented a more intense GFAP positive staining with longer differentiation time in the control laminin coating. On the other hand, S100β staining did not present such variation with time (DIV3 20.97±1.48%; DIV10 28.60±7.07%, $p>0.99$, One-way ANOVA). But the maturing glia presenting GFAP and S100β double stain, increased from DIV3 to DIV10 (DIV3 0.32±0.08%; DIV10 7.92±1.27%, $p < 0.05$, One-way ANOVA), showing the maturation of the cells over time.

Remarkably, the astroglial differentiation of cells seeded on the nanostructured scaffolds NanoPDA and NanoGO showed an increased amount of GFAP positive cells at DIV3 with respect to laminin (NanoPDA 75.25±4.10%, NanoGO 99.02±8.58%, laminin control 0.64±0.13%, $p < 0.05$, One-way ANOVA). Therefore, both, the nanopatterning and the presence of GO seemed to shorten the onset of the glial differentiation of NSCs. The induction of neurodifferentiation of stem cells thanks to a synthetic nanostructure has been previously reported [17], which may explain the accelerated differentiation towards immature glial-like cells. Besides, we found an increase on GFAP positive cells at early stages in the nanostructured scaffolds NanoGO compared to NanoPDA, but a better retention of GFAP positive cells on the NanoPDA compared to NanoGO over time. It has been reported before the positive GFAP staining of NSCs cultured from postnatal mouse forebrains [50], so these results may indicate the presence of undifferentiated NSCs in the culture only till DIV3 in the NanoGO and for longer periods till DIV7 on the NanoPDA scaffolds.

Regarding a more mature differentiation towards astroglial lineages, the percentage of S100β positive cells also increased in the NanoPDA and NanoGO scaffolds at DIV3 with respect to laminin control (NanoPDA 35.84±2.33%, NanoGO 71.94±4.37%, laminin 20.97±1.48%, $p < 0.05$, One-way ANOVA). Again, this quick maturation was more remarkable on the nanostructured scaffolds functionalized with GO. The amount of double stained GFAP and S100β+ positive cells was also higher on the nanostructured scaffolds tested, with respect to laminin control at DIV3 (NanoPDA 33.96±2.37%, NanoGO 70.94±6.37%, laminin 0.32±0.08%, $p < 0.05$, One-way ANOVA) and also higher on NanoGO than on NanoPDA, again suggesting a more rapid glial differentiation on the NanoGO scaffold. Interestingly, S100β is expressed in both mature astroglia and early oligodendrocyte precursor cells [51,52]. In agreement with previous works, we cannot exclude the possibility of S100β positive oligodendroglial cells at DIV3 on NanoGO scaffolds compared to NanoPDA [53].

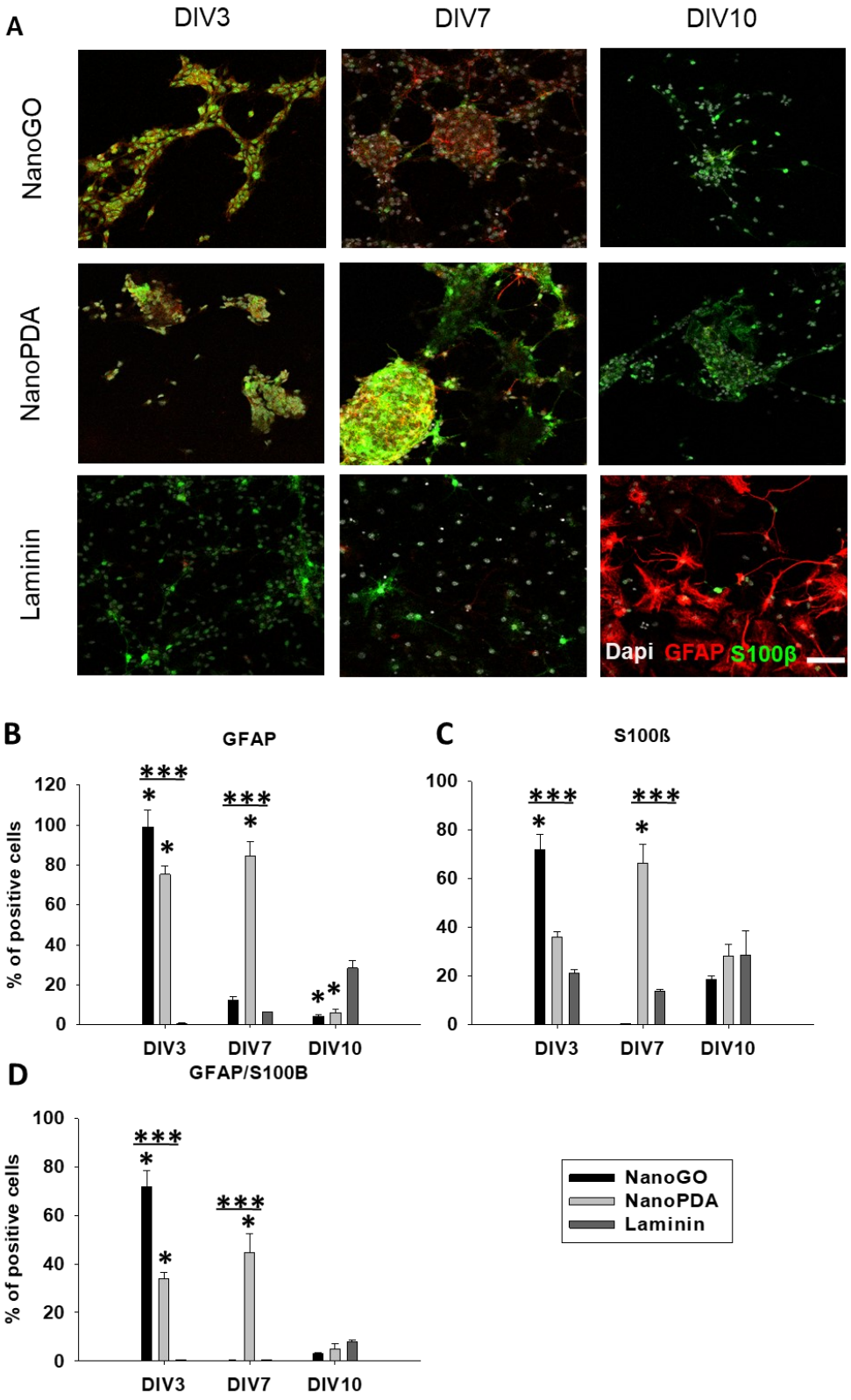

Figure 3.14.: Astroglial differentiation of NSCs over NanoGO and NanoPDA scaffolds.
(A) Double immunofluorescence for the astroglial lineage markers GFAP (red) and S100β (green) at DIV 3, 7 and 10 post-seeding in the different conditions. **(B)** Quantification of the proportion of GFAP+ **(C)** S100β+ and **(D)** GFAP+/S100β+ double stained positive cells. *$p < 0.05$ compared to laminin. ***$p < 0.001$ between the treatments NanoPDA and NanoGO, Holm-Šídák method One Way Analysis of Variance on Ranks. Scale bar, 50 µm.

It is also worth mentioning that the nanostructured scaffolds functionalized with GO, even though they showed the most rapid glial differentiation, presented a reduced amount of GFAP, S100β and double positive GFAP and S100β population at DIV7 (GFAP 12.07±1.83%; S100β 0.25±0.10%; GFAP/S100β 0.25±0.10%, $p < 0.05$, One-way ANOVA) and DIV10 (GFAP 4.33±0.50%; S100β 18.68±1.29%; GFAP/S100β 2.98±0.43%, $p < 0.05$, One-way ANOVA) with respect to the values observed at DIV3 (GFAP 99.02±8.58%; S100β 71.94±4.37%; GFAP/S100β 70.94±6.37%). On the other hand, the NanoPDA scaffolds also presented a lower population of GFAP positive cells at DIV10 compared to laminin control (NanoPDA 5.89±0.20%; laminin 28.35±3.13%, $p < 0.05$, One-way ANOVA). This may be ascribed to the accelerated glial differentiation of the NSCs on the scaffolds compared to laminin, which may contribute to the downregulation of immature glial markers towards more mature ones. Overall, our results suggested a more rapid glial differentiation on both nanostructured scaffolds NanoPDA and NanoGO than over laminin coated glass cover. Besides, NanoGO scaffold showed even a more rapid expression of both immature and mature astroglial markers in comparison with NanoPDA scaffold, but a lack of astroglia maintenance over time. In agreement with our results, other works claimed that nanostructured rGO microfibers were able to offer an alternative substrate for NSC adhesion when compared with 2D graphene films, and an increasing neuronal differentiation but with only few astroglial cells surrounding the microfibers [54]. In agreement with this work of Guo et al., we observed that neuronal differentiation was boosted at DIV7 on the NanoGO scaffolds, at the expense of the astroglial population. However, it is well reported in literature that glial cells are necessary to support neuronal cells [55–58]. Astrocytes for example, cooperate with neurons on several levels, including neurotransmitter trafficking and recycling, ion homeostasis, energy metabolism, and defense against oxidative stress [59,60]. Consequently, this faster differentiation may provoke a mid-term reduction of viability probably by changes of compensatory proportions of neurons and astroglial support. Following the same reasoning, GO has also been previously reported as a potential cytotoxic agent in chicken embryos [61,62]. However, we have not found a variation of apoptotic/pycnotic nuclei in immunostainings experiments, neither retracting cell process nor cell blebbing after SEM examination. This fact reinforces the arguments for the potential use of these systems.

3.4. Conclusions

In the present chapter, we describe the fabrication and characterization of biodegradable nanostructured poly(L-lactide-co-ε-caprolactone) (PLCL) scaffolds either with or without graphene oxide (GO) functionalization, to support the alignment, growth, guided migration and differentiation of neural stem and progenitor cells (NSCs) without a need of a extracellular matrix (ECM)-like compound coating. Furthermore, our scaffolds induce a fast and efficient cell differentiation towards neuronal lineages while maintaining glial cell population, which makes these materials a very attractive neural repair compounds for future therapeutic approaches.

References

[1] C.S. Ahuja, S. Nori, L. Tetreault, J. Wilson, B. Kwon, J. Harrop, D. Choi, M.G. Fehlings, Traumatic Spinal Cord Injury-Repair and Regeneration, Neurosurgery. 80 (2017) S9–S22. https://doi.org/10.1093/neuros/nyw080.

[2] X. Gu, F. Ding, Y. Yang, J. Liu, Construction of tissue engineered nerve grafts and their application in peripheral nerve regeneration, Prog. Neurobiol. 93 (2011) 204–230. https://doi.org/10.1016/j.pneurobio.2010.11.002.

[3] A. Rajaram, X.-B. Chen, D.J. Schreyer, Strategic design and recent fabrication techniques for bioengineered tissue scaffolds to improve peripheral nerve regeneration, Tissue Eng. Part B Rev. 18 (2012) 454–467. https://doi.org/10.1089/ten.TEB.2012.0006.

[4] R. Deumens, A. Bozkurt, M.F. Meek, M.A.E. Marcus, E.A.J. Joosten, J. Weis, G.A. Brook, Repairing injured peripheral nerves: Bridging the gap, Prog. Neurobiol. 92 (2010) 245–276. https://doi.org/10.1016/j.pneurobio.2010.10.002.

[5] S. Kehoe, X.F. Zhang, D. Boyd, FDA approved guidance conduits and wraps for peripheral nerve injury: a review of materials and efficacy, Injury. 43 (2012) 553–572. https://doi.org/10.1016/j.injury.2010.12.030.

[6] E.C. Spivey, Z.Z. Khaing, J.B. Shear, C.E. Schmidt, The fundamental role of subcellular topography in peripheral nerve repair therapies, Biomaterials. 33 (2012) 4264–4276. https://doi.org/10.1016/j.biomaterials.2012.02.043.

[7] Vascular-derived TGF-β increases in the stem cell niche and perturbs neurogenesis during aging and following irradiation in the adult mouse brain | EMBO Molecular Medicine, (n.d.). https://www.embopress.org/doi/full/10.1002/emmm.201202197 (accessed August 25, 2020).

[8] M. Ghidinelli, Y. Poitelon, Y.K. Shin, D. Ameroso, C. Williamson, C. Ferri, M. Pellegatta, K. Espino, A. Mogha, K. Monk, P. Podini, C. Taveggia, K.-A. Nave, L. Wrabetz, H.T. Park, M.L. Feltri, Laminin 211 inhibits protein kinase A in Schwann cells to modulate neuregulin 1 type III-driven myelination, PLoS Biol. 15 (2017) e2001408. https://doi.org/10.1371/journal.pbio.2001408.

[9] J.D. Lathia, M. Li, P.E. Hall, J. Gallagher, J.S. Hale, Q. Wu, M. Venere, E. Levy, M.S. Rani, P. Huang, E. Bae, J. Selfridge, L. Cheng, H. Guvenc, R.E. McLendon, I. Nakano, A.E. Sloan, H.S. Phillips, A. Lai, C. Gladson, M. Bredel, S. Bao, A.B. Hjelmeland, J.N. Rich, Laminin alpha 2 enables glioblastoma stem cell growth, Ann. Neurol. 72 (2012) 766–778. https://doi.org/10.1002/ana.23674.

[10] S. Zhang, B. Ma, F. Liu, J. Duan, S. Wang, J. Qiu, D. Li, Y. Sang, C. Liu, D. Liu, H. Liu, Polylactic Acid Nanopillar Array-Driven Osteogenic Differentiation of Human Adipose-Derived Stem Cells Determined by Pillar Diameter, Nano Lett. 18 (2018) 2243–2253. https://doi.org/10.1021/acs.nanolett.7b04747.

[11] Y. Ramot, A. Nyska, E. Markovitz, A. Dekel, G. Klaiman, M.H. Zada, A.J. Domb, R.R. Maronpot, Long-term Local and Systemic Safety of Poly(l-lactide-co-epsilon-caprolactone) after Subcutaneous and Intra-articular Implantation in Rats, Toxicol. Pathol. 43 (2015) 1127–1140. https://doi.org/10.1177/0192623315600275.

[12] J. Fernández, A. Larrañaga, A. Etxeberría, J.R. Sarasua, Effects of chain microstructures and derived crystallization capability on hydrolytic degradation of poly(l-lactide/ε-caprolactone) copolymers, Polym. Degrad. Stab. 98 (2013) 481–489. https://doi.org/10.1016/j.polymdegradstab.2012.12.014.

[13] J. Fernández, A. Larrañaga, A. Etxeberria, W. Wang, J.R. Sarasua, A new generation of poly(lactide/ε-caprolactone) polymeric biomaterials for application in the medical field, J. Biomed. Mater. Res. A. 102 (2014) 3573–3584. https://doi.org/10.1002/jbm.a.35036.

[14] Y. Li, Y. Xiao, C. Liu, The Horizon of Materiobiology: A Perspective on Material-Guided Cell Behaviors and Tissue Engineering, Chem. Rev. 117 (2017) 4376–4421. https://doi.org/10.1021/acs.chemrev.6b00654.

[15] D. Mohammed, M. Versaevel, C. Bruyère, L. Alaimo, M. Luciano, E. Vercruysse, A. Procès, S. Gabriele, Innovative Tools for Mechanobiology: Unraveling Outside-In and Inside-Out Mechanotransduction, Front. Bioeng. Biotechnol. 7 (2019) 162. https://doi.org/10.3389/fbioe.2019.00162.

[16] E.A. Silantyeva, W. Nasir, J. Carpenter, O. Manahan, M.L. Becker, R.K. Willits, Accelerated neural differentiation of mouse embryonic stem cells on aligned GYIGSR-functionalized nanofibers, Acta Biomater. 75 (2018) 129–139. https://doi.org/10.1016/j.actbio.2018.05.052.

[17] E.K. Yim, S.W. Pang, K.W. Leong, Synthetic Nanostructures Inducing Differentiation of Human Mesenchymal Stem Cells into Neuronal Lineage, Exp. Cell Res. 313 (2007) 1820–1829. https://doi.org/10.1016/j.yexcr.2007.02.031.

[18] A. Solanki, S.-T.D. Chueng, P.T. Yin, R. Kappera, M. Chhowalla, K.-B. Lee, Axonal alignment and enhanced neuronal differentiation of neural stem cells on graphene-nanoparticle hybrid structures, Adv. Mater. Deerfield Beach Fla. 25 (2013) 5477–5482. https://doi.org/10.1002/adma.201302219.

[19] S. Baek, J. Oh, J. Song, H. Choi, J. Yoo, G.-Y. Park, J. Han, Y. Chang, H. Park, H. Kim, S.-G. Cho, B.-S. Kim, J. Kim, Generation of Integration-Free Induced Neurons Using Graphene Oxide-Polyethylenimine, Small Weinh. Bergstr. Ger. 13 (2017). https://doi.org/10.1002/smll.201601993.

[20] M. Bramini, G. Alberini, E. Colombo, M. Chiacchiaretta, M.L. DiFrancesco, J.F. Maya-Vetencourt, L. Maragliano, F. Benfenati, F. Cesca, Interfacing Graphene-Based Materials With Neural Cells, Front. Syst. Neurosci. 12 (2018) 12. https://doi.org/10.3389/fnsys.2018.00012.

[21] J. Luzuriaga, O. Pastor-Alonso, J.M. Encinas, F. Unda, G. Ibarretxe, J.R. Pineda, Human Dental Pulp Stem Cells Grown in Neurogenic Media Differentiate Into Endothelial Cells and Promote Neovasculogenesis in the Mouse Brain, Front. Physiol. 10 (2019) 347. https://doi.org/10.3389/fphys.2019.00347.

[22] D.C. Silvestre, J.R. Pineda, F. Hoffschir, J.-M. Studler, M.-A. Mouthon, F. Pflumio, M.-P. Junier, H. Chneiweiss, F.D. Boussin, Alternative lengthening of telomeres in human glioma stem cells, Stem Cells Dayt. Ohio. 29 (2011) 440–451. https://doi.org/10.1002/stem.600.

[23] F.P. Cordelières, V. Petit, M. Kumasaka, O. Debeir, V. Letort, S.J. Gallagher, L. Larue, Automated Cell Tracking and Analysis in Phase-Contrast Videos (iTrack4U): Development of Java Software Based on Combined Mean-Shift Processes, PLoS ONE. 8 (2013). https://doi.org/10.1371/journal.pone.0081266.

[24] K. Baranes, M. Shevach, O. Shefi, T. Dvir, Gold Nanoparticle-Decorated Scaffolds Promote Neuronal Differentiation and Maturation, Nano Lett. 16 (2016) 2916–2920. https://doi.org/10.1021/acs.nanolett.5b04033.

[25] J.M. Lee, W.S. Kang, K.G. Lee, H.-Y. Cho, B. Conley, C.D. Ahrberg, J.H. Lim, S.J. Mo, S.G. Mun, E.-J. Kim, J.-W. Choi, K.-B. Lee, S.J. Lee, B.G. Chung, Combinatorial biophysical cue sensor array for controlling neural stem cell fate, Biosens. Bioelectron. 156 (2020) 112125. https://doi.org/10.1016/j.bios.2020.112125.

[26] S. Zhang, B. Ma, F. Liu, J. Duan, S. Wang, J. Qiu, D. Li, Y. Sang, C. Liu, D. Liu, H. Liu, Polylactic Acid Nanopillar Array-Driven Osteogenic Differentiation of Human Adipose-Derived Stem Cells Determined by Pillar Diameter, Nano Lett. 18 (2018) 2243–2253. https://doi.org/10.1021/acs.nanolett.7b04747.

[27] G. Bonaventura, R. Iemmolo, V. La Cognata, M. Zimbone, F. La Via, M.E. Fragalà, M.L. Barcellona, R. Pellitteri, S. Cavallaro, Biocompatibility between Silicon or Silicon Carbide surface and Neural Stem Cells, Sci. Rep. 9 (2019) 1–13. https://doi.org/10.1038/s41598-019-48041-3.

[28] J.H. Park, B.K. Lee, S.H. Park, M.G. Kim, J.W. Lee, H.Y. Lee, H.B. Lee, J.H. Kim, M.S. Kim, Preparation of Biodegradable and Elastic Poly(ε-caprolactone-co-lactide) Copolymers and Evaluation as a Localized and Sustained Drug Delivery Carrier, Int. J. Mol. Sci. 18 (2017) E671. https://doi.org/10.3390/ijms18030671.

[29] A. Larrañaga, P. Aldazabal, F.J. Martin, J.R. Sarasua, Hydrolytic degradation and bioactivity of lactide and caprolactone based sponge-like scaffolds loaded with bioactive glass particles, Polym. Degrad. Stab. 110 (2014) 121–128. https://doi.org/10.1016/j.polymdegradstab.2014.08.021.

[30] A. Larrañaga, E. Lizundia, A review on the thermomechanical properties and biodegradation behaviour of polyesters, Eur. Polym. J. 121 (2019) 109296. https://doi.org/10.1016/j.eurpolymj.2019.109296.

[31] J. Fernández, A. Etxeberria, J.M. Ugartemendia, S. Petisco, J.-R. Sarasua, Effects of chain microstructures on mechanical behavior and aging of a poly(L-lactide-co-ε-caprolactone) biomedical thermoplastic-elastomer, J. Mech. Behav. Biomed. Mater. 12 (2012) 29–38. https://doi.org/10.1016/j.jmbbm.2012.03.008.

[32] L. Wang, X. Liu, J. Fu, X. Ning, M. Zhang, Z. Jiang, G. Cheng, Y. Zhu, Z. Zhang, Release of methylene blue from graphene oxide-coated electrospun nanofibrous scaffolds to modulate functions of neural progenitor cells, Acta Biomater. 88 (2019) 346–356. https://doi.org/10.1016/j.actbio.2019.02.036.

[33] H. Lee, S.M. Dellatore, W.M. Miller, P.B. Messersmith, Mussel-inspired surface chemistry for multifunctional coatings, Science. 318 (2007) 426–430. https://doi.org/10.1126/science.1147241.

[34] J.-B. Wu, M.-L. Lin, X. Cong, H.-N. Liu, P.-H. Tan, Raman spectroscopy of graphene-based materials and its applications in related devices, Chem. Soc. Rev. 47 (2018) 1822–1873. https://doi.org/10.1039/C6CS00915H.

[35] Poly(vinyl alcohol) Reinforced and Toughened with Poly(dopamine)-Treated Graphene Oxide, and Its Use for Humidity Sensing | ACS Nano, (n.d.). https://pubs.acs.org/doi/abs/10.1021/nn500504s (accessed April 8, 2020).

[36] Frontiers | Innovative Tools for Mechanobiology: Unraveling Outside-In and Inside-Out Mechanotransduction | Bioengineering and Biotechnology, (n.d.). https://www.frontiersin.org/articles/10.3389/fbioe.2019.00162/full (accessed April 7, 2020).

[37] M. Pardo-Figuerez, N.R.W. Martin, D.J. Player, P. Roach, S.D.R. Christie, A.J. Capel, M.P. Lewis, Controlled Arrangement of Neuronal Cells on Surfaces Functionalized with Micropatterned Polymer Brushes, ACS Omega. 3 (2018) 12383–12391. https://doi.org/10.1021/acsomega.8b01698.

[38] A. Solanki, S.-T.D. Chueng, P.T. Yin, R. Kappera, M. Chhowalla, K.-B. Lee, Axonal alignment and enhanced neuronal differentiation of neural stem cells on graphene-nanoparticle hybrid structures, Adv. Mater. Deerfield Beach Fla. 25 (2013) 5477–5482. https://doi.org/10.1002/adma.201302219.

[39] G.A. Dunn, Characterising a kinesis response: time averaged measures of cell speed and directional persistence, Agents Actions. Suppl. 12 (1983) 14–33. https://doi.org/10.1007/978-3-0348-9352-7_1.

[40] H.G. Othmer, S.R. Dunbar, W. Alt, Models of dispersal in biological systems, J. Math. Biol. 26 (1988) 263–298. https://doi.org/10.1007/bf00277392.

[41] M.H. Gail, C.W. Boone, The locomotion of mouse fibroblasts in tissue culture, Biophys. J. 10 (1970) 980–993. https://doi.org/10.1016/S0006-3495(70)86347-0.

[42] M.E. van Strien, S.A. van den Berge, E.M. Hol, Migrating neuroblasts in the adult human brain: a stream reduced to a trickle, Cell Res. 21 (2011) 1523–1525. https://doi.org/10.1038/cr.2011.101.

[43] D. Inta, J. Alfonso, J. von Engelhardt, M.M. Kreuzberg, A.H. Meyer, J.A. van Hooft, H. Monyer, Neurogenesis and widespread forebrain migration of distinct GABAergic neurons from the

postnatal subventricular zone, Proc. Natl. Acad. Sci. U. S. A. 105 (2008) 20994–20999. https://doi.org/10.1073/pnas.0807059105.

[44] U. Englund, A. Björklund, K. Wictorin, Migration patterns and phenotypic differentiation of long-term expanded human neural progenitor cells after transplantation into the adult rat brain, Brain Res. Dev. Brain Res. 134 (2002) 123–141. https://doi.org/10.1016/s0165-3806(01)00330-3.

[45] L.F. Eng, R.S. Ghirnikar, Y.L. Lee, Glial fibrillary acidic protein: GFAP-thirty-one years (1969-2000), Neurochem. Res. 25 (2000) 1439–1451. https://doi.org/10.1023/a:1007677003387.

[46] J. Song, H. Gao, G. Zhu, X. Cao, X. Shi, Y. Wang, The preparation and characterization of polycaprolactone/graphene oxide biocomposite nanofiber scaffolds and their application for directing cell behaviors, Carbon. 95 (2015) 1039–1050. https://doi.org/10.1016/j.carbon.2015.09.011.

[47] Axonal Alignment and Enhanced Neuronal Differentiation of Neural Stem Cells on Graphene-Nanoparticle Hybrid Structures, (n.d.). https://www.ncbi.nlm.nih.gov/pmc/articles/PMC4189106/ (accessed April 7, 2020).

[48] H.P. Bei, Y. Yang, Q. Zhang, Y. Tian, X. Luo, M. Yang, X. Zhao, Graphene-Based Nanocomposites for Neural Tissue Engineering, Molecules. 24 (2019). https://doi.org/10.3390/molecules24040658.

[49] C. Fu, S. Pan, Y. Ma, W. Kong, Z. Qi, X. Yang, Effect of electrical stimulation combined with graphene-oxide-based membranes on neural stem cell proliferation and differentiation, Artif. Cells Nanomedicine Biotechnol. 47 (2019) 1867–1876. https://doi.org/10.1080/21691401.2019.1613422.

[50] T. Imura, H.I. Kornblum, M.V. Sofroniew, The Predominant Neural Stem Cell Isolated from Postnatal and Adult Forebrain But Not Early Embryonic Forebrain Expresses GFAP, J. Neurosci. 23 (2003) 2824–2832. https://doi.org/10.1523/JNEUROSCI.23-07-02824.2003.

[51] Evidence for a wide extra-astrocytic distribution of S100B in human brain, (n.d.). https://www.ncbi.nlm.nih.gov/pmc/articles/PMC1769505/ (accessed April 22, 2020).

[52] J.C. Deloulme, E. Raponi, B.J. Gentil, N. Bertacchi, A. Marks, G. Labourdette, J. Baudier, Nuclear expression of S100B in oligodendrocyte progenitor cells correlates with differentiation toward the oligodendroglial lineage and modulates oligodendrocytes maturation, Mol. Cell. Neurosci. 27 (2004) 453–465. https://doi.org/10.1016/j.mcn.2004.07.008.

[53] S. Shah, P.T. Yin, T.M. Uehara, S.-T.D. Chueng, L. Yang, K.-B. Lee, Guiding Stem Cell Differentiation into Oligodendrocytes Using Graphene-Nanofiber Hybrid Scaffolds, Adv. Mater. 26 (2014) 3673–3680. https://doi.org/10.1002/adma.201400523.

[54] W. Guo, J. Qiu, J. Liu, H. Liu, Graphene microfiber as a scaffold for regulation of neural stem cells differentiation, Sci. Rep. 7 (2017) 5678. https://doi.org/10.1038/s41598-017-06051-z.

[55] D.K. Wilton, L. Dissing-Olesen, B. Stevens, Neuron-Glia Signaling in Synapse Elimination, Annu. Rev. Neurosci. 42 (2019) 107–127. https://doi.org/10.1146/annurev-neuro-070918-050306.

[56] F. He, Y.E. Sun, Glial cells more than support cells?, Int. J. Biochem. Cell Biol. 39 (2007) 661–665. https://doi.org/10.1016/j.biocel.2006.10.022.

[57] A. Araque, M. Navarrete, Glial cells in neuronal network function, Philos. Trans. R. Soc. B Biol. Sci. 365 (2010) 2375–2381. https://doi.org/10.1098/rstb.2009.0313.

[58] C.N. Barber, D.M. Raben, Lipid Metabolism Crosstalk in the Brain: Glia and Neurons, Front. Cell. Neurosci. 13 (2019). https://doi.org/10.3389/fncel.2019.00212.

[59] M. Bélanger, P.J. Magistretti, The role of astroglia in neuroprotection, Dialogues Clin. Neurosci. 11 (2009) 281–295. https://www.ncbi.nlm.nih.gov/pmc/articles/PMC3181926/ (accessed April 8, 2020).

[60] B.J. Kim, J.Y. Choi, H. Choi, S. Han, J. Seo, J. Kim, S. Joo, H.M. Kim, C. Oh, S. Hong, P. Kim, I.S. Choi, Astrocyte-Encapsulated Hydrogel Microfibers Enhance Neuronal Circuit Generation, Adv. Healthc. Mater. 9 (2020) 1901072. https://doi.org/10.1002/adhm.201901072.

[61] E. Sawosz, S. Jaworski, M. Kutwin, A. Hotowy, M. Wierzbicki, M. Grodzik, N. Kurantowicz, B. Strojny, L. Lipińska, A. Chwalibog, Toxicity of pristine graphene in experiments in a chicken embryo model, Int. J. Nanomedicine. 9 (2014) 3913–3922. https://doi.org/10.2147/IJN.S65633.

[62] Y. Chen, X. Hu, J. Sun, Q. Zhou, Specific nanotoxicity of graphene oxide during zebrafish embryogenesis, Nanotoxicology. 10 (2016) 42–52. https://doi.org/10.3109/17435390.2015.1005032.

Chapter 4

Nanostructured scaffolds based on bioresorbable polymers and graphene oxide facilitate the adhesion, alignment, neural commitment and migration of human dental pulp stem cells and allow the intracerebral implantation to promote the restoration of the injured rostral migratory stream on a rodent brain model

Nanostructured scaffolds based on bioresorbable polymers and graphene oxide facilitate the adhesion, alignment, neural commitment and migration of human dental pulp stem cells and allow the intracerebral implantation to promote the restoration of the injured rostral migratory stream on a rodent brain model

Abstract

Regeneration of neural tissue represents an unmet clinical, scientific and social challenge. Nowadays, most therapies rely on the formulation of anchoring scaffolds that promote the regeneration of the tissue itself or on the direct implantation of grafted stem cells. However, both strategies find important limitations for their effective translation into the clinic. Firstly, anchoring scaffolds alone lack an effective restoration of the neural tissue for long periods, due to the incapability to replace the functionality of the lost neural tissue. Secondly, the therapeutic ability of grafted stem cells is limited due to their short half-life and rapid clearance *in vivo,* which is normally exacerbated after an injury. In the present chapter, we propose the combinatorial use of nanostructured bioresorbable polymeric scaffolds functionalized (NanoGO) or not (NanoPDA) with graphene oxide (GO) together with human dental pulp stem cells (hDPSCs) to promote the restoration of the injured neural tissue *in vivo*. Our findings suggested that our NanoPDA and NanoGO scaffolds permitted neural and glial differentiation of the hDPSCs *in vitro*. Moreover, in comparison with the hDPSCs grafted alone, the incorporation of the NanoPDA scaffold promoted the integration of the grafted hDPSCs in the tissue, thus facilitating the restoration of the injury after 3 months. Altogether, our findings demonstrated the beneficial outcome of the use of human stem cells together with bioresorbable polymeric scaffolds for the restoration of the damaged central nervous system.

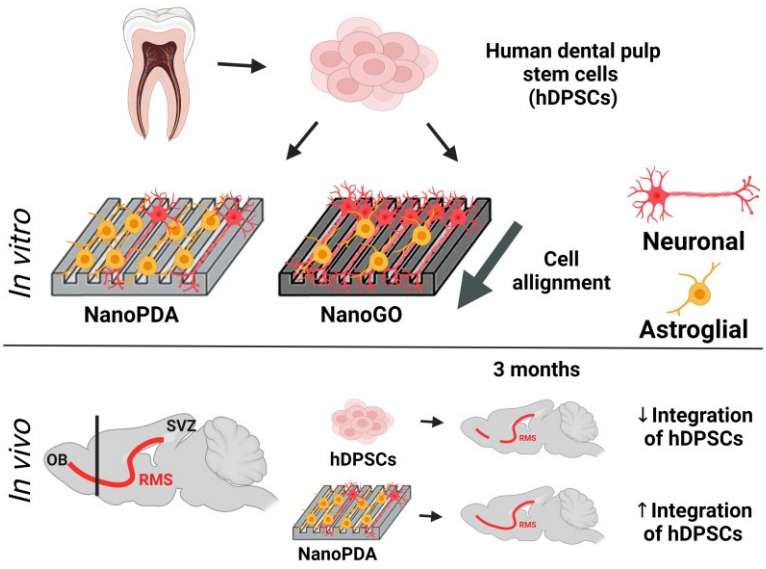

4.1. Introduction

Every year, neurological diseases result in the death or impairment of about 94 million individuals globally, and by 2030, this proportion is projected to increase to 103 million [1]. Therefore, new strategies are demanded to restore the damaged neural tissue and effectively promote its reconnection.

Ideally, biomaterials for neural regeneration should be biocompatible, bioresorbable and able to directionally reconnect and reorganize the tissue without the need of extracellular matrix-like compounds (ECM). In this sense, bioresorbable polymeric biomaterials based on DL-lactide and ε-caprolactone (PLCL) are of great interest due to their biocompatibility, adjustable degradation ratio and mechanical, geometrical and chemical characteristics that can be finely tuned to resemble the architecture of the ECM and boost neural differentiation [2]. Several studies have already demonstrated the beneficial effect of nanotopography on alignment, guided movement and differentiation of neural cells using bioresorbable polymeric scaffolds [3–5], but still more investigations are needed to gain more insights about their effectiveness in neural regeneration when challenging them in real *in vivo* situations [6]. As described in the previous chapter, we propose the use of nanostructured scaffolds based on bioresorbable polymeric materials to guide neural and axonal growth, while promoting a guided movement and neurodifferentiation of host cells. Aligned nanotopographical cues around 280 nm have been described to allow oligodendroglial and neuronal differentiation [7,8], while patterns between 350 and 480 nm have been described to better promote neurogenesis [8,9]. Moreover, we aim to functionalize the surface of our nanostructured scaffolds with advanced biocompatible and conductive entities by incorporating a surface coating of graphene oxide (GO). Previous studies working with neural stem cells (NSCs) have already shown the benefits of coating hydrophobic polymers like PLCL with GO, boosting attachment, aligned growth and movement of the cells and avoiding the need of potentially harmful ECM-like coating for *in vivo* studies [10–12].

Although promising in *in vitro* testing, bioresorbable polymeric scaffolds alone fail in the effective functional restoration of the neural tissue in clinical studies [13]. Hence, we aim to enhance here the functional restoration capabilities of our scaffolds by combining them with human stem cells. Several studies have shown promising results combining bioresorbable polymeric scaffolds and stem cells like NSCs, mesenchymal stem cells (MSCs) and induced pluripotent stem cells (iPSC), but there is still a long way to go before these cells can reach the clinic in a safe and efficient way [14,15]. Indeed, human fetal NSCs graft into the cerebellum of a youngster with ataxia telangiectasia created a glio-neuronal brain tumor in four years [16]. Thus, there exists the need of new autologous stem cell sources for future personalized therapies. Here, we propose the use of human dental pulp stem cells (hDPSCs), which are autologously obtained from the extraction of third molars. Their neural crest origin, ease of extraction, manipulation and expansion,

makes them an ideal alternative for personalized therapy [17,18]. Moreover, they have safe non-tumorigenic and immunomodulatory phenotype, while showing multi-linage differentiation capacity towards neuronal and glial lineages [19]. However, directly grafted stem cells have a poor therapeutic ability due to their short half-life and quick clearance *in vivo,* which is even aggravated after tissue damage. In addition, they normally fail on integrating on the host tissue and generating differentiated neural cells [20]. Here, we propose the combination of hDPSCs with nanostructured scaffolds to allow not only the attachment and functional integration of the cells, but also the modulation of important biological functions like survival and differentiation towards neural commitment, stimulating a more effective regeneration of the damaged neural tissue. This could provide underpinning work for the future use of this combinatorial approach for the treatment of traumatic central nervous system (CNS) disorders.

To test our hypothesis, in the present chapter we first studied the capabilities of our PLCL-based bioresorbable nanostructured scaffolds to promote the neural commitment towards both neuronal and astroglial lineages of the hDPSCs. Then, the impairment and subsequent restoration abilities of the rostral migratory stream (RMS) of athymic nude mice in the presence of the scaffolds was tested.

For a long time, it has been believed that there was no creation of new neurons in the adult brain. Nowadays, it is well accepted that neurogenesis is restricted to the subgranular zoned (SGZ) of the hippocampus and the subventricular zone (SVZ) of the lateral ventricles [21]. Indeed, even there are migration paths that permit the redistribution of those neural stem cells to specific regions of the brain. In rodents, neuronal precursors that are originated in the SVZ travel through the RMS, a specific migration pathway, to reach the major olfactory bulb (OB) for structural brain plasticity and functional cellular turnover [22,23]. Here, we propose the physical impairment of the RMS to study the *in vivo* reconnection capabilities of our nanostructured scaffolds either grafted or not with hDPSCs.

4.2. Materials and methods

4.2.1. Fabrication and characterization of the scaffolds

Fabrication and characterization of the scaffolds was done as stated in chapter 3 with a newly synthetized amorphous polymer.

4.2.1.1. Synthesis and characterization of the polymer

First, a biodegradable copolymer of DL-lactide and ε-caprolactone was synthetized by one step ring-opening polymerization to obtain large quantities of statistical copolymer based on ε-caprolactone (assay > 98%, Merk Millipore, USA) and DL-lactide (assay > 99.5%, Purac Biochem, The Netherlands). The synthesis reaction was conducted in a flask submerged in an oil bath at 130 ^{o}C for 24 h. DL-lactide and ε-caprolactone were placed into a round bottom glass flask in 80:20 feed weight composition. Once melted, the catalyst (triphenylbismuth, Ph_3Bi) was added in 1000:1 comonomer:catalyst molar ratio. Afterwards, the resulting copolymer (i.e., PLCL) was dissolved in dichloromethane and precipitated in an excess of methanol to remove catalyst impurities and those monomers that had not reacted. Finally, the copolymer was air-dried at room temperature overnight and a heat treatment was carried out (100 ^{o}C under vacuum for 1 h) to ensure the complete elimination of any remaining solvent.

The characterization of the synthetized PLCL was done by proton nuclear magnetic resonance (NMR), gel permeation chromatography (GPC) and differential scanning calorimetry (DSC).

All NMR spectra were recorded in a Bruker Avance III HD Fourier 300 at 300.13 MHz and 75.5 MHz of resonance frequency, with deuterated chloroform ($CDCl_3$, 0.7 mL) as solvent and at room temperature (25 ^{o}C), using 5 mm O.D. sample tubes. H-NMR spectra were recorded using 10 mg of sample, 3 s acquisition time, 10 s delay time, 14 µs pulse, spectral width of 6000 Hz and 16 scans. For the ^{13}C-NMR, 40 mg of sample were used, inverse gated decoupling sequence, 1.7 s acquisition time, 5.3 s delay time, 10 µs pulse, spectral width of 19,200 Hz and over 5,000 scans. Copolymer composition, average sequence lengths and randomness character value were calculated by averaging the values of molar contents and the LA-CL dyad relative molar fractions that were obtained by means of ^{1}H spectroscopy. Equations 1-4 were employed to obtain the number-average sequence lengths (l_i), the Bernouillian random number-average sequence lengths $(l_{i,})_{random}$ and the randomness character (R), considering the lactide (LA) and ε-caprolactone (CL) molar fractions, and the average dyad relative molar fractions of LA-CL, LA-LA and CL-CL respectively:

$$l_{LA} = \frac{(LA - LA) + \frac{1}{2}(LA - CL)}{\frac{1}{2}(LA - CL)} = \frac{2(LA)}{(LA - CL)} \qquad (1)$$

$$l_{EB} = \frac{(CL - CL) + \frac{1}{2}(LA - CL)}{\frac{1}{2}(LA - CL)} = \frac{2(CL)}{(LA - CL)} \qquad (2)$$

$$(l_{LA})_{random} = \frac{1}{(CL)};\ (l_{CL})_{random} = \frac{1}{(LA)} \qquad (3)$$

$$R = \frac{(\mathrm{l_{LA}})_{\mathrm{random}}}{\mathrm{l_{LA}}} = \frac{(\mathrm{l_{CL}})_{\mathrm{random}}}{\mathrm{l_{CL}}} \qquad (4)$$

The molecular weight of the resulting copolymer was determined by GPC using a Waters 1515 GPC device equipped with two Styragel columns (10^2–10^4 Å). Chloroform was used as eluent at a flow rate of 1 mL/min and polystyrene standards (Shodex Standards, SM-105) were used to obtain a primary calibration curve. All samples were prepared at a concentration of 10 mg/mL.

Thermal properties were studied on a DSC Q200 (TA Instruments). 5-10 mg of copolymer were heated from -40 ^{o}C to 150 ^{o}C at 20 ^{o}C/min. After the first scan, the sample was quenched in the DSC and a second scan was conducted from -40 ^{o}C to 150 ^{o}C at 20 ^{o}C/min. This second scan was used to determine the glass transition temperature (T_g).

4.2.1.2. Fabrication and characterization of the scaffolds

For the fabrication of the scaffolds, PLCL films of around 150 µm were first obtained by compression molding and nanostructured by a thermo-pressing process to replicate the period of a commercially available silicon stamp (Nano). Subsequently, the functionalization of the surface was done with polydopamine (PDA) and GO as previously described in chapter 3, obtaining NanoPDA and NanoGO samples. Circular samples of 6 mm diameter were punched out for characterization and cell culture studies and sterilized afterwards with 70% ethanol for 15 min and washed with sterile phosphate buffer saline (PBS) 3 times prior to an exposure of 30 min of ultraviolet (UV) light. For *in vivo* studies, nanostructured films were first sterilized with 70% ethanol for 15 min and washed with sterile PBS 3 times and exposed to UV light for 30 min. Afterwards, samples of around 1x1 mm were obtained with a scalper in sterile conditions.

The degradation and mechanical properties of the scaffolds were studied to better understand their performance *in vivo*. For the *in vitro* degradation, round samples of 6 mm in diameter were placed in a 24-well plate containing PBS (pH = 7.2) (5–9 mg of initial weight (W_o) and n = 3). The samples were kept at 37 ^{o}C. Three samples of each scaffold Nano, NanoPDA or NanoGO were taken out from the PBS after 1, 3, 7, 14, 23, 32, 49, 63, 77 or 91 days and wiped with filter paper to eliminate any surface water and

determine the wet weight (W_w). Afterwards, they were air-dried overnight and weighed again to determine the dry weight (W_d). The remaining weight (%RW) and water absorption (%WA) were determined by using the equations 5 and 6.

$$\% WA = \frac{W_w - W_d}{W_d} * 100 \qquad (5)$$

$$\% RW = \frac{W_d}{W_0} * 100 \qquad (6)$$

The molecular weight of the samples during degradation was determined by GPC as previously described. The thermal properties of the samples were determined on dried samples by means of DSC as previously described. Scanning electron microscopy (SEM) was used to evaluate the surface morphology (HITACHI S-4800) of the samples during the degradation process. Samples were coated with a 150 Å layer of gold in a JEL Ion Sputter JFC-1100 at 1200 V and 5 mA prior to analysis.

The mechanical properties of the initial samples were determined by tensile test on an Instron 5565 testing machine with a crosshead displacement rate of 10 mm/min (Instron, Nordwood, MA, USA). According to ISO 527-3/1995, these tests were conducted at human body temperature (37 ^{o}C). Either non-coated films (No Nano) of 150-250 µm thick, coated with PDA (No NanoPDA) or PDA and GO (No NanoGO) were cut into the following dimensions: total length of 100 mm, distance between clamps of 50 mm, and width of 10 mm. The mechanical characteristics (secant modulus at 2%, elongation at break and yield strength) correspond to average values of at least five measurements. A temperature chamber was used for mechanical testing at 37 ^{o}C and due to the temperature chamber's size restrictions, the testing was terminated at 180% of strain. Due to the elastomeric behavior of the tested samples, the secant modulus at 2% was determined instead of the Young´s modulus.

4.2.2. Cell culture

Extraction, isolation and amplification of hDPSCs was performed as previously described [19]. Briefly, hDPSCs of at least 15 different patients (ages between 18-42 years old) were mixed to avoid possible interference derived from age, sex or genetic variants. 60,000 cells were seeded in Neurocult proliferation medium on each 6 mm-diameter scaffold for immunostaining and videomicroscopy characterization. After 24 h, medium was changed to Neurocult differentiation to promote neural differentiation of the cells as previously described in chapter 3 and cultured at 37 ^{o}C and 5% CO_2. The media was changed every 3 days to ensure a proper supply of nutrients. For *in vivo* experiments, 100,000 cells were seeded on each 1x1 mm scaffold in Neurocult proliferation medium and cells were incubated for 24 h at 37 ^{o}C and 5% CO_2 to allow them to attach.

4.2.2.1. Immunostaining

As previously described [12], hDPSCs were fixed, permeabilized, and stained after 7 and 14 days *in vitro* (DIV). Immunopositive Nestin (1:200, ab6142, Abcam, United Kingdom) labeling was used to detect the maintenance of the stem phenotype. Positive DCX (1:300, sc8066, Santa Cruz, USA) and NeuN (1:200, ab177487, Abcam, Cambridge, UK) labeling was used to identify cells that were committed to the neuronal lineage. GFAP (1:500, G9269, Sigma-Aldrich, USA), S100 β (1:200, Dako Cytomation, Denmark) and p75 (1:500, G9269, Sigma-Aldrich, USA) were used to analyze the commitments to astroglial and Schwann cell lineages. Alexa Fluor donkey anti-mouse, anti-rabbit or anti-goat secondary antibodies were employed in 488, 594 or 647 fluorophores (1:200, Life Technologies, USA).

4.2.2.2. Videomicroscopy

Dentospheres were disaggregated and 60,000 hDPSCs were cultured in a petri µ-Dish 35 mm (Ibidi, Gräfelfing, Germany) containing nanostructured scaffolds as previously described in chapter 3. Nikon BioStation IM-Q videomicroscopy was used to capture cells for a total of 24 h after they had been allowed to attach for 30 min (Nikon Instruments Europe BV, Amsterdam, Netherlands). A constant 37 ^{o}C, 5% CO_2, and 95% relative humidity were maintained for imaging. Every 10 minutes, images of eight to twelve fields in each condition were obtained with a 10x objective. Using the MTrackJ plugin in ImageJ, individual cell tracks were tracked and overlaid over a shorter 8-hour period. Using an Excel macro created by F. Cordelières (Bordeaux imaging center, UMS 3420 CNRS, Bordeaux, France), the dynamic parameters (migration velocity and persistence) were determined [24].

4.2.3. *In vivo* experiments

Athymic Swissnu/nu mice were used to study the reconnection capacity of the nanostructured scaffolds implanted with or without hDPSCs. Briefly, mice were anesthetized intraperitoneally using a mixture of ketamine and medetomidine. A subcutaneous dose of buprenorphine analgesic and ophthalmic ointment was also administered to reduce animal discomfort and protect against dry eyes. Then, a scalper was used to make a small incision on the skin. The RMS was interrupted permanently sectioning the connection brain-OB at the stereotaxic coordinates 3.5 mm from bregma and 7.3 mm from interaural coordinate (1 mm from coronal suture and 2 mm from sagittal suture) on both hemispheres using a drill coupled to a stereotaxic apparatus (Kopf model 900) (Figure 4.1.). Afterwards, either NanoGO or NanoPDA grafted or not with hDPSCs were inserted only into the RMS of the left hemisphere, using the right hemisphere as an internal control of the restoration capacities of each animal. The intrinsic restoration capacities were also assessed in animals containing neither scaffold nor grafted cells on the left hemisphere. As a control of the restoration capacities of the

hDPSCs alone, disaggregated hDPSCs dentospheres in the active growth phase were collected in Neurocult proliferation media and 2 µl containing 100,000 cells were unilaterally injected into the left hemisphere injured RMS at 0.5 µL/min using a 10 µL Hamilton with a micropump coupled to the stereotaxic apparatus (Kopf model 900). Animals were kept in a colony isolator at a constant temperature of 19–22 ^{o}C and humidity (40–50%) with a 12–12 h light/dark cycle. Animal care was provided before and after surgery as previously mentioned [25].

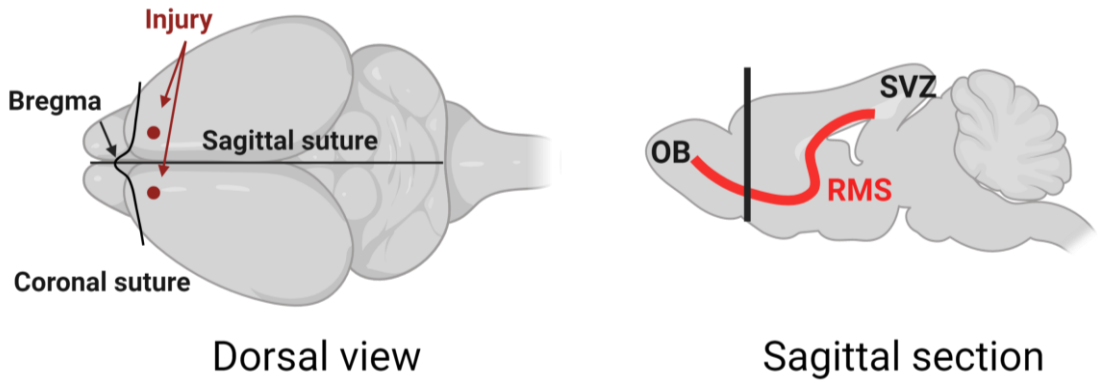

Figure 4.1.: Schematic representation of the injured site.
Schematic representation of the dorsal view of a mouse brain, representing the bregma, coronal suture and sagittal suture of the sculp and the injured site at 1 mm from the coronal suture and 2 mm from the sagittal suture, just close to the bregma. On the right, the schematic representation of the sagittal section represents the interruption of the rostral migratory stream (RMS) that connects the subventricular zone (SVZ) with the olfactory bulb (OB).

4.2.3.1. Animal behavior experiments by buried food test (BFT)

The effect of neurogenesis on olfactory-mediated behaviors has been controversial in the last years, while some authors stated that neurogenesis has little or no effects on olfactory-mediated behaviors, others claimed that olfactory loss even may be considered as an early biomarker of neurodegenerative diseases [26]. Today, there is a consensus that after pronounced changes on OB newborn neurons have a role in odor learning, discrimination, short-term olfactory memory and olfactory-guided behavior in mammals [27–29]. To study the interruption and functional restoration of the RMS, we assessed the olfactory ability of food-deprived mice to identify and find the odor from a hidden food pellet beneath the bedding of the cage by the buried food test (BFT). BFT is a key assay to evaluate the ability to smell odorants and the main parameter observed in this test is the latency to uncover a small piece of food [30]. The 66 animals used in the study were kept with water *ad libitum* but deprived of food for 12 h prior to the BFT test. For the BFT test, a regular size cage (50 cm length x 30 cm width x 16 cm height) with clean bedding was placed under a chemical hood with laminar and filtered air flow. Afterwards, a small piece of 4 g of food was hidden for 6 rounds always in the same order (middle, upper right, upper left, down right, down left, middle) for each animal. The

elapsed time spent to find the food was recorded and compared between different groups by mean values and standard error of mean (SEM). The experiments were carried out in an isolated and silent experimentation room to avoid any disturbance or entrance of people, and always performed by the same experimenter at the same time of the day, respecting the animal's circadian cycle, as previously reported [31,32].

4.2.3.2. Immunostaining of brain slices

After 7, 14 or 90 days, animals were sacrificed, prefunded and the selected organs (brains with OBs, liver, kidney, spleen and heart) dissected as stated before [19]. Brains with OBs were kept at 4 ^{o}C in PBS containing 0.2% sodium azide (Sigma-Aldrich, USA) until use. To obtain 50 µm thick brain slices without compromising the bioresorbable scaffold and the surrounded tissue, the brains were embedded in 2% ultrapure agarose (Thermo Fisher Scientific, USA), serially cut using a Microm Hm 650v vibratome from Thermo Fisher and stored in PBS containing sodium azide (Sigma-Aldrich, USA). Prior to immunostaining, agarose was removed and slices immunostained as described in chapter 3 using the same conditions and antibodies described in 4.2.2.1.

4.2.3.3. Toxicological evaluation

According to ISO 10993, perfused liver, kidney, spleen and heart were dehydrated in increasing alcohol concentrations and embedded in paraffin for 5 µm sectioning using a paraffin microtome (Reichert Jung motorized microtome). Slices were collected in a 37ºC warm bath in gelatin-coated slices, rehydrated, stained for hematoxylin and eosin staining, dehydrated and mounted for histopathological analysis.

4.2.3.4. Study approval

The competent authorities (Diputación Foral de Bizkaia) approved the animal tests, which were carried out in accordance with European Communities Council Directive 86/609/EEC of November 24, 1986.

4.2.4. Statistical analysis

When comparing two or more groups, the Kruskal-Wallis test was used followed by Dunn's post hoc test or the Holm-Šídák techniques. The U-Mann Whitney test was used to compare only two groups, with a p-value of 0.05 denoting statistical significance. The results were shown as mean ±SD or SEM (indicated accordingly). The relevant figure legend displays the number of separate experiments.

4.3. Results

4.3.1. PLCL scaffolds were successfully fabricated, nanostructured and functionalized

A bioresorbable copolymer with a molar fraction of 78% of DL-lactide (DL-LA) and 22% of ε-caprolactone (ε-DL) was satisfactorily synthesized (Figure 4.2. A). The synthesis was carried out in bulk by one-pot-step ring-opening polymerization (ROP), with a weight feed composition of 80% DL-lactide and 20% ε-caprolactone, 1000:1 comonomers:catalyst molar ratio, at 130 ^{o}C for 24 h. Afterwards, the copolymer was dissolved in dichloromethane and precipitated in an excess of methanol followed by a thermal treatment to remove all impurities and remaining solvent. As determined by NMR, the obtained copolymer had a final mass composition of 78.0% DL-lactide, with a molecular weight (M_w) of 97.1 kDa and a dispersity (D) value of 2.6 as concluded from GPC analysis (Figure 4.2. B). Further characterization by NMR showed a random distribution of the repetitive units in the polymeric chain, with a randomness character value (R) of 1.1, a DL-lactide sequence length (l_{LA}) of 4.1 and of ε-caprolactone of 1.2 (l_{CL}) (Figure 4.2. B and C). As expected, we achieved a completely amorphous PLCL copolymer with no melting (T_m) or crystallization points and a single glass transition temperature (T_g) of 24.0 ^{o}C (Figure 4.2. B and D). Hence, it is expected that our amorphous PLCL copolymer will not crystallize during its use, thus avoiding the formation of crystalline residues that may activate the immunoreaction after CNS damage observed when using other non-amorphous polymers [33].

A

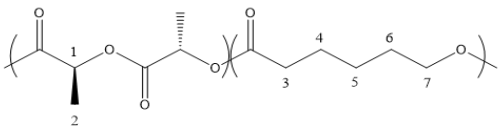

B

Sample	% DL-LA	% ε-CL	M_w (kDa)	D	l_{LA}	l_{CL}	R	T_g (°C)
PLCL 8020	78.0	22.0	97.1	2.6	4.1	1.2	1.1	24.0

C

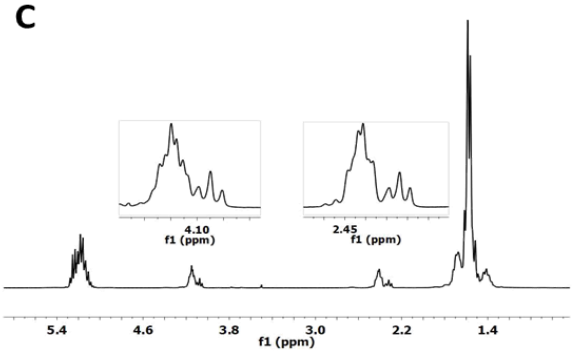

D

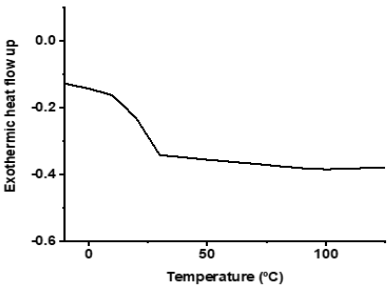

Figure 4.2.: Characterization of the poly(DL-lactide-co-ε-caprolactone) (PLCL) copolymer.
(A) Chemical structure of the poly(DL-lactide-co-ε-caprolactone) copolymer. **(B)** Table showing the different parameters of the PLCL copolymer: the content of DL-lactide and ε-caprolactone, the molecular weight (M_w) and dispersity index (D), the DL-lactide (l_{LA}) and ε-caprolactone (l_{CL}) sequence length, the randomness character and the glass transition temperature. **(C)** Proton nuclear magnetic resonance (NMR) spectra of the PLCL copolymer. **(D)** DSC thermogram showing the first scan of the synthesized copolymer.

Following the procedure described in chapter 3, the nanotopography of a silicon stamp was faithfully replicated in a PLCL film, producing nanostructured PLCL scaffolds with a clearly discernible grooved pattern of 155±27 nm grooves and 554±13 nm ridges (Figure 4.3. A). Due to the soft mechanical properties of PLCL at room temperature [34], certain ridges seemed slightly deformed after functionalization with polydopamine (PDA) and GO, but resulted in no detrimental effects on the original nanotopography. To prevent an excessive buildup of PDA and GO agglomerates that would harm the original nanostructured topography of the scaffolds, the concentration and reaction time were carefully regulated. PDA coating played a pivotal role in the subsequent functionalization with GO, acting as an adlayer between the polymeric film and GO [35], as described in chapter 3.

For a successful CNS regeneration, the degradation of the scaffolds must be carefully controlled [36]. For CNS reconnection of the RMS, the nanostructured scaffolds must support the adhesion, alignment and guided migration of the cells at the beginning but must also allow the gradual regeneration of the tissue without becoming a physical barrier. Our PLCL nanostructured scaffolds were able to maintain their nanostructure for 7 days (Figure 4.3. A), which presumably should permit the guidance of the cells for at least that period of time. Remarkably, the coatings with PDA (NanoPDA) and subsequent functionalization with GO (NanoGO) helped on the maintenance of the nanostructure for 49 days, which might be beneficial for guiding DCX-positive cells in the *in vivo* restoration of the rodent RMS.

To better asses the degradation profile of the nanostructured scaffolds, we incubated the nanostructured scaffolds in PBS at 37 ^{o}C and studied the hydrolytic degradation of the samples by studying the variations in the water absorption (%WA), and remaining weight (%RW). RW curves derived from the degradation study of the scaffolds displayed a constant RW for up to 91 days (Figure 4.3. B). These results are in agreement with other studies where PLCL scaffolds displayed a constant weight during the degradation process, but an uptake in WA, due to its dominating bulk degradation mechanism [37]. WA ability is a crucial element in the bulk degradation process since weight loss is mostly caused by water attacking the ester bonds [38]. In this regard, all the scaffolds showed an increase on WA from day 49 on (Nano 123±37%; NanoPDA 102±33%; NanoGO 226±87%) (Figure 4.3. C). Although NanoGO scaffold exhibited a higher WA at day 49, there was no statistical difference compared to NanoPDA and Nano scaffolds ($p = 0.53$, One-way ANOVA) and the %WA was similar in the three scaffolds after 91 days (Nano 294±20%; NanoPDA 277±48%; NanoGO 277±59%, $p = 0.99$, One-way ANOVA). Our results are in accordance with previous studies where PLCL scaffolds also exhibited an increase on WA after 49 days [39].

For a better characterization, the molecular weight (M_w) was monitored by GPC analysis. All the samples displayed a similar M_w at day 0 (Nano 80.4 kDa; NanoPDA 91.0 kDa; NanoGO 82.8 kDa, $p > 0.1$, One-way ANOVA), showing a low M_w lost after the processing of the original film to create the nanostructured surface and its subsequent coating/functionalization. As expected, M_w was constant in the first days, but the three samples showed a linear decrease on the M_w with a 50% of molecular weight loss after 23 days independent of the functionalization with PDA and GO (Nano 52.1 kDa; NanoPDA 52.9 kDa; NanoGO 44.0 kDa, $p > 0.1$, One-way ANOVA) (Figure 4.3. D). This molecular weight reduction is mandatory to allow mass loss through solubilization of the oligomers [40] and is in accordance with other PLCL degradation studies [41]. Indeed, after 91 days, Nano, NanoPDA and NanoGO scaffolds exhibited a similar M_w loss (Nano 8.1 kDa; NanoPDA 8.1 kDa; NanoGO 7.8 kDa, $p = 0.94$, One-way ANOVA), demonstrating that the functionalization of the surface had no effect on the degradation profile. In line with the molecular weight loss, the DSC results demonstrated that the T_g was also reduced over the degradation time in Nano, NanoPDA and NanoGO independently of the coatings (Figure 4.3. E). Indeed, in line with the results observed on the WA absorption and the M_w, there is a decrease in the T_g on the three scaffolds from day 32 (Nano 21.5 ^oC; NanoPDA 20.5 ^oC; NanoGO 21.0 ^oC) to day 49 (Nano 18.0 ^oC; NanoPDA 16.0 ^oC; NanoGO 15.0 ^oC) due to the degradation process. The three samples achieved a similar value on their T_g after 91 days (Nano 16.5 ^oC; NanoPDA 14.0 ^oC; NanoGO 14.0 ^oC), demonstrating again no effect of surface functionalization on the degradation profile. Moreover, as expected from chain microstructure, DSC thermograms did not show melting or crystallization peaks (Figure 4.3. F).

Overall, the hydrolytic degradation studies demonstrated that both NanoGO and NanoPDA scaffolds were able to maintain the necessary nanostructure for the aligned migration of the cells at least for 7 days with a minimal release of degradation by-products. Hence, a minimal interference from the degradation by-products with the cell mobility, integration, differentiation or restoration of the CNS proposed herein is expected.

Due to the rising importance of the brain's physiological mechanical environment in normal brain functioning and its involvement in the evolution of disease [42], bioengineered scaffolds must mimic the mechanical properties of the ECM for a correct restoration of the tissue. For example, during neuroinflammation and glial scar formation, a diminution of the mechanical properties of the affected CNS region have been reported [43,44]. Here, we studied the mechanical properties of our 150-250 µm scaffolds at 37 ^oC. Tensile studies demonstrated that the mechanical properties of our scaffolds were among those exhibited by other elastomeric polymers, showing large elastic deformation and relatively low secant modulus (17.6±1.5 MPa for No Nano sample) and offset yield strength (0.35±0.03 MPa for No Nano) [45].

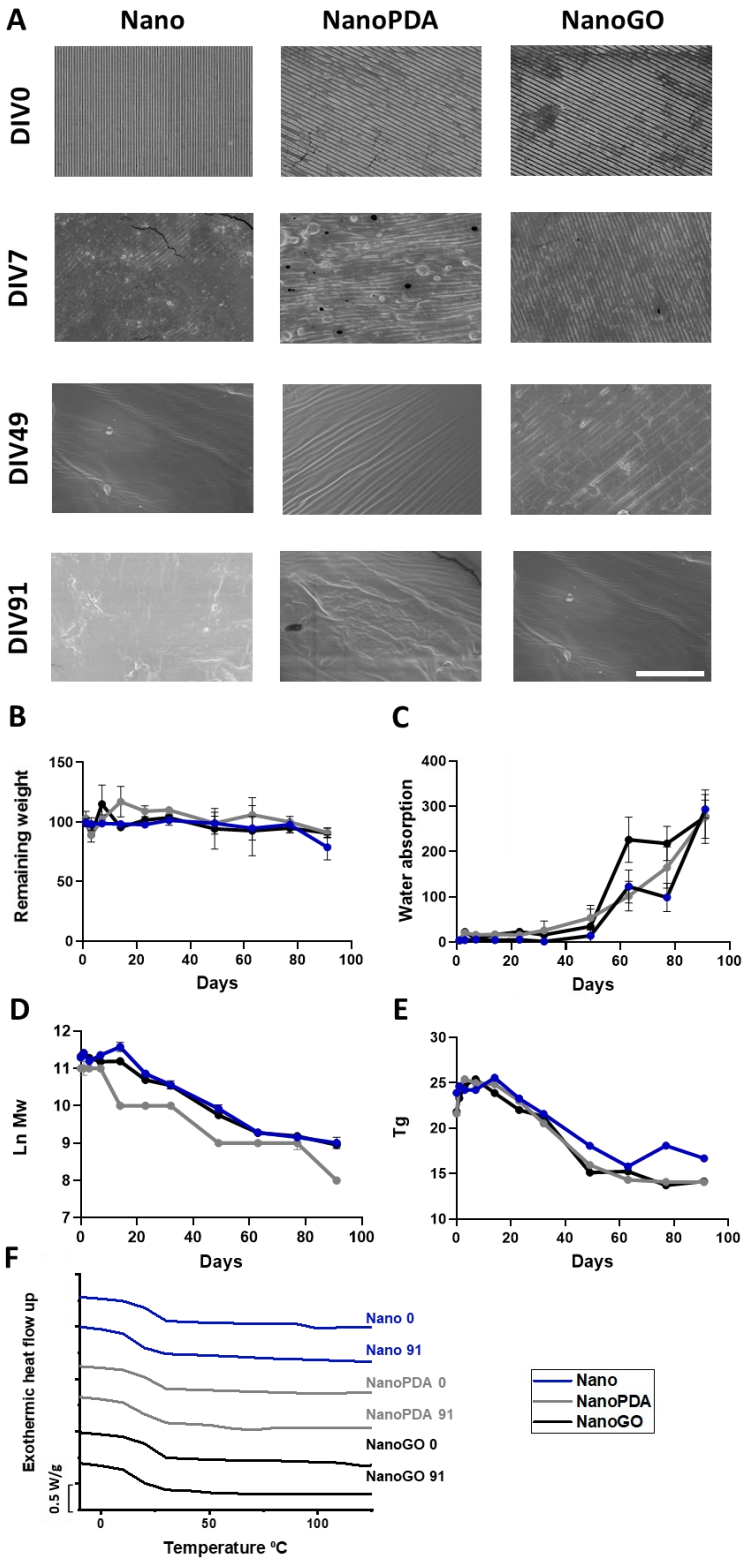

Figure 4.3.: ***In vitro*** **degradation of the nanostructured scaffolds.**

(A) SEM micrographs showing the nanostructured surface of the scaffolds without any coating (Nano), coated with PDA (NanoPDA) and coated with PDA and functionalized with GO (NanoGO) from DIV0 to 91. Scale bar 10 µm. **(B)** Graphs showing the remaining weight (%RW), **(C)** water absorption (%WA), **(D)** molecular weight (M_w) and **(E)** glass-transition temperature (T_g) over the degradation time. **(F)** 1st DSC thermograms of the Nano, NanoPDA and NanoGO scaffolds at day 0 and 91 showing no melting (T_m) or crystallization peaks.

The further functionalization with PDA and GO reduced the strength-related properties of the No Nano sample. Accordingly, both the secant modulus (No NanoPDA 10.5±2.0 MPa; No NanoGO 10.4±3.2 MPa) and the offset yield strength (No NanoPDA 0.22±0.04 MPa; No NanoGO 0.21±0.07 MPa) (Figure 4.4. A and B) showed lower values with respect to the non-functionalized sample (i.e., No Nano). The T_g values of the three samples were very similar, with a slight decrease in the transition temperature after the coating/functionalization step (No Nano 21.5 ^{o}C; No NanoPDA 21.0 ^{o}C; No NanoGO 20.0 ^{o}C) (Figure 4.4. C). This phenomena could be ascribed to some water molecules inside the polymeric structure that may act as a plasticizer [46]. Despite our synthesized polymeric scaffolds are clearly stiffer than the mouse brain (17.6±1.5 MPa vs 0.007 MPa) [47–49], other materials regularly considered for CNS regeneration and stimulation (e.g., platinum) display much higher elastic moduli even in the range of several GPa [50–53]. Thus, we believe that our polymeric material will minimize the mechanical mismatch between the implant (i.e., PLCL) and the host tissue (i.e., brain) with respect to other considered metallic counterparts.

A

Temperature 37 ^{o}C	Secant modulus 2% (MPa)	Elongation at break (%)	Offset yield strength (MPa)	T_g (^{o}C)
No Nano	17.6 ± 1.5	> 180	0.35 ± 0.03	21.5
No NanoPDA	10.5 ± 2.0	> 180	0.22 ± 0.04	21.0
No NanoGO	10.4 ± 3.2	> 180	0.21 ± 0.07	20.0

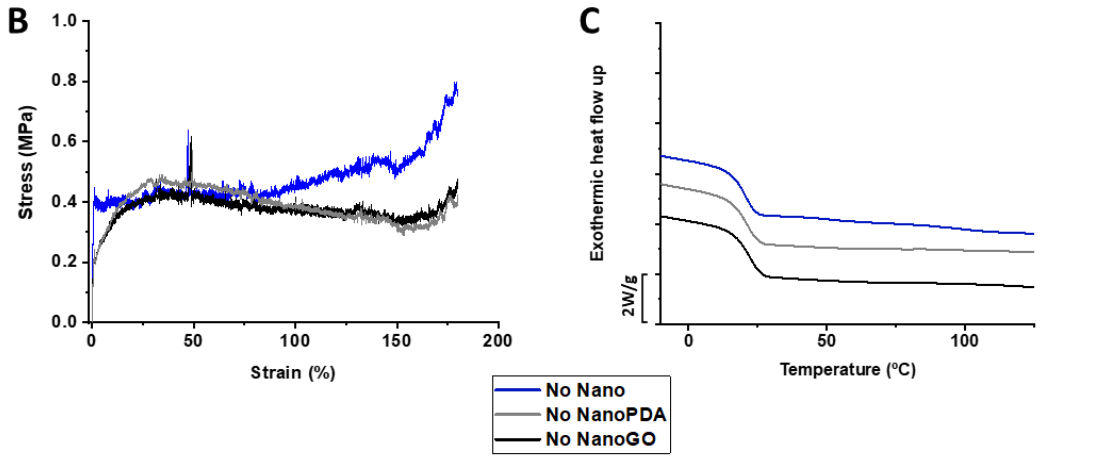

Figure 4.4.: Mechanical characterization of the PLCL films.
(A) Table showing the secant modulus at 2%, percentage of the elongation at break, offset yield strength and the T_g of the non-coated PLCL films (No Nano), coated with PDA (No NanoPDA) and further functionalized with GO (No NanoGO). **(B)** Stress-strain curves for the studied samples. **(C)** DSC thermograms of the samples used on the tensile test.

4.3.2. Surface nanostructured grooves allow oriented migration of human dental pulp stem cells

Apart from the use of NanoGO and NanoPDA scaffolds alone for the treatment of CNS injuries, here, we also propose their combination with stem cells for a better restoration of the CNS in future personalized clinical applications. Regardless of cell donor origin, stem cell treatments require to minimize the risk for cancer, eliminate unclear variables for cell differentiation, and purify the differentiated cells before transplantation [54]. In this regard, we propose the preselection of hDPSCs with neural differentiation capacity thanks to the preamplification with Neurocult proliferation as stated in chapter 3 prior to cell graft. Moreover, hDPSCs, in comparison with other stem cell sources like embryonic stem cells, have no tumorigenic features. Besides, their immunomodulatory and multi-linage differentiation capacities (including neural differentiation towards neuronal and glial lineages), make them excellent candidates for personalized therapies [55].

First, we studied the dynamics of cell growth and adhesion regarding attachment, elongation and migration of hDPSCs over the NanoGO and NanoPDA scaffolds in comparison with the commonly used laminin-coated glass cover. Laminin is known to prime the proliferation of brain tumoral cells [56]. However, in our model, hDPSCs were able to attach, align and elongate with no need of ECM-like compounds in both NanoGO and NanoPDA scaffolds (Figure 4.5. A), although the number of cells was greater on NanoPDA than NanoGO scaffolds, suggesting a possible better attachment on NanoPDA and demonstrating the capability of these supports to act as anchoring scaffolds for the transplantation of hDPSCs into the injured CNS.

To evaluate the migratory capacity of hDPSCs on the scaffolds, cells were seeded and videorecorded for 16 h. Cells cultured over nanostructured scaffolds NanoGO and NanoPDA displayed no statistical difference neither in the mean velocity (NanoGO 0.05±0.03 μm/min; NanoPDA 0.05±0.02 μm/min; laminin 0.09±0.03 μm/min, $p > 0.3$, One-way ANOVA) nor in the persistence (NanoGO 11.2±0.9%; NanoPDA 9.9±1.5% laminin 15.0±2.1%, $p > 0.1$, One-way ANOVA) in comparison with hDPSCs cultured over laminin (Figure 4.5. B). The persistence measures the interval between major shifts in cell direction, enabling a quantitative examination of the variations in migratory patterns [57–59]. Although this quantitative measurement showed no statistical difference in the recorded time, the trajectories demonstrated a directional pattern on the movement over the NanoGO and NanoPDA scaffolds. Nevertheless, hDPSCs cultured on Neurocult proliferation serum free medium exhibited a lower mobility capacity than other cells like the NSCs studied on chapter 3, which may explain the lack of statistical differences. Hence, this preliminary data clearly encourages to increase either the number of cells counted or the time of the records to better understand the movement pattern. Anyway, the fact that hDPSCs were able to attach, elongate and move following the nanograting

axis made NanoGO and NanoPDA suitable anchoring scaffolds for the combinatorial treatment of CNS injuries together with grafted stem cells of human origin.

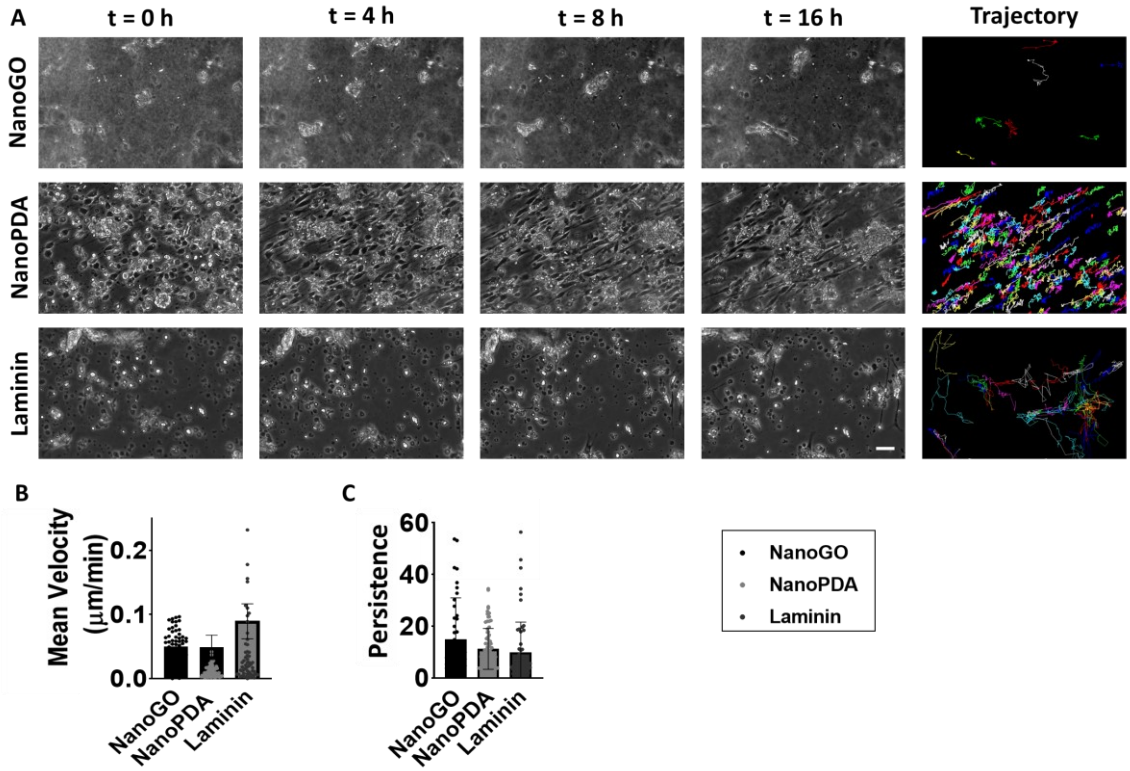

Figure 4.5.: Dynamic movement pattern of human dental pulp stem cell (hDPSCs) and progenitor cells over NanoGO and NanoPDA scaffolds.
(A) Videomicroscopy snapshots at 0, 4, 8 and 16 h post seeding in nanostructured scaffolds illustrating the dynamic process of the parallel cell alignment. On the contrary, hDPSCs seeded on laminin-coated glass covers showed a random trajectory over time. **(B)** Mean cell velocity and **(C)** cell persistence over NanoGO and NanoPDA scaffolds compared to laminin control. Bars showed mean ± SEM and dots correspond to individual data, Kruskal-Wallis One Way Analysis of Variance on Ranks. Scale bars, 50 μm.

4.3.3. Human dental pulp stem cells cultured on nanostructured scaffolds are able to generate neuronal and astroglial lineage cells

The neural crest origin of hDPSCs make them ideal for personalized CNS restoration purposes after injury [55]. Indeed, the neurodifferentiation capabilities of these cells towards both neuronal and astroglial lineages in laminin coated glass covers have been recently reported [19]. Here, we aim to study the neurodifferentiation commitment of hDPSCs over our NanoGO and NanoPDA scaffolds towards both neuronal and astroglial lineages to ensure a correct neurodifferentiation process of the integrated grafted cells towards all the neural descendants after *in vivo* graft. The need of stem capabilities is also vital for a correct integration of the grafted cells in the neural tissue [60]. Therefore, the stemness of the hDPSCs cultured over NanoGO and NanoPDA scaffolds for 7 or 14

days was also assessed. The presence of Nestin, an intermediate filament of neural precursor cells in adult CNS [61], was used to determine if the seeded cells maintained their stemness. Nestin is also an important multipotent stem cell marker with signaling implications on the development of immature cells [62], including neural progenitor cells [63,64]. We found that, although both scaffolds showed a lower amount of stem cells than laminin, NanoPDA better supported Nestin positive cells compared to NanoGO at DIV7 (NanoGO 8.3±0.4%; NanoPDA 25.7±1.5%; laminin 47.7±2.6%, $p < 0.001$, One-way ANOVA) and DIV14 (NanoGO 3.0±0.5%; NanoPDA 20.1±2.7%; laminin 65.6±1.8%, $p < 0.001$, One-way ANOVA) (Figure 4.6.). Together with Nestin, the glial fibrillary acidic protein (GFAP) is also expressed by astrocytes and non-differentiated neural stem cells [65]. The number of cells expressing GFAP was greater than that observed with Nestin, but again, both scaffolds showed a lower amount of GFAP positive cells in comparison to laminin. NanoPDA scaffold better supported the GFAP marker expression compared to NanoGO both at DIV7 (NanoGO 18.9±1.0%; NanoPDA 29.1±3.2%; laminin 89.4±5.6% $p < 0.001$, One-way ANOVA) and DIV14 (NanoGO 15.8±2.0%; NanoPDA 30.1±3.9%; laminin 50.0±1.9%, $p < 0.001$, One-way ANOVA). Altogether, our results demonstrated that hDPSCs cultured over NanoGO and NanoPDA scaffolds were able to retain the stem phenotype for up to 14 days, although in lower cellular proportion than in laminin, suggesting a possible faster differentiation and less tumorigenic potential. Nevertheless, these findings point out the prevalence of the necessary stem population on the NanoGO and NanoPDA scaffolds, which will be presumably needed for a correct integration of the grafted hDPSCs on the host neural tissue.

GFAP is also an astroglial marker and together with other specific markers allowed us to study the differentiation capabilities of the hDPSCs towards astroglial lineages. First, we studied the differentiation capabilities towards more mature astroglial lineages by the appearance of the S100 calcium-binding protein β (S100β). Astroglial differentiation is characterized by the loss of Nestin, preservation of GFAP and the appearance of the S100β [66,67]. We found that while NanoPDA scaffold presented a non-statistical difference of S100β positive cells compared to laminin, NanoGO expressed lower amounts at DIV7 (NanoGO 2.3±0.2%; NanoPDA 10.7±1.6%; laminin 22.6±1.6%, $p < 0.001$, One-way ANOVA), suggesting a more rapid mature astroglial differentiation on NanoPDA scaffold, compared to NanoGO. Surprisingly, at DIV14, NanoGO scaffold augmented the amount of S100β positive cells compared to both NanoPDA and laminin, while NanoPDA maintained the population of the mature astroglial lineage (NanoGO 21.5±3.4%; NanoPDA 10.8±1.0%; laminin 9.5±0.5%, $p < 0.001$; One-way ANOVA) (Figure 4.7.). In accordance with the loss of Nestin and the conservation of GFAP, we can conclude that both NanoGO and NanoPDA were able to support the astroglial differentiation, without excluding other glial lineages. Interestingly, S100β is also a marker of myelinating cells like oligodendrocytes (in the CNS) or Schwann cells (in the PNS) [68–70]. Thus, due to the peripheric origin of the hDPSCs, we studied the

differentiation towards Schwann precursor cells by p75 neurotrophin receptor (p75(NTR)). This immature no-myelinating Schwann cell marker has been reported to be implicated on the remyelination and restoration of motor function driven by Schwann cells *in vivo* [71], making its expression interesting for future restoration of neural tissue after an injury. We found that both scaffolds showed a lower p75 expression than laminin, but again, NanoPDA scaffold supported a greater p75 marker expression than NanoGO at DIV7 (NanoGO 7.9±0.7%; NanoPDA 31.9±4.3%; laminin 80.6±5.8%, $p < 0.001$, One-way ANOVA). This result is in accordance with those found with GFAP, suggesting that NanoPDA provoked a faster differentiation towards glial cells compared to NanoGO scaffold. Nevertheless, both scaffolds were able to support greater p75 marker expression for longer periods with no statistical difference between them at DIV14 (NanoGO 42.9±3.5%; NanoPDA 36.4±2.5%; laminin 15.4±0.1%). There must be taken in consideration that p75 has been found to be essential for neuronal cell survival and the activation of reparative processes after rodent CNS injury [72]. Hence, the fact that both of our scaffolds were able to support p75 differentiation and maintenance for greater periods, further support the use of NanoGO and NanoPDA scaffolds grafted with hDPSCs for the future treatment of CNS injuries like traumatic brain injury (TBI) or spinal cord injury (SCI).

To truly recognize the differentiation towards Schwann cell precursors, we studied the coexpression of both S100β with p75. We found that although laminin exhibited a faster coexpression of both markers at DIV7 than NanoGO and NanoPDA scaffolds (NanoGO 2.4±0.2%; NanoPDA 10.7±1.7%; laminin 22.6±1.6%, $p < 0.001$, One-way ANOVA), there was no statistical difference compared to NanoPDA, suggesting again a faster glial differentiation on this scaffold than in NanoGO. Moreover, the amount of Schwann precursors was stabilized at DIV14 in both NanoGO and NanoPDA scaffolds compared to laminin, being even higher on NanoGO, despite non-statistical difference was found (NanoGO 21.6±3.4%; NanoPDA 10.8±1.0%; laminin 9.5±0.5%, $p > 0.1$, One-way ANOVA). These results suggested that NanoGO was also able to support glial differentiation, but in a slower manner. Remarkably, although originally from the PNS, Schwann cells contribute to Wallerian degeneration and regrowth [73] and have the ability to remyelinate demyelinated axons in the CNS [74]. Wallerian degeneration is the active deterioration of the more distal point of an axon after an injury to both PNS and CNS and has been described in degenerative diseases such as Alzheimer or amyotrophic lateral sclerosis (ALS) [75]. Indeed, after damage to the nervous system, Schwann cells are transformed into repair Schwann cells and migrate close to the injured area to better support regeneration. These repair Schwann cells provide the different features required for the survival of wounded neurons, axonal regeneration, and reinnervation [76]. Hence, they play a key role in the regeneration process after injury of both PNS and CNS. Here, we demonstrated the differentiation of hDPSCs towards glial cells including most likely Schwann cell precursors over NanoGO and NanoPDA scaffolds, offering an alternative combined treatment for damaged PNS and CNS in future experiments.

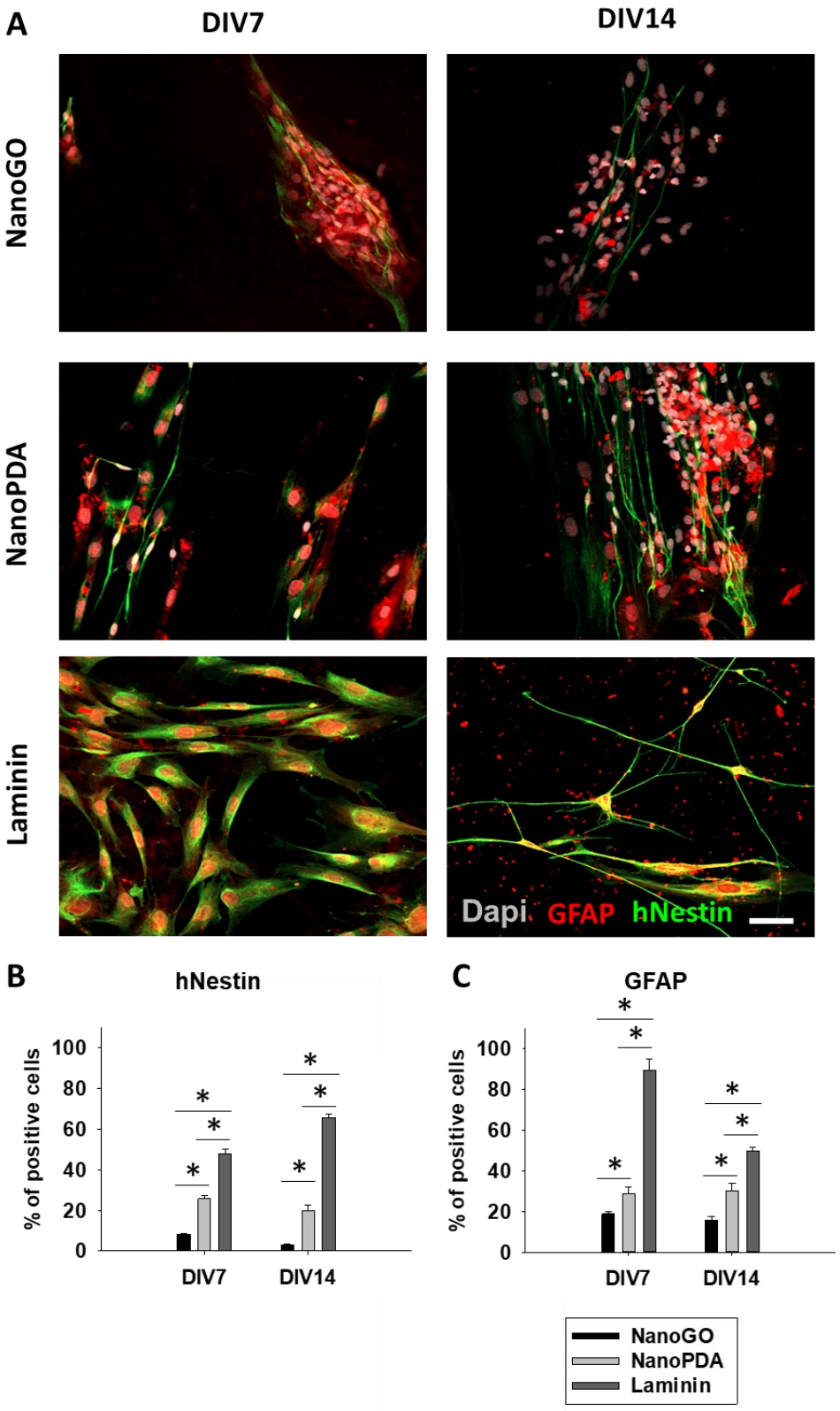

Figure 4.6.: Stemness maintenance of the hDPSCs over NanoPDA and NanoGO scaffolds.
(A) Double immunofluorescence for the stemness lineage markers GFAP (red) and hNesting (green) at DIV 7 and 14 post-seeding in the different conditions. **(B)** Quantification of the proportion of hNestin and **(C)** GFAP positive cells. *p < 0.001 between laminin and the treatments NanoGO and NanoPDA, Holm-Šídák method One Way Analysis of Variance on Ranks. Scale bar, 50 µm.

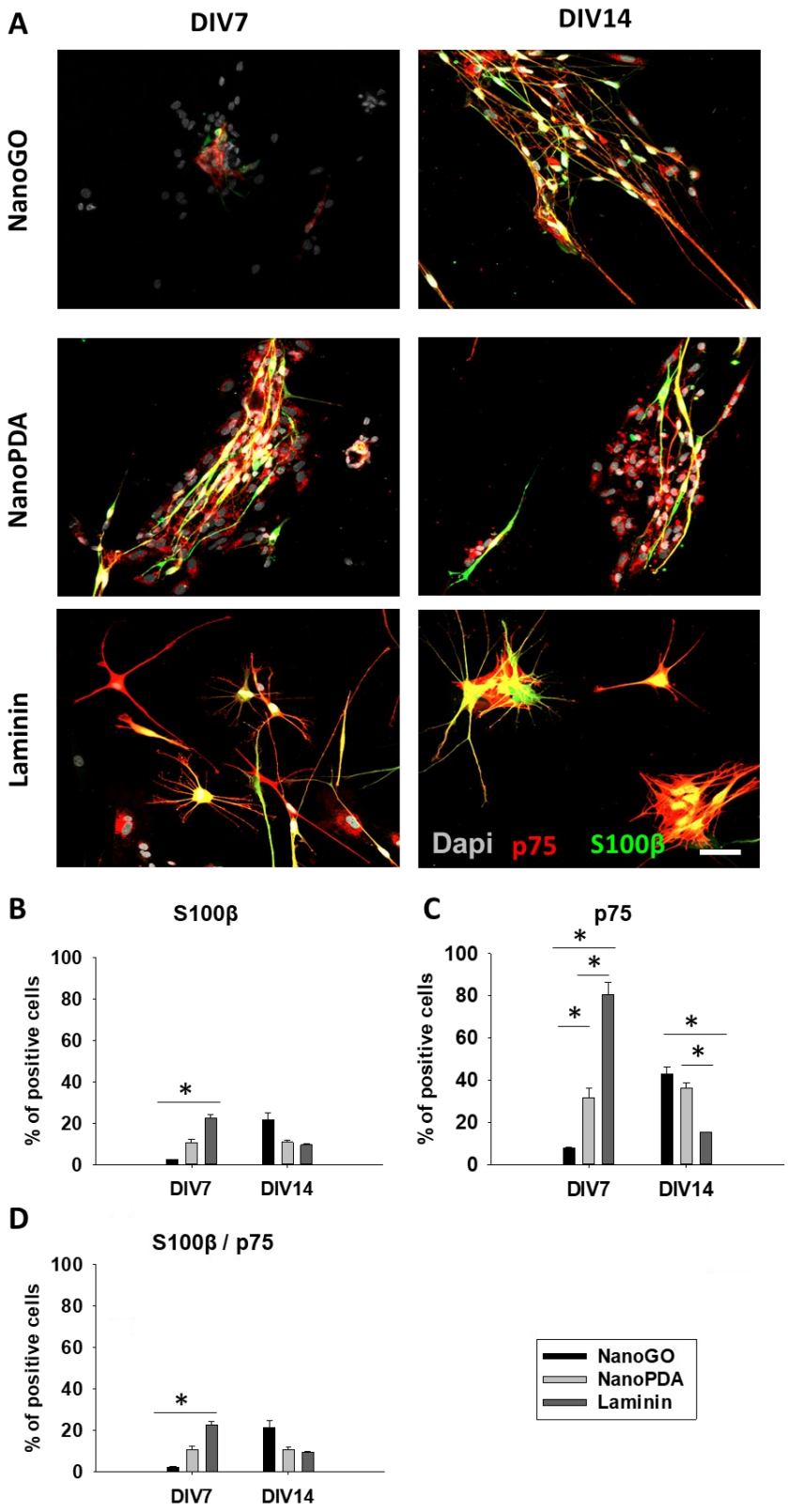

Figure 4.7.: Glial differentiation of the hDPSCs over NanoPDA and NanoGO scaffolds.
(A) Double immunofluorescence for the astroglial lineage markers p75 (red) and S100β (green) at DIV 7 and 14 post-seeding in the different conditions. **(B)** Quantification of the proportion of S100β, **(C)** p75 **(D)** and double stained S100β/p75 positive cells. *$p < 0.001$ between laminin and the treatments NanoGO and NanoPDA, Holm-Šídák method One Way Analysis of Variance on Ranks. Scale bar, 50 µm.

For a complete reinnervation after injury, grafted stem cells need to be able to differentiate towards all the lineages from the neural tissue, including neuronal cells [60]. Thus, we studied neuronal-like cell differentiation of the hDPSCs over NanoGO and NanoPDA scaffolds. We first studied the differentiation towards immature neuronal-like cells with doublecortin (DCX) marker. In both the developing and adult brains [77], DCX expression is restrained to neuronal origin premature cells and multipotent-precursors, including the cells on the RMS [78,79], which here we aim to regenerate *in vivo*. We found that NanoGO promoted a greater differentiation towards DCX positive neuronal-like cells, even achieving the proportions found in laminin, at both DIV7 (NanoGO 92.2±6.6%; NanoPDA 34.5±5.3%; laminin 99.2±8.1%, $p < 0.001$, One-way ANOVA) and DIV14 (NanoGO 82.6±8.9%; NanoPDA 0±0%; laminin 92.1±5.6%, $p < 0.001$, One-way ANOVA) (Figure 4.8.). In line with these results, the differentiation towards more mature neuronal-like phenotype expressing nuclear neuronal marker NeuN was also boosted on NanoGO scaffold compared to NanoPDA at DIV14. However, both of them displayed a lower mature neuronal differentiation than the cells cultured over laminin (NanoGO 14.1±2.0%; NanoPDA 0±0%; laminin 92.1±5.6%, $p < 0.001$, One-way ANOVA). Previous studies have similarly reported that GO induces cellular neurodifferentiation and also a faster neuronal-like phenotype of stem cells, including DCX and NeuN positive cells [80].

Remarkably, there was neither DCX nor NeuN positive cells on the NanoPDA scaffold at DIV14. The fact that there were neuronal-like cells at DIV7 in NanoPDA can be ascribed to: i) a maturation of hDPSCs over NanoPDA scaffolds towards neuronal-like cells expressing other markers not tested here; or ii) a disparity on the compensatory proportions of neurons and astroglial support in favor of the glial differentiation at DIV14. It can be generally concluded that NanoGO and NanoPDA scaffolds achieved lower neuronal differentiation than laminin in favor of other cell types that have not been studied in this chapter. It can be also concluded that hDPSCs cultured over NanoGO scaffolds had a more balanced differentiation towards both glial and neuronal-like cells, while NanoPDA scaffold might have boosted glial differentiation at the expense of the neuronal-like cell commitment. Considering that NanoPDA scaffolds promoted a more balanced glial and neuronal-like cell commitment with mouse NSCs on chapter 3, the use of both NanoGO and NanoPDA were considered for the subsequent *in vivo* experiments.

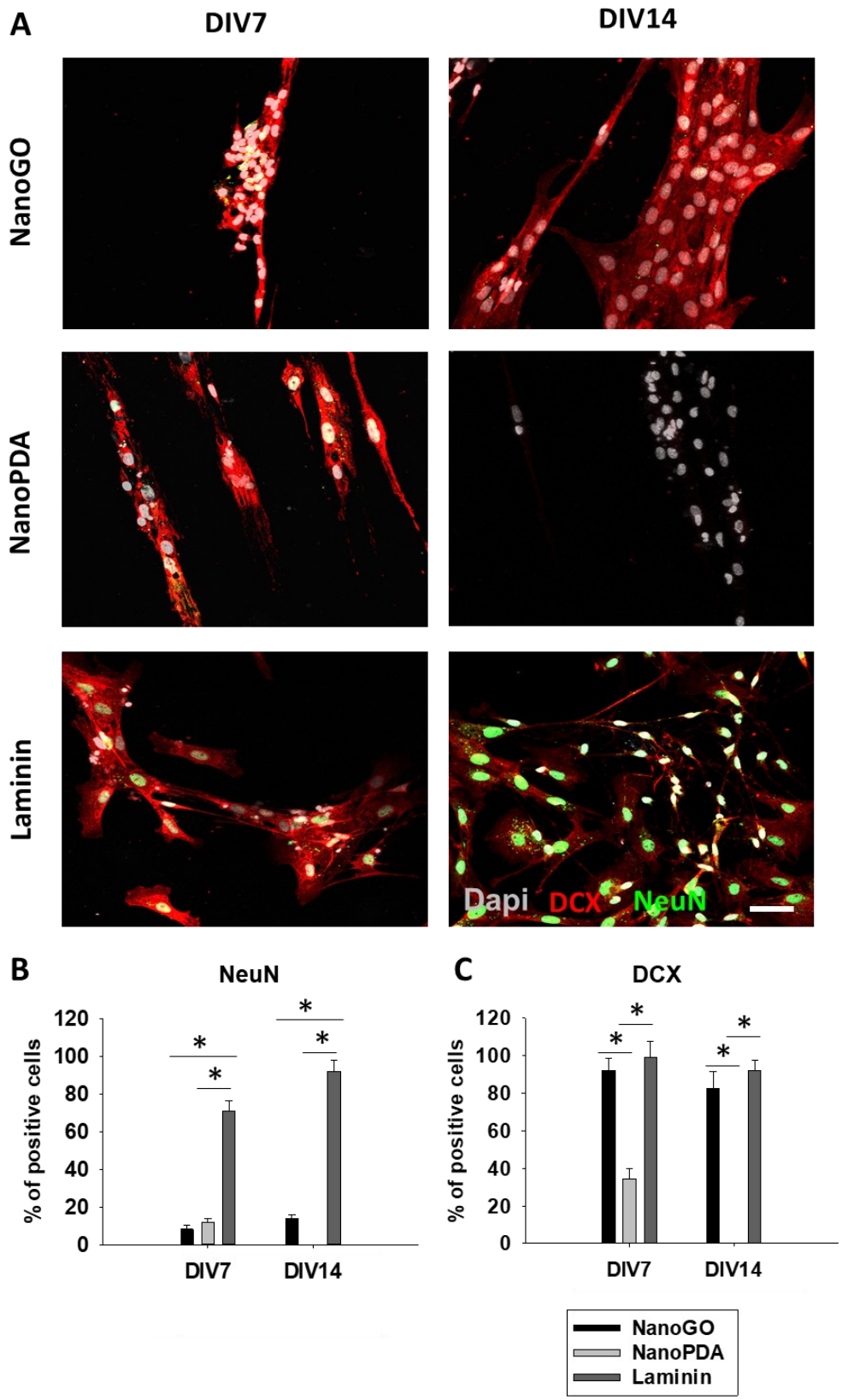

Figure 4.8.: Neuronal differentiation of the hDPSCs over NanoPDA and NanoGO scaffolds. **(A)** Double immunofluorescence for the neuronal lineage markers DCX (red) and NeuN (green) at DIV 7 and 14 post-seeding in the different conditions. **(B)** Quantification of the proportion of NeuN and **(C)** DCX positive cells. *$p < 0.001$ between laminin and the treatments NanoGO and NanoPDA, Holm-Šídák method One Way Analysis of Variance on Ranks. Scale bar, 50 µm.

4.3.4. *In vivo* restoration of the rostral migratory stream

After assessing the aligned attachment and neurodifferentiation capabilities of the hDPSCs over NanoGO and NanoPDA scaffolds *in vitro*, we tested the effect of the nanostructured scaffolds in an *in vivo* context. For that, the RMS of athymic nude mice was first interrupted, provoking a damage on the migratory stream and the consequent spatial restriction of the DCX positive neuroblasts from the subventricular zone to the olfactory bulb (OB) [81]. Within the first days after the lesion on the CNS, the inflammation produces the activation of the astrocytes towards the injured tissue. The proliferation and migration of the astrocytes results in the production of a glial scar to isolate the rest of the brain from the damaged area, impairing tissue regeneration [82]. In the last years, animal experiments have showed that when these physical glial barriers are altered, removed, or circumvented, neurons can significantly reorganize their circuits and undergo protracted regeneration [42,43]. Hence, it is herein proposed the use of NanoGO and NanoPDA scaffolds to support the attachment and guided migration of the neural cells, to characterize the reconnection of the damaged RMS and the glial scar formation. Besides, we aimed to study the effect of the NanoGO and NanoPDA scaffolds grafted with hDPSCs on their migration and integration *in vivo* to ultimately lead the potential of exogenous cells as an alternative cell therapy.

First, the possible *in vivo* interference and accumulation of our NanoGO and NanoPDA scaffolds was studied. None of the animals implanted with the NanoGO and NanoPDA scaffolds showed any alteration in movement, social, grooming, feeding or food deposition compared to the sham (interruption of the RMS with the same procedure but without the introduction of any scaffold or hDPSCs) or controls (no intervention). To better asses the possible accumulation on the main organs, after 91 days (3 months), animals were sacrificed, prefunded and the heart, liver, kidney and spleen dissected, processed and stained via hematoxylin and eosin (H&E) according to ISO 10993-11 [83]. None of the scaffolds provoked macroscopic histopathological alterations in any of the organs studied after 91 days (3 months) compared to control and Sham animals (Figure 4.9.), suggesting a good tolerance with no apparent toxicity of both NanoGO and NanoPDA scaffolds.

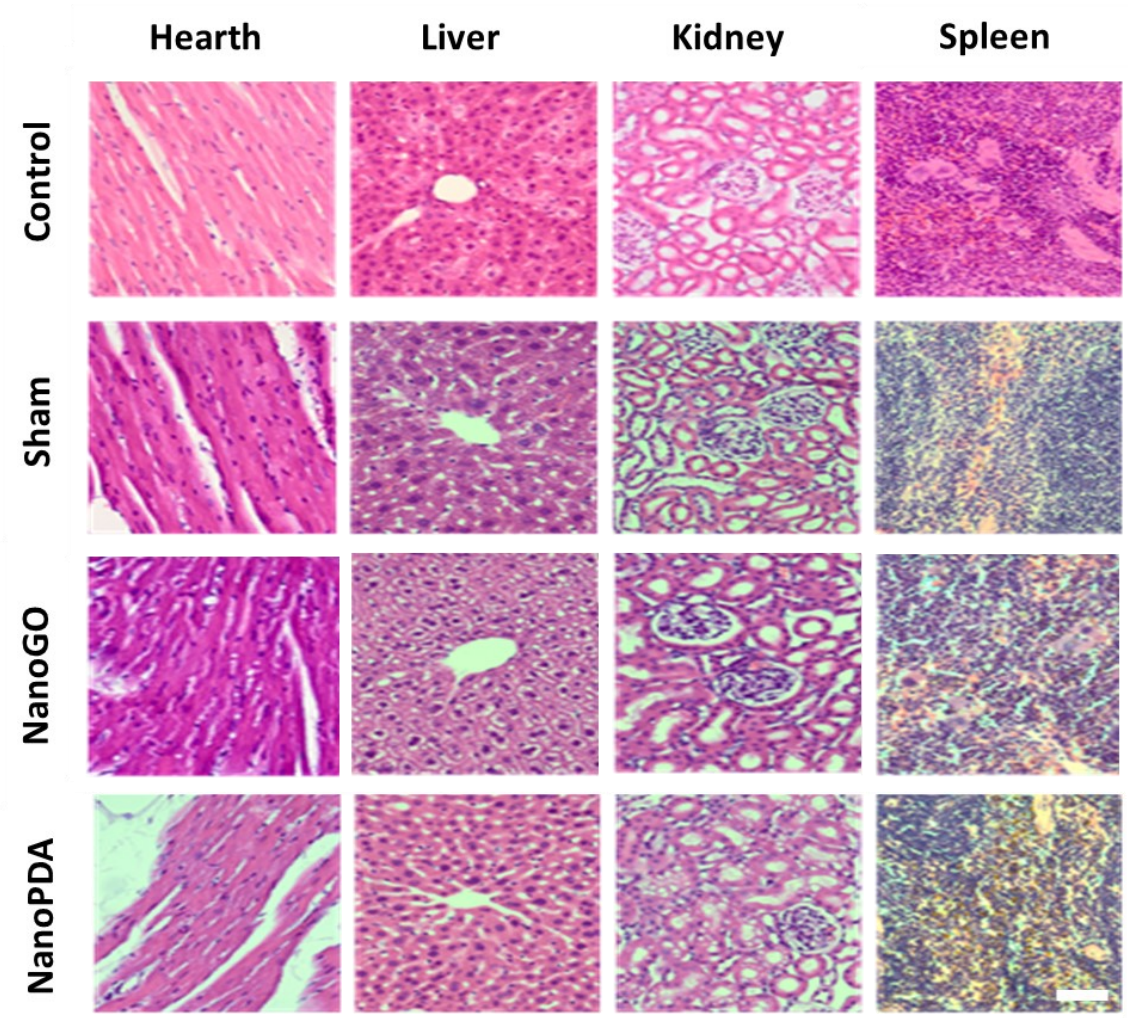

Figure 4.9.: *In vivo* toxicity and accumulation of NanoGO and NanoPDA scaffolds
Hematoxylin and eosin (H&E) staining of mice spleen, kidney, liver and hearth with no apparent toxicity, massive neoplasia or cell death after 91 days. Scale bar 100 µm.

The interruption of the RMS provoked a restriction of DCX positive neural progenitors on the OB. Thus, death or damaged cells were unable to be replaced and the mice suffered from an impaired olfactory sense [84]. To address the functional recovery of the RMS reconnection, we studied the olfactory capacity of the mice after 7, 14 and 91 days (3 months) after surgery by the buried food test (BFT). We found that when the RMS was interrupted in the Sham mice, after 7 days, the time consumed to find the food was duplicated in comparison to the control mice (Control 64.8±11.0 s; Sham 125.6±18.7 s, $p < 0.05$, One-way ANOVA) (Figure 4.10. A), suggesting a functional impairment either on the olfactory sense itself or on the association of the smell with food. Interestingly, both NanoGO and NanoPDA alone were able to diminish the time needed to find the food to basal levels (NanoGO 62.1±12.7 s; NanoPDA 48.9±5.4 s; $p < 0.05$, One-way ANOVA). To assess the function of hDPSCs on the restoration of the RMS, we also performed the BFT test when grafting the hDPSCs alone or in combination with NanoGO and NanoPDA scaffolds. Surprisingly, there was no statistical difference when hDPSCs

were grafted either alone or in combination with NanoGO or NanoPDA scaffolds, compared neither to Sham nor the control (Control 64.8±11.0 s; Sham 70.6±11.5 s; hDPSCs 81.6±10.2 s; NanoGO+hDPSCs 87.3±16.0 s; NanoPDA+hDPSCs 71.8±11.7 s, One-way ANOVA), suggesting a real alternative to stereotaxic cell injection (Figure 4.10. B). The physical impairment of the RMS hinders the replacement of DCX positive cells on the OB, but cause no damage on the actual population of DCX cells that had already reached the OB. Hence, it is possible to have a delayed functional effect on the olfactory sense or its recognition, despite the actual damage on the RMS [81,85].

After 3 months, both NanoGO and NanoPDA were able to lower the time needed to find the food to basal levels in female mice (Control 64.8±11.0 s; Sham 98.8±9.9 s; NanoGO 47.9±6.1 s; NanoPDA 43.1±8.3 s, $p < 0.05$, One-way ANOVA respect to Sham) (Figure 4.10. C). Remarkably, in males, functional recovery was only observed in NanoGO scaffold and there was a spontaneous functional recovery on the two Sham lesioned males (Control 64.8±11.0 s; Sham 32.4±3.8 s; NanoGO 42.7±11.3 s; NanoPDA 100.1±22.8 s, $p < 0.05$, One-way ANOVA) (Figure 4.10. D). It must be taken into consideration that gender dimension is a key factor regarding neural regeneration. Besides, in animal models, females generally show a greater neurological and functional recovery in comparison with males [86–89]. Hence, the experiments with hDPSCs at 3 months were performed only in females, where both scaffolds showed a similar recovery. After 3 months, there was no statistical difference between Sham and the hDPSCs either alone or grafted together with NanoGO and NanoPDA scaffolds (Control 64.8±11.0 s; Sham 105.4±11.8 s; hDPSCs 107.4±19.3 s; NanoGO+hDPSCs 76.6±15.8 s; NanoPDA+hDPSCs 76.0±14.5 s, One-way ANOVA), showing again that maybe the delayed functional recovery was caused by the hDPSCs (Figure 4.10. E). In conclusion, regarding olfactory function, both NanoGO and NanoPDA scaffolds showed promising results, even better than the combinatorial treatment with hDPSCs and showed no worsening behavior caused by the implantation of a foreign body. Although athymic nude mice had a defect in thymus affecting the maturation of T-Cells and thus an impaired immune system, they still preserved astrocytes, microglia and macrophages, which may had detected the grafted hDPSCs, provoking an inflammatory response surrounding the grafted area [90]. This activation of the brain immune and surveillance systems by grafted stem cells can be both helpful and harmful. Indeed, the effectiveness of endogenous regenerative responses and the method of action, as well as the fate and functional integration of exogenous cells, appear to be influenced by the interaction between immune cells, grafted stem cells, and their offspring, by promoting cell replacement, immunomodulation, and trophic support [91], but might have induced death of the grafted stem cells, delaying the restoration [92].

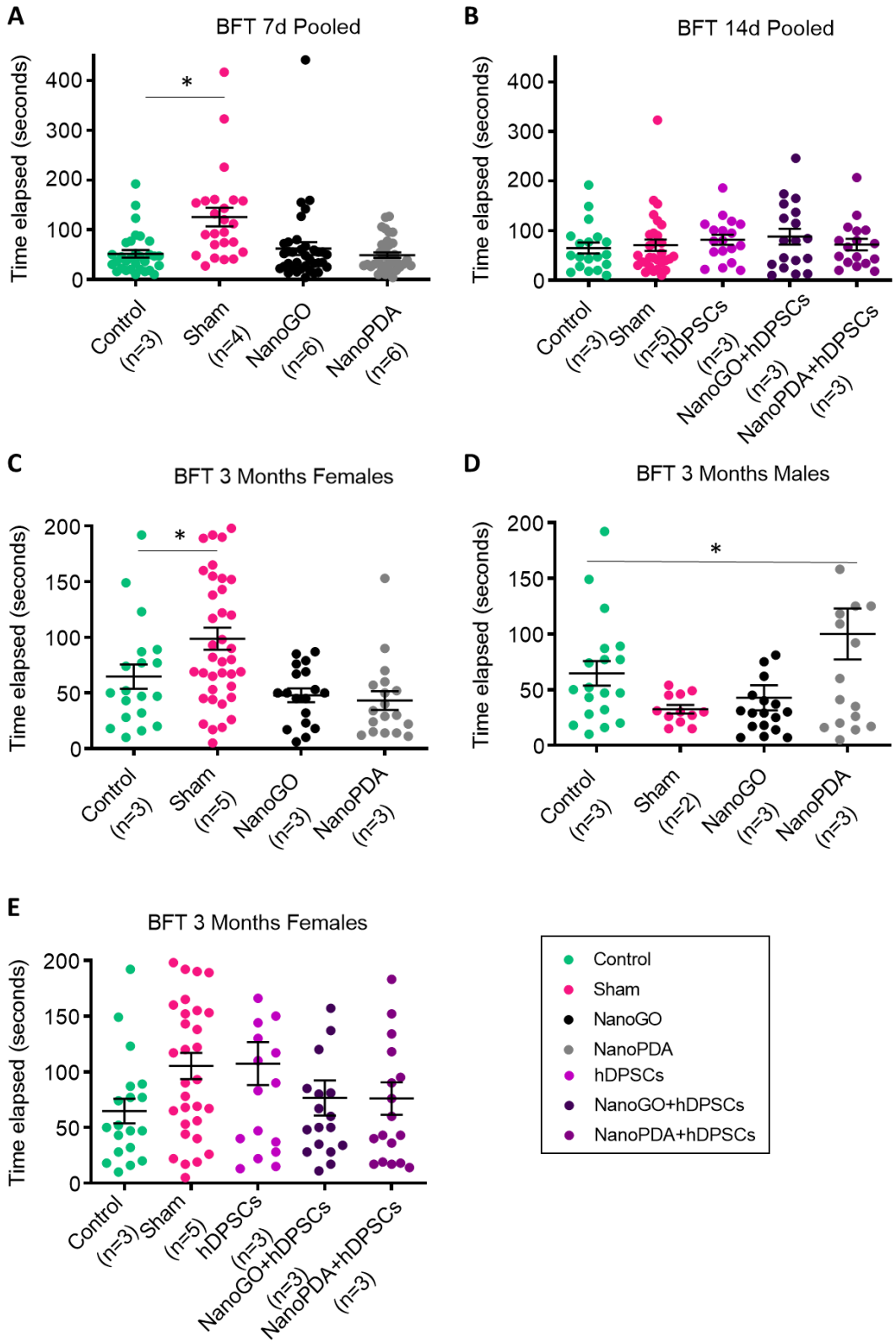

Figure 4.10.: Buried Food Test (BFT) results.

Graphical representation showing the mean time and standard error of the mean (SEM) acquired to find the food in the buried food test (BFT) **(A)** 7 days after the injury, **(B)** 14 days after the injury or **(C)** 3 months after the injury in females **(D)** males and **(E)** females combined with hDPSCs. *$p < 0.05$ between the non-injured control and the treatments, Holm-*Šídák* method One Way Analysis of Variance on Ranks.

To better assess the restoration of the RMS, an immunostaining against DCX, GFAP and hNestin was performed. As explained before, in rodents, DCX positive neuronal precursors that are originated in the SVZ of the brain travel through the RMS to reach the OB and replace the damaged cells [81]. Moreover, RMS is surrounded by GFAP positive glial cells that, together with blood vessels, act as a plath for neuroblast migration [93]. Remarkably, during neural damage, GFAP positive astrocytes migrate to the injured site producing the glial scar which impairs tissue regeneration [82]. Hence, GFAP marker will allow to detect the RMS and the possible glial scar formation. Finally, hNestin positive staining was used to detect the migration and integration of hDPSCs. This marker specifically detects human Nestin making possible to differentiate the mouse cells from the grafted human stem cells. Preliminary data showed that, 7 days after the lesion, the RMS was successfully impaired (Figure 4.11.) and both NanoGO and NanoPDA scaffolds showed a lower RMS impairment but a higher astrogliosis on the injured site. Maybe, the scaffolds were able to serve as migration paths for DCX positive neuroblast at short periods, but activated the astrocyte recruitment to the injured site to create the well-known astroglial scar [82]. Therefore, experiments with hDPSCs were performed at longer periods to better assess the integration capabilities of the cells and the restoration of the RMS.

To overcome the restoration capabilities of the hDPSCs, we again impaired the RMS and either introduced hDPSCs incubated for 24 h over NanoGO (NanoGO+hDPSCs), NanoPDA (NanoPDA+hDPSCs) scaffolds or resuspended hDPSCs. Given the lack of restoration after 7 days with the scaffolds alone, to better assess the possible short-term regenerative effects, together with cell presence under differentiation, the experiments were conducted and 14 days after the injury and cell graft, animals were sacrificed and histologically analyzed. We observed that after 14 days, the RMS was successfully impaired and a reduction of astrogliosis was observed due to the grafted hDPSCs. hNestin positive cells alone had migrated from the grafted area to the SVZ, OB, even to the hippocampus and cerebral cortex in the left hemisphere (LH) and no hDPSCs appeared on the right hemisphere (RH) (Figure 4.12.). When hDPSCs were grafted with NanoGO scaffolds (NanoGO+hDPSCs), cells were able to migrate also to SVZ, OB, hippocampus, and cerebral cortex in the LH, but astrogliosis was found around the injured site, suggesting that the presence of GO on the scaffolds boosted the migration and activation of the GFAP positive astrocytes towards the grafted area. Interestingly, less hDPSCs dispersion in the brain and astrogliosis was observed when hDPSCs were grafted together with NanoPDA scaffold (NanoPDA+hDPSCs). Indeed, NanoPDA scaffolds provoked the accumulation of the hDPSCs on the grafted area and reduced the migration of the hDPSCs towards only the SVZ (neurogenic region) on the LH, suggesting a possible reduction of cell dispersion on the grafted area thanks to the nanostructured scaffold. These results are in accordance with other studies where the direct administration of GO sheets in the mouse brain provoked the activation of proinflammatory cascades

without any neuronal loss or microglial activation [94]. Some studies even reported that the activation of astrocytes and maybe microglia is somehow beneficial for the regeneration of the neural tissue [91]. Hence, studies at longer periods may be done to better understand the possible activation of both astrocytes and microglia after GO implantation and its effect in regeneration. Overall, our results demonstrated that grafted hDPSCs integrated mostly in the SVZ, one of the natural niche of stem cells in the mouse brain full off capillaries that run inside and around neuroblast chains [95]. Due to the stem phenotype of the hDPSCs, they may have stayed on the injured site or migrated towards the natural stem niches most probably using the RMS itself or the blood vessels that compose it.

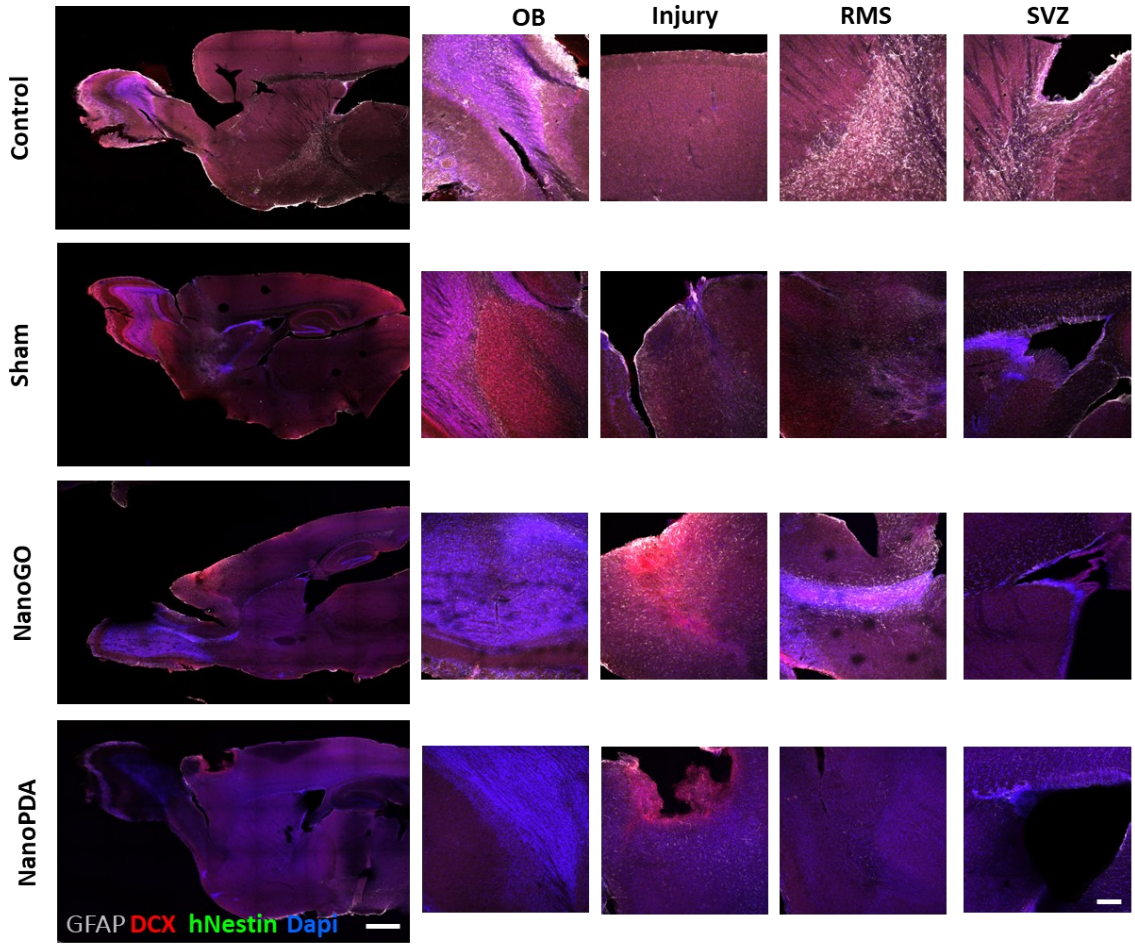

Figure 4.11.: Immunofluorescence of the mouse brain with the RMS interrupted after 7 days post-surgery.

Triple immunofluorescence for the neuronal (DCX), astroglial (GFAP) lineages and human stem cells (hNestin) at the murine sagittal left hemisphere brain slices showing in detail the olfactory bulb (OB), injured site (injury), the restoration of the rostral migratory stream (RMS) and the dorsal RMS and subventricular zone (SVZ) after 7 days of the Sham (injured on both hemispheres), control (not injured) and after the introduction of the NanoPDA and NanoGO scaffolds on the left hemisphere (LH). The right hemisphere (RH) was only injured to serve as an internal control. Scale bars 2 mm and 200 µm in the detailed images.

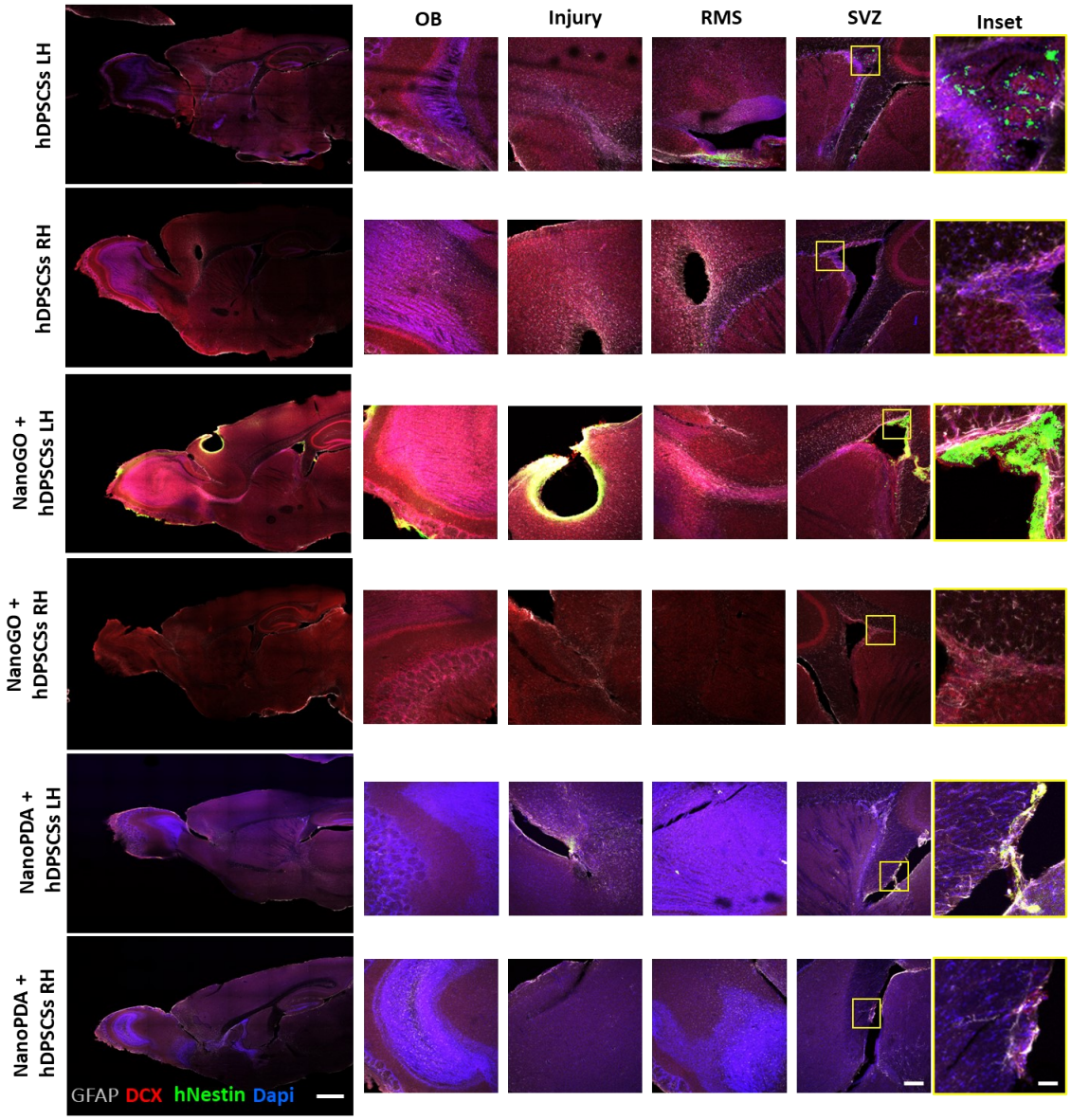

Figure 4.12.: Immunofluorescence images for grafted hDPSCs in combination with NanoGO and NanoPDA scaffolds or not in mouse brains after 14 days post-surgery.

Triple immunofluorescence for the neuronal (DCX), astroglial (GFAP) and human stem (hNestin) lineages of murine sagittal brain slices showing in detail the olfactory bulb (OB), injured site (injury), the restoration of the rostral migratory stream (RMS) and the the dorsal RMS and subventricular zone (SVZ) after 14 days of the hDPSCs grafted alone or in combination with the NanoGO and NanoPDA scaffolds. The graft was placed only in the left hemisphere (LH) and the right hemisphere (RH) was only injured to serve as an internal control. Scale bars 2 mm, 200 µm in the detailed images and 40 µm in the insets.

Experiments at longer periods of time demonstrated that, remarkably, after 3 months, there was an astroglial reaction around the injured grafted site, but no hDPSCs were found on the LH, where they were grafted, when hDPSCSs were grafted alone. In contrast, hDPSCs had migrated to the RH and were able to integrate in the SVZ and the injured site, the natural niches of stem cells [95]. In contrast, in NanoPDA+hDPSCs samples, RMS was restored in both LH and RH and hDPSCs were detected on both SVZs, suggesting a better survival and integration of the cells on both hemispheres for longer periods of time together with a better restoration of the tissue. These findings also suggested a possible migration of the hDPSCs through the blood vessels of the RMS and the cerebral cortex. Indeed, the integration of the hDPSCs into the blood vessels and their differentiation towards endothelial cells when grafted into murine brain has been previously reported [19]. Therefore, the fact that hDPSCs appeared in both SVZ in NanoPDA+hDPSCs might suggest a long-term survival and possible integration of the hDPSCs on the actual stem niches. Overall, our results demonstrated a beneficial effect of the NanoPDA scaffold on the integration and survival of the hDPSCs and a more rapid restoration of the damaged tissue in both hemispheres, compared with the cells grafted alone. Although more studies should be done to assess the restoration capacity of the NanoGO and NanoPDA scaffolds alone or grafted with hDPSCs, our preliminary data clearly encourage the combination of polymeric nanostructured scaffolds with human stem cells for the restoration of damaged CNS.

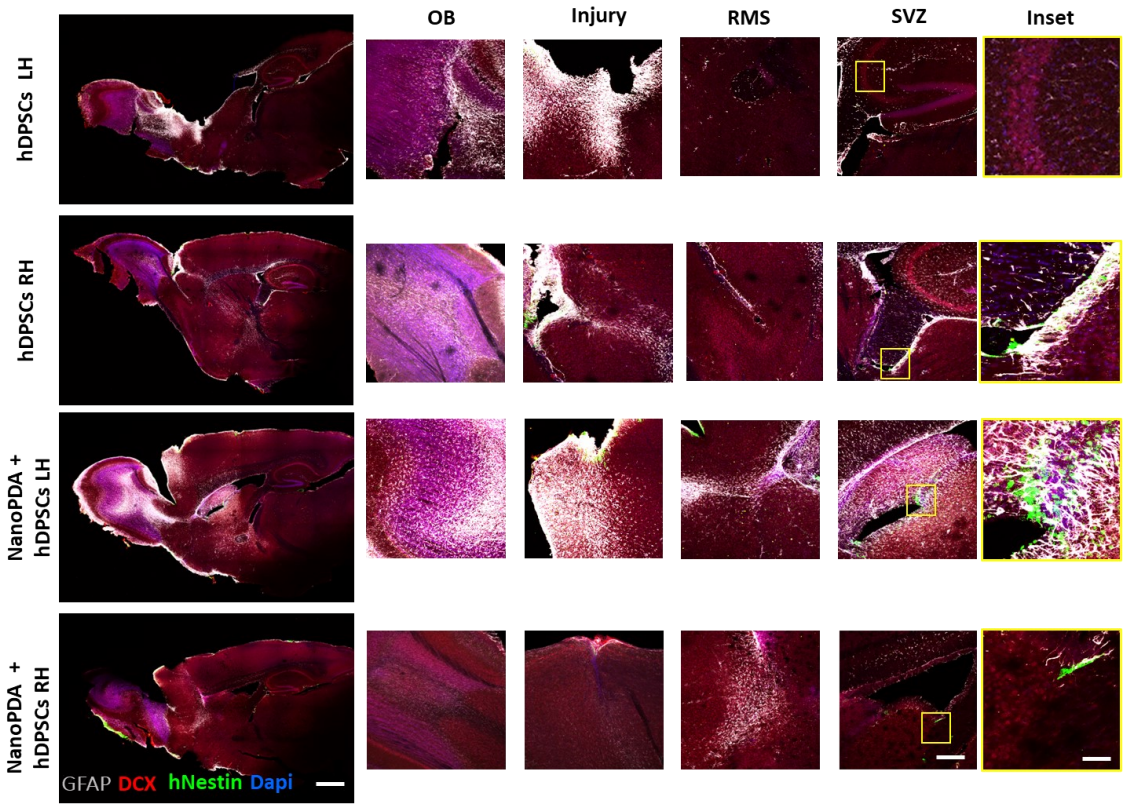

Figure 4.13.: Immunofluorescence of hDPSCs when grafted together or not with the NanoPDA scaffold after 91 days (3 months) post-surgery.

Triple immunofluorescence for the neuronal (DCX), astroglial (GFAP) and human stem (hNestin) lineages of murine sagittal brain slices showing in detail the olfactory bulb (OB), injured site (injury), the restoration of the rostral migratory stream (RMS) and the the dorsal RMS and subventricular zone (SVZ) after 3 months of the hDPSCs grafted alone or in combination with NanoPDA scaffold. The graft was placed only in the left hemisphere (LH) and the right hemisphere (RH) was only injured to serve as an internal control. Scale bars 2 mm and 200 µm in the detailed images and 40 µm in the insets.

4.4. Conclusions

In this chapter, a totally amorphous PLCL was synthetized and subsequently nanostructured to create cell anchoring scaffolds. Afterwards, the surface was further coated with PDA (NanoPDA) and functionalized with GO (NanoGO) to test separately the effect of the nanostructure and the GO on the attachment and integration of hDPSCs into the injured neural tissue. NanoGO and NanoPDA scaffolds were able to promote the neurodifferentiation of hDPSCs *in vitro* towards glial and neuronal-like cells, including myelinating-precursor cells, while retaining some stem phenotype, necessary for a correct integration of the cells on the grafted area. Although, more research is needed, *in vivo* preliminary data showed a better integration of hDPSCs together with our NanoGO and NanoPDA scaffolds, compared to the cells grafted alone at longer periods. Regarding the restoration of the rostral migratory stream (RMS), hDPSCs grafted together with NanoPDA scaffolds promoted a better integration into the neural tissue and restoration of the RMS after 3 months compared with hDPSCs grafted alone.

References

[1] C.S. Ahuja, S. Nori, L. Tetreault, J. Wilson, B. Kwon, J. Harrop, D. Choi, M.G. Fehlings, Traumatic Spinal Cord Injury-Repair and Regeneration, Neurosurgery. 80 (2017) S9–S22. https://doi.org/10.1093/neuros/nyw080.

[2] L. Gong, L. Cao, Z. Shen, L. Shao, S. Gao, C. Zhang, J. Lu, W. Li, Materials for Neural Differentiation, Trans-Differentiation, and Modeling of Neurological Disease, Adv. Mater. Deerfield Beach Fla. 30 (2018) e1705684. https://doi.org/10.1002/adma.201705684.

[3] S. Pisani, I. Genta, R. Dorati, P. Kavatzikidou, D. Angelaki, A. Manousaki, K. Karali, A. Ranella, E. Stratakis, B. Conti, Biocompatible polymeric electrospun matrices: Micro–nanotopography effect on cell behavior, J. Appl. Polym. Sci. 137 (2020) 49223. https://doi.org/10.1002/app.49223.

[4] P. Wieringa, I. Tonazzini, S. Micera, M. Cecchini, Nanotopography induced contact guidance of the F11 cell line during neuronal differentiation: a neuronal model cell line for tissue scaffold development, Nanotechnology. 23 (2012) 275102. https://doi.org/10.1088/0957-4484/23/27/275102.

[5] B. Zhu, Q. Zhang, Q. Lu, Y. Xu, J. Yin, J. Hu, Z. Wang, Nanotopographical guidance of C6 glioma cell alignment and oriented growth, Biomaterials. 25 (2004) 4215–4223. https://doi.org/10.1016/j.biomaterials.2003.11.020.

[6] D.Y. Wong, S.J. Hollister, P.H. Krebsbach, C. Nosrat, Poly(epsilon-caprolactone) and poly (L-lactic-co-glycolic acid) degradable polymer sponges attenuate astrocyte response and lesion growth in acute traumatic brain injury, Tissue Eng. 13 (2007) 2515–2523. https://doi.org/10.1089/ten.2006.0440.

[7] G.T. Christopherson, H. Song, H.-Q. Mao, The influence of fiber diameter of electrospun substrates on neural stem cell differentiation and proliferation, Biomaterials. 30 (2009) 556–564. https://doi.org/10.1016/j.biomaterials.2008.10.004.

[8] S.Y. Chew, W.C. Low, Scaffold-based approach to direct stem cell neural and cardiovascular differentiation: An analysis of physical and biochemical effects, J. Biomed. Mater. Res. A. 97A (2011) 355–374. https://doi.org/10.1002/jbm.a.33064.

[9] J. Xie, S.M. Willerth, X. Li, M.R. Macewan, A. Rader, S.E. Sakiyama-Elbert, Y. Xia, The differentiation of embryonic stem cells seeded on electrospun nanofibers into neural lineages, Biomaterials. 30 (2009) 354–362. https://doi.org/10.1016/j.biomaterials.2008.09.046.

[10] P. Bellet, M. Gasparotto, S. Pressi, A. Fortunato, G. Scapin, M. Mba, E. Menna, F. Filippini, Graphene-Based Scaffolds for Regenerative Medicine, Nanomater. Basel Switz. 11 (2021). https://doi.org/10.3390/nano11020404.

[11] M. Bramini, G. Alberini, E. Colombo, M. Chiacchiaretta, M.L. DiFrancesco, J.F. Maya-Vetencourt, L. Maragliano, F. Benfenati, F. Cesca, Interfacing Graphene-Based Materials With Neural Cells, Front. Syst. Neurosci. 12 (2018) 12. https://doi.org/10.3389/fnsys.2018.00012.

[12] W. Guo, J. Qiu, J. Liu, H. Liu, Graphene microfiber as a scaffold for regulation of neural stem cells differentiation, Sci. Rep. 7 (2017) 5678. https://doi.org/10.1038/s41598-017-06051-z.

[13] InVivo Therapeutics, The INSPIRE Study: InVivo Study of Probable Benefit of the Neuro-Spinal Scaffold(TM) for Safety and Neurologic Recovery in Subjects With Complete Thoracic AIS A Spinal Cord Injury, clinicaltrials.gov, 2021. https://clinicaltrials.gov/ct2/show/NCT02138110 (accessed August 25, 2022).

[14] T. Führmann, R.Y. Tam, B. Ballarin, B. Coles, I. Elliott Donaghue, D. van der Kooy, A. Nagy, C.H. Tator, C.M. Morshead, M.S. Shoichet, Injectable hydrogel promotes early survival of induced pluripotent stem cell-derived oligodendrocytes and attenuates longterm teratoma formation in a spinal cord injury model, Biomaterials. 83 (2016) 23–36. https://doi.org/10.1016/j.biomaterials.2015.12.032.

[15] X. Lu, T. Perera, A. Aria, L. Smith Callahan, Polyethylene glycol in spinal cord injury repair: A critical review, J. Exp. Pharmacol. Volume 10 (2018) 37–49. https://doi.org/10.2147/JEP.S148944.

[16] N. Amariglio, A. Hirshberg, B.W. Scheithauer, Y. Cohen, R. Loewenthal, L. Trakhtenbrot, N. Paz, M. Koren-Michowitz, D. Waldman, L. Leider-Trejo, A. Toren, S. Constantini, G. Rechavi, Donor-Derived Brain Tumor Following Neural Stem Cell Transplantation in an Ataxia Telangiectasia Patient, PLOS Med. 6 (2009) e1000029. https://doi.org/10.1371/journal.pmed.1000029.

[17] R. Khanna-Jain, B. Mannerström, A. Vuorinen, G.K. Sándor, R. Suuronen, S. Miettinen, Osteogenic differentiation of human dental pulp stem cells on β-tricalcium phosphate/poly (l-lactic acid/caprolactone) three-dimensional scaffolds, J. Tissue Eng. 3 (2012) 2041731412467998. https://doi.org/10.1177/2041731412467998.

[18] G. Ibarretxe, O. Crende, M. Aurrekoetxea, V. García-Murga, J. Etxaniz, F. Unda, Neural Crest Stem Cells from Dental Tissues: A New Hope for Dental and Neural Regeneration, Stem Cells Int. 2012 (2012) 103503. https://doi.org/10.1155/2012/103503.

[19] J. Luzuriaga, O. Pastor-Alonso, J.M. Encinas, F. Unda, G. Ibarretxe, J.R. Pineda, Human Dental Pulp Stem Cells Grown in Neurogenic Media Differentiate Into Endothelial Cells and Promote Neovasculogenesis in the Mouse Brain, Front. Physiol. 10 (2019) 347. https://doi.org/10.3389/fphys.2019.00347.

[20] L.H. Forbes, M.R. Andrews, Advances in human stem cell therapies: pre-clinical studies and the outlook for central nervous system regeneration, Neural Regen. Res. 16 (2020) 614–617. https://doi.org/10.4103/1673-5374.295287.

[21] Glial Neurobiology: A Textbook | Wiley, Wiley.Com. (n.d.). https://www.wiley.com/en-us/Glial+Neurobiology%3A+A+Textbook-p-9780470015643 (accessed August 14, 2022).

[22] M.A. Curtis, R.L.M. Faull, P.S. Eriksson, The effect of neurodegenerative diseases on the subventricular zone, Nat. Rev. Neurosci. 8 (2007) 712–723. https://doi.org/10.1038/nrn2216.

[23] M. Biebl, C.M. Cooper, J. Winkler, H.G. Kuhn, Analysis of neurogenesis and programmed cell death reveals a self-renewing capacity in the adult rat brain, Neurosci. Lett. 291 (2000) 17–20. https://doi.org/10.1016/s0304-3940(00)01368-9.

[24] F.P. Cordelières, V. Petit, M. Kumasaka, O. Debeir, V. Letort, S.J. Gallagher, L. Larue, Automated Cell Tracking and Analysis in Phase-Contrast Videos (iTrack4U): Development of Java Software Based on Combined Mean-Shift Processes, PLoS ONE. 8 (2013). https://doi.org/10.1371/journal.pone.0081266.

[25] A preclinical mouse model of glioma with an alternative mechanism of telomere maintenance (ALT) - Jeitany - 2015 - International Journal of Cancer - Wiley Online Library, (n.d.). https://onlinelibrary.wiley.com/doi/full/10.1002/ijc.29171 (accessed August 13, 2022).

[26] D. Marín-Pardo, L. Giménez-Llort, Olfactory Signatures in the Food Finding Test in Mice With Normal and Alzheimer's Disease-Pathological Aging With Special Concerns on the Effects of Social Isolation, Front. Neurosci. 0 (2021). https://doi.org/10.3389/fnins.2021.733984.

[27] V. Breton-Provencher, M. Lemasson, M.R. Peralta, A. Saghatelyan, Interneurons produced in adulthood are required for the normal functioning of the olfactory bulb network and for the execution of selected olfactory behaviors, J. Neurosci. Off. J. Soc. Neurosci. 29 (2009) 15245–15257. https://doi.org/10.1523/JNEUROSCI.3606-09.2009.

[28] S. Bragado Alonso, J.K. Reinert, N. Marichal, S. Massalini, B. Berninger, T. Kuner, F. Calegari, An increase in neural stem cells and olfactory bulb adult neurogenesis improves discrimination of highly similar odorants, EMBO J. 38 (2019) e98791. https://doi.org/10.15252/embj.201798791.

[29] B. Tepper, P. Koguc-Sobolewska, K. Jaslan, K. Turlejski, K. Bartkowska, R. Djavadian, Impaired olfactory neurogenesis affects the performance of olfactory-guided behavior in aged female opossums, Sci. Rep. 11 (2021) 4418. https://doi.org/10.1038/s41598-021-83834-5.

[30] C.F. Machado, T.M. Reis-Silva, C.S. Lyra, L.F. Felicio, B. Malnic, Buried Food-seeking Test for the Assessment of Olfactory Detection in Mice, Bio-Protoc. 8 (2018) e2897. https://doi.org/10.21769/BioProtoc.2897.

[31] P. Jr, J. M, A. A, J. Mp, C. H, F.D. Boussin, Intranasal Administration of Temozolomide Delayed the Development of Brain Tumors Initiated by Human Glioma Stem-Like Cell in Nude Mice, J. Cancer Sci. Ther. 09 (2017). https://doi.org/10.4172/1948-5956.1000445.

[32] C.A. Duncan-Lewis, R.L. Lukman, R.K. Banks, Effects of zinc gluconate and 2 other divalent cationic compounds on olfactory function in mice, Comp. Med. 61 (2011) 361–365.

[33] J.R. Sarasua, N. López-Rodríguez, E. Zuza, S. Petisco, B. Castro, M. del Olmo, T. Palomares, A. Alonso-Varona, Crystallinity assessment and in vitro cytotoxicity of polylactide scaffolds for biomedical applications, J. Mater. Sci. Mater. Med. 22 (2011) 2513–2523. https://doi.org/10.1007/s10856-011-4425-1.

[34] J. Fernández, A. Etxeberria, J.M. Ugartemendia, S. Petisco, J.-R. Sarasua, Effects of chain microstructures on mechanical behavior and aging of a poly(L-lactide-co-ε-caprolactone) biomedical thermoplastic-elastomer, J. Mech. Behav. Biomed. Mater. 12 (2012) 29–38. https://doi.org/10.1016/j.jmbbm.2012.03.008.

[35] S. Wang, J. Zhu, Y. Rao, B. Li, S. Zhao, H. Bai, J. Cui, Polydopamine Modified Graphene Oxide-TiO2 Nanofiller for Reinforcing Physical Properties and Anticorrosion Performance of Waterborne Epoxy Coatings, Appl. Sci. 9 (637035840000000000). https://doi.org/10.3390/app9183760.

[36] F.K. Ma, J. Li, M. Kong, Y. Liu, Y. An, X.G. Chen, Preparation and hydrolytic erosion of differently structured PLGA nanoparticles with chitosan modification, Int. J. Biol. Macromol. 54 (2013) 174–179. https://doi.org/10.1016/j.ijbiomac.2012.12.019.

[37] G. Sabbatier, A. Larrañaga, A.-A. Guay-Bégin, J. Fernandez, F. Diéval, B. Durand, J.-R. Sarasua, G. Laroche, Design, Degradation Mechanism and Long-Term Cytotoxicity of Poly(l-lactide) and Poly(Lactide-co-ϵ-Caprolactone) Terpolymer Film and Air-Spun Nanofiber Scaffold, Macromol. Biosci. 15 (2015) 1392–1410. https://doi.org/10.1002/mabi.201500130.

[38] J. Fernández, A. Etxeberria, J.-R. Sarasua, Synthesis, structure and properties of poly(L-lactide-co-ε-caprolactone) statistical copolymers, J. Mech. Behav. Biomed. Mater. 9 (2012) 100–112. https://doi.org/10.1016/j.jmbbm.2012.01.003.

[39] J. Fernández, A. Larrañaga, A. Etxeberria, W. Wang, J.R. Sarasua, A new generation of poly(lactide/ε-caprolactone) polymeric biomaterials for application in the medical field, J. Biomed. Mater. Res. A. 102 (2014) 3573–3584. https://doi.org/10.1002/jbm.a.35036.

[40] J. Fernández, A. Etxeberria, J.-R. Sarasua, In vitro degradation studies and mechanical behavior of poly(ε-caprolactone-co-δ-valerolactone) and poly(ε-caprolactone-co-L-lactide) with random and semi-alternating chain microstructures, Eur. Polym. J. 71 (2015) 585–595. https://doi.org/10.1016/j.eurpolymj.2015.09.001.

[41] E. Díaz, I. Puerto, In Vitro Degradation of PLCL/nHA Biodegradable Scaffolds, Polym.-Plast. Technol. Eng. 54 (2015) 556–564. https://doi.org/10.1080/03602559.2014.961087.

[42] J.M. Barnes, L. Przybyla, V.M. Weaver, Tissue mechanics regulate brain development, homeostasis and disease, J. Cell Sci. 130 (2017) 71–82. https://doi.org/10.1242/jcs.191742.

[43] K. Riek, J.M. Millward, I. Hamann, S. Mueller, C.F. Pfueller, F. Paul, J. Braun, C. Infante-Duarte, I. Sack, Magnetic resonance elastography reveals altered brain viscoelasticity in experimental autoimmune encephalomyelitis, NeuroImage Clin. 1 (2012) 81–90. https://doi.org/10.1016/j.nicl.2012.09.003.

[44] E. Moeendarbary, I.P. Weber, G.K. Sheridan, D.E. Koser, S. Soleman, B. Haenzi, E.J. Bradbury, J. Fawcett, K. Franze, The soft mechanical signature of glial scars in the central nervous system, Nat. Commun. 8 (2017) 14787. https://doi.org/10.1038/ncomms14787.

[45] A. Larrañaga, A.-A. Guay-Bégin, P. Chevallier, G. Sabbatier, J. Fernández, G. Laroche, J.-R. Sarasua, Grafting of a model protein on lactide and caprolactone based biodegradable films for biomedical applications, Biomatter. 4 (2014) e27979. https://doi.org/10.4161/biom.27979.

[46] H. Levine, L. Slade, Water as a plasticizer: physico-chemical aspects of low-moisture polymeric systems, in: F. Franks (Ed.), Water Sci. Rev. 3 Water Dyn., Cambridge University Press, Cambridge, 1988: pp. 79–185. https://doi.org/10.1017/CBO9780511552083.002.
[47] N. Antonovaite, L.A. Hulshof, E.M. Hol, W.J. Wadman, D. Iannuzzi, Viscoelastic mapping of mouse brain tissue: Relation to structure and age, J. Mech. Behav. Biomed. Mater. 113 (2021) 104159. https://doi.org/10.1016/j.jmbbm.2020.104159.
[48] A. Weltman, J. Yoo, E. Meng, Flexible, Penetrating Brain Probes Enabled by Advances in Polymer Microfabrication, Micromachines. 7 (2016) 180. https://doi.org/10.3390/mi7100180.
[49] N. Antonovaite, S.V. Beekmans, E.M. Hol, W.J. Wadman, D. Iannuzzi, Regional variations in stiffness in live mouse brain tissue determined by depth-controlled indentation mapping, Sci. Rep. 8 (2018) 12517. https://doi.org/10.1038/s41598-018-31035-y.
[50] S. Ali, I.B. Wall, C. Mason, A.E. Pelling, F.S. Veraitch, The effect of Young's modulus on the neuronal differentiation of mouse embryonic stem cells, Acta Biomater. 25 (2015) 253–267. https://doi.org/10.1016/j.actbio.2015.07.008.
[51] P.D. Dalton, L. Flynn, M.S. Shoichet, Manufacture of poly(2-hydroxyethyl methacrylate-co-methyl methacrylate) hydrogel tubes for use as nerve guidance channels, Biomaterials. 23 (2002) 3843–3851. https://doi.org/10.1016/s0142-9612(02)00120-5.
[52] Z. Álvarez, O. Castaño, A.A. Castells, M.A. Mateos-Timoneda, J.A. Planell, E. Engel, S. Alcántara, Neurogenesis and vascularization of the damaged brain using a lactate-releasing biomimetic scaffold, Biomaterials. 35 (2014) 4769–4781. https://doi.org/10.1016/j.biomaterials.2014.02.051.
[53] R.W. Griffith, D.R. Humphrey, Long-term gliosis around chronically implanted platinum electrodes in the Rhesus macaque motor cortex, Neurosci. Lett. 406 (2006) 81–86. https://doi.org/10.1016/j.neulet.2006.07.018.
[54] T. Yasuhara, S. Kawauchi, K. Kin, J. Morimoto, M. Kameda, T. Sasaki, B. Bonsack, C. Kingsbury, N. Tajiri, C.V. Borlongan, I. Date, Cell therapy for central nervous system disorders: Current obstacles to progress, CNS Neurosci. Ther. 26 (2020) 595–602. https://doi.org/10.1111/cns.13247.
[55] J. Luzuriaga, Y. Polo, O. Pastor-Alonso, B. Pardo-Rodríguez, A. Larrañaga, F. Unda, J.-R. Sarasua, J.R. Pineda, G. Ibarretxe, Advances and Perspectives in Dental Pulp Stem Cell Based Neuroregeneration Therapies, Int. J. Mol. Sci. 22 (2021) 3546. https://doi.org/10.3390/ijms22073546.
[56] J.D. Lathia, M. Li, P.E. Hall, J. Gallagher, J.S. Hale, Q. Wu, M. Venere, E. Levy, M.R.S. Rani, P. Huang, E. Bae, J. Selfridge, L. Cheng, H. Guvenc, R.E. McLendon, I. Nakano, A.E. Sloan, H.S. Phillips, A. Lai, C.L. Gladson, M. Bredel, S. Bao, A.B. Hjelmeland, J.N. Rich, Laminin alpha 2 enables glioblastoma stem cell growth, Ann. Neurol. 72 (2012) 766–778. https://doi.org/10.1002/ana.23674.
[57] G.A. Dunn, Characterising a kinesis response: time averaged measures of cell speed and directional persistence, Agents Actions. Suppl. 12 (1983) 14–33. https://doi.org/10.1007/978-3-0348-9352-7_1.
[58] H.G. Othmer, S.R. Dunbar, W. Alt, Models of dispersal in biological systems, J. Math. Biol. 26 (1988) 263–298. https://doi.org/10.1007/bf00277392.
[59] M.H. Gail, C.W. Boone, The locomotion of mouse fibroblasts in tissue culture, Biophys. J. 10 (1970) 980–993. https://doi.org/10.1016/S0006-3495(70)86347-0.
[60] D. Henriques, R. Moreira, J. Schwamborn, L. Pereira de Almeida, L.S. Mendonça, Successes and Hurdles in Stem Cells Application and Production for Brain Transplantation, Front. Neurosci. 13 (2019). https://www.frontiersin.org/articles/10.3389/fnins.2019.01194 (accessed August 22, 2022).
[61] U. Lendahl, L.B. Zimmerman, R.D. McKay, CNS stem cells express a new class of intermediate filament protein, Cell. 60 (1990) 585–595. https://doi.org/10.1016/0092-8674(90)90662-x.

[62] S. Suzuki, J. Namiki, S. Shibata, Y. Mastuzaki, H. Okano, The neural stem/progenitor cell marker nestin is expressed in proliferative endothelial cells, but not in mature vasculature, J. Histochem. Cytochem. Off. J. Histochem. Soc. 58 (2010) 721–730. https://doi.org/10.1369/jhc.2010.955609.

[63] A. Bernal, L. Arranz, Nestin-expressing progenitor cells: function, identity and therapeutic implications, Cell. Mol. Life Sci. 75 (2018) 2177–2195. https://doi.org/10.1007/s00018-018-2794-z.

[64] J. Dahlstrand, M. Lardelli, U. Lendahl, Nestin mRNA expression correlates with the central nervous system progenitor cell state in many, but not all, regions of developing central nervous system, Brain Res. Dev. Brain Res. 84 (1995) 109–129. https://doi.org/10.1016/0165-3806(94)00162-s.

[65] F. Doetsch, J.M. García-Verdugo, A. Alvarez-Buylla, Cellular composition and three-dimensional organization of the subventricular germinal zone in the adult mammalian brain, J. Neurosci. Off. J. Soc. Neurosci. 17 (1997) 5046–5061.

[66] E. Raponi, F. Agenes, C. Delphin, N. Assard, J. Baudier, C. Legraverend, J.-C. Deloulme, S100B expression defines a state in which GFAP-expressing cells lose their neural stem cell potential and acquire a more mature developmental stage, Glia. 55 (2007) 165–177. https://doi.org/10.1002/glia.20445.

[67] J.R. Pineda, M. Daynac, A. Chicheportiche, A. Cebrian-Silla, K. Sii Felice, J.M. Garcia-Verdugo, F.D. Boussin, M.-A. Mouthon, Vascular-derived TGF-β increases in the stem cell niche and perturbs neurogenesis during aging and following irradiation in the adult mouse brain, EMBO Mol. Med. 5 (2013) 548–562. https://doi.org/10.1002/emmm.201202197.

[68] G. Santos, A. Barateiro, D. Brites, A. Fernandes, S100B Impairs Oligodendrogenesis and Myelin Repair Following Demyelination Through RAGE Engagement, Front. Cell. Neurosci. 14 (2020) 279. https://doi.org/10.3389/fncel.2020.00279.

[69] M. Mata, D. Alessi, D.J. Fink, S100 is preferentially distributed in myelin-forming Schwann cells, J. Neurocytol. 19 (1990) 432–442. https://doi.org/10.1007/BF01188409.

[70] Z. Liu, Y.-Q. Jin, L. Chen, Y. Wang, X. Yang, J. Cheng, W. Wu, Z. Qi, Z. Shen, Specific marker expression and cell state of Schwann cells during culture in vitro, PloS One. 10 (2015) e0123278. https://doi.org/10.1371/journal.pone.0123278.

[71] K. Tomita, T. Kubo, K. Matsuda, T. Fujiwara, K. Yano, J.M. Winograd, M. Tohyama, K. Hosokawa, The neurotrophin receptor p75NTR in Schwann cells is implicated in remyelination and motor recovery after peripheral nerve injury, Glia. 55 (2007) 1199–1208. https://doi.org/10.1002/glia.20533.

[72] G.K.T. Chu, W. Yu, M.G. Fehlings, The p75 neurotrophin receptor is essential for neuronal cell survival and improvement of functional recovery after spinal cord injury, Neuroscience. 148 (2007) 668–682. https://doi.org/10.1016/j.neuroscience.2007.05.028.

[73] M. Dezawa, Central and peripheral nerve regeneration by transplantation of Schwann cells and transdifferentiated bone marrow stromal cells, Anat. Sci. Int. 77 (2002) 12–25. https://doi.org/10.1046/j.0022-7722.2002.00012.x.

[74] C.Z. Chen, B. Neumann, S. Förster, R.J.M. Franklin, Schwann cell remyelination of the central nervous system: why does it happen and what are the benefits?, Open Biol. 11 (n.d.) 200352. https://doi.org/10.1098/rsob.200352.

[75] A. Llobet Rosell, L.J. Neukomm, Axon death signalling in Wallerian degeneration among species and in disease, Open Biol. 9 (2019) 190118. https://doi.org/10.1098/rsob.190118.

[76] K.R. Jessen, R. Mirsky, The repair Schwann cell and its function in regenerating nerves, J. Physiol. 594 (2016) 3521–3531. https://doi.org/10.1113/JP270874.

[77] T.L. Walker, T. Yasuda, D.J. Adams, P.F. Bartlett, The Doublecortin-Expressing Population in the Developing and Adult Brain Contains Multipotential Precursors in Addition to Neuronal-Lineage Cells, J. Neurosci. 27 (2007) 3734–3742. https://doi.org/10.1523/JNEUROSCI.5060-06.2007.

[78] T. Kremer, R. Jagasia, A. Herrmann, H. Matile, E. Borroni, F. Francis, H.G. Kuhn, C. Czech, Analysis of adult neurogenesis: evidence for a prominent “non-neurogenic” DCX-protein pool in rodent brain, PloS One. 8 (2013) e59269. https://doi.org/10.1371/journal.pone.0059269.

[79] Y. Aoyagi, T. Hibi, Y. Kimori, M. Sawada, R. Kawakami, K. Sawamoto, T. Nemoto, Heterogeneous distribution of doublecortin-expressing cells surrounding the rostral migratory stream in the juvenile mouse, J. Comp. Neurol. 526 (2018) 2631–2646. https://doi.org/10.1002/cne.24521.

[80] J. Song, H. Gao, G. Zhu, X. Cao, X. Shi, Y. Wang, The preparation and characterization of polycaprolactone/graphene oxide biocomposite nanofiber scaffolds and their application for directing cell behaviors, Carbon. 95 (2015) 1039–1050. https://doi.org/10.1016/j.carbon.2015.09.011.

[81] W. Sun, H. Kim, Y. Moon, Control of neuronal migration through rostral migratory stream in mice, Anat. Cell Biol. 43 (2010) 269–279. https://doi.org/10.5115/acb.2010.43.4.269.

[82] J. Silver, M.E. Schwab, P.G. Popovich, Central Nervous System Regenerative Failure: Role of Oligodendrocytes, Astrocytes, and Microglia, Cold Spring Harb. Perspect. Biol. 7 (2015) a020602. https://doi.org/10.1101/cshperspect.a020602.

[83] 14:00-17:00, ISO 10993-11:2017, ISO. (n.d.). https://www.iso.org/cms/render/live/en/sites/isoorg/contents/data/standard/06/84/68426.html (accessed August 22, 2022).

[84] M.A. Curtis, H.J. Monzo, R.L.M. Faull, The rostral migratory stream and olfactory system: smell, disease and slippery cells, Prog. Brain Res. 175 (2009) 33–42. https://doi.org/10.1016/S0079-6123(09)17503-9.

[85] D.R. Kornack, P. Rakic, The generation, migration, and differentiation of olfactory neurons in the adult primate brain, Proc. Natl. Acad. Sci. U. S. A. 98 (2001) 4752–4757. https://doi.org/10.1073/pnas.081074998.

[86] J.A. Chowen, L.M. Garcia-Segura, Role of glial cells in the generation of sex differences in neurodegenerative diseases and brain aging, Mech. Ageing Dev. 196 (2021) 111473. https://doi.org/10.1016/j.mad.2021.111473.

[87] M.L. Sipski, A.B. Jackson, O. Gómez-Marín, I. Estores, A. Stein, Effects of gender on neurologic and functional recovery after spinal cord injury, Arch. Phys. Med. Rehabil. 85 (2004) 1826–1836. https://doi.org/10.1016/j.apmr.2004.04.031.

[88] G.J. Farkas, A.S. Gorgey, D.R. Dolbow, A.S. Berg, D.R. Gater, Sex dimorphism in the distribution of adipose tissue and its influence on proinflammatory adipokines and cardiometabolic profiles in motor complete spinal cord injury, J. Spinal Cord Med. 42 (2019) 430–436. https://doi.org/10.1080/10790268.2018.1436125.

[89] A.B. Ghnenis, D.T. Burns, W. Osimanjiang, G. He, J.S. Bushman, A Long-Term Pilot Study on Sex and Spinal Cord Injury Shows Sexual Dimorphism in Functional Recovery and Cardio-Metabolic Responses, Sci. Rep. 10 (2020) 2762. https://doi.org/10.1038/s41598-020-59628-6.

[90] Y. Pan, M. Xiong, R. Chen, Y. Ma, C. Corman, M. Maricos, U. Kindler, M. Semtner, Y.-H. Chen, S. Dahiya, D.H. Gutmann, Athymic mice reveal a requirement for T-cell–microglia interactions in establishing a microenvironment supportive of Nf1 low-grade glioma growth, Genes Dev. 32 (2018) 491–496. https://doi.org/10.1101/gad.310797.117.

[91] Z. Kokaia, G. Martino, M. Schwartz, O. Lindvall, Cross-talk between neural stem cells and immune cells: the key to better brain repair?, Nat. Neurosci. 15 (2012) 1078–1087. https://doi.org/10.1038/nn.3163.

[92] A. Morizane, D. Doi, T. Kikuchi, K. Okita, A. Hotta, T. Kawasaki, T. Hayashi, H. Onoe, T. Shiina, S. Yamanaka, J. Takahashi, Direct Comparison of Autologous and Allogeneic Transplantation of iPSC-Derived Neural Cells in the Brain of a Nonhuman Primate, Stem Cell Rep. 1 (2013) 283–292. https://doi.org/10.1016/j.stemcr.2013.08.007.

[93] M.C. Whitman, W. Fan, L. Rela, D.J. Rodriguez-Gil, C.A. Greer, Blood Vessels Form a Migratory Scaffold in the Rostral Migratory Stream, J. Comp. Neurol. 516 (2009) 94–104. https://doi.org/10.1002/cne.22093.

[94] C. Portioli, C. Bussy, M. Mazza, N. Lozano, D.A. Jasim, M. Prato, A. Bianco, M. Bentivoglio, K. Kostarelos, Intracerebral Injection of Graphene Oxide Nanosheets Mitigates Microglial Activation Without Inducing Acute Neurotoxicity: A Pilot Comparison to Other Nanomaterials, Small Weinh. Bergstr. Ger. (2020) e2004029. https://doi.org/10.1002/smll.202004029.

[95] Q. Shen, Y. Wang, E. Kokovay, G. Lin, S.-M. Chuang, S.K. Goderie, B. Roysam, S. Temple, Adult SVZ stem cells lie in a vascular niche: A quantitative analysis of niche cell-cell interactions, Cell Stem Cell. 3 (2008) 289–300. https://doi.org/10.1016/j.stem.2008.07.026.

Chapter 5

Self-assembled three-dimensional hydrogels based on graphene derivatives and cerium oxide nanoparticles: scaffolds for co-culture of oligodendrocytes and neurons derived from neural stem cells

Self-assembled three-dimensional hydrogels based on graphene derivatives and cerium oxide nanoparticles: scaffolds for co-culture of oligodendrocytes and neurons derived from neural stem cells

Abstract

Stem cell-based therapies have shown promising results for the regeneration of the nervous system. However, the survival and integration of the stem cells in the neural circuitry is suboptimal and might compromise the therapeutic outcomes of this approach. The development of functional scaffolds capable of actively interacting with stem cells may overcome the current limitations of stem cell-based therapies. In this last experimental chapter, three-dimensional hydrogels based on graphene derivatives and cerium oxide (CeO_2) nanoparticles are presented as prospective supports allowing neural stem cell adhesion, migration and differentiation. The morphological, mechanical and electrical properties of the resulting hydrogels can be finely tuned by controlling several parameters of the self-assembly of graphene oxide sheets, namely the amount of incorporated reducing agent (ascorbic acid) and CeO_2 nanoparticles. The intrinsic properties of the hydrogels, as well as the presence of CeO_2 nanoparticles, clearly influence the cell fate. Thus, stiffer adhesion substrates promote differentiation to glial cell lineages, while softer substrates enhance mature neuronal differentiation. Remarkably, CeO_2 nanoparticle-containing hydrogels support the differentiation of neural stem cells to neuronal, astroglial and oligodendroglial lineage cells, promoting the *in vitro* generation of nerve tissue grafts that might be employed in neuroregenerative cell therapies.

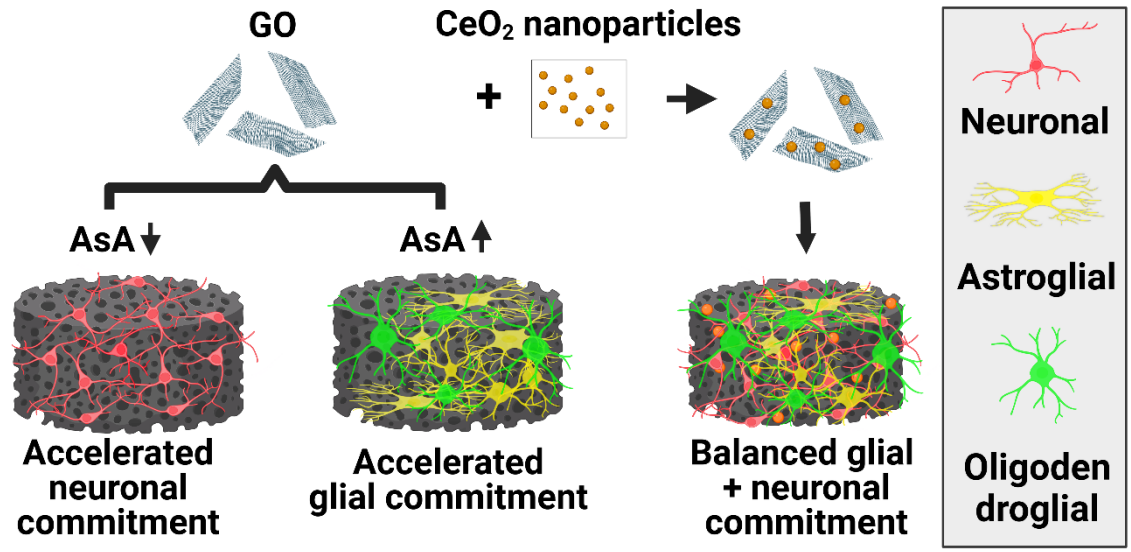

5.1. Introduction

Neurological disorders cause death or disability to more than 94 million people worldwide every year and this number is expected to rise to 103 million by 2030 [1,2]. Among them, stroke is the main cause of chronic impairment and the third leading cause of mortality worldwide [3]. Stroke, like traumatic injuries, causes the death of the neural tissue in the affected area, but also provokes a dysfunction of the surrounding cells, inhibiting an efficient restoration or functional recovery of the damaged tissue [3,4]. Despite their huge socioeconomic impact, there is no available treatment for these conditions nowadays [5]. Therefore, there is a need to explore new therapies that replace the injured neural network and promote the integration of new neurons and glial cells into the central nervous system (CNS).

Among the different approaches to regenerate the CNS, cell-based therapies, particularly those based on neural stem cells (NSCs), offer the most straightforward alternative to reestablish a functional neural network by producing therapeutic factors, promoting the self-restoration of the damaged tissue and ultimately replacing the lost neural cells [4,6]. However, the integration of the cells into the host CNS remains challenging [7]. In this regard, tissue engineering offers the possibility to combine NSCs with scaffolds to enhance cell integration on the damaged area [6]. Within the recently coined field of materiobiology, scaffolds are considered multifunctional devices with the capability to finely tune biological functions [8]. In the particular case of nervous system regeneration, materials based on graphene derivatives have attracted considerable attention [9,10] thanks to the possibility to create moldable platforms (e.g., with tailored chemical, mechanical and electrical features) to promote the adhesion and differentiation of NSCs towards functional glial and neuronal lineages [11]. Graphene consists of a single layer of carbon atoms organized in a honeycomb lattice monolayer that can be arranged either in two- (2D) or three-dimensional (3D) scaffolds, thus resembling the complex architecture of the extracellular matrix [12–14]. Although most of the studies with NSCs have been performed in 2D graphene derivative-based scaffolds, recently, 3D scaffolds have been reported to better promote the proliferative ability of NSCs, while maintaining similar adhesion features [15]. Moreover, the physical properties of these 3D scaffolds including stiffness or pore geometry can modulate the adhesion, proliferation and differentiation capabilities of the NSCs [16]. Understanding how these features interact in the formation of complex neural networks that support mature neuronal and glial interplay will be vital to ensure the successful integration of the NSCs into the graphene derivative-based 3D scaffolds.

Three-dimensional composite scaffolds offer several benefits concerning single material scaffolds since they allow a simple modulation of their physicochemical, mechanical and electrical properties by simply modifying their composition while exploiting potential synergistic effects among their constituents [17,18]. Herein, the combination of 3D scaffolds made of graphene-derivatives and cerium oxide (CeO_2) nanoparticles will be

explored as a platform for the regeneration of the CNS. CeO_2 nanoparticles comprise a cubic fluorite arrangement that acts as redox reaction sites thanks to the oxygen deficiencies at the nanoscale order [19]. This oxygen deprivation endows antioxidant features to the CeO_2 nanoparticles that resemble the activity of antioxidant natural enzymes (i.e., superoxide dismutase (SOD) and catalase (CAT)), which is beneficial for the promotion of the angiogenesis and the restoration of the neural architecture [20,21]. Accordingly, CeO_2 nanoparticles have been reported to provide neuroprotective effects, as demonstrated on an adult spinal neuron model [22] and *in vivo* on a pharmacologically induced brain oxidative stress model [23].

In the present chapter, we combine the potential of graphene-based materials to promote the adhesion, proliferation and differentiation of NSCs, with the additional antioxidant and neuroprotective effects associated with CeO_2 nanoparticles as a prospective approach for the restoration of the injured CNS. To achieve this aim, we engineered and characterized 3D hydrogels based on the combination of graphene derivatives and CeO_2 nanoparticles with tunable stiffness, porous geometry and electrical conductivity. We further studied the adhesion, integration and differentiation capabilities of the NSCs towards neuronal, astroglial, and oligodendroglial lineages at different time points. This allowed us to establish heterocellular cultures for *in vitro* studies that mimicked the *in vivo* CNS tissue architecture.

5.2. Materials and methods

5.2.1. Fabrication of the hydrogels

Graphene oxide (GO) solution (4 mg/ml aqueous dispersion from Graphenea, Spain) was pre-diluted with distilled water to a concentration of 2 mg/ml and sonicated for 30 min. Cerium oxide (CeO_2) nanoparticles (246 mg/ml, Cerium (IV) oxide, 20% in water from Thermo Fisher Scientific, USA) were also sonicated for 30 min to ensure a homogeneous dispersion. For those hydrogels containing CeO_2 nanoparticles, the two dispersions were mixed in the corresponding GO:CeO_2 weight ratios (10:0.25; 10:0.5; 10:0.6; 10:0.75 or 10:1) and the mixture was then incubated under magnetic stirring for 3 h at 90 ^{o}C to facilitate the electrostatic interactions between the negatively charged GO sheets and the positively charged CeO_2 nanoparticles [24]. Samples containing only GO were also treated for 3 h at 90 ^{o}C to ensure equal thermal treatment in all the samples. Afterwards, L-ascorbic acid (AsA) (Sigma Aldrich, Spain) was added to reduce the GO sheets and enable hydrogel formation. The corresponding GO:AsA weight ratio (1:1; 1:4; 1:10) was mixed for 30 min under stirring and the self-assembly of the GO was promoted by incubating the solution at 60 ^{o}C overnight. The medium of the resulting hydrogels was replaced with distilled water every 12 h for 7 days to ensure the complete elimination of the unreacted AsA. Hydrogels were either lyophilized for characterization or sterilized with 70% ethanol every 12 h for 5 times. Sterilized hydrogels were washed with sterile phosphate buffered saline (PBS) every 12 h for 4 times and finally replaced by Neurocult basal medium (Stem Cell Technologies, Canada) one day prior to cell culture experiments.

5.2.2. Physico-chemical and functional characterization

5.2.2.1. Transmission electron microscopy (TEM)

The successful decoration of the GO sheets with CeO_2 nanoparticles was studied with TEM. Either a previously sonicated dispersion of GO (2 mg/ml) alone or together with CeO_2 nanoparticles was incubated for 3 h at 90 ^{o}C under constant magnetic stirring. Afterwards, the aqueous solution containing either GO sheets, CeO_2 nanoparticles, or GO sheets decorated with CeO_2 nanoparticles was deposited onto carbon-coated grids and imaged in a JEOL 1400 Plus transmission electron microscope (JEOL, Tokyo, Japan).

5.2.2.2. X-ray diffraction (XRD)

The X-ray powder diffraction patterns of the previously lyophilized hydrogels were collected by using a Philips X'pert PRO automatic diffractometer (Malvern Panalyticals, Malvern, UK) operating at 40 kV and 40 mA, in theta-theta configuration, secondary monochromator with Cu-Kα radiation (λ = 1.5418 Å) and a PIXcel solid state detector (active length in 2θ equal to 3.347^{o}). Data were collected at a 2θ from 5 to 60^{o}, step size equal to 0.026^{o} and time per step of 600 s at room temperature (RT) (total time: 1 h). 1^{o}

fixed soller and divergence slit giving a constant volume of sample illumination were used.

5.2.2.3. Energy-dispersive X-ray spectroscopy (EDX)

The elemental analysis (spectra and mapping) of the previously lyophilized graphene-based hydrogels containing increasing amounts of CeO_2 nanoparticles was performed using a built-in Bruker Nano XFlash 5010 detector (Bruker, Coventry, UK). Before analysis, the samples were placed on a dual-side conductive carbon tape and were coated with gold at 25 mA for 70 s.

5.2.2.4. Raman spectroscopy

Raman spectroscopy was performed on the previously lyophilized graphene-based hydrogels containing increasing amounts of CeO_2 nanoparticles using a Horiba LabRAM HR Evolution Raman microscope (Horiba, Kyoto, Japan). The laser excitation wavelength was 532 nm and the scanning range was set from 400 to 3000 1/cm. The samples were placed on top of a silicon wafer and the analysis was performed in at least three random areas of the sample to ensure its homogeneity. The mean values are represented in the graph.

5.2.2.5. Scanning electron microscopy (SEM)

Previously lyophilized hydrogels were directly observed (i.e., without gold or carbon coating) in a scanning electron microscope Hitachi S-3400 N (Hitachi, Tokio, Japan).

5.2.2.6. Rheology

The mechanical properties of the hydrogels were studied applying a torque of 5 μN·m, at room temperature and in a range of frequencies from 0.1 to 10 rad/s in the linear viscoelastic region (LVR) using a TA instruments AR G2 rheometer (TA Instruments, New Castle, USA).

5.2.2.7. Electrical conductivity

Conductivity measurements were carried out using a Novocontrol Alpha impedance analyzer (Novocontrol Technologies GmbH, Montabaur, Germany). The previously lyophilized hydrogels were pressed between gold electrodes, and an AC electric field was applied (1.5 VRMS, frequency range 1 Hz to 1 MHz). All measurements were performed at room conditions (22 ^{o}C, 50 RH%).

5.2.2.8. Antioxidant capabilities

The antioxidant capacity of the hydrogels decorated with increasing amounts of CeO_2 nanoparticles was evaluated under 50 µM hydrogen peroxide concentration. Each hydrogel was exposed to 50 µM hydrogen peroxide solution from the Fluorimetric Hydrogen Peroxide Assay Kit (Sigma Aldrich) for 30 min. Thereafter, 50 µL of the medium were placed in a 96-well plate and mixed with 50 µl of the horseradish peroxidase and red peroxidase substrate mastermix solution. After 20 min, a Biotek Synergy H1M microplate reader (Agilent, Santa Clara, CA, USA) was used to measure the fluorescence intensity (λ_{ex} = 540 nm/λ_{em} = 590 nm) and determine the remaining hydrogen peroxide concentration.

5.2.2.9. ζ-potential measurements

Fresh solutions of pure GO, CeO_2, or GO:CeO_2 10:1 were made as stated in section 5.2.1.. Prior to the addition of AsA, the ζ-potential was determined using a a Zetasizer Nano ZS analyzer (Malvern Panalytical, United Kingdom). A minimum of 3 runs were performed for each sample at 25 ºC in 5 mM NaCl aqueous solution.

5.2.3. Cell culture

5.2.3.1. Seeding and induction of cell differentiation

Mouse neural stem cells (NSCs) were collected, passaged and seeded in Neurocult proliferation medium as described in chapter 3. To compare the effect of the morphology, mechanical properties and electrical conductivity, hydrogels containing a similar proportion of GO:AsA (GO:AsA 1:1) and four times more AsA (GO:AsA 1:4) were selected for cell experiments. The effect of the incorporation of CeO_2 nanoparticles was studied with the GO:AsA 1:4 hydrogel containing a proportion of GO:CeO_2 of 10:0.25 (GO:AsA 1:4 + CeO_2 0.25).

As the hydrogels have different diameters, 60,000 cells were seeded on the GO:AsA 1:1 and 30,000 cells were seeded on the GO:AsA 1:4 and GO:AsA 1:4 + CeO_2 0.25 hydrogels to keep a similar cell density. After 24 h, medium was changed to Neurocult differentiation medium and cells were cultured as previously described in chapter 3.

5.2.3.2. Scanning electron microscopy (SEM)

To study the attachment of the cells to the hydrogels, NSCs were incubated for 24 h over GO:AsA 1:1; GO:AsA 1:4 and GO:AsA 1:4 + CeO_2 0.25 hydrogels and subsequently fixed for 1 h at room temperature using 2% glutaraldehyde (cat# 50-262-19, Fisher Scientific, Pittsburgh, USA) diluted in 0.1 M cacodylate buffer (cat# C0250, Sigma-Aldrich, Spain). Cacodylate buffer and isosmolar sucrose (cat# S7903, Sigma-Aldrich, Spain) were then used to rinse the fixative solution. The samples were post-fixed for 1 h in the dark using

1% osmium tetraoxide (OsO_4) in cacodylate (cat# O5500, Sigma-Aldrich, Spain). Then, OsO_4 was eliminated by rinsing for 10 min each hydrogel with cacodylate buffer. Hydrogels were dehydrated with increasing series of EtOH (30º, 50º, 70º, 90º, 96º, 100º, and 2x100º absolute) for 20 min each and air dried for 5 h. Afterwards, conductive cement was used to mount the hydrogels on the scanning electron microscope supports. Finally, gold particles flashed in an argon environment were used to create a metallic coating. A Hitachi S-3400 N scanning electron microscope was used to observe the samples (Hitachi, Tokio, Japan).

5.2.3.3. Immunostaining

NSCs were fixed, permeabilized and immunostained as previously documented in chapter 3. The maintenance of the stem phenotype was determined by immunopositive Nestin labeling (1:200, ab6142, Abcam, United Kingdom). Cell commitment towards neuronal lineage was determined by positive staining for DCX (1:300, sc8066, Santa Cruz, USA) and MAP2 (1:500, ab5392, Abcam, United Kingdom). On the other hand, the commitments towards astroglial and oligodendroglial cell lineages were determined using GFAP (1:500, G9269, Sigma-Aldrich, USA), S100β (1:200, Dako Cytomation, Denmark) and Olig2 (1:200, MABN50, Millipore, USA). Alexa Fluor donkey anti-mouse, anti-rabbit, anti-goat or anti-chicken secondary antibodies coupled with 488 or 594 fluorophores (1:200, Life Technologies, USA) and goat anti-chicken Texas Red (1:200, ab6875, Abcam, United Kingdom) were used as secondary antibodies. To study the migration of cells into the hydrogels, serial cuts of 250 µm thickness slices of previously immunostained and 1% agarose embedded hydrogels were made and collected using a Microm HM650 V vibratome (Microm, International GmbH, Walldorf, Germany).

5.2.3.4. Intracellular reactive oxygen species measurements

To study the possible antioxidant benefits of the CeO_2 nanoparticles, NSCs were seeded over GO:AsA 1:1; GO:AsA 1:4 and GO:AsA 1:4 + CeO_2 0.25 hydrogels. After 14 days *in vitro,* NSCs were labeled with 50 µM of the 2',7'-Dichlorodihydrofluorescein diacetate cell-permeable probe (H2DCFDA; Invitrogen, USA) for 30 min at 37 ºC and 5% CO_2 to evaluate the accumulation of reactive oxygen species (ROS) within cells. Fluorescence intensity of 3 independent samples of each condition was determined on Fluoroskan Ascent plate fluorimeter (Thermo Labsystems, Santa Rosa, California, USA) to determine the fluorescence intensity (λ_{ex} = 488 nm/λ_{em} = 520 nm) in the area.

5.2.3.5. Cell count and statistical analysis

Cell counts for each condition were performed in triplicate samples taking five aleatory hydrogel images of 0.1 mm^2. The total number of cells was counted using nuclear DAPI staining and the percentage of positive cells was determined in cell counts for each respective marker with respect to the total number of cells. The results were presented as the mean average ±SD or SEM. Multiple group comparisons were done with One-way

Anova non-parametric Holm-Šídák or Kruskal-Wallis tests followed by Dunn´s post hoc test. *$p < 0.05$ was taken as statistically significant.

5.3. Results

5.3.1. Effect of AsA on the morphology, mechanical and electrical properties of the self-assembled three-dimensional hydrogels

Graphene oxide (GO) is a carbon-based material bearing oxygenated functional groups, which improve the solubility and induce the expansion of the interlayer distance in aqueous solutions [25,26]. The reduction of the GO provokes the deletion of oxygen and other atomic-scale lattice defects, thus enhancing the hydrophobic nature and promoting the accumulation of the sheets via non-covalent interactions [25,27,28] (Figure 5.1. A). GO can be reduced in several ways, including chemical, thermal, electrochemical or light-driven approaches [25,27]. Chemical reduction, in combination with thermal annealing, results more effective in repairing vacancy defects and removing out-of-plane carbonyl groups [25]. Herein, we combined the chemical reduction with an overnight thermal treatment at 60 ^{o}C, using AsA as a reducing agent to overcome the limitations of more toxic alternatives [29]. This represents an easy and quick manner to synthesize 3D hydrogels by self-assembly with high C/O ratios and good electrical properties [29–31].

The absence or presence of oxygen functionalities will have a direct impact on the final properties of the hydrogels [32]. The different proportions of GO:AsA allowed us to modulate both the reduction level and the arrangement of the GO sheets, which determined the pore size of the hydrogels (Figure 5.1. B). Scanning electron micrographs revealed the large porous structures formed by atomic wide walls of GO sheets. Increasing the amount of AsA diminished the repulsion forces between the GO sheets and enabled the formation of more compact structures with smaller pores. The GO:AsA 1:1 hydrogel showed the largest pores with respect to the other two formulations (i.e., GO:AsA 1:4 & 1:10). In agreement with these results, X-ray diffraction demonstrated that the addition of an increasing amount of AsA triggered the reduction of GO sheets, resulting in the displacement of the diffraction peak to higher values (i.e, from 10^{o} in the commercial GO to 24^{o} in the GO:AsA 1:4 & 1:10) (Figure 5.1. C). According to Bragg´s law, the interlayer distance of the commercial GO was 0.85 nm and decreased till 0.77 nm in the GO:AsA 1:1 sample. The chemical reduction of GO stimulated the self-assembly of the reduced GO sheets thanks to the reduction of hydroxyl, epoxy, carboxyl and carbonyl groups [33], that enabled the formation of new π-π binding sites between the GO sheets. The deletion of oxygenated functional groups also raised the hydrophobicity of the graphene sheets. The combined effect of these two events provoked a random overlapping of flexible graphene sheets, thus favouring the self-assembly of the 3D hydrogels [34]. Remarkably, the addition of more AsA decreased the interlayer distance in the GO:AsA 1:4 and GO:AsA 1:10 hydrogels till 0.37 nm in both cases, but no differences were observed between these two formulations, suggesting that the reduction level was similar in both cases.

The mechanical properties of the hydrogels were measured by rheology. The GO:AsA 1:1 hydrogel showed the lowest shear modulus (G') (22.8±0.3 kPa), which in viscous materials is directly correlated with the elastic capabilities (Figure 5.1. D). The GO:AsA 1:4 and GO:AsA 1:10 presented increased shear modulus (178.4±2.8 kPa vs. 186.4±2.6 kPa), demonstrating that we were able to modulate the mechanical properties in almost one order of magnitude by controlling the reduction level through simply modifying the amount of AsA added. As shown in other studies, once the maximum reduction level is achieved, the mechanical properties of the hydrogels remain stable [35]. Even if the human brain presents a shear modulus of around 1-2.5 kPa [36], other central nervous system areas like the spinal cord recorded shear modulus of 250-300 kPa [37] and the peripheral nervous system like ulnar and median nerves register a shear modulus around 10-20 kPa [38]. It is also reported in the literature that the acquirement of well differentiated neural cultures of stem cells *in vitro* and *in vivo* can be achieved with scaffolds that present quite higher stiffness values [39,40].

GO is a poor electrical conductor due to the lack of percolating conduits between sp^2 carbon atoms that act as electron carriers in graphene. The reduction process with AsA induces the deletion of oxygen functionalities and raises the amount of sp^2 or π-π binding sites which consequently increases the conductivity of the material [41]. In accordance with the data of other studies [42,43], the electrical capacities of the hydrogels increased with the addition of AsA. The GO:AsA 1:1 hydrogel exhibited the lowest electrical conductivity (0.6 S/m), which increased in GO:AsA 1:4 (27 S/m) and GO:AsA 1:10 (35 S/m) (Figure 5.1. E). Accordingly, we were able to enhance the electrical conductivity thanks to the deletion of atomic-scale lattice defects of the GO sheets via the thermochemical reduction process [25]. According to these results, other groups have reported electrical conductivities between 0.045 and 600 S/m on graphene-based hydrogels [44–46]. Remarkably, as it has been reported before, the impedance or the electrical conductivity are constant in graphene oxide as usually observed for highly conducting systems [47,48]. Nevertheless, the human brain has an electrical conductivity of around 0.33 S/m, where grey matter exhibits a conductivity of around 0.47±0.24 S/m and white matter around 0.22±0.17 S/m [49,50]. However, materials showing electrical conductivity values between 0.08-1.3 S/m or even higher values are able to electrically stimulate neurons [51,52]. Therefore, all our hydrogels showed conductivity values compatible with neural stimulation.

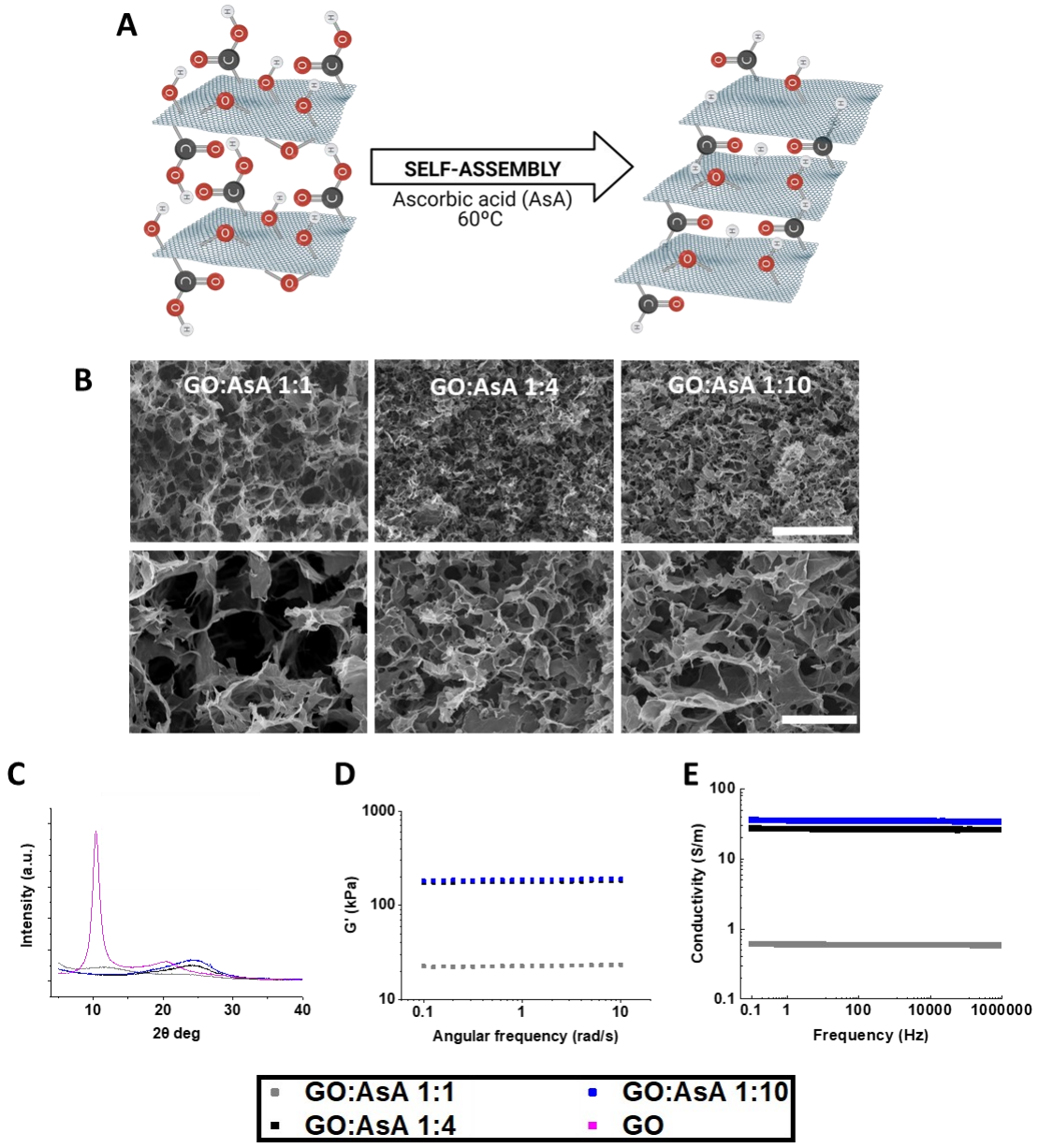

Figure 5.1.: Characterization of GO:AsA hydrogels.
(A) Schematic representation of the reduction process and self-assembly of the hydrogels. **(B)** SEM images of the GO:AsA 1:1, GO:AsA 1:4 and GO:AsA 1:10 hydrogels. Scale bar 100 µm on the upper images and 20 µm on the lower images. **(C)** XRD spectra, **(D)** shear modulus determined by rheology and **(E)** electrical conductivity of the hydrogels.

5.3.2. Effect of CeO_2 nanoparticles on the morphology, mechanical, electrical and antioxidant properties of the self-assembled three-dimensional hydrogels

Cerium oxide (CeO_2) nanoparticles are widely known for possessing antioxidant [53] and neuroprotective [54] properties. Here, CeO_2 nanoparticles were incorporated during the self-assembly of the graphene-based hydrogels, a process that is favored by electrostatic interactions between the negatively charged GO sheets (-29.1±0.36 mV) and the positively charged CeO_2 (24.3±0.57 mV) nanoparticles [24], as demonstrated by dynamic light scattering (DLS) (Figures 5.2. A, B).

To confirm the presence of CeO_2 nanoparticles in our samples, we performed transmission electron microscopy (TEM). TEM micrographs showed the GO sheets successfully decorated with CeO_2 nanoparticles prior to their reduction with AsA (Figure 5.2. C). Moreover, the amount of CeO_2 nanoparticles on the surface of the GO sheets increased with the addition of more CeO_2 to the samples (data not shown). These results were further corroborated with Raman spectroscopy and energy-dispersive X-ray spectrometry (EDX) (Figures 5.2. D, E and 5.3.). Raman spectroscopy demonstrated that all the samples that contained CeO_2 nanoparticles showed a band at 453 cm^{-1} that can be ascribed to the first order scattering of CeO_2 [55,56] and increased in intensity as the amount of CeO_2 nanoparticles raised. As expected, the GO:AsA 1:4 sample only exhibited the characteristic D and G bands (1350 and 1580 cm^{-1} respectively) which are related to the disarranged sp^2-hybridized carbon structure and expansion of the C-C bond in graphitic materials [57]. In accordance with these results, the EDX demonstrated the presence of Ce in the samples containing CeO_2 nanoparticles and presented similar proportions for carbon (C) (73.22 - 79.74%) and oxygen (O) (19.75 - 25.19%) in all the samples.

SEM images demonstrated that the addition of CeO_2 nanoparticles had no impact on the large porous structures formed by atomic wide walls of GO sheets (Figure 5.2. F). In accordance with these results, the XRD showed a peak at 24^o in all the samples (Figure 5.2. G), demonstrating that the interlayer distance was not affected by the addition of CeO_2 nanoparticles. Nevertheless, the intensity of the peak dropped down with the addition of CeO_2 nanoparticles to the samples in a dose dependent manner, denoting an interlayer distortion of the GO sheets, mediated by the CeO_2 nanoparticles. Remarkably, in all the samples there was a peak at 43^o which corresponded to the plane of the graphene layer [58] and indicated that the CeO_2 nanoparticles were localized on the interlayer space without inducing any variation in the GO sheets [59,60].

The mechanical behavior of the hydrogels decorated with CeO_2 nanoparticles was again measured by rheology. The GO:AsA 1:4 + CeO_2 0.25 and GO:AsA 1:4 + CeO_2 0.5 (187.7±7.5 kPa and 164.6±1.6, respectively) showed a shear modulus similar to the GO:AsA 1:4 hydrogel (178.4±2.8 kPa). A gradual decrease on the mechanical properties was however observed in the GO:AsA 1:4 + CeO_2 0.6 (71.6±0.7 kPa), GO:AsA 1:4 + CeO_2

0.75 (11.8±0.1 kPa) and GO:AsA 1:4 + CeO_2 1 (9.7±0.1 kPa) hydrogels (Figure 5.2. H). The fact that the shear modulus decreased with the addition of more CeO_2 nanoparticles to the samples indicated the possibility to tune the mechanical properties of the hydrogel by just modifying the CeO_2 nanoparticle concentration. These results are in concordance with those obtained by other groups using dopant nanoparticle substances like platinum [61] and can be explained due to the less organized structures associated to the incorporation of the CeO_2 nanoparticles in the interlayer space of the GO sheets [60,61], as suggested by XRD.

We also measured the electrical properties of the hydrogels. GO:AsA 1:4 + CeO_2 0.25 and GO:AsA 1:4 + CeO_2 0.5 (22 S/m and 17 S/m) maintained almost the same electrical properties of the GO:AsA 1:4 (27 S/m) (Figure 5.2. I). However, the addition of an increasing amount of CeO_2 nanoparticles resulted in a decline of the electrical conductivity of the GO:AsA 1:4 + CeO_2 0.6, GO:AsA 1:4 + CeO_2 0.75 and GO:AsA 1:4 + CeO_2 1 hydrogels (8.5 S/m; 2.8 S/m and 1.6 S/m respectively), which may be attributed to the more disordered arrangement of the GO sheets due to the incorporation of the CeO_2 nanoparticles in the interlayer space. Nevertheless, the electrical values obtained proved that all our hydrogels could potentially trigger the electrical excitation of the seeded neural cells [51,52].

It is well known that cerium oxide can exhibit +3 and +4 states that support the formation of CeO_2 and CeO_{2-x} and provides antioxidant properties [62,63]. CeO_2 nanoparticles resemble the antioxidant enzymes superoxide dismutase (SOD) and catalase (CAT) and, hence, scavenge reactive oxygen species (ROS) and free radicals [63,64] in physiological conditions [54,65,66]. Here, we applied a concentration of 50 µM hydrogen peroxide (H_2O_2) and measured the antioxidant capabilities of the hydrogels containing increasing amounts of CeO_2 nanoparticles. It was reported in the literature that this H_2O_2 concentration is able to mimic the pro-oxidative environment found *in vivo* which may cause a detrimental effect on important cellular structures, thus leading to oxidative distress [67]. As expected, all the hydrogels containing CeO_2 nanoparticles were able to reduce the hydrogen peroxide concentration in a dose dependent manner. In contrast, the GO:AsA 1:4 sample had no antioxidant properties, demonstrating that the CeO_2 nanoparticles were responsible of the decline on the hydrogen peroxide concentration (Figure 5.2. J). These results are in agreement with other studies were CeO_2 nanoparticles have demonstrated to possess antioxidant properties *in vitro* and *in vivo,* creating a more favorable microenvironment for angiogenesis and nerve reconstruction, resulting accordingly in a neuroprotective effect [21,68].

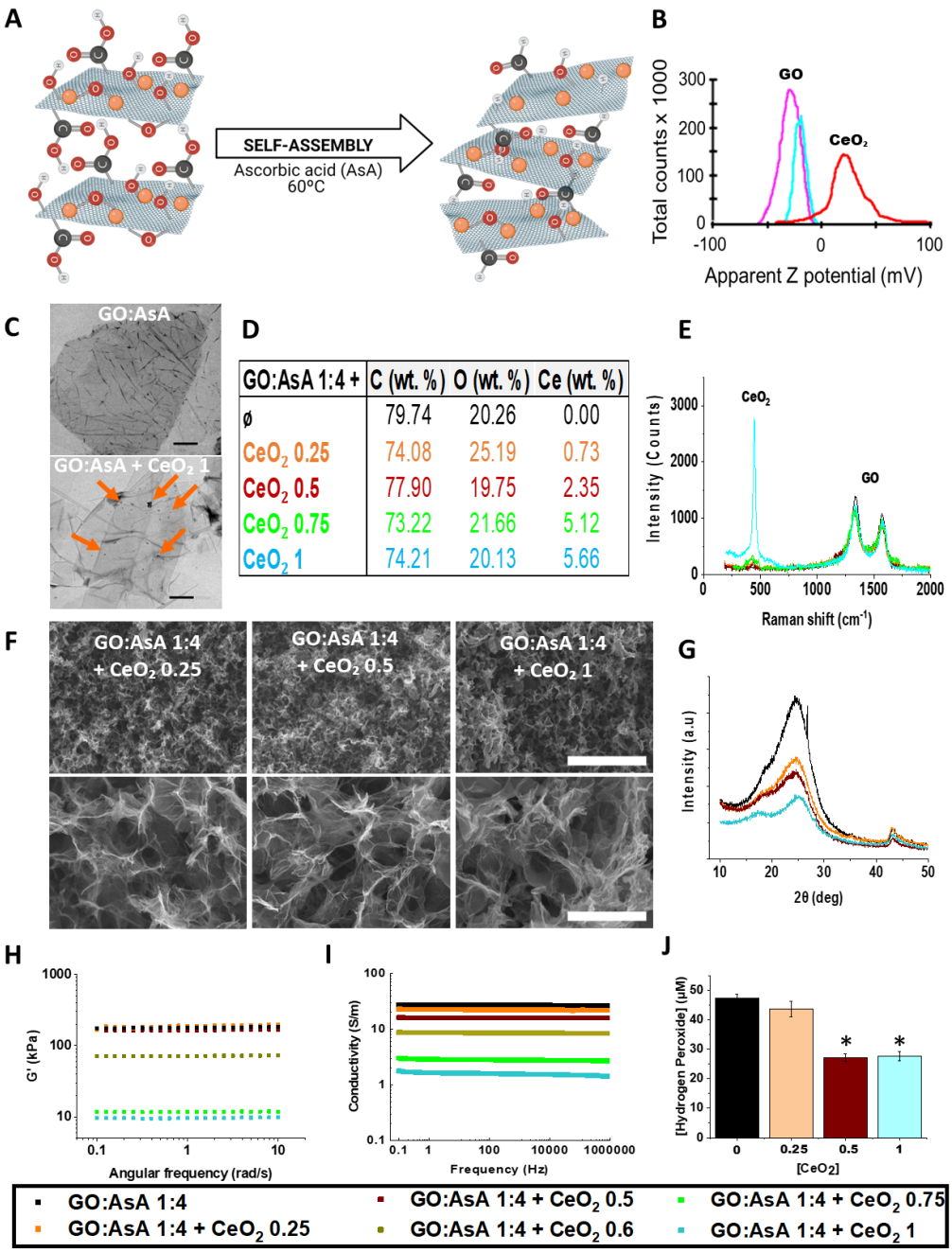

Figure 5.2.: Characterization of GO:AsA + CeO_2 nanoparticles hydrogels.

(A) Schematic representation of the decoration of the GO sheets with CeO_2 nanoparticles (orange) and the subsequent self-assembly process. **(B)** ζ-potential values of the negatively charged GO sheets in pink, the positively charged CeO_2 nanoparticles in dark orange and the shift on the surface charge of the GO sheets when combined at a GO:CeO_2 10:1 proportion in light blue. **(C)** TEM micrographs showing the GO sheets decorated with CeO_2 nanoparticles. Orange arrows highlight the presence of CeO_2 nanoparticles. Scale bar 1 µm on top and 200 nm in the bottom image. **(D)** EDX analysis showing the C, O and Ce wt %. **(E)** Raman spectra and **(F)** SEM images of the GO:AsA 1:4 + CeO_2 0.25, GO:AsA 1:4 + CeO_2 0.5 and GO:AsA 1:4 + CeO_2 1 hydrogels. Scale bar 100 µm on the upper images and 20 µm on the lower images. **(G)** XRD spectra of the hydrogels with different amounts of CeO_2 nanoparticles. **(H)** Shear modulus determined by rheology, **(I)** electrical conductivity and **(J)** antioxidant capacity of the hydrogels. *$p < 0.05$ compared to GO:AsA 1:4, Holm-Šídák method One Way Analysis of Variance on Ranks.

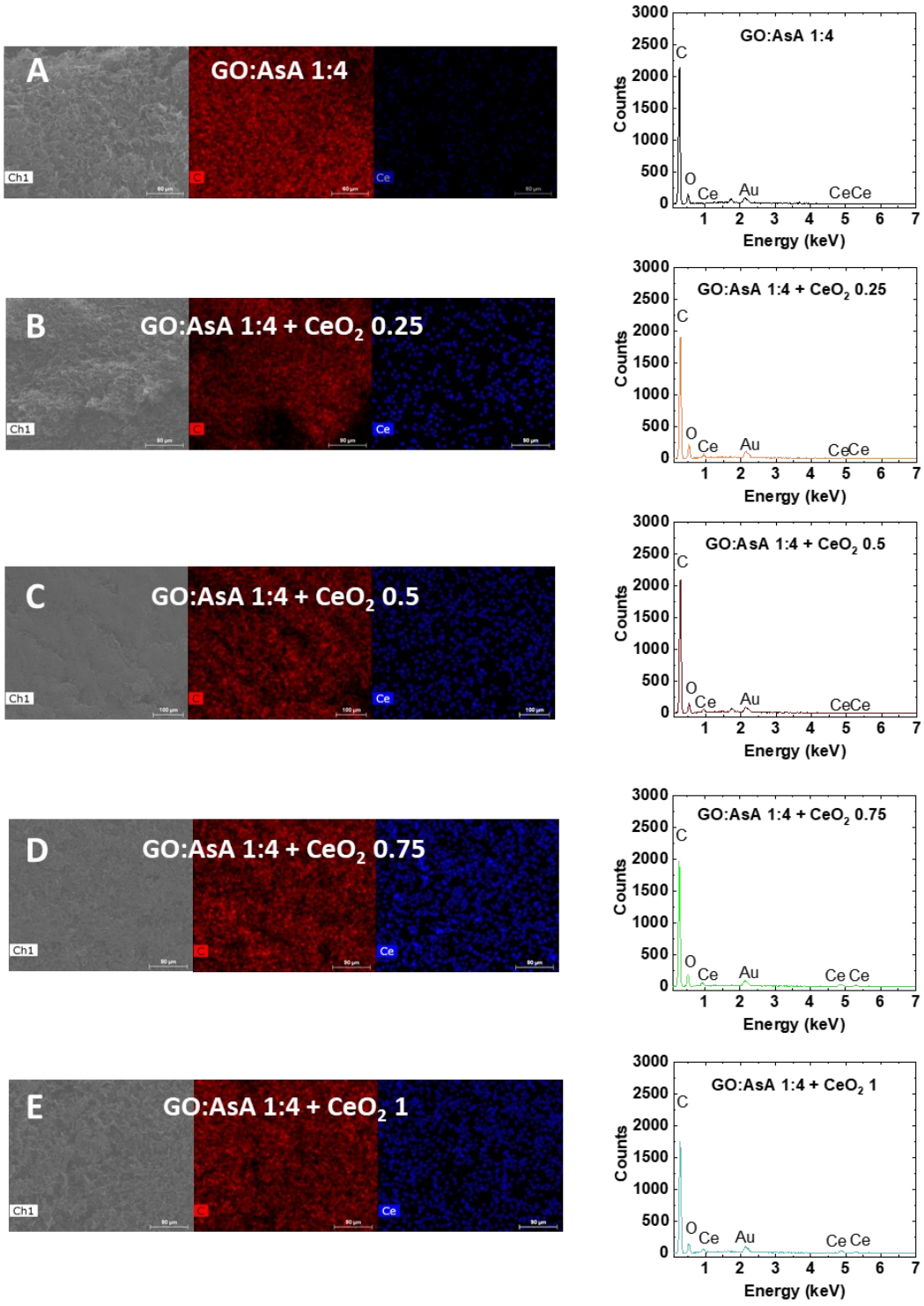

Figure 5.3.: EDX mapping and spectra of the hydrogels containing increasing amounts of CeO_2 nanoparticles.

(A) GO:AsA 1:4, **(B)** GO:AsA 1:4 + CeO_2 0.25, **(C)** GO:AsA 1:4 + CeO_2 0.5, **(D)** GO:AsA 1:4 + CeO_2 0.75, and **(E)** GO:AsA 1:4 + CeO_2 1 showing the peaks of the C, O and Ce.

5.3.3. Adhesion and integration of NSCs on the hydrogels

Materials based on graphene derivatives, when arrested in hydrogel form, have been shown not only to minimize the direct toxicity on cells, but also to promote the growth and differentiation of neural cells [69,70]. Herein, we wanted to explore the effect of different configurations of GO-based hydrogels with varying morphological, mechanical and electrical properties (which are dependant one from the other) on the neural commitment of NSCs. Therefore, we compared GO:AsA 1:1 that exhibited the larger pores and lowest stiffness and electrical conductivity with the GO:AsA 1:4, which exhibited smaller pores, but higher stiffness and electrical conductivity. To compare the influence of the CeO_2 nanoparticles on the neural differentiation, we selected the GO:AsA 1:4 + CeO_2 0.25, which shows morphological, electrical and mechanical properties comparable to the GO:AsA 1:4 configuration.

NSCs were seeded directly on the hydrogels and were able to attach without a need of Fetal Bovine Serum (FBS) supplementation (Figure 5.4.). They could also migrate inside the hydrogels without a need of coating with any extracellular matrix (ECM)-derived compound (Figure 5.5.). Both NSC survival and adhesion are crucial to facilitate the bench to clinic implementation of these materials. After 7, 14 and 21 days *in vitro* (DIV), cells were fixed and immunostained for neural stem (Nestin), astroglial (GFAP & S100β), oligodendroglial (Olig2) or neuronal lineage markers (DCX and MAP2) to study the effect of each hydrogel on the differentiation fate of the NSCs.

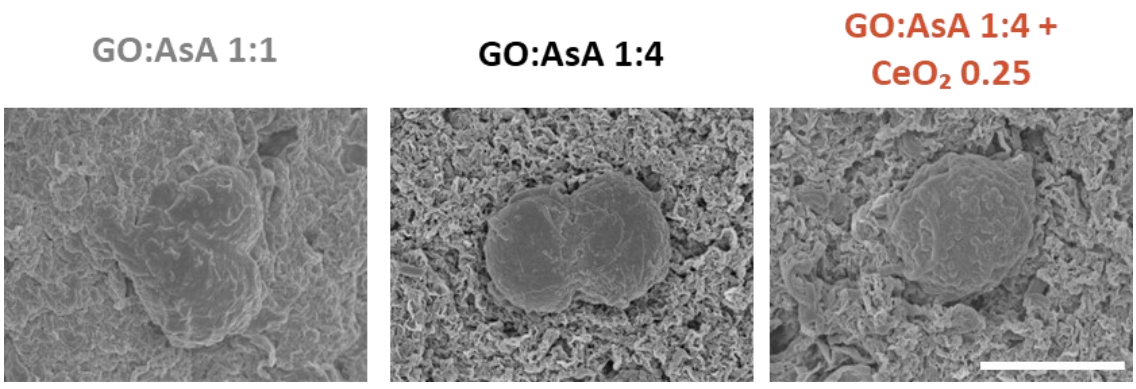

Figure 5.4.: Images of the surface of the hydrogels showing the attachment of the cells over the 3D structure.
Scanning electron micrographs showing the cells attached after 24 h in the GO:AsA 1:1, GO:AsA 1:4 and GO:AsA 1:4 + CeO_2 0.25. Scale bar 10 µm.

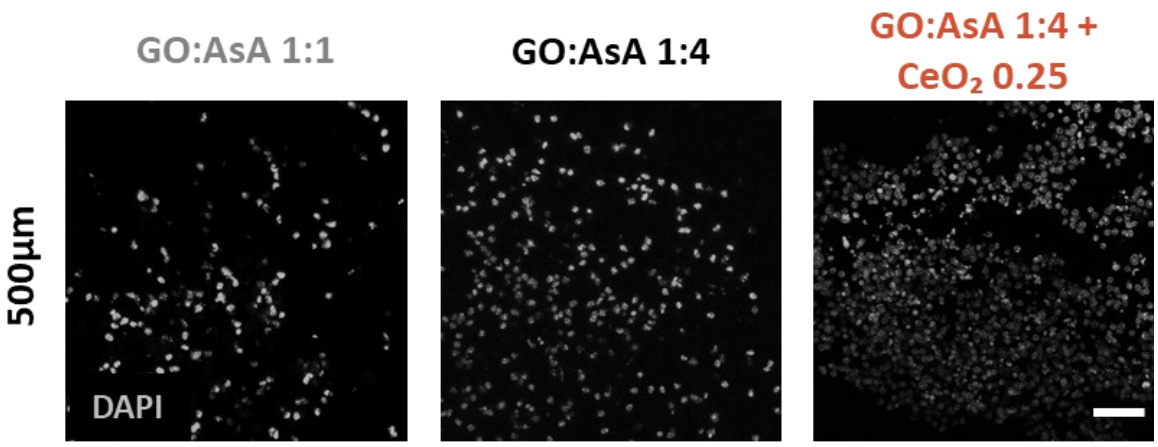

Figure 5.5.: Sectioned hydrogels showing the integration of the cells over the 3D structure. Immunofluorescence images for DAPI on hydrogel pieces cut by the vibratome. Cells were found until 500 µm deep on the GO:AsA 1:1, GO:AsA 1:4 and GO:AsA 1:4 + CeO_2 0.25. Scale bar 50 µm.

5.3.4. Stemness and glial cell differentiation of NSCs on the hydrogels

The maintenance of the NSC phenotype of the seeded cells was assessed by the presence of the intermediate filament Nestin. Nestin is a marker of neural precursor cells in embryonic and adult CNS tissue [71] and it is also considered to be a multipotent stem cell marker with crucial regulatory roles on the proliferation of immature cells [72] including neural progenitor cells [73,74]. Thus, non-differentiated NSCs are characterized by the expression of both Nestin and GFAP markers, but during the differentiation process, Nestin is progressively downregulated and replaced by other markers of more differentiated cells [75]. We found that GO:AsA 1:4 + CeO_2 0.25 hydrogel showed a more rapid decrease in the proportion of the Nestin positive stem cell population (3.7±0.2%, $p < 0.05$, One-way ANOVA) followed by the GO:AsA 1:1 (37.8±6.4%, $p < 0.05$, One-way ANOVA) and the GO:AsA 1:4 (28.4±2.2%, $p < 0.05$, One-way ANOVA) at DIV7 (Figure 5.6.), suggesting a faster expansion and subsequent differentiation of the seeded NSCs. By DIV14-21, Nestin expression was progressively lost in all the conditions, showing the exhaustion and progressive replacement of the stem cell population with differentiated cells. Interestingly, in GO:AsA 1:4 + CeO_2 0.25 hydrogels the proportion of Nestin positive cells at DIV14 was reduced in a slower manner (34.0±6.7%, $p < 0.05$, One-way ANOVA) compared to the other two conditions (GO:AsA 1:1 10.6±2.2% and GO:AsA 1:4 0.6±0.1%, $p < 0.05$, One-way ANOVA). This result goes in accordance with other studies where it is reported that more disordered arranges induced the maintenance of the stemness [76]. Moreover, non-differentiated NSCs can secrete neurotrophic factors that protect the developing neural tissue and help on its regeneration process [77]. Therefore, the better preservation of stem cells on the GO:AsA 1:4 + CeO_2 0.25 hydrogel might be helpful for the generation of a functional neural tissue *in vitro*.

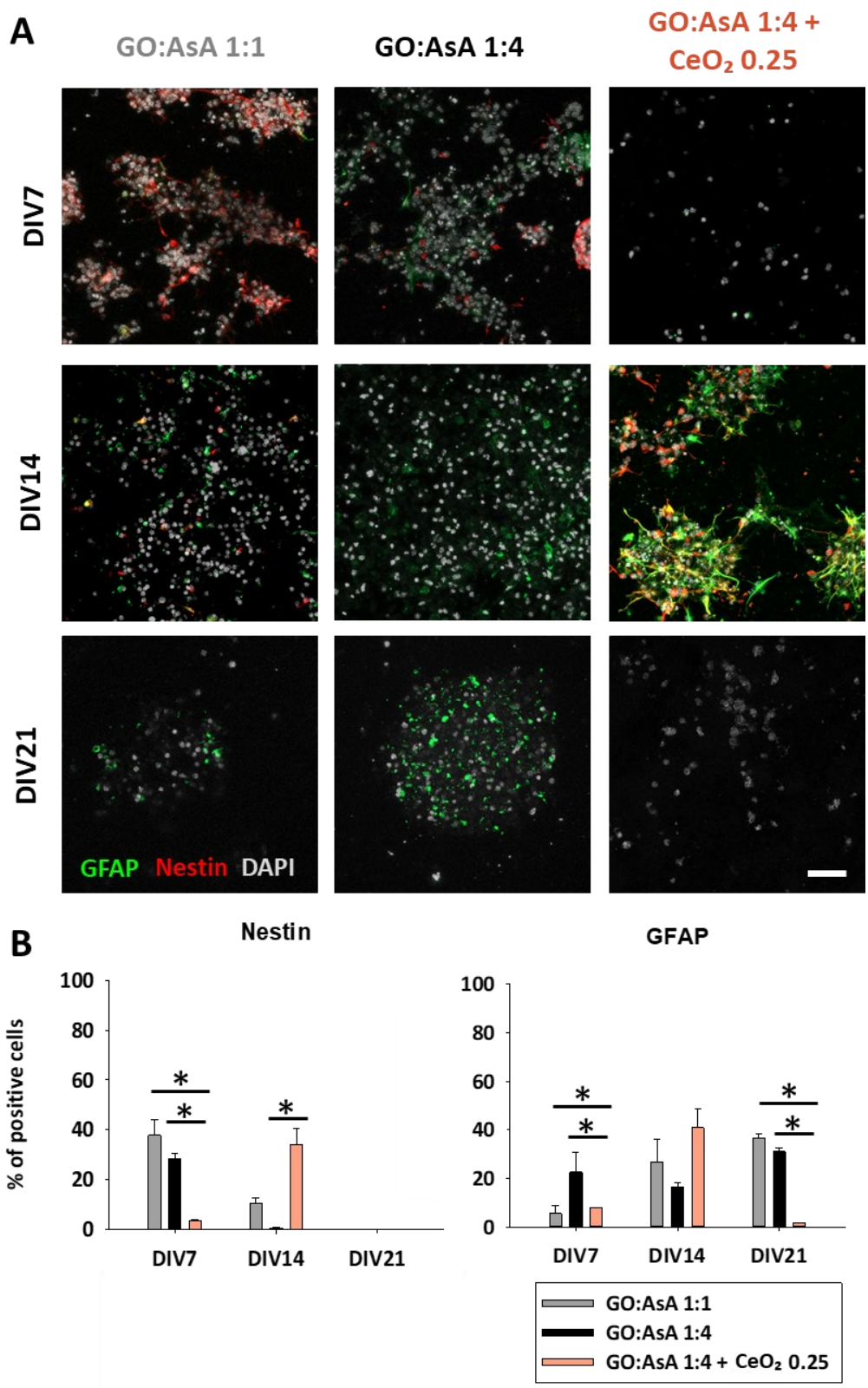

Figure 5.6.: Immature neural stem phenotype cells on the hydrogels.
(A) Double immunofluorescence showing GFAP (green) and Nestin (red) positive cells in GO:AsA 1:1, GO:AsA 1:4 and GO:AsA 1:4 + CeO_2 0.25 hydrogels after DIV 7, 14 and 21. Scale bar 50 µm. **(B)** Quantification of the percentage of positive cells of each of the markers tested (*$p < 0.05$ compared to the other hydrogels at the same time-points. Dunn´s or Holm-Šídák method One-way ANOVA Analysis of Variance on Ranks).

NSC are remnant cells of the CNS development restricted in neurogenic niches and maintain the ability to differentiate towards neuronal and glial lineages [78]. A balanced neuronal and glial cell differentiation is important for the long-term survival of the NSC-derived cell cultures due to the supporting function of the glial cells over the new-born neurons on the regulation of their oxidative and metabolic balance, and the neurophysiological processes of ion and neurotransmitter uptake and release, among others [79]. Thus, in this work we also characterized the NSC differentiation process towards astroglial lineages, by the loss of Nestin, the maintenance of the expression of glial fibrillary acidic protein (GFAP) and the appearance of the S100 calcium-binding protein β(S100β) marker during the astroglial differentiation (Figure 5.6. and 5.7.). The percentage of GFAP positive cells at DIV7 indicated that GO:AsA 1:4 substrate promoted more astroglial differentiation (22.6±8.2%, $p < 0.05$, One-way ANOVA) than GO:AsA 1:1 (5.6±3.4%, $p < 0.05$, One-way ANOVA) or GO:AsA 1:4 + CeO_2 0.25 (7.9±0.2%, $p < 0.05$, One-way ANOVA) hydrogels. This result suggest that, as previously described, stiffer substrates like GO:AsA 1:4 promoted the differentiation towards the glial lineages compared to softer ones [16,80]. However, the presence of CeO_2 nanoparticles could modulate the final fate of this astroglial phenotype into not only astrocytes, but also other types of glial cells. Interestingly, at DIV21 we found an abundant GFAP positive astroglial cell subpopulation in GO:AsA 1:1 (36.5±1.8%, $p < 0.05$, One-way ANOVA) and GO:AsA 1:4 (31.1±1.7%, $p < 0.05$, One-way ANOVA) hydrogels, compared to GO:AsA 1:4 + CeO_2 0.25, where those cells were relatively much less frequent (1.7±0.1%, $p < 0.05$, One-way ANOVA). From the point of view of tissue engineering therapies, the presence of GFAP positive astrocytes may pose both advantages and disadvantages. On the one hand, mature astrocytes are an important supporting glial cell of the CNS, sustaining neuronal metabolism and function. On the other hand, astroglial cells have also been described to be involved in glial scar formation after CNS injury [81]. Scar tissue has a dual component: first, the glial scar formed by glial precursors, reactive astrocytes and microglia found at the periphery of the lesion, and second, the fibrotic scar composed by phagocytic cells and fibroblasts at the lesion core [82,83]. This biological process has been reported detrimental for an effective reinnervation of the damaged CNS [84,85]. Taking into account that reactive astroglial phenotypes can be induced when these cells are exposed to a damaged CNS environment, the presence of high amounts of astrocytes (GFAP positive astroglial subpopulation) in the tissue engineered grafts may constitute a limitation for therapeutic purposes [83].

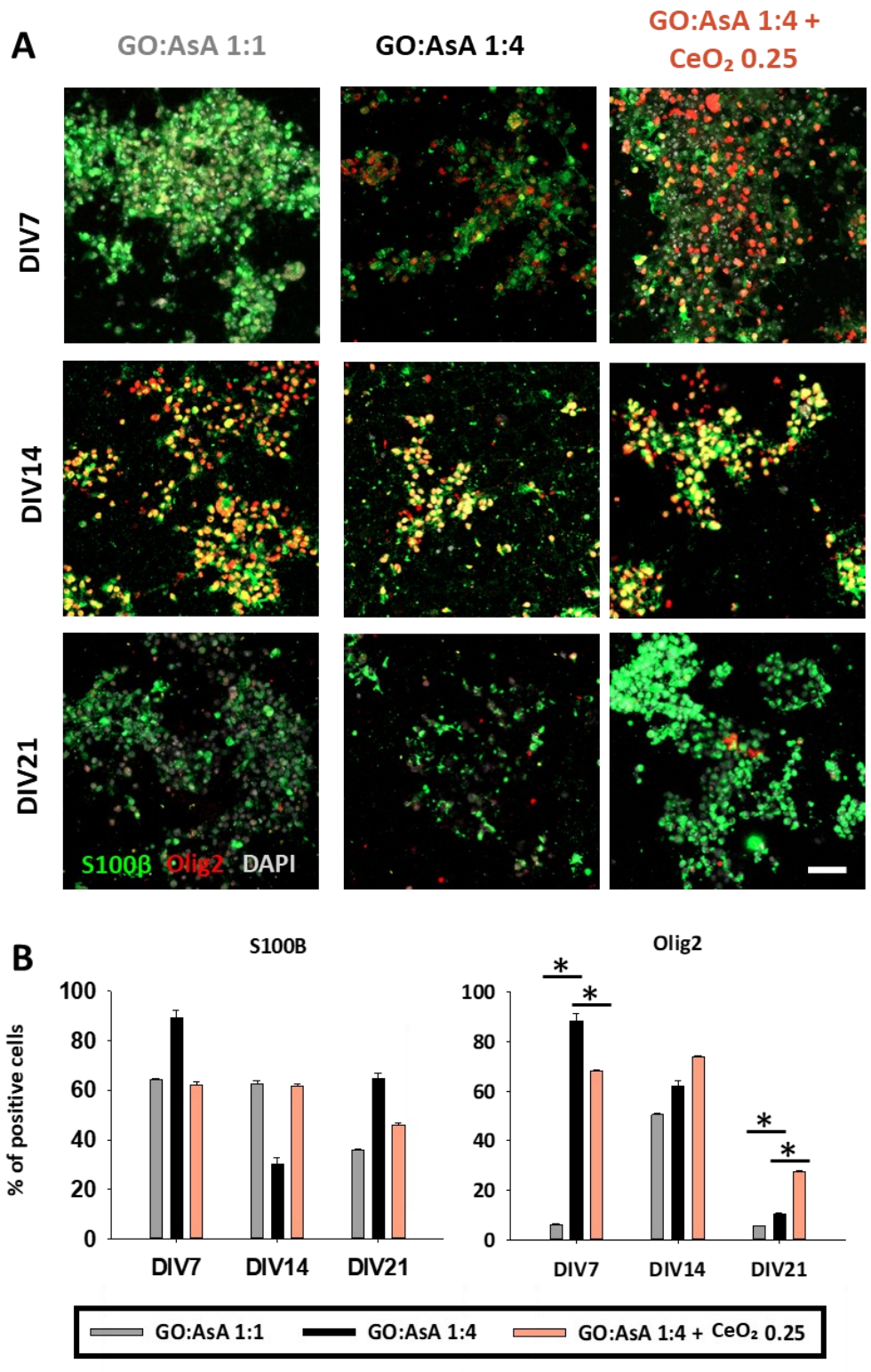

Figure 5.7.: Astroglial and oligodendroglial differentiation on the hydrogels.
(A) Double immunofluorescence showing S100β (green) mature astroglial and Olig2 (red) positive oligodendroglial-like cells in GO:AsA 1:1, GO:AsA 1:4 and GO:AsA 1:4 + CeO_2 0.25 hydrogels after DIV 7, 14 and 21. Scale bar 50 µm. **(B)** Quantification of the percentage of positive cells of each of the markers tested (*$p < 0.05$ compared to the other hydrogels at the same time-points. Dunn´s or Holm-Šídák method One-way ANOVA Analysis of Variance on Ranks).

During the maturation of the astrocytes, together with the expression of GFAP, cells acquire the expression of S100β [86,87]. All the tested hydrogels presented a mature astroglial-like lineage population over time since the proportion of S100β positive cells were always higher than that of GFAP positive cells in all the conditions (Figure 5.7.). It is remarkable that S100β, apart from mature astroglial cells, is also a marker of oligodendroglial lineage cells [88]. Oligodendrocyte precursors are known to express both S100β and Olig2 markers [88]. Therefore, in view of this result we also studied the expression of oligodendrocyte transcription factor Olig2 on the cell-seeded hydrogels. The expression of Olig2 in oligodendrocyte progenitors has been reported to be increased during the remyelination process of injured axons in multiple sclerosis (MS) [89], and is characteristic of an *in situ* expanding oligodendrocyte population. At DIV7, the proportion of the oligodendroglial lineage population on the GO:AsA 1:1 (5.9±0.4%, $p < 0.05$, One-way ANOVA) was also lower compared to GO:AsA 1:4 (88.5±3.0%, $p < 0.05$, One-way ANOVA) and GO:AsA 1:4 + CeO_2 0.25 (68.2±0.2%, $p < 0.05$, One-way ANOVA), demonstrating that stiffer substrates promoted a faster differentiation towards glial cell lineages. Interestingly, GO:AsA 1:4 + CeO_2 was able to support much better the oligodendroglial cell population until DIV21 (27.6±0.2%, $p < 0.05$, One-way ANOVA) compared to GO:AsA 1:1 (5.4±0.1%, $p < 0.05$, One-way ANOVA) and GO:AsA 1:4 (10.3±0.5%, $p < 0.05$, One-way ANOVA). These results suggested that the presence of CeO_2 nanoparticles might have helped on the establishment of a mature and healthy oligodendroglial lineage subpopulation within the hydrogel. Oligodendrocytes are known to be a particularly sensitive cell type to oxidative stress [90,91]. Although the antioxidant effect of CeO_2 0.25 using a concentrated source of exogenous H_2O_2 was limited, it might modulate the physiologic levels of biological metabolic intracellular free radicals' production, which may explain the beneficial effect of the CeO_2 nanoparticles addition on oligodendroglial survival in the scaffolds. Indeed, CeO_2 nanoparticles have been reported to possess antioxidant and neuroprotective capabilities and even attenuate the inflammation and help on the recovery of demyelinating pathologies like MS [92], further suggesting their implication on oligodendrocyte function and survival. Our results also suggest that, even if no statistical difference was observed for the GO:AsA 1:4 + 0.25 CeO_2 formulation on H_2O_2 reduction, the amount of CeO_2 nanoparticles added is enough to lower the amount of intracellular reactive oxygen species (GO:AsA 1:1 71.6±5.3, GO:AsA 1:4 62.6±5.9 and GO:AsA 1:4 + CeO_2 0.25 34.8±2.1, $p < 0.05$, One-way ANOVA) (Figure 5.8.) and modulate the differentiation pattern of the cells. This may be ascribed to the reduction of other reactive oxygen species or via other mechanisms beyond the scope of this chapter.

Overall, our results indicated that stiffer substrates like GO:AsA 1:4 promoted astroglial and oligodendrogial differentiation. Nevertheless, both GO:AsA 1:1 and GO:AsA 1:4 were able to support a GFAP positive astrocyte-like subpopulation, until DIV21. Remarkably, the addition of CeO_2 nanoparticles on the GO:AsA 1:4 + CeO_2 hydrogel was

able to better maintain both a Nestin positive stem population and also oligodendroglial lineage cell populations for longer culture periods.

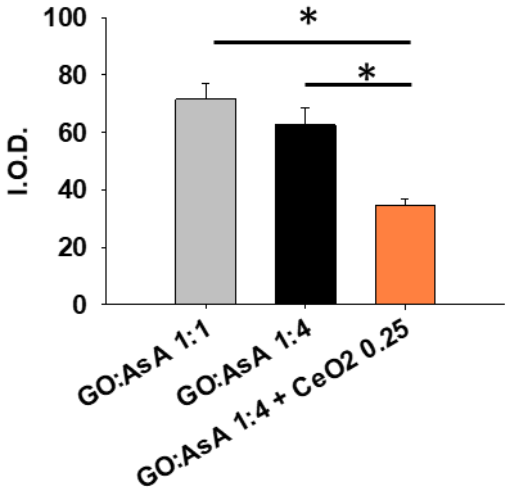

Figure 5.8.: Intracellular reactive oxygen species measurements.
Quantification of the intracellular reactive oxygen species on NSCs cultured for 14 days over GO:AsA 1:1, GO:AsA 1:4 and GO:AsA 1:4 + CeO_2 0.25 hydrogels. (*$p < 0.05$ compared to GO:AsA 1:1 and GO:AsA 1:4, Holm-Šídák method One Way Analysis of Variance on Rank).

5.3.5. Neuronal differentiation pattern and establishment of neuron-oligodendrocyte co-cultures on graphene-derivatives and CeO_2 nanoparticles-based hydrogels

Glial cells play a key role on regeneration, but mature and immature neurons are also needed to promote and coordinate innervation and, hence, the regeneration process [93]. The presence of neuronal progenitor cells also needs to be assessed to predict an effective neuroregeneration outcome. Hence, we performed immunofluorescence to detect doublecortin (DCX) [94–96], an immature neuronal marker. DCX expression is restricted to neuronal lineage immature cells and multipotent-precursors in both the developing and adult brain [97] and also in regions of adult neurons undergoing a plastic reorganization of their dendrites [98]. We found that the GO:AsA 1:4 hydrogel was not able to support DCX positive cells at any of the periods tested and GO:AsA 1:1 only supported them till DIV7. By contrast, GO:AsA 1:4 + CeO_2 0.25 was able to maintain a substantial population of DCX positive cells till DIV21 (28.4±0.3%, $p < 0.05$, One-way ANOVA) (Figure 5.9.). These results may indicate the presence of DCX+ multipotent-precursors and are in accordance with the increase in Nestin positive cells that occurred in GO:AsA 1:4 + CeO_2 0.25 at DIV14 and with other studies where more disordered structures supressed differentiation and enhanced stem cell lineage markers compared to more organized arrangements [76]. Nevertheless, the persistence of DCX positive population in the GO:AsA 1:4 + CeO_2 0.25 hydrogels at DIV21 may be attributed to a better long-term survival of neuronal lineage cells in culture.

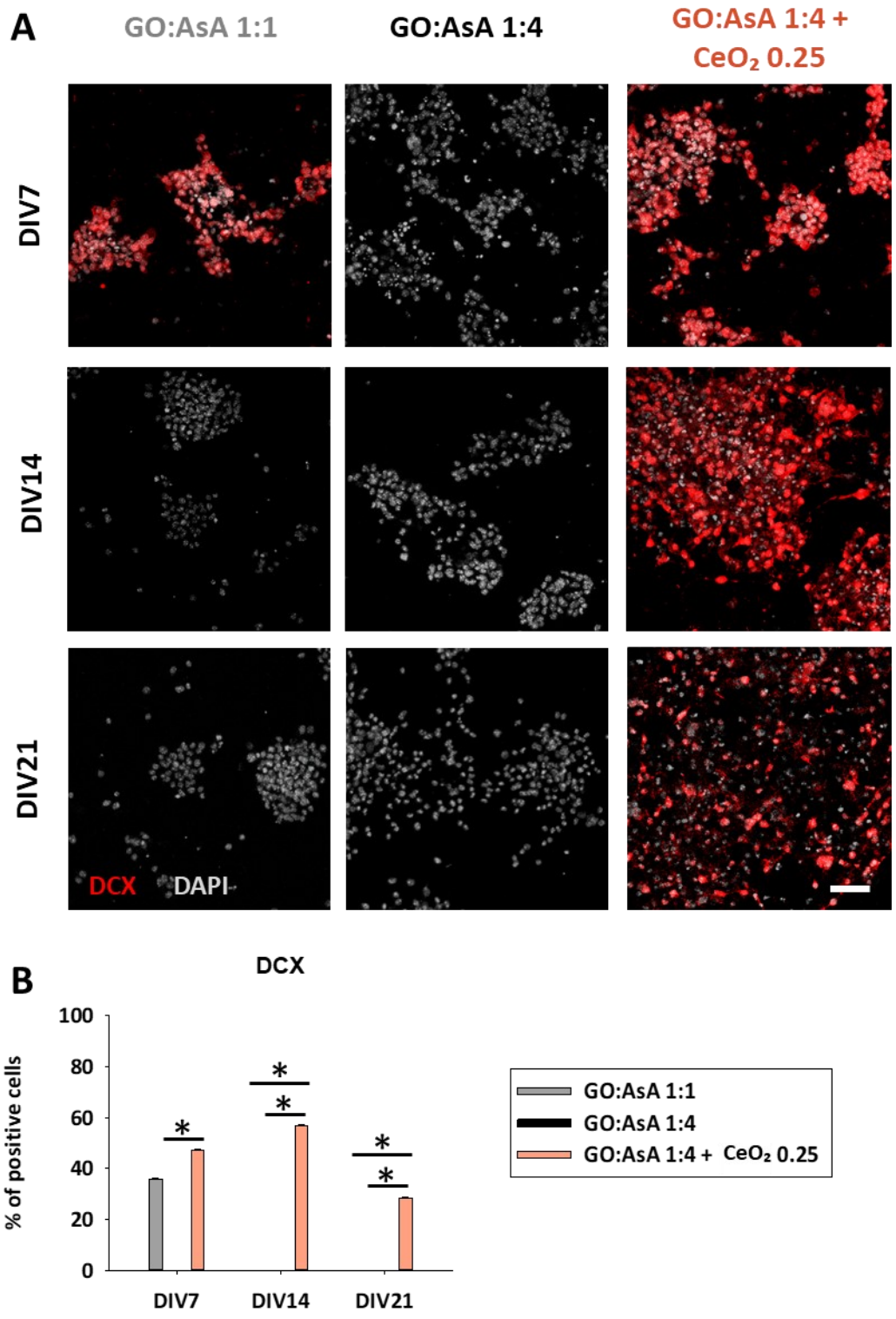

Figure 5.9.: Immature neuronal cells on the hydrogels at different time points.
(A) Immunofluorescence showing immature DCX (red) positive neuronal-like cells in GO:AsA 1:1, GO:AsA 1:4 and GO:AsA 1:4 + CeO_2 0.25 hydrogels after DIV 7, 14 and 21. Scale bar 50 µm. **(B)** Quantification of the percentage of DCX positive cells (*$p < 0.05$ compared to the other hydrogels at the same time-points. Dunn´s or Holm-Šídák method One-way Anova Analysis of Variance on Ranks).

The functionality and successful engraftment of bioengineered nerve tissues implies a balanced generation of both mature and immature glial and neuronal cells. Hence, we also studied the expression of other neuronal markers like microtubule-associated protein 2 (MAP2), which is expressed in the dendrites of fully mature neurons [99,100]. The percentage of MAP2 positive neurons in our hydrogels was much higher in GO:AsA 1:4 + CeO_2 0.25 (35.4±0.2%, $p < 0.05$, One-way ANOVA), than in GO:AsA 1:1 (0.04±0.03% $p < 0.05$, One-way ANOVA) and GO:AsA 1:4 (0.03±0.02%, $p < 0.05$, One-way ANOVA), which exhibited almost none mature neuronal generation at DIV7 (Figure 5.10. A and B). Interestingly, GO:AsA 1:1 showed an increase on MAP2 positive cells (22.9±0.4%, $p < 0.05$, One-way ANOVA) at DIV14, compared to GO:AsA 1:4, where no significant populations of MAP2 positive cells were ever found at any time point. These results are in agreement with DCX results in GO:AsA 1:1 at DIV7, which exhibited an increase in DCX positive cells. It might be assumed that some of these progenitor cells would proceed through their differentiation process to eventually give rise to mature neurons at DIV14 and corroborates the findings of other studies in the literature, where softer substrates were reported to promote the differentiation towards neuronal lineages [16,80]. However, the GO:AsA 1:1 hydrogel was unable to support the survival of the MAP2 positive cells for longer periods. On the contrary, the GO:AsA 1:4 + CeO_2 0.25 hydrogel managed to support a subpopulation of MAP2 positive mature neurons till DIV21. Our findings suggested that the addition of CeO_2 nanoparticles to the hydrogels allowed them to support the terminal differentiation of NSCs towards fully mature neurons. It is noteworthy that here CeO_2 nanoparticles were physically attached to the hydrogels, thus possibly preventing their cellular internalization and possible detrimental effects on the neuronal lineage differentiation of the seeded NSCs, as it was suggested in other studies [101]. Moreover, in accordance with our study, CeO_2 nanoparticles have also been shown to stimulate neuronal survival and growth [102], protecting against oxidative stress, improving neuronal function and delaying neuronal death after a traumatic brain injury both *in vitro* and *in vivo* [103].

As previously stated in chapter 3, a glial and neuronal equilibrium is primordial for cell survival and functionality of nerve tissues. Herein, in the absence of CeO_2 nanoparticles (GO:AsA 1:1 vs 1:4 configurations), the larger pores and lower stiffness and electrical conductivity of the GO:AsA 1:1 hydrogel enhanced the generation of neuronal lineage cells with respect to the smaller pores and greater mechanical and electrical properties of the GO:AsA 1:4, where there is a promotion towards glial lineages at shorter differentiation periods (Figure 5.10. C). But, remarkably, at DIV21, in both hydrogels, GO:AsA 1:1 and GO:AsA 1:4, astrocytes were the major persisting cell type. This result comes in agreement with the fact that astrocytes are the metabolically most resistant (least demanding) cell type of the CNS, whose high endogenous antioxidant and glycolytic capacity endows them with a higher ability to survive in adverse conditions [91,104,105]. Interestingly, in the presence of CeO_2 nanoparticles, the GO:AsA 1:4 + CeO_2 0.25 hydrogel supported the co-generation of both MAP2 positive mature

neuronal lineage cells together with Olig2 positive oligodendroglial lineage cells until DIV21. The results of this work clearly encourage the incorporation of neuroprotective and antioxidant systems like CeO_2 nanoparticles trapped in tissue engineering scaffolds, to boost survival of these two extremely necessary and highly vulnerable cell types of the CNS. The balanced generation of neurons, astrocytes and oligodendrocytes within the bioengineered construct is fundamental for an eventual success of CNS regeneration therapies. It should be emphasized that once a balanced oligodendrocytes, neurons and astrocytes population has been established within the graft, the close contact of the three different cell types may protect each other and improve xenocell survival prior to the integration into the host tissue [106,107]. Indeed, several studies highlighted the necessary integrin mediated connexion between neuronal axons and oligodendrocytes for the survival of both neuronal and oligodendroglial cells *in vitro* [108,109]. Moreover, oligodendrocytes have also been shown to be a glial cell subpopulation that play a key role on axonal regeneration [109,110], hence the importance of preserving both neurons and oligodendrocytes together in the same bioengineered construct. Here we present a 3D hydrogel based on graphene derivatives and cerium oxide nanoparticles as a promising therapeutic tool for neurodegenerative and demyelinating pathologies involving neuronal and/or oligodendroglial cell death.

Overall, our results showed that hydrogels based on graphene-derivatives supported both glial and neuronal lineage differentiation of NSCs in short-term cultures. Softer substrates like GO:AsA 1:1 with larger pores and lower electrical conductivities promoted cell differentiation towards neuronal lineages, while stiffer substrates like GO:AsA 1:4 with smaller pores and greater electrical properties enhanced glial cell differentiation. However, for long-term cultures, graphene derivatives-based hydrogels alone were unable to sustain a balanced long-term survival of neurons and oligodendrocytes. In contrast, thanks to the antioxidant and neuroprotective capabilities of CeO_2 nanoparticles embedded on GO:AsA 1:4 + CeO_2 0.25, this hydrogel was able to support the generation of astroglial, oligodendroglial and neuronal cells until DIV21, providing a promising approach for CNS regeneration therapies.

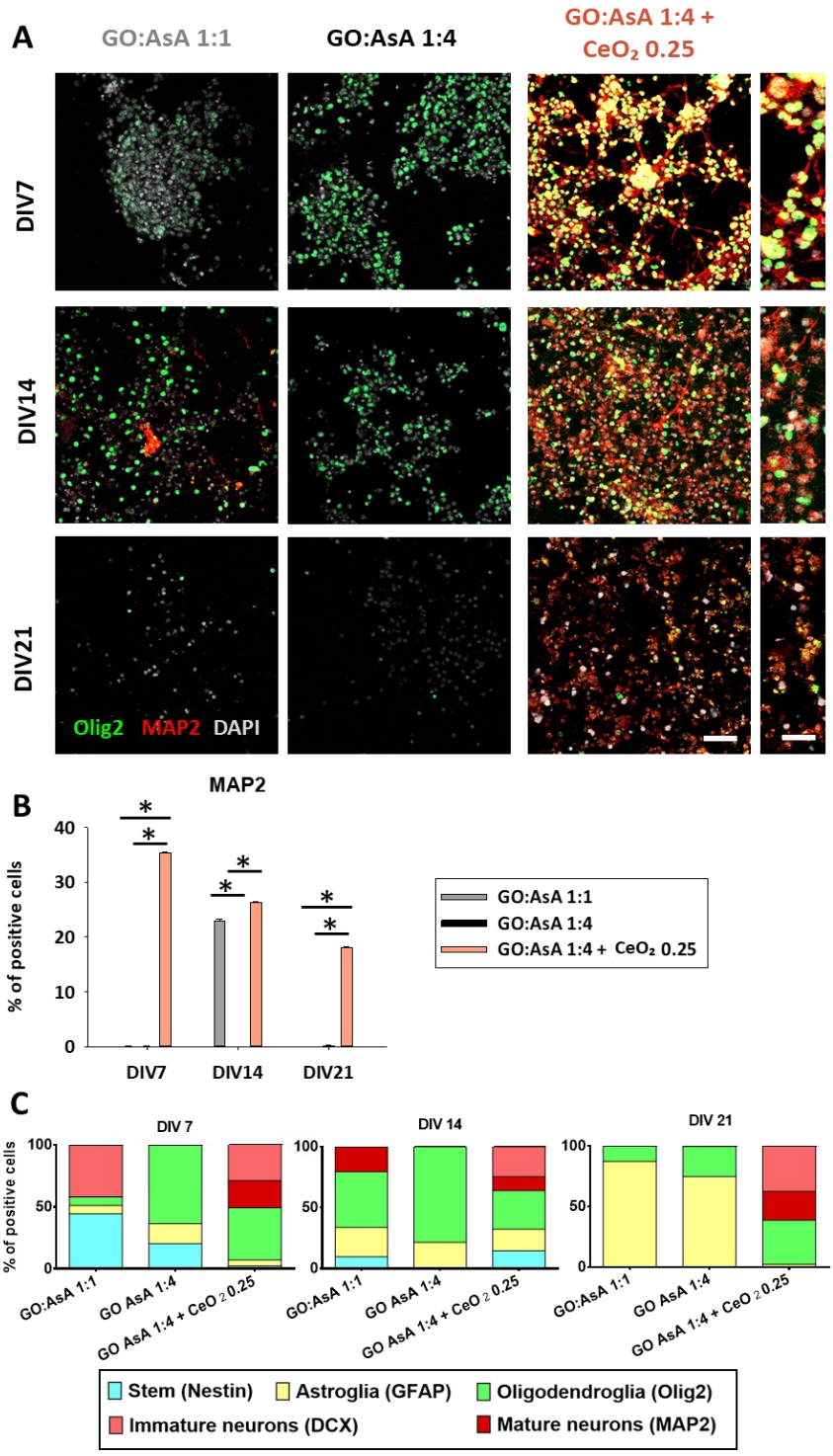

Figure 5.10.: Generation of *in vitro* co-cultures of neuronal and oligodendroglial lineage cells. **(A)** Double immunofluorescence showing oligodendroglial Olig2 (green) positive cells together with neuronal MAP2 (red) and positive cells in GO:AsA 1:1, GO:AsA 1:4 and GO:AsA 1:4 + CeO_2 0.25 hydrogels after DIV 7, 14 and 21. Scale bar 50 µm. Scale bar of the insets 20 µm. **(B)** Quantification of the percentage of MAP2 positive cells (*p < 0.05 compared to the other hydrogels at the same time-points. Dunn´s or Holm-Šídák method One-way ANOVA Analysis of Variance on Ranks). **(C)** Relative proportions of each of the cell lineages in the hydrogels over time. Neural stem (Nestin positive), astroglial (GFAP positive cells), oligodendroglial (Olig2 positive cells), immature neuronal (DCX positive), mature neuronal (MAP2 positive).

5.4. Conclusions

This chapter describes a simple and scalable method to fabricate 3D hydrogels based on graphene derivatives and CeO_2 nanoparticles promoted by a self-assembly process. The resulting hydrogels showed highly porous structures with tunable electrical, morphological and mechanical properties that can be finely regulated by the addition of AsA and CeO_2 nanoparticles. The final properties of the scaffolds, together with the advanced functionalities provided by the CeO_2 nanoparticles, clearly determined the fate of NSCs, which were seeded on the hydrogels without any ECM-like compound coating or FBS supplementation. Accordingly, we found that softer hydrogels with larger pores and lower electrical conductivity (i.e., GO:AsA 1:1) induced an increase of neuronal lineage differentiation, whereas the stiffer ones with smaller pores and greater electrical properties (i.e., GO:AsA 1:4) promoted glial cell lineage differentiation. Remarkably, the hydrogel containing CeO_2 nanoparticles (i.e., GO:AsA 1:4 + CeO_2 0.25) was the only one allowing the long-term establishment of a mature co-culture containing abundant populations of both neuronal and oligodendroglial lineage cells, which are the two most delicate and difficult to sustain cell types of the CNS. Our findings provide valuable insight on the creation and optimization of differentiated glial and neuronal 3D co-culture systems that enable the integration of both neurons and oligodendrocytes in a same hydrogel scaffold, which could be very useful for future CNS regeneration therapies.

References

[1] V.L. Feigin, A.A. Abajobir, K.H. Abate, F. Abd-Allah, A.M. Abdulle, S.F. Abera, G.Y. Abyu, M.B. Ahmed, A.N. Aichour, I. Aichour, M.T.E. Aichour, R.O. Akinyemi, S. Alabed, R. Al-Raddadi, N. Alvis-Guzman, A.T. Amare, H. Ansari, P. Anwari, J. Ärnlöv, H. Asayesh, S.W. Asgedom, T.M. Atey, L. Avila-Burgos, E. Frinel, G.A. Avokpaho, M.R. Azarpazhooh, A. Barac, M. Barboza, S.L. Barker-Collo, T. Bärnighausen, N. Bedi, E. Beghi, D.A. Bennett, I.M. Bensenor, A. Berhane, B.D. Betsu, S. Bhaumik, S.M. Birlik, S. Biryukov, D.J. Boneya, L.N.B. Bulto, H. Carabin, D. Casey, C.A. Castañeda-Orjuela, F. Catalá-López, H. Chen, A.A. Chitheer, R. Chowdhury, H. Christensen, L. Dandona, R. Dandona, G.A. de Veber, S.D. Dharmaratne, H.P. Do, K. Dokova, E.R. Dorsey, R.G. Ellenbogen, S. Eskandarieh, M.S. Farvid, S.-M. Fereshtehnejad, F. Fischer, K.J. Foreman, J.M. Geleijnse, R.F. Gillum, G. Giussani, E.M. Goldberg, P.N. Gona, A.C. Goulart, H.C. Gugnani, R. Gupta, V. Hachinski, R. Gupta, R.R. Hamadeh, M. Hambisa, G.J. Hankey, H.A. Hareri, R. Havmoeller, S.I. Hay, P. Heydarpour, P.J. Hotez, M. (Michael) B. Jakovljevic, M. Javanbakht, P. Jeemon, J.B. Jonas, Y. Kalkonde, A. Kandel, A. Karch, A. Kasaeian, A. Kastor, P.N. Keiyoro, Y.S. Khader, I.A. Khalil, E.A. Khan, Y.-H. Khang, A. Tawfih, A. Khoja, J. Khubchandani, C. Kulkarni, D. Kim, Y.J. Kim, M. Kivimaki, Y. Kokubo, S. Kosen, M. Kravchenko, R.V. Krishnamurthi, B.K. Defo, G.A. Kumar, R. Kumar, H.H. Kyu, A. Larsson, P.M. Lavados, Y. Li, X. Liang, M.L. Liben, W.D. Lo, G. Logroscino, P.A. Lotufo, C.T. Loy, M.T. Mackay, H.M.A.E. Razek, M.M.A.E. Razek, A. Majeed, R. Malekzadeh, T. Manhertz, L.G. Mantovani, J. Massano, M. Mazidi, C. McAlinden, S. Mehata, M.M. Mehndiratta, Z.A. Memish, W. Mendoza, M.A. Mengistie, G.A. Mensah, A. Meretoja, H.B. Mezgebe, T.R. Miller, S.R. Mishra, N.M. Ibrahim, A. Mohammadi, K.E. Mohammed, S. Mohammed, A.H. Mokdad, M. Moradi-Lakeh, I.M. Velasquez, K.I. Musa, M. Naghavi, J.W. Ngunjiri, C.T. Nguyen, G. Nguyen, Q.L. Nguyen, T.H. Nguyen, E. Nichols, D.N.A. Ningrum, V.M. Nong, B. Norrving, J.J.N. Noubiap, F.A. Ogbo, M.O. Owolabi, J.D. Pandian, P.G. Parmar, D.M. Pereira, M. Petzold, M.R. Phillips, M.A. Piradov, R.G. Poulton, F. Pourmalek, M. Qorbani, A. Rafay, M. Rahman, M.H. Rahman, R.K. Rai, S. Rajsic, A. Ranta, S. Rawaf, A.M.N. Renzaho, M.S. Rezai, G.A. Roth, G. Roshandel, E. Rubagotti, P. Sachdev, S. Safiri, R. Sahathevan, M.A. Sahraian, A.M. Samy, P. Santalucia, I.S. Santos, B. Sartorius, M. Satpathy, M. Sawhney, M.I. Saylan, S.G. Sepanlou, M.A. Shaikh, R. Shakir, M. Shamsizadeh, K.N. Sheth, M. Shigematsu, H. Shoman, D.A.S. Silva, M. Smith, E. Sobngwi, L.A. Sposato, J.D. Stanaway, D.J. Stein, T.J. Steiner, L.J. Stovner, R.S. Abdulkader, C.E. Szoeke, R. Tabarés-Seisdedos, D. Tanne, A.M. Theadom, A.G. Thrift, D.L. Tirschwell, R. Topor-Madry, B.X. Tran, T. Truelsen, K.B. Tuem, K.N. Ukwaja, O.A. Uthman, Y.Y. Varakin, T. Vasankari, N. Venketasubramanian, V.V. Vlassov, F. Wadilo, T. Wakayo, M.T. Wallin, E. Weiderpass, R. Westerman, T. Wijeratne, C.S. Wiysonge, M.A. Woldu, C.D.A. Wolfe, D. Xavier, G. Xu, Y. Yano, H.H. Yimam, N. Yonemoto, C. Yu, Z. Zaidi, M.E.S. Zaki, J.R. Zunt, C.J.L. Murray, T. Vos, Global, regional, and national burden of neurological disorders during 1990–2015: a systematic analysis for the Global Burden of Disease Study 2015, Lancet Neurol. 16 (2017) 877–897. https://doi.org/10.1016/S1474-4422(17)30299-5.

[2] World Health Organization - 2006 - Neurological disorders public health challenges.pdf, (n.d.). https://www.who.int/mental_health/neurology/neurological_disorders_report_web.pdf (accessed July 2, 2021).

[3] P.M. Rossini, C. Calautti, F. Pauri, J.-C. Baron, Post-stroke plastic reorganisation in the adult brain, Lancet Neurol. 2 (2003) 493–502. https://doi.org/10.1016/S1474-4422(03)00485-X.

[4] I. Fischer, J.N. Dulin, M.A. Lane, Transplanting neural progenitor cells to restore connectivity after spinal cord injury, Nat. Rev. Neurosci. 21 (2020) 366–383. https://doi.org/10.1038/s41583-020-0314-2.

[5] X. Tian, T. Fan, W. Zhao, G. Abbas, B. Han, K. Zhang, N. Li, N. Liu, W. Liang, H. Huang, W. Chen, B. Wang, Z. Xie, Recent advances in the development of nanomedicines for the

treatment of ischemic stroke, Bioact. Mater. 6 (2021) 2854–2869. https://doi.org/10.1016/j.bioactmat.2021.01.023.
[6] S. Jarrin, S. Cabré, E. Dowd, The potential of biomaterials for central nervous system cellular repair, Neurochem. Int. 144 (2021) 104971. https://doi.org/10.1016/j.neuint.2021.104971.
[7] S. Grade, M. Götz, Neuronal replacement therapy: previous achievements and challenges ahead, Npj Regen. Med. 2 (2017) 1–11. https://doi.org/10.1038/s41536-017-0033-0.
[8] Y. Li, Y. Xiao, C. Liu, The Horizon of Materiobiology: A Perspective on Material-Guided Cell Behaviors and Tissue Engineering, Chem. Rev. 117 (2017) 4376–4421. https://doi.org/10.1021/acs.chemrev.6b00654.
[9] R. Kumar, R. Rauti, D. Scaini, M. Antman-Passig, O. Meshulam, D. Naveh, L. Ballerini, O. Shefi, Graphene-Based Nanomaterials for Neuroengineering: Recent Advances and Future Prospective, Adv. Funct. Mater. 31 (2021) 2104887. https://doi.org/10.1002/adfm.202104887.
[10] E. López-Dolado, A. González-Mayorga, M.T. Portolés, M.J. Feito, M.L. Ferrer, F. Del Monte, M.C. Gutiérrez, M.C. Serrano, Subacute Tissue Response to 3D Graphene Oxide Scaffolds Implanted in the Injured Rat Spinal Cord, Adv. Healthc. Mater. 4 (2015) 1861–1868. https://doi.org/10.1002/adhm.201500333.
[11] A. Capasso, J. Rodrigues, M. Moschetta, F. Buonocore, G. Faggio, G. Messina, M.J. Kim, J. Kwon, E. Placidi, F. Benfenati, M. Bramini, G.-H. Lee, N. Lisi, Interactions between Primary Neurons and Graphene Films with Different Structure and Electrical Conductivity, Adv. Funct. Mater. 31 (2021) 2005300. https://doi.org/10.1002/adfm.202005300.
[12] R. Guo, S. Zhang, M. Xiao, F. Qian, Z. He, D. Li, X. Zhang, H. Li, X. Yang, M. Wang, R. Chai, M. Tang, Accelerating bioelectric functional development of neural stem cells by graphene coupling: Implications for neural interfacing with conductive materials, Biomaterials. 106 (2016) 193–204. https://doi.org/10.1016/j.biomaterials.2016.08.019.
[13] C. Tapeinos, Graphene-Based Nanotechnology in Neurodegenerative Disorders, Adv. NanoBiomed Res. 1 (2021) 2000059. https://doi.org/10.1002/anbr.202000059.
[14] Q. Ma, L. Yang, Z. Jiang, Q. Song, M. Xiao, D. Zhang, X. Ma, T. Wen, G. Cheng, Three-Dimensional Stiff Graphene Scaffold on Neural Stem Cells Behavior, ACS Appl. Mater. Interfaces. 8 (2016) 34227–34233. https://doi.org/10.1021/acsami.6b12305.
[15] Q. Fang, Y. Zhang, X. Chen, H. Li, L. Cheng, W. Zhu, Z. Zhang, M. Tang, W. Liu, H. Wang, T. Wang, T. Shen, R. Chai, Three-Dimensional Graphene Enhances Neural Stem Cell Proliferation Through Metabolic Regulation, Front. Bioeng. Biotechnol. 7 (2020). https://doi.org/10.3389/fbioe.2019.00436.
[16] Three-Dimensional Stiff Graphene Scaffold on Neural Stem Cells Behavior | ACS Applied Materials & Interfaces, (n.d.). https://pubs.acs.org/doi/10.1021/acsami.6b12305 (accessed July 14, 2021).
[17] N. Sultana, M.I. Hassan, M.M. Lim, Composite Synthetic Scaffolds for Tissue Engineering and Regenerative Medicine, Springer International Publishing, Cham, 2015. https://doi.org/10.1007/978-3-319-09755-8.
[18] N. Mansouri, S.F. Al-Sarawi, J. Mazumdar, D. Losic, Advancing fabrication and properties of three-dimensional graphene–alginate scaffolds for application in neural tissue engineering, RSC Adv. 9 (2019) 36838–36848. https://doi.org/10.1039/C9RA07481C.
[19] K.R. Singh, V. Nayak, T. Sarkar, R.P. Singh, Cerium oxide nanoparticles: properties, biosynthesis and biomedical application, RSC Adv. 10 (2020) 27194–27214. https://doi.org/10.1039/D0RA04736H.
[20] C. Xu, X. Qu, Cerium oxide nanoparticle: a remarkably versatile rare earth nanomaterial for biological applications, NPG Asia Mater. 6 (2014) e90–e90. https://doi.org/10.1038/am.2013.88.
[21] Y. Qian, Q. Han, X. Zhao, H. Li, W.-E. Yuan, C. Fan, Asymmetrical 3D Nanoceria Channel for Severe Neurological Defect Regeneration, IScience. 12 (2019) 216–231. https://doi.org/10.1016/j.isci.2019.01.013.

[22] M. Das, S. Patil, N. Bhargava, J.-F. Kang, L.M. Riedel, S. Seal, J.J. Hickman, Auto-catalytic ceria nanoparticles offer neuroprotection to adult rat spinal cord neurons, Biomaterials. 28 (2007) 1918–1925. https://doi.org/10.1016/j.biomaterials.2006.11.036.

[23] A. Ranjbar, S. Soleimani Asl, F. Firozian, H. Heidary Dartoti, S. Seyedabadi, M. Taheri Azandariani, M. Ganji, Role of Cerium Oxide Nanoparticles in a Paraquat-Induced Model of Oxidative Stress: Emergence of Neuroprotective Results in the Brain, J. Mol. Neurosci. 66 (2018) 420–427. https://doi.org/10.1007/s12031-018-1191-2.

[24] Z. Ji, X. Shen, M. Li, H. Zhou, G. Zhu, K. Chen, Synthesis of reduced graphene oxide/CeO2 nanocomposites and their photocatalytic properties, Nanotechnology. 24 (2013) 115603. https://doi.org/10.1088/0957-4484/24/11/115603.

[25] S. Pei, H.-M. Cheng, The reduction of graphene oxide, Carbon. 50 (2012) 3210–3228. https://doi.org/10.1016/j.carbon.2011.11.010.

[26] R.K. Singh, R. Kumar, D.P. Singh, Graphene oxide: strategies for synthesis, reduction and frontier applications, RSC Adv. 6 (2016) 64993–65011. https://doi.org/10.1039/C6RA07626B.

[27] Y. SHANG, D. ZHANG, Y. LIU, C. GUO, Preliminary comparison of different reduction methods of graphene oxide, Bull. Mater. Sci. 38 (2015) 7–12. https://doi.org/10.1007/s12034-014-0794-7.

[28] V. Agarwal, P.B. Zetterlund, Strategies for reduction of graphene oxide – A comprehensive review, Chem. Eng. J. 405 (2021) 127018. https://doi.org/10.1016/j.cej.2020.127018.

[29] C.K. Chua, M. Pumera, Chemical reduction of graphene oxide: a synthetic chemistry viewpoint, Chem. Soc. Rev. 43 (2013) 291–312. https://doi.org/10.1039/C3CS60303B.

[30] K.K.H. De Silva, H.-H. Huang, R.K. Joshi, M. Yoshimura, Chemical reduction of graphene oxide using green reductants, Carbon. 119 (2017) 190–199. https://doi.org/10.1016/j.carbon.2017.04.025.

[31] N. Ormategui, A. Veloso, G.P. Leal, S. Rodriguez-Couto, R. Tomovska, Design of Stable and Powerful Nanobiocatalysts, Based on Enzyme Laccase Immobilized on Self-Assembled 3D Graphene/Polymer Composite Hydrogels, ACS Appl. Mater. Interfaces. 7 (2015) 14104–14112. https://doi.org/10.1021/acsami.5b03325.

[32] K.K.H. De Silva, H.-H. Huang, M. Yoshimura, Progress of reduction of graphene oxide by ascorbic acid, Appl. Surf. Sci. 447 (2018) 338–346. https://doi.org/10.1016/j.apsusc.2018.03.243.

[33] O.C. Compton, S.T. Nguyen, Graphene Oxide, Highly Reduced Graphene Oxide, and Graphene: Versatile Building Blocks for Carbon-Based Materials, Small. 6 (2010) 711–723. https://doi.org/10.1002/smll.200901934.

[34] K. Sheng, High-performance self-assembled graphene hydrogels prepared by chemical reduction of graphene oxide, New Carbon Mater. (2011) 6.

[35] Y. Xu, K. Sheng, C. Li, G. Shi, Self-assembled graphene hydrogel via a one-step hydrothermal process, ACS Nano. 4 (2010) 4324–4330. https://doi.org/10.1021/nn101187z.

[36] E. Nicolas, S. Callé, S. Nicolle, D. Mitton, J.-P. Remenieras, Biomechanical characterization of ex vivo human brain using ultrasound shear wave spectroscopy, Ultrasonics. 84 (2018) 119–125. https://doi.org/10.1016/j.ultras.2017.10.009.

[37] S. Cheng, E.C. Clarke, L.E. Bilston, Rheological properties of the tissues of the central nervous system: a review, Med. Eng. Phys. 30 (2008) 1318–1337. https://doi.org/10.1016/j.medengphy.2008.06.003.

[38] Z. Ma, S. Hu, J.S. Tan, C. Myer, N.M. Njus, Z. Xia, In vitro and in vivo mechanical properties of human ulnar and median nerves, J. Biomed. Mater. Res. A. 101 (2013) 2718–2725. https://doi.org/10.1002/jbm.a.34573.

[39] K. Pradhan, G. Das, J. Khan, V. Gupta, S. Barman, A. Adak, S. Ghosh, Neuro-Regenerative Choline-Functionalized Injectable Graphene Oxide Hydrogel Repairs Focal Brain Injury, ACS Chem. Neurosci. 10 (2019) 1535–1543. https://doi.org/10.1021/acschemneuro.8b00514.

[40] A.F. Girão, J. Sousa, A. Domínguez-Bajo, A. González-Mayorga, I. Bdikin, E. Pujades-Otero, N. Casañ-Pastor, M.J. Hortigüela, G. Otero-Irurueta, A. Completo, M.C. Serrano, P.A.A.P. Marques, 3D Reduced Graphene Oxide Scaffolds with a Combinatorial Fibrous-Porous Architecture for Neural Tissue Engineering, ACS Appl. Mater. Interfaces. 12 (2020) 38962–38975. https://doi.org/10.1021/acsami.0c10599.

[41] S. Chae, T.-H. Le, C.S. Park, Y. Choi, S. Kim, U. Lee, E. Heo, H. Lee, Y.A. Kim, O.S. Kwon, H. Yoon, Anomalous restoration of sp2 hybridization in graphene functionalization, Nanoscale. 12 (2020) 13351–13359. https://doi.org/10.1039/D0NR03422C.

[42] S. Rao, J. Upadhyay, K. Polychronopoulou, R. Umer, R. Das, Reduced Graphene Oxide: Effect of Reduction on Electrical Conductivity, J. Compos. Sci. 2 (2018) 25. https://doi.org/10.3390/jcs2020025.

[43] J. Zhang, H. Yang, G. Shen, P. Cheng, J. Zhang, S. Guo, Reduction of graphene oxide via L-ascorbic acid, Chem. Commun. Camb. Engl. 46 (2010) 1112–4. https://doi.org/10.1039/b917705a.

[44] Z. Tan, S. Ohara, H. Abe, M. Naito, Synthesis and processing of graphene hydrogels for electronics applications, RSC Adv. 4 (2014) 8874–8878. https://doi.org/10.1039/C3RA46856A.

[45] X. Jing, H.-Y. Mi, B.N. Napiwocki, X.-F. Peng, L.-S. Turng, Mussel-inspired electroactive chitosan/graphene oxide composite hydrogel with rapid self-healing and recovery behavior for tissue engineering, Carbon. 125 (2017) 557–570. https://doi.org/10.1016/j.carbon.2017.09.071.

[46] J. Park, J.H. Choi, S. Kim, I. Jang, S. Jeong, J.Y. Lee, Micropatterned conductive hydrogels as multifunctional muscle-mimicking biomaterials: Graphene-incorporated hydrogels directly patterned with femtosecond laser ablation, Acta Biomater. 97 (2019) 141–153. https://doi.org/10.1016/j.actbio.2019.07.044.

[47] J.E. Hirsch, Apparent violation of the conductivity sum rule in certain superconductors, Phys. C Supercond. 199 (1992) 305–310. https://doi.org/10.1016/0921-4534(92)90415-9.

[48] Y. Nioua, S. El Bouazzaoui, B.M.G. Melo, P.R.S. Prezas, M.P.F. Graça, M.E. Achour, L.C. Costa, C. Brosseau, Analyzing the frequency and temperature dependences of the ac conductivity and dielectric analysis of reduced graphene oxide/epoxy polymer nanocomposites, J. Mater. Sci. 52 (2017) 13790–13798. https://doi.org/10.1007/s10853-017-1462-2.

[49] L. Koessler, S. Colnat-Coulbois, T. Cecchin, J. Hofmanis, J.P. Dmochowski, A.M. Norcia, L.G. Maillard, In-vivo measurements of human brain tissue conductivity using focal electrical current injection through intracerebral multicontact electrodes, Hum. Brain Mapp. 38 (2017) 974–986. https://doi.org/10.1002/hbm.23431.

[50] H. McCann, G. Pisano, L. Beltrachini, Variation in Reported Human Head Tissue Electrical Conductivity Values, Brain Topogr. 32 (2019) 825–858. https://doi.org/10.1007/s10548-019-00710-2.

[51] P. Zarrintaj, S. Manouchehri, Z. Ahmadi, M.R. Saeb, A.M. Urbanska, D.L. Kaplan, M. Mozafari, Agarose-based biomaterials for tissue engineering, Carbohydr. Polym. 187 (2018) 66–84. https://doi.org/10.1016/j.carbpol.2018.01.060.

[52] A. Saberi, F. Jabbari, P. Zarrintaj, M.R. Saeb, M. Mozafari, Electrically Conductive Materials: Opportunities and Challenges in Tissue Engineering, Biomolecules. 9 (2019). https://doi.org/10.3390/biom9090448.

[53] A. Pesaraklou, M.M. Matin, Cerium oxide nanoparticles and their importance in cell signaling pathways for predicting cellular behavior, Nanomed. (2020). https://doi.org/10.2217/nnm-2020-0104.

[54] A.Y. Estevez, J.S. Erlichman, The potential of cerium oxide nanoparticles (nanoceria) for neurodegenerative disease therapy, Nanomed. 9 (2014) 1437–1440. https://doi.org/10.2217/nnm.14.87.

[55] J. Cui, G.A. Hope, Raman and Fluorescence Spectroscopy of CeO2, Er2O3, Nd2O3, Tm2O3, Yb2O3, La2O3, and Tb4O7, J. Spectrosc. 2015 (2015) e940172. https://doi.org/10.1155/2015/940172.
[56] P. Nayak, P.N. Santhosh, S. Ramaprabhu, Cerium Oxide Nanoparticles Decorated Graphene Nanosheets for Selective Detection of Dopamine, J. Nanosci. Nanotechnol. 15 (2015) 4855–4862. https://doi.org/10.1166/jnn.2015.9812.
[57] J.-B. Wu, M.-L. Lin, X. Cong, H.-N. Liu, P.-H. Tan, Raman spectroscopy of graphene-based materials and its applications in related devices, Chem. Soc. Rev. 47 (2018) 1822–1873. https://doi.org/10.1039/C6CS00915H.
[58] B. Gupta, N. Kumar, K. Panda, V. Kanan, S. Joshi, I. Visoly-Fisher, Role of oxygen functional groups in reduced graphene oxide for lubrication, Sci. Rep. 7 (2017) 45030. https://doi.org/10.1038/srep45030.
[59] Y. Yang, C. Tian, L. Sun, R. Lü, W. Zhou, K. Shi, K. Kan, J. Wang, H. Fu, Growth of small sized CeO2 particles in the interlayers of expanded graphite for high-performance room temperature NOx gas sensors, J. Mater. Chem. A. 1 (2013) 12742. https://doi.org/10.1039/c3ta12399e.
[60] N.L. Hamidah, M. Shintani, A.S. Ahmad Fauzi, G.K. Putri, S. Kitamura, K. Hatakeyama, M. Sasaki, A.T. Quitain, T. Kida, Graphene Oxide Membranes with Cerium-Enhanced Proton Conductivity for Water Vapor Electrolysis, ACS Appl. Nano Mater. 3 (2020) 4292–4304. https://doi.org/10.1021/acsanm.0c00439.
[61] Y. Si, E.T. Samulski, Exfoliated Graphene Separated by Platinum Nanoparticles, Chem. Mater. 20 (2008) 6792–6797. https://doi.org/10.1021/cm801356a.
[62] A. Dhall, W. Self, Cerium Oxide Nanoparticles: A Brief Review of Their Synthesis Methods and Biomedical Applications, Antioxidants. 7 (2018) 97. https://doi.org/10.3390/antiox7080097.
[63] S.M. Hirst, A.S. Karakoti, R.D. Tyler, N. Sriranganathan, S. Seal, C.M. Reilly, Anti-inflammatory Properties of Cerium Oxide Nanoparticles, Small. 5 (2009) 2848–2856. https://doi.org/10.1002/smll.200901048.
[64] G. Song, N. Cheng, J. Zhang, H. Huang, Y. Yuan, X. He, Y. Luo, K. Huang, Nanoscale Cerium Oxide: Synthesis, Biocatalytic Mechanism, and Applications, Catalysts. 11 (2021) 1123. https://doi.org/10.3390/catal11091123.
[65] C. Korsvik, S. Patil, S. Seal, W.T. Self, Superoxide dismutase mimetic properties exhibited by vacancy engineered ceria nanoparticles, Chem. Commun. (2007) 1056–1058. https://doi.org/10.1039/B615134E.
[66] S.M. Hirst, A. Karakoti, S. Singh, W. Self, R. Tyler, S. Seal, C.M. Reilly, Bio-distribution and in vivo antioxidant effects of cerium oxide nanoparticles in mice, Environ. Toxicol. 28 (2013) 107–118. https://doi.org/10.1002/tox.20704.
[67] H. Sies, Hydrogen peroxide as a central redox signaling molecule in physiological oxidative stress: Oxidative eustress, Redox Biol. 11 (2017) 613–619. https://doi.org/10.1016/j.redox.2016.12.035.
[68] G. Ciofani, G.G. Genchi, I. Liakos, V. Cappello, M. Gemmi, A. Athanassiou, B. Mazzolai, V. Mattoli, Effects of cerium oxide nanoparticles on PC12 neuronal-like cells: proliferation, differentiation, and dopamine secretion, Pharm. Res. 30 (2013) 2133–2145. https://doi.org/10.1007/s11095-013-1071-y.
[69] J. Kim, Y.-R. Kim, Y. Kim, K. Taek Lim, H. Seonwoo, S. Park, S.-P. Cho, B. Hee Hong, P.-H. Choung, T. Dong Chung, Y.-H. Choung, J. Hoon Chung, Graphene -incorporated chitosan substrata for adhesion and differentiation of human mesenchymal stem cells, J. Mater. Chem. B. 1 (2013) 933–938. https://doi.org/10.1039/C2TB00274D.
[70] J. Yi, G. Choe, J. Park, J.Y. Lee, Graphene oxide-incorporated hydrogels for biomedical applications, Polym. J. 52 (2020) 823–837. https://doi.org/10.1038/s41428-020-0350-9.
[71] U. Lendahl, L.B. Zimmerman, R.D. McKay, CNS stem cells express a new class of intermediate filament protein, Cell. 60 (1990) 585–595. https://doi.org/10.1016/0092-8674(90)90662-x.

[72] S. Suzuki, J. Namiki, S. Shibata, Y. Mastuzaki, H. Okano, The neural stem/progenitor cell marker nestin is expressed in proliferative endothelial cells, but not in mature vasculature, J. Histochem. Cytochem. Off. J. Histochem. Soc. 58 (2010) 721–730. https://doi.org/10.1369/jhc.2010.955609.

[73] A. Bernal, L. Arranz, Nestin-expressing progenitor cells: function, identity and therapeutic implications, Cell. Mol. Life Sci. 75 (2018) 2177–2195. https://doi.org/10.1007/s00018-018-2794-z.

[74] J. Dahlstrand, M. Lardelli, U. Lendahl, Nestin mRNA expression correlates with the central nervous system progenitor cell state in many, but not all, regions of developing central nervous system, Brain Res. Dev. Brain Res. 84 (1995) 109–129. https://doi.org/10.1016/0165-3806(94)00162-s.

[75] F. Doetsch, J.M. García-Verdugo, A. Alvarez-Buylla, Cellular composition and three-dimensional organization of the subventricular germinal zone in the adult mammalian brain, J. Neurosci. Off. J. Soc. Neurosci. 17 (1997) 5046–5061.

[76] C. Yang, F.W. DelRio, H. Ma, A.R. Killaars, L.P. Basta, K.A. Kyburz, K.S. Anseth, Spatially patterned matrix elasticity directs stem cell fate, Proc. Natl. Acad. Sci. U. S. A. 113 (2016) E4439–E4445. https://doi.org/10.1073/pnas.1609731113.

[77] L. Ottoboni, B. von Wunster, G. Martino, Therapeutic Plasticity of Neural Stem Cells, Front. Neurol. 11 (2020) 148. https://doi.org/10.3389/fneur.2020.00148.

[78] F.H. Gage, S. Temple, Neural Stem Cells: Generating and Regenerating the Brain, Neuron. 80 (2013) 588–601. https://doi.org/10.1016/j.neuron.2013.10.037.

[79] K.H. Lee, M. Cha, B.H. Lee, Crosstalk between Neuron and Glial Cells in Oxidative Injury and Neuroprotection, Int. J. Mol. Sci. 22 (2021) 13315. https://doi.org/10.3390/ijms222413315.

[80] K. Saha, A.J. Keung, E.F. Irwin, Y. Li, L. Little, D.V. Schaffer, K.E. Healy, Substrate Modulus Directs Neural Stem Cell Behavior, Biophys. J. 95 (2008) 4426–4438. https://doi.org/10.1529/biophysj.108.132217.

[81] M.V. Sofroniew, H.V. Vinters, Astrocytes: biology and pathology, Acta Neuropathol. (Berl.). 119 (2010) 7–35. https://doi.org/10.1007/s00401-009-0619-8.

[82] T. Yang, Y. Dai, G. Chen, S. Cui, Dissecting the Dual Role of the Glial Scar and Scar-Forming Astrocytes in Spinal Cord Injury, Front. Cell. Neurosci. 14 (2020) 78. https://doi.org/10.3389/fncel.2020.00078.

[83] H. Kawano, J. Kimura-Kuroda, Y. Komuta, N. Yoshioka, H.P. Li, K. Kawamura, Y. Li, G. Raisman, Role of the lesion scar in the response to damage and repair of the central nervous system, Cell Tissue Res. 349 (2012) 169–180. https://doi.org/10.1007/s00441-012-1336-5.

[84] A. McKeon, E.E. Benarroch, Glial fibrillary acid protein: Functions and involvement in disease, Neurology. 90 (2018) 925–930. https://doi.org/10.1212/WNL.0000000000005534.

[85] M.K. Gottipati, J.M. Zuidema, R.J. Gilbert, Biomaterial strategies for creating in vitro astrocyte cultures resembling in vivo astrocyte morphologies and phenotypes, Curr. Opin. Biomed. Eng. 14 (2020) 67–74. https://doi.org/10.1016/j.cobme.2020.06.004.

[86] E. Raponi, F. Agenes, C. Delphin, N. Assard, J. Baudier, C. Legraverend, J.-C. Deloulme, S100B expression defines a state in which GFAP-expressing cells lose their neural stem cell potential and acquire a more mature developmental stage, Glia. 55 (2007) 165–177. https://doi.org/10.1002/glia.20445.

[87] J.R. Pineda, M. Daynac, A. Chicheportiche, A. Cebrian-Silla, K. Sii Felice, J.M. Garcia-Verdugo, F.D. Boussin, M.-A. Mouthon, Vascular-derived TGF-β increases in the stem cell niche and perturbs neurogenesis during aging and following irradiation in the adult mouse brain, EMBO Mol. Med. 5 (2013) 548–562. https://doi.org/10.1002/emmm.201202197.

[88] G. Santos, A. Barateiro, D. Brites, A. Fernandes, S100B Impairs Oligodendrogenesis and Myelin Repair Following Demyelination Through RAGE Engagement, Front. Cell. Neurosci. 14 (2020) 279. https://doi.org/10.3389/fncel.2020.00279.

[89] A. Wegener, C. Deboux, C. Bachelin, M. Frah, C. Kerninon, D. Seilhean, M. Weider, M. Wegner, B. Nait-Oumesmar, Gain of Olig2 function in oligodendrocyte progenitors

promotes remyelination, Brain J. Neurol. 138 (2015) 120–135. https://doi.org/10.1093/brain/awu375.

[90] G. Ibarretxe, M.V. Sánchez-Gómez, M.R. Campos-Esparza, E. Alberdi, C. Matute, Differential oxidative stress in oligodendrocytes and neurons after excitotoxic insults and protection by natural polyphenols, Glia. 53 (2006) 201–211. https://doi.org/10.1002/glia.20267.

[91] S.K. Thorburne, B.H.J. Juurlink, Low Glutathione and High Iron Govern the Susceptibility of Oligodendroglial Precursors to Oxidative Stress, J. Neurochem. 67 (1996) 1014–1022. https://doi.org/10.1046/j.1471-4159.1996.67031014.x.

[92] E. Eitan, E.R. Hutchison, N.H. Greig, D. Tweedie, H. Celik, S. Ghosh, K.W. Fishbein, R.G. Spencer, C.Y. Sasaki, P. Ghosh, S. Das, S. Chigurapati, J. Raymick, S. Sarkar, S. Chigurupati, S. Seal, M.P. Mattson, Combination Therapy with Lenalidomide and Nanoceria Ameliorates CNS Autoimmunity, Exp. Neurol. 273 (2015) 151–160. https://doi.org/10.1016/j.expneurol.2015.08.008.

[93] N. Pirotte, N. Leynen, T. Artois, K. Smeets, Do you have the nerves to regenerate? The importance of neural signalling in the regeneration process, Dev. Biol. 409 (2016) 4–15. https://doi.org/10.1016/j.ydbio.2015.09.025.

[94] M.E. van Strien, S.A. van den Berge, E.M. Hol, Migrating neuroblasts in the adult human brain: a stream reduced to a trickle, Cell Res. 21 (2011) 1523–1525. https://doi.org/10.1038/cr.2011.101.

[95] D. Inta, J. Alfonso, J. von Engelhardt, M.M. Kreuzberg, A.H. Meyer, J.A. van Hooft, H. Monyer, Neurogenesis and widespread forebrain migration of distinct GABAergic neurons from the postnatal subventricular zone, Proc. Natl. Acad. Sci. U. S. A. 105 (2008) 20994–20999. https://doi.org/10.1073/pnas.0807059105.

[96] U. Englund, A. Björklund, K. Wictorin, Migration patterns and phenotypic differentiation of long-term expanded human neural progenitor cells after transplantation into the adult rat brain, Brain Res. Dev. Brain Res. 134 (2002) 123–141. https://doi.org/10.1016/s0165-3806(01)00330-3.

[97] T.L. Walker, T. Yasuda, D.J. Adams, P.F. Bartlett, The Doublecortin-Expressing Population in the Developing and Adult Brain Contains Multipotential Precursors in Addition to Neuronal-Lineage Cells, J. Neurosci. 27 (2007) 3734–3742. https://doi.org/10.1523/JNEUROSCI.5060-06.2007.

[98] T. Kremer, R. Jagasia, A. Herrmann, H. Matile, E. Borroni, F. Francis, H.G. Kuhn, C. Czech, Analysis of adult neurogenesis: evidence for a prominent “non-neurogenic” DCX-protein pool in rodent brain, PloS One. 8 (2013) e59269. https://doi.org/10.1371/journal.pone.0059269.

[99] L. Dehmelt, S. Halpain, The MAP2/Tau family of microtubule-associated proteins, Genome Biol. 6 (2005) 204. https://doi.org/10.1186/gb-2004-6-1-204.

[100] J.G. Izant, J.R. McIntosh, Microtubule-associated proteins: a monoclonal antibody to MAP2 binds to differentiated neurons, Proc. Natl. Acad. Sci. U. S. A. 77 (1980) 4741–4745. https://doi.org/10.1073/pnas.77.8.4741.

[101] A.R. Gliga, K. Edoff, F. Caputo, T. Källman, H. Blom, H.L. Karlsson, L. Ghibelli, E. Traversa, S. Ceccatelli, B. Fadeel, Cerium oxide nanoparticles inhibit differentiation of neural stem cells, Sci. Rep. 7 (2017). https://doi.org/10.1038/s41598-017-09430-8.

[102] A. Arya, A. Gangwar, S.K. Singh, M. Roy, M. Das, N.K. Sethy, K. Bhargava, Cerium oxide nanoparticles promote neurogenesis and abrogate hypoxia-induced memory impairment through AMPK–PKC–CBP signaling cascade, Int. J. Nanomedicine. 11 (2016) 1159–1173. https://doi.org/10.2147/IJN.S102096.

[103] Z.S. Bailey, E. Nilson, J.A. Bates, A. Oyalowo, K.S. Hockey, V.S.S.S. Sajja, C. Thorpe, H. Rogers, B. Dunn, A.S. Frey, M.J. Billings, C.A. Sholar, A. Hermundstad, C. Kumar, P.J. VandeVord, B.A. Rzigalinski, Cerium Oxide Nanoparticles Improve Outcome after In Vitro and In Vivo Mild Traumatic Brain Injury, J. Neurotrauma. 37 (2020) 1452–1462. https://doi.org/10.1089/neu.2016.4644.

[104] B.H.J. Juurlink, S.K. Thorburne, L. Hertz, Peroxide-scavenging deficit underlies oligodendrocyte susceptibility to oxidative stress, Glia. 22 (1998) 371–378. https://doi.org/10.1002/(SICI)1098-1136(199804)22:4<371::AID-GLIA6>3.0.CO;2-6.

[105] A. Almeida, J. Almeida, J.P. Bolaños, S. Moncada, Different responses of astrocytes and neurons to nitric oxide: The role of glycolytically generated ATP in astrocyte protection, Proc. Natl. Acad. Sci. 98 (2001) 15294–15299. https://doi.org/10.1073/pnas.261560998.

[106] M.J. Rigby, T.M. Gomez, L. Puglielli, Glial Cell-Axonal Growth Cone Interactions in Neurodevelopment and Regeneration, Front. Neurosci. 14 (2020) 203. https://doi.org/10.3389/fnins.2020.00203.

[107] A. Amaral, T. Meisingset, M. Kotter, U. Sonnewald, Metabolic Aspects of Neuron-Oligodendrocyte-Astrocyte Interactions, Front. Endocrinol. 4 (2013) 54. https://doi.org/10.3389/fendo.2013.00054.

[108] E.E. Frost, P.C. Buttery, R. Milner, C. ffrench-Constant, Integrins mediate a neuronal survival signal for oligodendrocytes, Curr. Biol. 9 (1999) 1251-S1. https://doi.org/10.1016/S0960-9822(99)80506-5.

[109] L. Gang, Y. Yao, Y. Liu, Y. Li, K. Yang, L. Lu, Y. Cheng, X. Chen, Y. Tu, Co-culture of oligodendrocytes and neurons can be used to assess drugs for axon regeneration in the central nervous system, Neural Regen. Res. 10 (2015) 1612–1616. https://doi.org/10.4103/1673-5374.167759.

[110] K.A. Chamberlain, S.E. Nanescu, K. Psachoulia, J.K. Huang, Oligodendrocyte regeneration: Its significance in myelin replacement and neuroprotection in multiple sclerosis, Neuropharmacology. 110 (2016) 633–643. https://doi.org/10.1016/j.neuropharm.2015.10.010.

Chapter 6

General conclusions and future perspectives

General conclusions and future perspectives

6.1. General conclusions

Chapter 3. Nanostructured scaffolds based on bioresorbable polymers and graphene oxide induce the aligned migration and accelerate the neuronal differentiation of neural stem cells.

1. **Successful generation of bioresorbable polymeric nanostructured scaffolds functionalized with graphene oxide (GO).**
   Poly(L-lactide-co-ε-caprolactone) (PLCL) films of around 150 μm were first obtained by compression molding at 175 ^{o}C and subsequently thermo-pressed at 190 ^{o}C and 20 N with the aid of a commercially available silicon stamp. For surface functionalization, precoating with 2 mg/ml dopamine-hydrocholoride was a must for the successful deposition of GO on the surface. Besides, GO concentrations above 0.25 mg/ml or incubation times longer than 30 min were demonstrated to have a detrimental effect on the original shape of the nanostructure.

2. **Nanostructured scaffolds either functionalized or not with GO enable the aligned attachment of neural stem cells (NSCs) to the surface.**
   In the absence of extracellular matrix (ECM)-like compounds, non-nanostructured scaffolds showed attachment of NSCs in spherical form (i.e., neurospheres), independent of the functionalization with GO. Contrarily, when scaffolds were nanostructured, independent of the functionalization with GO, cells oriented and aligned according to the nanograting axis. Besides, the functionalization with GO resulted in higher directionality of the cell processes.

3. **Nanostructured scaffolds either functionalized or not with graphene oxide create migration paths according to the nanograting axis.**
   The pausing time was greater and the mean velocity and the total travel distances were lower on our nanostructured scaffolds either functionalized or not with GO in comparison with the control (i.e., glass cover coated with laminin). However, the persistence (i.e., the time a cell follows the same direction) was greater on our scaffolds than on laminin, suggesting the creation of preferential migration paths.

4. **Nanostructured scaffolds either functionalized or not with GO allow the neural differentiation of mouse NSCs towards both astroglial and neuronal lineages even faster than the extracellular matrix (ECM)-like compound laminin.**
   Neuronal and glial differentiation was boosted over our nanostructured scaffolds in comparison with the glass cover coated with laminin. Both immature (DCX) and mature (NeuN) neurons were more abundant on our nanostructured scaffolds coated with polydopamine (NanoPDA) or coated with polydopamine and functionalized with GO (NanoGO) at days *in vitro* (DIV) 10. Similarly, glial immature (GFAP) and mature (S100β) differentiation was also boosted even at DIV3 on both NanoPDA and NanoGO.

Chapter 4. Nanostructured scaffolds based on bioresorbable polymers and graphene oxide facilitate the adhesion, alignment, neural commitment and migration of human dental pulp stem cells and allow the intracerebral implantation to promote the restoration of the injured rostral migratory stream on a rodent brain model.

1. **Nanostructured scaffolds based on bioresorbable polymers and graphene oxide allow the differentiation of hDPSCs towards, astroglial, neuronal and myelinating precursor committed cells.**
   In vitro studies demonstrated an enhanced differentiation towards immature (DCX) and mature (NeuN) neuronal lineages on NanoGO scaffolds, while NanoPDA accelerated the glial differentiation towards astroglial immature (GFAP) and mature (S100β) cells and also possible myelinating Schwann cell precursors (S100β/p75).

2. **The combination of the nanostructured scaffolds NanoPDA and NanoGO together with grafted hDPSCs allowed the survival and implantation of the hDPSCs on the stem cell neural niches.**
   Preliminary studies showed that after 3 months, when hDPSCs were grafted alone, they were able to migrate towards the subventricular zone and promote the restoration of the RMS on the left hemisphere, where they were grafted. But, when hDPSCs were grafted together with the NanoPDA scaffold, they were able to migrate towards the right hemisphere even permitting the restoration of the RMS on both sides.

Chapter 5. Self-assembled three-dimensional hydrogels based on graphene derivatives and cerium oxide nanoparticles: scaffolds for co-culture of oligodendrocytes and neurons derived from neural stem cells.

1. **Increasing the amount of ascorbic acid (AsA) resulted in a more collapsed morphology with greater mechanical and electrical properties of the graphene derivatives-based hydrogels.**
   Increasing four times the ratio between GO and AsA (from GO:AsA 1:1 to GO:AsA 1:4) provoked the augmentation of both mechanical stiffness (from 22.8±0.3 kPa to 178.4±2.8 kPa) and electrical conductivity (from 0.6 S/m to 35 S/m) , while resulting in hydrogels with a more collapsed porous architecture. Further increasing the proportion of AsA had almost no effect on the morphology, the mechanical or electrical properties of the resulting hydrogels, suggesting that a plateau has been reached in terms of GO reduction level.

2. **Including cerium oxide (CeO_2) nanoparticles in an increasing amount resulted in graphene derivatives-based hydrogels with lower mechanical stiffness and electrical conductivity.**
   Including CeO_2 nanoparticles had no effect on the morphology in any of the concentrations tested. Regarding the mechanical and the electrical properties, ratios of GO:CeO_2 up to 10:0.5 had no effect, but higher ratios like GO:CeO_2 10:1 decreased both the mechanical stiffness (from 178.4±2.8 kPa to 9.7±0.1 kPa) and the electrical conductivity (from 27 S/m to 1.6 S/m) of the hydrogels.

3. **Graphene derivatives-based hydrogels with larger pores and lower mechanical stiffness and electrical conductivity promoted the differentiation towards neuronal lineages.**
   Differentiation studies with immature (DCX) and mature (MAP2) neuronal markers suggested that GO:AsA 1:1 hydrogels with larger pores and lower mechanical stiffness and electrical conductivity were able to support both immature and mature neurons at DIV7 and DIV14 respectively. Contrarily, GO:AsA 1:4 hydrogels with smaller pores and higher mechanical stiffness and electrical conductivity did not allow neuronal differentiation at any studied time-point.

4. **Graphene derivatives-based hydrogels with smaller pores and higher mechanical stiffness and electrical conductivity promoted the differentiation towards astroglial lineages.**
   Differentiation studies with immature (GFAP) and mature astroglial markers (S100β) suggested that both GO:AsA 1:1 and GO:AsA 1:4 hydrogels supported astroglial differentiation at DIV7, 14 and 21. But GO:AsA 1:4 supported a faster astroglial (GFAP) and oligodendroglial differentiation (Olig2) at DIV3.

5. **The incorporation of CeO_2 nanoparticles enabled the establishment of mature oligodendrocytes and neurons thanks to their antioxidant properties.**
   Differentiation studies showed a co-culture of oligodendrocytes (Olig2) and mature neurons (MAP2) up to DIV21 only in the hydrogels containing CeO_2 nanoparticles. Moreover, the intracellular reactive oxygen species (ROS) were also lower (GO:AsA 1:1 71.6±5.3, GO:AsA 1:4 62.6±5.9 and Go:AsA 1:4 + CeO_2 0.25 34.8±2.1, $p < 0.05$, One-way ANOVA), suggesting that the possible reason behind the oligodendroglial and the mature neuron survival was thanks to the reduction of the intracellular ROS.

6.2. Future perspectives

In the present PhD work, we successfully synthesized bioresorbable poly(L-lactide-co-ε-caprolactone) (PLCL) nanostructured two-dimensional films either functionalized (NanoGO) or not (NanoPDA) with graphene oxide (GO) for expansion and differentiation of mouse and human stem cells. The experiments with primary mouse neural stem cells (NSCs) demonstrated the good biocompatibility and enhanced neural and glial differentiation of the NSCs over our NanoGO and NanoPDA scaffolds. Interestingly, these studies also highlighted the necessity of topographical cues for the adequate attachment of the stem cells over the scaffolds. On the other hand, these experiments demonstrated enhanced biocompatibility when the scaffolds were functionalized with conductive substances like polydopamine (PDA) or graphene oxide (GO), even in the absence of extracellular matrix (ECM)-like compounds like laminin. Future experiments should investigate the addition of other conductive substances like non-absorbable polymers, carbon nanotubes or inorganic nanoparticles (e.g., gold or cerium oxide (CeO_2) nanoparticles) to enhance the attachment of stem cells and avoid ECM-like compounds coatings that mask the direct interaction of the cells with the biomaterials. Besides, future investigations should include a negative control of non-coated nanostructured scaffolds and nanostructured scaffolds coated with ECM-like compounds together with a more complete proteomic analysis to study the effects of the combination of the nanostructure and the conductive substance coating on the biocompatibility and attachment of stem cells over the synthesized scaffolds.

In addition, when our nanostructured scaffolds were incubated with NSCs, they were able to create migration paths along with the nanograting axis, which highly encourages the use of nanostructured scaffolds for the treatment of neural diseases that demand aligned axonal and neural growth. Nevertheless, as the acquisition of autologous NSCs together with their possible tumorigenic features are huge handicaps for their use in clinic, future experiments should include human stem cells from different sources like mesenchymal stem cells (MSCs) or induced pluripotent stem cells (iPSCs). Indeed, our experiments with MSCs like human dental pulp stem cells (hDPSCs) also demonstrated the alignment of the cells according to the nanostructure, which supports the use of other stem cells for treating aligned tissue regeneration like neuromuscular or vascular diseases, peripheral system reinnervation or even spinal cord injury (SCI). Anyways, the controversial results obtained on the creation of migration paths thanks to the nanostructure with NSCs and hDPSCs require further experiments together with complete biocompatibility, aligned migration and differentiation pattern towards the astroglial, neuronal and myelinating precursor lineages before our bioresorbable nanostructured scaffolds-based technology can reach the clinic. Anyways, the obtained results highly encourage the use of PLCL-based nanostructured scaffolds functionalized or not with GO for the restoration of traumatic central nervous system (CNS) injuries like traumatic brain injury (TBI) and spinal cord injury (SCI).

In the treatment of traumatic diseases like TBI and SCI, the remyelination of the axons is reported to enhance functional recovery. Thus, future studies may investigate the differentiation of the cells towards oligodendrocytes and Schwann cells before implantation into the injured neural tissue. Indeed, our *in vitro* experiments with hDPSCs demonstrated the capacity of the nanostructured scaffolds NanoGO and NanoPDA on the commitment of hDPSCs towards myelinating precursors expressing both S100 calcium-binding protein β (S100β) and p75 neurotrophin receptor (p75(NTR)), but further studies must be performed to ensure the promotion of functional myelinization cells over our nanostructured NanoGO and NanoPDA scaffolds.

Similarly, we reported the achievement of both immature (DCX) and mature (NeuN) neurons thanks to the enhanced neuronal commitment of both mouse NSCs and hDPSCs over our nanostructured NanoGO and NanoPDA scaffolds, but there is still the need to test the functionality of those neurons. In this regard, future studies should test the possibility of achieving neurons with the ability to undergo action potentials by electrophysiological studies. These electrophysiological studies must not be only performed *in vitro*, but they may also ensure the integration of the grafted stem cells in the actual neural network by electrophysiological studies *in vivo* either using optogenetics or studying the integration of the grafted stem cells with *ex vivo* patch clamp studies in animal brain or spinal cord slices.

Stem cells with the ability to differentiate towards neural tissue may also have the ability to create pericytes and microglia. Indeed, the creation of both may delay the restoration of the injured neural tissue *in vivo*. Hence, future experiments combining nanostructured scaffolds like NanoGO and NanoPDA with stem cells should also test the commitment toward these lineages before implanting them inside the traumatic injured site. Here, we focused on the implantation of hDPSCs and actual restoration of the rostral migratory stream (RMS) but we only presented a proof-of-concept study where either NanoGO or NanoPDA scaffolds grafted or not with hDPSCs were able to restore the damaged CNS. However, further studies are needed to truly investigate the effect of the nanostructure alone either functionalized or not with GO and the effect of the hDPSCs on the modulation of the inflammation and the immune response, the restoration of the tissue and the possible integration of the hDPSCs on the neural networks. In this regard, due to modulatory features of the hDPSCs, activation of the microglia should be studied together with the migration of macrophages and leukocytes that could have migrated inside the brain due to the mechanical distribution of the extracellular matrix and the interstitial system after the injury. In other studies, grafted hDPSCs on a healthy mouse have shown integration of the hDPSCs in the vascular system instead of the stem neural niches. Hence, to better study the actual effect of the nanostructured scaffolds like NanoPDA and NanoGO on the functional integration of the hDPSCs in the neural network, further studies may include the analysis of endothelial

markers like cluster of differentiation 31 (CD31), 105 (CD105), 146 (CD146) and von Willebrand factor (vWF).

Finally, our *in vitro* testing of 3D scaffolds demonstrated the successful generation of graphene derivatives-based scaffolds with tunable morphological, mechanical and electrical properties dependent on the amount of ascorbic acid (AsA). The *in vitro* testing demonstrated good biocompatibility and integration of the stem cells with a clear differentiation toward astroglial lineages on scaffolds with smaller pores and higher mechanical stiffness and electrical conductivity, while the neuronal commitment was enhanced on scaffolds with larger pores and lower mechanical stiffness and electrical conductivity. Nevertheless, our studies were unable to identify which of the properties was enhancing this astroglial or neuronal commitment, nor the biological mechanism underneath. Thus, future studies should include the formation of hydrogels with variation in only one of the features to better understand the independent effect of the morphology, mechanical and electrical properties. Interestingly, our studies also suggested that independent of the geometry, mechanical and electrical cues, the addition of antioxidant entities enhanced the establishment of a mature culture with oligodendroglial and neuronal committed cells. Although future studies should focus on the biological mechanism underlying these findings, our studies highly encourage the incorporation of antioxidant features on 3D scaffolds for a more stabilized differentiation and a better prognostic in animal studies and in the clinic.

In the future, other human stem cells (e.g., hDPSCs) should be tested over the 3D graphene derivatives-based scaffolds to investigate the effect of the tunable geometrical, mechanical, electrical conductivity and antioxidant properties on the proliferation and differentiation pattern towards the neural lineage. Besides, to better understand the impact of the incorporation of antioxidant features, experiments should be done by adding only CeO_2 nanoparticles to the cell medium and studying proliferation and differentiation patterns. If results are satisfactory, the incorporation of more complex features either 3D or nanostructured scaffolds might be studied, like bioresorbable antioxidant nanoparticles or nanogels loaded with antioxidant enzymes like superoxide-dismutase (SOD) or catalase (CAT). Indeed, the incorporation of antioxidant features has been reported to be beneficial in SCI and TBI, which will enhance the bench-to-clinic approach of our technology.

Overall, although more investigation is needed, our studies highly encourage the use of the combination of nanostructured bioresorbable scaffolds based on PLCL and stem cells like hDPSCs on the restoration of pathological CNS lesions where the directionality of the cells or the axons are an actual problem like in SCI. They also encourage the use of our nanotechnology in other pathologies that need an aligned restoration like neuromuscular diseases and finally our results highly support the implementation of antioxidant features when designing materials for CNS restoration.